Lecture Notes in Electrical Engineering 396

Daya K. Lobiyal
Durga Prasad Mohapatra
Atulya Nagar
Manmath N. Sahoo
Editors

Proceedings of the International Conference on Signal, Networks, Computing, and Systems

ICSNCS 2016, Volume 2

Springer

Lecture Notes in Electrical Engineering

Volume 396

About this Series

"Lecture Notes in Electrical Engineering (LNEE)" is a book series which reports the latest research and developments in Electrical Engineering, namely:

- Communication, Networks, and Information Theory
- Computer Engineering
- Signal, Image, Speech and Information Processing
- Circuits and Systems
- Bioengineering

LNEE publishes authored monographs and contributed volumes which present cutting edge research information as well as new perspectives on classical fields, while maintaining Springer's high standards of academic excellence. Also considered for publication are lecture materials, proceedings, and other related materials of exceptionally high quality and interest. The subject matter should be original and timely, reporting the latest research and developments in all areas of electrical engineering.

The audience for the books in LNEE consists of advanced level students, researchers, and industry professionals working at the forefront of their fields. Much like Springer's other Lecture Notes series, LNEE will be distributed through Springer's print and electronic publishing channels.

More information about this series at http://www.springer.com/series/7818

Daya K. Lobiyal · Durga Prasad Mohapatra
Atulya Nagar · Manmath N. Sahoo
Editors

Proceedings of the International Conference on Signal, Networks, Computing, and Systems

ICSNCS 2016, Volume 2

Springer

Editors
Daya K. Lobiyal
School of Computer and Systems Sciences
Jawaharlal Nehru University
New Delhi, Delhi
India

Atulya Nagar
Faculty of Science
Liverpool Hope University
Liverpool
UK

Durga Prasad Mohapatra
Department of Computer Science and Engineering
National Institute of Technology
Rourkela, Odisha
India

Manmath N. Sahoo
Department of Computer Science and Engineering
National Institute of Technology
Rourkela, Odisha
India

ISSN 1876-1100 ISSN 1876-1119 (electronic)
Lecture Notes in Electrical Engineering
ISBN 978-81-322-3587-3 ISBN 978-81-322-3589-7 (eBook)
DOI 10.1007/978-81-322-3589-7

Library of Congress Control Number: 2016942038

Printed on acid-free paper

This Springer imprint is published by Springer Nature
The registered company is Springer (India) Pvt. Ltd.

Preface

International Conference on Signal, Networks, Computing, and Systems (ICSNCS 2016), organized by School of Computer and Systems Sciences, Jawaharlal Nehru University, India, during February 25–27, 2016, certainly marks a success toward bringing researchers, academicians, and practitioners to the same platform. It is indeed a pleasure to receive overwhelming response from researchers of premier institutes of the country and abroad for participating in ICSNCS 2016, which makes our endeavor successful. Being the first conference of its series, it was challenging for us to broadcast the conference among researchers and scientists and to receive their valuable works for review. A very systematic workflow by the committee has made it possible. We have received 296 articles and have selected 73 articles of the highest quality among them for presentation and publication through peer-review done by at least two experts for each article. We are unable to accommodate many promising works as we restricted our selection to limited articles which could be elaborately presented in a three-day conference. We are thankful to have the advice of dedicated academicians and experts from industry to organize the conference. We thank all researchers who participated and submitted their valued works in our conference. The articles presented in the proceedings discuss the cutting-edge technologies and recent advances in the domain of the conference. We conclude with our heartiest thanks to everyone associated with the conference and seeking their support to organize the next editions of the conference in subsequent years.

New Delhi, India — Daya K. Lobiyal
Rourkela, India — Durga Prasad Mohapatra
Liverpool, UK — Atulya Nagar
Rourkela, India — Manmath N. Sahoo

Conference Organization

General Chair

Daya K. Lobiyal, Jawaharlal Nehru University, India

Organizing Chairs

Ram Shringar Rao, Ambedkar Institute of Advanced Communication Technologies and Research, India
Sushil Kumar, Jawaharlal Nehru University, India
Buddha Singh, Jawaharlal Nehru University, India

Program Chairs

Manmath N. Sahoo, National Institute of Technology, Rourkela, India
Zaheeruddin, Jamia Millia Islamia University, India
Yulei Wu, University of Exeter, Exeter

Program Co-Chairs

Sandip Rakshit, Kaziranga University, Assam, India
Syed Rizvi, Pennsylvania State University, USA
Yogesh H. Dandawate, SMIEEE, Vishwakarma Institute of Information Technology, India

Publication Chairs

Soubhagya Sankar Barpanda, National Institute of Technology, Rourkela, India
Sambit Bakshi, National Institute of Technology, Rourkela, India

Area Chairs

ASIA: Ompraksh Kaiwartya, Faculty of Computing Universiti Teknologi, Malaysia
EUROPE: Atilla Elci, Aksaray University, Turkey
USA: Adam Schmidt, Poznan University of Technology, Poland

Technical Track Chairs

Signal: Binod K. Kanaujia, AIACTR, India
Networking: Sanjay K. Soni, Delhi Technological University, Delhi, India
Computing: Nanhay Singh, AIACTR, India
Systems: Naveen Kumar, Indira Gandhi National Open University, India

Web Chairs

Sanjoy Das, Galgotias University, India
Rahul Raman, National Institute of Technology, Rourkela, India

Technical Program Committee

Anand Paul, SMIEEE, Kyungpook National University, Republic of Korea
Andrey V. Savchenko, National Research University Higher School of Economics, Russia
Ch. Aswani Kumar, Vellore Institute of Technology, India
Dilip Singh Sisodia, National Institute of Technology, Raipur, India
Ediz Saykol, Beykent University, Turkey
Flavio Lombardi, Roma Tre University of Rome, Italy
Jamuna Kanta Sing, SMIEEE, Jadavpur University, India
Jaya Sil, Bengal Engineering and Science University, India

Krishnan Nallaperumal, SMIEEE, Manonmaniam Sundaranar University, India
Lopamudra Chowdhury, Jadavpur University, India
Narayan C. Debnath, Winona State University, USA
Nidul Sinha, SMIEEE, National Institute of Technology, Silchar, India
Paulo Quaresma, University of Evora, Portugal
Patrick Siarry, SMIEEE, Université de Paris, France
Pradeep Singh, National Institute of Technology, Raipur, India
Raghvendra Mall, University of Leuven, Belgium
Rajarshi Pal, Institute for Development and Research in Banking Technology, India
Sotiris Kotsiantis, University of Patras, Greece
Yogesh H. Dandawate, SMIEEE, Vishwakarma Institute of Information Technology, Pune, India
Zhiyuan (Thomas) Tan, University of Twente, the Netherlands

Organizing Committee

Adesh Kumar, Shri Lal Bahadur Shastri Rashtriya Sanskrit Vidyapeetha, India
Ajay Sikandar, Jawaharlal Nehru University, India
Anil Kumar Sagar, Galgotias University, India
Arvind Kumar, Ambedkar Institute of Advanced Communication Technologies and Research, India
Ashok Kumar Yadav, Amity School of Engineering and Technology, India
Indrani Das, Jawaharlal Nehru University, India
Kamlesh Kumar Rana, Galgotias College of Engineering and Technology (GCET), India
Karan Singh, Jawaharlal Nehru University, India
Mahendra Ram, Jawaharlal Nehru University, India
Meenakshi Sihag, Guru Tegh Bahadur Institute of Technology, India
Prashant Singh, Northern India Engineering College, India
Rajesh Kumar Yadav, Delhi Technological University, India
Rameshwar Lal Ujjwal, Guru Gobind Singh Indraprastha University, India
Sanjeev Kumar, Ambedkar Institute of Advanced Communication Technologies and Research, India
Shailender Kumar, Ambedkar Institute of Advanced Communication Technologies and Research, India
Sunil Kumar, Jawaharlal Nehru University, India
Suresh Kumar, Ambedkar Institute of Advanced Communication Technologies and Research, India

External Reviewers

Ajay Shankar Shukla, Central Council for Research in Ayurvedic Sciences, India
Amar Jeet Singh, Himachal Pradesh University, India
R. Kingsy Grace, Anna University, India
Shiv Prakash, Indian Institute of Technology, Delhi, India
Snehasis Banerjee, Tata Consultancy Services Research, India
Taymaz Farshi, Gazi University, Turkey
Omprakash Kaiwartya, Jawaharlal Nehru University, India
Xavier Bellekens, University of Strathclyde, Glasgow

Contents

About the Editors

Dr. Daya K. Lobiyal is currently serving as Professor in School of Computer and Systems Sciences in Jawaharlal Nehru University, India. His research works have been published in many journals and conference proceedings. He is a Fellow of Institution of Electronics and Telecommunication Engineers, India.

Prof. Durga Prasad Mohapatra received his Ph.D. from the Indian Institute of Technology Kharagpur and is presently serving as Associate Professor in NIT Rourkela, Odisha. His research interests include software engineering, real-time systems, discrete mathematics, and distributed computing. He has published more than 30 research papers in these fields in various international journals and conference proceedings. He has received several project grants from DST and UGC, Government of India. He has received the Young Scientist Award for the year 2006 from Orissa Bigyan Academy. He has also received the Prof. K. Arumugam National Award and the Maharashtra State National Award for outstanding research work in Software Engineering for the years 2009 and 2010, respectively, from the Indian Society for Technical Education (ISTE), New Delhi. He is going to receive the Bharat Sikshya Ratan Award for significant contribution in academics awarded by the Global Society for Health and Educational Growth, Delhi.

Prof. Atulya Nagar holds the Foundation Chair as Professor of Mathematical Sciences at Liverpool Hope University where he is the Dean of Faculty of Science. He has been the Head of Department of Mathematics and Computer Science since December 2007. A mathematician by training, he is an internationally recognized scholar working at the cutting edge of applied nonlinear mathematical analysis, theoretical computer science, operations research, and systems engineering and his work is underpinned by strong complexity-theoretic foundations. He has an extensive background and experience of working in universities in UK and India. He has edited volumes on Intelligent Systems and Applied Mathematics; he is the Editor-in-Chief of the International Journal of Artificial Intelligence and Soft Computing (IJAISC) and serves on editorial boards for a number of prestigious journals such as the Journal of Universal Computer Science (JUCS). Professor Nagar received a prestigious Commonwealth Fellowship for pursuing his Doctorate

(D.Phil.) in Applied Non-Linear Mathematics, which he earned from the University of York in 1996. He holds B.Sc. (Hons.), M.Sc., and M.Phil. (with Distinction) from the MDS University of Ajmer, India.

Dr. Manmath N. Sahoo received his M.Tech and Ph.D. degrees in Computer Science in the year 2009 and 2014, respectively, from National Institute of Technology (NIT) Rourkela, India. He is Assistant Professor in the Department of Computer Science and Engineering, NIT Rourkela, India. He has served as reviewer, guest editor, track chair, and program chair in many reputed journals and conferences. His research interests include mobile ad hoc networks, fault tolerance, and sensor networks. He is a professional member of prestigious societies like IEEE, CSI, and IEI.

Part I
Advanced Computing Paradigms

Interactions with Human CD4 Protein Leads to Helix-to-Coil Transition in HIV-gp120 Aiding CCR5 Attachment and Viral Entry: An *In Silico* Structural Biology Approach for AIDS

Sujay Ray and Arundhati Banerjee

Abstract Human immuno-deficiency virus (HIV) is assisted by its glycoprotein; gp120 for its human host cell invasion via fusion to cause AIDS. Documentation documents a structural change in gp120, after its first interaction with human CD4 protein which further attracts CCR5 protein, thereby paving its way for viral entry. So, gp120 was homology modeled efficiently. Trio docking analysis led to the disclosure of the responsible residues from protein complexes. Polar-charged residues from CD4 protein played a pivotal role. The trio complex was optimized and simulated. Conformational switches and other stability parameters for gp120 was computed, compared, and analyzed at three different stages; before any interaction and after CD4 and CCR5 interaction separately. They were statistically significant with an overall helix-to-coil transition.

Keywords Modeling · Conformational switches · Docked Protein–Protein interaction · AIDS · Stability parameters · Biostatistics

1 Introduction

In AIDS (acquired immuno-deficiency syndrome), HIV uses glycoprotein (gp) subunit-120 to participate in the interaction with CD4 receptor on the host target cell [1, 2]. A structural and conformational change occurs in gp120 protein. This further helps to activate the binding of chemokine coreceptors (CCR5) to

S. Ray (✉)
Department of Biochemistry and Biophysics, University of Kalyani, Kalyani, WB, India
e-mail: raysujay@gmail.com

A. Banerjee
Department of Biotechnology, National Institute of Technology, Durgapur, WB, India
e-mail: arundhati.92star@gmail.com

D.K. Lobiyal et al. (eds.), *Proceedings of the International Conference on Signal, Networks, Computing, and Systems*, Lecture Notes in Electrical Engineering 396, DOI 10.1007/978-81-322-3589-7_1

gp120 [3]. HIV thus invades into the cell [3]. T-cells compromise the immune system, expire and secondary infection is caused because of HIV's eventual replication. However, detailed molecular level interaction between these proteins along with analysis in the conformational variations in gp120 at three different stages (before any interaction, after interacting with CD4 and further with CCR5 protein) has not been dealt with yet.

Therefore, this study involves primarily the homology modeling of gp120 from human immuno-deficiency virus (HIV) and analysis of the 3D functional state of all the essential proteins. After simulation, the protein–protein docking studies helped to examine the residual contribution. Further, the study delved into the conformational alterations, energy calculations, net solvent accessibility, and electrostatic surface potentials in the gp120 protein at each individual stage of interaction with statistical significances. This is an unexplored and novel description where the probe provides clear information regarding the respective residue level disclosure for understanding the molecular background for HIV entry. The overall study contributes to future molecular and therapeutic research.

2 Materials and Methods

2.1 Sequence-Template Exploration and Homology Modeling for gp120 Protein

The amino acid sequence of human immuno-deficiency virus (HIV) protein from *Human Immuno-Deficiency Virus* was extracted and obtained from Uniprot KB (Accession No.: P03378). It was validated using NCBI too. Results from PSI-BLASTP [4] against PDB helped to distinguish the templates for building the homology model. The template was from *Human Immuno-Deficiency Virus* (PDB code: 3J5M_A with 98 % query coverage sharing 72 % sequence identity).

For the homology modeling of gp120 protein, MODELLER9.14 software tool [5] was operated. Root mean-squared deviations (RMSD) from the backbone superimposition on its crystal template (i.e., A chain of 3J5M) was 0.244 Å from both PyMOL [6].

2.2 Optimization, Refinement, and Stereochemical Validation of the Structure

The modeled protein was subjected to ModLoop [7] and further ModRefiner tool [8] to resolve the distortions in the loop regions and refinement in the 3D geometry of gp120. A steady conformation [8] was achieved by overall energy optimization. Energy minimization technique using CHARMM force field [9] was performed by

steepest descend technique and conjugate gradient using Discovery studio software, until the modeled gp120 structure attained a RMS value of 0.0001. Corroboration of the stereochemical features of the modeled gp120 protein was performed with the estimation of Verify3D [10] and ERRAT [11] values. Ramachandran Plot [12] had zero residues in the unfavored regions.

2.3 Structure Analysis of gp120-CD4 Complex and Human CCR5 Protein

The necessary search results for gp120-CD4 bound complex for the purpose of effective cooperation of gp120 with human CD4, selected its X-ray crystal structure from *Homo sapiens*, having PDB ID: 2B4C with chain G and C for gp120 protein and human CD4 protein [13]. The entire protein complex of interest had 496 amino acids. Search results for human CCR5 protein selected its X-ray crystal structure from *Homo sapiens* having PDB ID: 4MBS, chain A [14]. It was 346 amino acid residues long.

2.4 Protein–Protein Docking with Human CCR5 Protein and Simulation

For the protein–protein interaction study of gp120-CD4 complex with human CCR5 protein, the protein complex and human CCR5 protein was docked operating Cluspro2.0 [15]. Preeminent cluster size among all the complexes was opted.

Two-step molecular dynamics simulation was performed to achieve a stable conformation of the protein with a diminished overall energy. First, FG-MD (fragment-guided molecular-dynamics) [16] aided to reconstruct the energy funnel via MD simulations. Next, this rebuilt simulated trio protein complex structure from its fragments was subjected to Chiron Energy Minimization tool [17], to diminish the overall energy using CHARMM force field [9] and perform Molecular Dynamics [17]. Therefore, besides eliminating the steric clashes rapidly, minimal deformation of the protein backbone was produced.

2.5 Conformational Variations and Stability for the gp120 Protein

The conformational switching in the gp120 HIV protein was estimated and analyzed at its three different stages; before any kind of interaction (S1), after interacting with CD4 protein (S2) and after interacting with CCR5 protein (S3) further.

So, the individual secondary structure distribution was analyzed using DSSP method [18] and PyMOL [6]. Documentation suggests [19] that increase in the helical structures and β-sheets leads to stronger and better interaction.

At three different stages; S1, S2, and S3, the stability and strength of the protein was explored by evaluating the free energy of folding (using VADAR2.0 [20]) and net area of solvent accessibility [21] of the individual gp120 protein. The surface electrostatic potential for all the three gp120 structures was generated through vacuum electrostatics with the assistance of PyMOL [6].

2.6 Calculation of Interaction Patterns and Binding Modes in the Complexes

Protein Interaction Calculator (P.I.C) web server [22] was operated to delve into the responsible relevant amino acid residues (specially, predominant ionic interactions [23]) participating in the protein–protein complexes from their individual positions.

2.7 Evaluation and Substantiation Through Statistical Significance

For the purpose of statistical significance analysis and substantiation of the estimated outcomes, the paired T-test was evaluated. The difference between the two means turns-out to be statistically significant ($P < 0.05$) and thus, validates the outcomes.

3 Results

3.1 Structural Portrayal of the Human Immuno-Deficiency Virus gp120

The functionally potent 3D-modeled structure of the human immuno-deficiency virus gp120 protein was 478 amino acids long. The modeled protein was akin to its crystal template belonging from *Human Immuno-deficiency Virus* (PDB code: 3J5M, chain A). It comprises mainly 7 sets of α-helices interspersed with 21 sets of parallel and anti-parallel β-sheets. The structure is well illustrated in Fig. 1 with α-helices and β-sheets in marine blue and yellow shades connected by red-shaded coils.

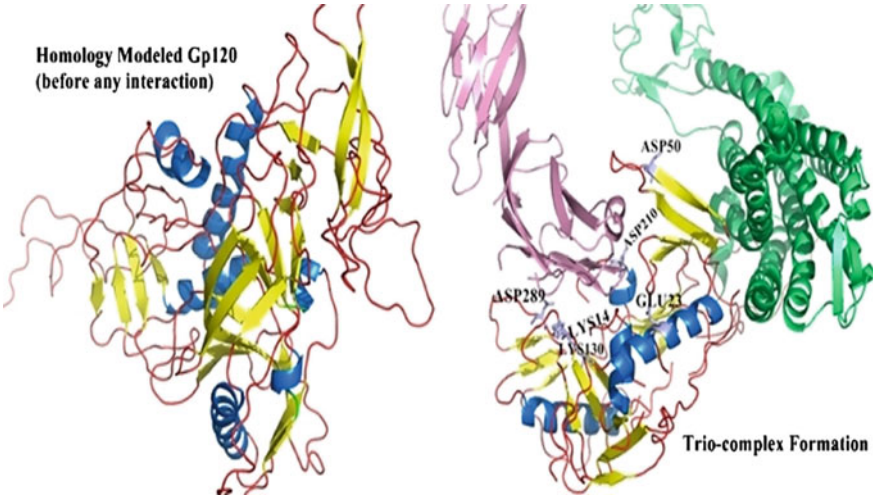

Fig. 1 HIV gp120 protein with α-helices, β-sheets and coils in *marine-blue*, *yellow* and *red shades*. Interacting residues from gp120 are labeled. CCR5 and CD4 in *pink* and *green shades* (colour online)

3.2 Analysis of Conformational Transitions in gp120

The conformational switching in the gp120 HIV protein at S1, S2, and S3 stages was evaluated and compared. Figure 2 represents the conformational alterations of gp120.

3.3 Stability Analysis Deductions for gp120 Protein

3.3.1 Estimation of Free Energy of Folding, Net Solvent Accessibility, and Electrostatic Potential on gp120 Protein Surface

After the two interactions, the free energy of folding and net solvent accessible area was observed to get an abrupt increase and decrease (respectively). Thus, it apprehends the structure to become more unstable (Table 1) but interact firmly for the viral entry to occur efficiently.

Fascinatingly, the alteration in the vacuum electrostatic potential calculation from ±68.740 to ±64.562 to ±53.640 (as in Fig. 3), also infers the gp120 protein to become more unstable and be benefitted by the CD4 and CCR5 proteins individually for the viral entry via membrane fusion (Fig. 3).

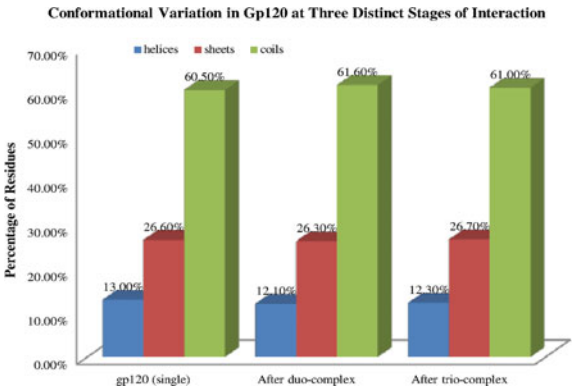

Fig. 2 Conformational switches in gp120 at three different stages of interaction

Table 1 Stability calculation of gp120 protein after duo and trio protein complex formation

Stability parameters	gp120 single	gp120 duo complex	gp120 trio complex
Free energy of folding	−421.49 kcal/mol	−271.36 kcal/mol	−235.45 kcal/mol
Net solvent accessible area	26258.74 $Å^2$	19819.41 $Å^2$	18366.99 $Å^2$

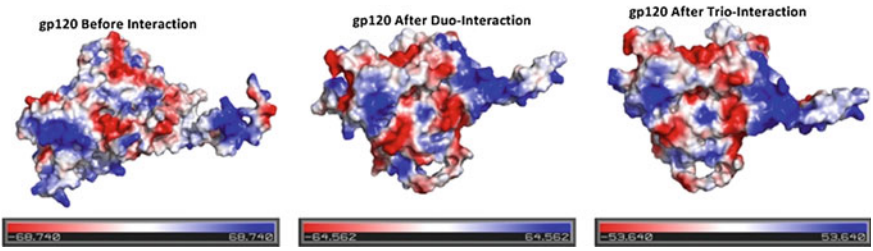

Fig. 3 Comparative view of the surface electrostatic potential change on the surfaces of gp120

3.4 Analysis in Docked Protein–Protein Interactions

The comparative analysis for interaction between essentially paramount gp120 and CD4 protein from the gp120-CD4 complex and gp120-CD4-CCR5 complex (Table 2 and Fig. 1) revealed that the interaction grew stronger in the trio complex.

Table 2 Ionic interactions among gp120 and CD4 after the duo and trio complex formation

	Position	Residue	Protein	Position	Residue	Protein
gp120-CD4	14	LYS	G	410	ASP	C
	130	LYS	G	410	ASP	C
	210	ASP	G	381	ARG	C
	289	ASP	G	357	LYS	C
gp120-CD4-CCR5	23	GLU	G	345	LYS	C
	289	ASP	G	357	LYS	C
	50	ASP	G	380	ARG	C
	210	ASP	G	381	ARG	C
	130	LYS	G	410	ASP	C
	14	LYS	G	410	ASP	C

Protein G and Protein C represents HIV gp120 protein and human CD4 protein respectively

3.5 Substantiation Through Statistical Significance

All the estimated outcomes were observed to statistically significant ($P < 0.5$). The paired T-test calculations revealed $P = 0.010245$, $P = 0.024431$ and $P = 0.031382$ for the free energy of folding, net solvent accessibility area, and conformational switching to coils, respectively.

4 Discussion

In the current scenario, the functional tertiary modeled 3D protein structure of HIV gp120 was efficiently built. Further, the gp120–CD4 complex was docked with CCR5. The statistically significant conformational switches after simulation disclosed that there was a shift from helix-to-coil (predominant) as well as from β-sheets-to-coils in gp120 protein. Furthermore, statistically significant decrease in electrostatic potential along with altered free energy of folding disclosed the instability of gp120 protein after the trio interaction. Four ionic strong interactions were observed in the duo complex (Table 2) which increased to net six, after the interaction of the duo protein complex with CCR5 (Table 2). From the duo complex, predominantly, Asp410 formed solely two ionic interactions from CD4 with Lys14 and Lys130 of gp120 protein. On the other hand, from the trio complex, leadingly, Asp410 formed uniquely two ionic interactions with Lys14 and Lys130 of gp120 protein. Additionally, from the trio complex two adjacent residues; Arg380 and Arg381 from CD4 interacted with Asp50 and Asp210 of gp120. The stronger interaction is further affirmed from the abrupt decrease in solvent accessible area for gp120 after trio complex formation. Altogether, it led to instability in gp120 protein with a stronger interaction after the participation of CCR5 to perform the viral entry into human host.

This residual-level in silico study to scrutinize the basis of the interaction and conformational switches presents to be one of the most crucial zones. This computational investigation therefore, also delves into the disclosure of the residual participation, binding demonstration, and analysis of the stability parameters in gp120 at different stages of interaction for the viral entry to cause deadly disease like AIDS. It prompts with an outlook for the future therapeutic research in a distinct mode.

5 Conclusion and Future Prospect

The cooperative participation of the residues from the two essential proteins (gp120 and CD4) for HIV entry and AIDS was the chief focus of this current study. Furthermore, the conformational switches in gp120 at three distinct stages and stability parameters unveiled the instability of gp120 for the viral entry in AIDS consequently. Therefore, the present study indulged into the molecular and computational basis of HIV entry. The structural and computational molecular contribution of gp120 and its interactions was essential to be elucidated for instigating the future clinical progress in new therapeutics for AIDS.

Acknowledgments Authors are thankful for the immense help by Dr. Angshuman Bagchi, Assistant Professor, Department of Biochemistry and Biophysics, University of Kalyani, Kalyani, Nadia, India. Moreover, our deepest regards would be for the Department of Biotechnology, National Institute of Technology Durgapur as well as the Department of Biotechnology, Bengal College of Engineering and Technology, Durgapur for their immense support.

References

1. Alain, Bernard: Leucocyte typing: human leucocyte differentiation antigens detected by monoclonal antibodies: specification, classification, nomenclature: [report on the first international references workshop sponsored by INSERM, WHO and IUIS]. Berlin: Springer. pp. 45–48 (1984) ISBN 0-387-12056-4.
2. Kwong, P.D., Wyatt, R., Robinson, J., Sweet, R.W., Sodroski, J., Hendrickson, W.A.: Structure of an HIV gp120 envelope glycoprotein in complex with the CD4 receptor and a neutralizing human antibody. Nature. 393 (6686), 648–59 (1998) doi:10.1038/31405. PMID9641677.
3. Dalgleish, A.G., Beverley, P.C., Clapham, P.R., Crawford, D.H., Greaves, M.F., Weiss, R.A.: The CD4 (T4) antigen is an essential component of the receptor for the AIDS retrovirus. Nature. 312 (5996), 763–7 (1984).
4. Altschul, S.F., et al.: Basic local alignment search tool. Journal of Molecular Biology. 25, 403–410 (1990).
5. Sali, A., Blundell, T.L.: Comparative protein modelling by satisfaction of spatial restraints. Journal of Molecular Biology. 234, 779–815 (1993).
6. DeLano, W.L.: The PyMOL Molecular Graphics System DeLano Scientific, San Carlos, CA, USA (2002) doi:10.1093/nar/gki408.

7. Fiser, A., Sali, A.: ModLoop: automated modeling of loops in protein structures. Bioinformatics. 19(18), 2500–2501 (2003).
8. Xu, D., Zhang, Y.: Improving the Physical Realism and Structural Accuracy of Protein Models by a Two-step Atomic-level Energy Minimization. Biophysical Journal. 101, 2525–2534 (2001) http://dx.doi.org/10.1016/j.bpj.2011.10.024.
9. Brooks, B.R., Bruccoleri, R.E., Olafson, B.D., States, D.J., Swaminathan, S., Karplus, M.: CHARMM: a program for macromolecular energy, minimization, and dynamics calculations. J.Comp. Chem. 4(2), 187–217 (1983).
10. Eisenberg, D., et al.: VERIFY3D: Assessment of protein models with three-dimensional profiles. Methods in Enzymology. 277, 396–404 (1997).
11. Colovos, C., Yeates, T.O.: Verification of protein structures: patterns of nonbonded atomic interactions. Protein Science. 2, 1511–1519 (1993).
12. Ramachandran, G.N., Sashisekharan, V.: Conformation of polypeptides and proteins. Advances in Protein Chemistry. 23, 283–438 (1968).
13. Huang, C.C., Tang, M., Zhang, M.Y., Majeed, S., Montabana, E., Stanfield, R.L., Dimitrov, D.S., Korber, B., Sodroski, J., Wilson, I.A., Wyatt, R., Kwong, P.D.: Structure of a V3-containing HIV-1 gp120 core. Science. 310, 1025–1028 (2005).
14. Tan, Q., Zhu, Y., Li, J., Chen, Z., Han, G.W., Kufareva, I., Li, T., Ma, L., Fenalti, G., Li, J., Zhang, W., Xie, X., Yang, H., Jiang, H., Cherezov, V., Liu, H., Stevens, R.C., Zhao, Q., Wu, B.: Structure of the CCR5 chemokine receptor-HIV entry inhibitor maraviroc complex. Science. 341, 1387–1390 (2013).
15. Comeau, S.R., et al.: ClusPro: An automated docking and discrimination method for the prediction of protein complexes. Bioinformatics. 20, 45–50 (2004).
16. Jian, Zhang, Yu, Liang, Yang, Zhang: Atomic-Level Protein Structure Refinement Using Fragment-Guided Molecular Dynamics Conformation Sampling. Structure. 19, 1784–1795 (2011).
17. Ramachandran, S., Kota, P., Ding, F., Dokholyan, N.V.: PROTEINS: Structure, Function and Bioinformatics. 79, 261—270 (2011).
18. Kabsch, W., Sander, C. Dictionary of protein secondary structure: pattern recognition of hydrogen-bonded and geometrical features. Biopolymes. 22(12), 2577–2637 (1983).
19. Paul, D., Thomas, Ken, A. Dill: Local and nonlocal interactions in globular proteins and mechanisms of alcohol denaturation. Protein Science. 2, 2050–2065 (1993).
20. Tartaglia, G. G., Pawar, A. P., Campioni, S., Dobson, C. M., Chiti, F., Vendruscolo, M.: Prediction of aggregation-prone regions in structured proteins. J. Mol. Biol. 380, 425–436 (2008).
21. Gerstein, M.: A Resolution-Sensitive Procedure for Comparing Protein Surfaces and its Application to the Comparison of Antigen-Combining Sites. Acta Cryst. A48, 271–276 (1992).
22. Tina, K.G, Bhadra, R., Srinivasan, N.: PIC: Protein Interactions Calculator. Nucleic Acids Research. 35, W473–W476 (2007).
23. Baldwin, R.L.: How Hofmeister ion interactions affect protein stability. Biophys. J. 71(4), 2056–2063 (1996).

A Support Vector Machine Approach for LTP Using Amino Acid Composition

N. Hemalatha and N.K. Narayanan

Abstract Identifying the functional characteristic in new annotated proteins is a challenging problem. With the existing sequence similarity search method like BLAST, scope is limited and accuracy is less. Rather than using sequence information alone, we have explored the usage of several composition, hybrid methods, and machine learning to improve the prediction of lipid-transfer proteins. In this paper, we have discussed an approach for genome wide prediction of LTP proteins in rice genome based on amino acid composition using support vector machine (SVM) algorithm. A predictive accuracy of 100 % was obtained for the module implemented with SVM using polynomial kernel. This approach was compared with an All-plant method comprising of six different plants (wheat, maize, barley, arabidopsis, tomato and soybean) which gave an accuracy of only 70 % for SVM.

Keywords SVM · LTP · All-Plant · Machine learning

1 Introduction

Among the various abiotic stresses that affect the rice production, high temperature is one of the main concerns. Development of high-temperature tolerant rice variety has become a major area for rice scientists to work upon [1].

Lipid-transfer proteins (LTP) are basic 9-kDa proteins. They are present in flowering plants in large amounts and can boost in vitro phospholipids transfer between membranes. They can also bind acyl chains. These properties help them to further participate in membrane biogenesis and also regulation of the intracellular fatty acid pools [2]. Studies by Wang and Liu have shown that the expression of

N. Hemalatha (✉)
AIMIT, St. Aloysius College, Mangalore 575022, India
e-mail: hemasree71@gmail.com

N.K. Narayanan
Department of Information Science Technology, Kannur University, Kannur 670567, India

D.K. Lobiyal et al. (eds.), *Proceedings of the International Conference on Signal, Networks, Computing, and Systems*, Lecture Notes in Electrical Engineering 396, DOI 10.1007/978-81-322-3589-7_2

LTPs can be induced by environmental stresses like extreme temperatures, osmotic pressures, and drought [3, 4].

Rice being one of the major food crops is a subject of research worldwide. Because of the advances in the sequencing techniques in the past few years, whole genomic sequences of rice which includes subspecies *japonica* and *indica* is publicly available. Manual annotation of these sequences is not feasible because data is large. This paper discusses a novel approach of prediction for high-temperature resistant protein LTP using amino acid composition features and hybrid information of proteins. The problem undertaken in this paper is the identification of functional characteristic of newly annotated proteins. Many varieties of *indica*, the subspecies of *Oryza*, are yet to be sequenced and has to be annotated which manually is impossible. Hence, development of prediction approaches will definitely help the biologists for future annotations. The machine-learning approach SVM with three different kernels and nine feature extraction techniques was used. An All-plant model with six different plants (wheat, maize, barley, arabidopsis, tomato, and soybean) using amino acid composition was also created and compared with the new developed method to prove the species-specific property of the classifier.

The paper is organized as follows: Sect. 2 present the data sets to be used in the experiments and steps to extract features from the sequences involved. This section also covers the feature extraction methods applied on the data sets and classification model building. Section 3 presents the performance measures to evaluate SVM with different kernel and feature methods. Comparison of newly developed model in SVM with existing sequence search algorithm PSI-BLAST is discussed in Sect. 4. Section 5 discusses the experimental results over the testing dataset and species-specific property of the developed model. Finally, Sect. 6 concludes with recommendations for future research.

2 Materials and Methods

2.1 Materials

A total of 105 LTPs and non LTP's belonging to both *japonica* and *indica* were collected from Uniprot Knowledgebase (UniProt KB) and National Centre for Biotechnology Information (NCBI). To make the dataset completely nonredundant, CD-HIT software was applied for removing sequences highly similar to other sequences with a threshold of 90 % [5]. Majority of data collected were computationally predicted, and hence to confirm the sequences to be of LTP family Prosite and PFam databases were used. Finally, 105 LTPs were retained for positive dataset and a set of negative samples was constructed from 105 non LTPs from *Oryza sativa*. To check the species-specific property of the approach, another set of negative samples of 105 non LTPs from other plants were taken.

2.2 Methods

Binary SVM Support Vector Machine (SVM) is a classification algorithm based on statistical learning theory. SVM can be applied to pattern classification by mapping the input vectors to a feature space which is of higher dimension [6]. A binary SVM is used in this work to classify sequences into LTP's and non LTP's. Let $s = s_1, s_2 \ldots s_n$ denote a protein sequence of length n where $s_i \in \{A, C, D, E, F, G, H, I, K, L, M, N, P, Q, R, S, T, V, W, Y\}$ and dimension $R = R_1, R_2 \ldots R_9$. An ideal mapping for classifying sequences into LTP's and non LTP's from R^9 space into $-1, +1$, where +1 corresponds to LTP class and -1 to non LTP classes, respectively [7].

Let $(r_j, q_j); j = 1, 2 \ldots N$ denote the set of N training sets, where q_j denotes the either class LTP or non LTP, for the input feature vector r_j. Kernel functions are introduced for nonlinearly separable problems as training sets on normalization contain random values and which makes optimization problem more simpler. SVM first maps the input feature vector to a higher dimensional space H with a kernel function k and then is combined linearly with a weight vector w to obtain the output. The binary SVM is trained to classify whether the input protein sequence belongs to the LTP or non LTP class.

SVM develops a discriminant function for classifying LTP by solving the following optimization problem:

$$\max \sum_{i=1}^{N} \alpha_i - \frac{1}{2} \sum_{i=1}^{N} \sum_{i=1}^{N} y_i y_j k(r_i, r_j) \alpha_i \alpha_j$$

subject to

$$0 \leq \alpha_i, \text{for } i = 1, 2, \ldots n;$$

$$\sum_{i=1}^{N} y_i \alpha_i = 0$$

The kernel function $k(r_i, r_j) = \phi(r_j)^T \phi(r_i)$ and the weight vector $w = \sum_{i=1}^{N} \alpha_i q_i \phi(r_i)$, where ϕ represents the mapping function to a higher dimension and α represents Lagrange multiplier. The optimization gives the values for the parameters α_j and the resulting discriminant function f is given by

$$f(r_i) = \sum_{j=1}^{N} \alpha_j q_j k(r_i, r_j) + b = w^T \phi(r_i) + b$$

where bias b is chosen so that $q_j f(r_j) = 1$ for all j with $0 < \alpha_j < \gamma$. The class corresponding to input pattern r_i is LTP if $f(r_i) \geq 0$ or non LTP if $f(r_i) < 0$.

3 Features

For converting the protein characteristics to feature vectors, effective mathematical expressions should be formulated. This is necessary for applying machine-learning technique that is relevant to the prediction tasks. In this paper, we have used five different composition methods and four hybrid methods which are discussed in the following section.

3.1 Composition-Based Features

Amino acid composition This composition provides a 20-dimensional feature vector. This is an important attribute since this feature denotes a fundamental structural aspect of a protein encapsulating the information regarding the occurrence of each amino acid in the particular protein sequence. The fraction of each amino acid a_i in the given sequence is given by the formula:

$$P(a_i) = \frac{Na_i}{\sum_{i=1}^{20} Na_i} \tag{1}$$

where Na_i represents the total number of a particular amino acid a_i present in the sequence and $\sum_{i=1}^{20} Na_i$ represents the total number of amino acids present in the given protein sequence.

Dipeptide composition This composition provides a 400 (20×20) dimensional vector. This feature encapsulates the local information of each protein sequence utilizing the sequence order effects. The fraction of each dipeptide $a_i a_j$ in the given sequence is given by the formula:

$$P(a_i a_j) = \frac{Na_i a_j}{\sum_{i=1}^{20} \sum_{j=1}^{20} Na_i a_j} \tag{2}$$

where $Na_i a_j$ gives the total number of $a_i a_j$ dipeptides in the sequence and $\sum_{i=1}^{20} \sum_{j=1}^{20} Na_i a_j$ represents the total number of all dipeptides present in the given protein sequence.

Tripeptide composition This composition provides a 8000 (20×400) dimensional vector. This composition gives the properties of the neighboring amino acids The fraction of each tripeptide $a_i a_j a_k$ in the given sequence is given by the formula:

$$P(a_i a_j a_k) = \frac{Na_i a_j a_k}{\sum_{i=1}^{20} \sum_{j=1}^{20} \sum_{k=1}^{20} Na_i a_j a_k} \tag{3}$$

where $Na_i a_j a_k$ gives the total number of $a_i a_j a_k$ and $\sum_{i=1}^{20} \sum_{j=1}^{20} \sum_{k=1}^{20} Na_i a_j a_k$ represents the total number of all tripeptides present in the given protein sequence.

3.2 Four-Parts Composition

This composition is based on the assumption that different parts of a sequence can provide valuable information. In this composition, query sequence is divided into four fragments of equal length and amino acid composition from each fragments are calculated separately using Eq. (1). Each fragment of 20 dimensions gets concatenated to form 80 dimensional feature vector.

3.3 Three Parts Composition

This composition is also otherwise called as terminal-based N-center-C composition. This determines the signal peptides at N or C terminal region of different proteins. To identify these signal peptides, amino acid composition has to be calculated separately from the terminals N and C and remaining from the center region. For each region a 20-dimensional vector will be created using Eq. (1), so for the three regions the combined feature will have a dimension vector of 60.

3.4 Hybrid-Based Features

Hybrid1 approach This approach combines amino acid and dipeptide composition features of a protein sequence and is calculated using Eqs. (1) and (2), respectively. Because amino acid and dipeptide compositions are combined, feature vector will have a dimension of 420, i.e., 20 for amino acid and 400 for dipeptide.

Hybrid2 approach This approach combines amino acid and tripeptide composition features of a protein sequence using Eqs. (1) and (3), respectively. This approach has a feature dimension of 8020, i.e., 20 for amino acid and 8000 for tripeptide.

Hybrid3 approach In this approach, amino acid was combined with four part composition which was calculated using Eq. (1) and has a dimension of 100.

Hybrid4 approach In this approach, we combined amino acid composition calculated using Eq. (1), dipeptide calculated using Eq. (2) and three parts calculated using Eq. (1) to have an input feature dimension of 480 (20 for amino acid, 400 for dipeptide and 60 for three parts composition).

4 Performance Measure

Some standard evaluation methods are used to measure the performance of the algorithm. The two methods which have been used for this purpose are cross validation and independent data test. Cross-validation techniques can be used to test the predictive performance of models as well as to help prevent a model being over fitted. This technique can be of various folds like 10-fold, 20-fold, etc. In the *k*th fold cross validation, the data set is divided into k subsets and each subsets contains equal number of proteins. The k subsets are then grouped into $(k-1)$ training set and remaining one as testing set. This procedure is repeated k times so that every subset is at least used once for testing. In the independent dataset test, testing dataset is totally independent of the training set. Selection of data for training and testing are independent of each other.

The standard evaluation metric used are sensitivity (Sn), specificity (Sp), precision (Pr), accuracy (Acc), F-measure (F), and Mathew correlation coefficient (MCC). Actual prediction of positive and negative data of LTP is measured by sensitivity and specificity respectively. Precision defines the proportion of the predicted positive cases of correct LTP. Accuracy measures the proportion of the total number of correct predictions of LTP. Recall calculates the correctly identified proportion of positive cases of LTP. MCC is used especially when number of positive and negative data differs too much from each other. The value of MCC ranges between −1 and 1 and a positive value indicates a better prediction performance. TP, FP, TN, FN are the numbers of true positives, false positives, true negatives, and false negatives, respectively. Following are the equations used for their calculations:

$$\text{Sensitivity} = \left(\frac{\text{TP}}{\text{TP}+\text{FN}}\right) \times 100 \tag{4}$$

$$\text{Specificity} = \left(\frac{\text{TN}}{\text{FP}+\text{TN}}\right) \times 100 \tag{5}$$

$$\text{F-measure} = \left(\frac{2 \times \text{Pr} \times \text{Sn}}{\text{Pr}+\text{Sn}}\right) \times 100 \tag{6}$$

$$\text{Accuracy} = \left(\frac{\text{TP}+\text{TN}}{\text{TP}+\text{TN}+\text{FP}+\text{FN}}\right) \times 100 \tag{7}$$

$$\text{MCC} = \frac{(\text{TP} \times \text{TN}) - (\text{FP} \times \text{FN})}{\sqrt{(\text{TP}+\text{FP})(\text{TP}+\text{FN})(\text{TN}+\text{FP})(\text{TN}+\text{FN})}} \tag{8}$$

5 Similarity Search

In sequence similarity searching, a query sequence is searched against sequence databases using alignment which can be statistically assessed. This information can be used to infer homology and transfer information to the query sequence about its match with the database. This similarity between sequences can give clues to similarities in molecular structure and function as well to discover evolutionary relationships between the sequences.

PSI-BLAST tool is widely used in bioinformatics for sequence similarity search. This tool was used for sequence similarity search to find the similarity of the given sequences with other related sequences. This tool compared a protein sequence with a created database [8]. In this paper this tool is used for a comparative study of search using PSI-BLAST to the one presented in this paper using the classifier discussed in Sect. 2.

6 Experiments and Results

Binary SVM was implemented using SVM^{light} [9] which is known to be a fast optimization algorithm. We use a tenfold cross validation and independent data test with different types of kernels to evaluate the accuracy in the LTP classification. The kernel type and parameters were set based on best accuracy.

6.1 Statistical Tests of SVM Classifiers

Applying independent data test in SVM with three different kernels for a total of nine different compositions, an accuracy of 100 % was obtained for amino acid, dipep, and tripep compositions with linear kernel (Table 1). Applying 10-fold cross-validation test in SVM, 98 % accuracy was obtained for four-parts and hybrid1 composition with linear kernel (Table 1).

Amino acid involves less number of features and less complexity, hence we considered amino acid as the best composition. Also linear kernel is the most simplest among the three kernels in SVM. Hence for this classifier, we have chosen amino acid composition with linear kernel which has only 20 dimension obtained for independent test. Cross-validation result was not considered because it could obtain only 98 % for four-parts and hybrid1 composition whose feature size is 80 and 420 which is much higher than amino acid composition. The performance comparison of SVM is depicted in the Fig. 1.

Table 1 Validation of Independent and cross-validation test results with SVM

Composition	Independent test			Cross-validation test		
	Acc	F	MCC	Acc	F	MCC
Aminoacid	100	100	1	90	94	0.85
Dipeptide	100	100	1	96	98	0.92
Tripep	100	100	1	53	53	0
3-parts	80	88	0.61	89	11	0.73
4-parts	95	100	0.9	98	97	0.95
Hybrid1	50	50	0	98	97	0.95
Hybrid2	50	50	0	96	0	0.91
Hybrid3	95	100	0.9	92	92	0.81
Hybrid4	85	100	0.73	52	19	0.11

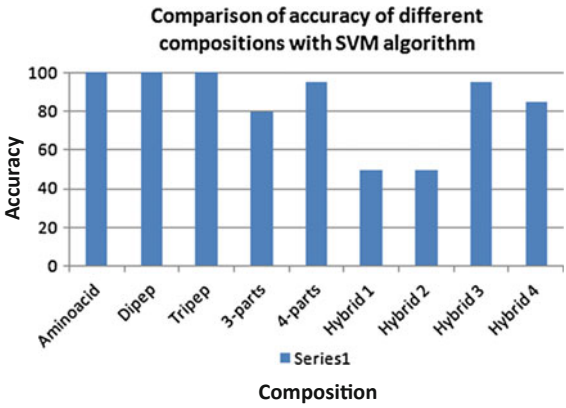

Fig. 1 Performance comparison of accuracy of 9 different compositions

6.2 *Similarity Search*

PSI-BLAST, the sequence similarity search tool, was compared to the newly developed approach. For this, 10-fold cross validation was conducted for similarity search tool which generated a very less accuracy of 67.6 % Table 2. This result shows that similarity search is not an efficient tool for comparison compared to feature based approach.

6.3 *Species-Specific Classifier*

To find what happens to the classifier when non-rice LTP patterns are included in the training set, two tests were conducted. In the first, an All-plant method consisting of six plants namely arabidopsis, wheat, maize, barley, tomato, and soybean

Table 2 Prediction result of LTP with similarity search (tenfold cross validation used)

Test	No. of Test sets	No. of correctly predicted	Average
1	19	12	63
2	19	13	68
3	19	14	73.6
4	19	12	63
5	19	13	68
6	19	14	73.6
7	19	13	68
8	19	14	73.6
9	19	12	63
10	8	5	62.5
			67.6

was developed and compared to the rice-specific classifier. In the second test, the newly developed method was tested with the above six plants.

Comparison with All-plant method In this test, an All-plant method was developed in SVM using all the three kernels. For creating this, six plants were taken namely arabidopsis (*Arabidopsis thaliana*), wheat (*Triticum aestivum*), maize (*Zea mays*), barley (*Hordeum vulgare*), tomato (*Solanum lycopersicum*) and soybean (*Glycine max*), including a total of 174 data in the training set. In the case of newly developed All-plant model, we have used the simple amino acid approach, which was having an accuracy of 100 % for rice-specific classifier.

On comparison of newly created rice-specific classifier with corresponding All-plant module based on the rice independent training set, the former showed an increase of 50 % accuracy with respect to linear kernel. From Table 3, it can be seen that All-plant method is having 70 % accuracy for both polynomial and RBF kernel and only 50 % for linear kernel. These results clearly indicate the advantage of species-specific classifier. Methodology for creating both the model were identical, i.e., have used the amino acid composition approach. This strongly suggests that species-specific prediction systems are much better compared to general ones.

Performance on other Plants In the second validation, we checked the performance of newly developed method on six plants namely arabidopsis, wheat, maize, barley, soybean, and tomato. The results obtained are tabulated in Table 4. The result of SVM model with RBF kernel revealed accuracy of 96 % for four

Table 3 Comparison of All-plant model with new model

Method	Algorithm	Sn	Sp	Acc	MCC
All-plant	Linear	100	0	50	0.00
	Polynomial	40	100	70	0.50
	RBF	40	100	70	0.50
New model SVM	Linear	100	100	100	1.00
	Polynomial	100	100	100	1.00
	RBF	100	100	100	1.00

Table 4 Performance of SVM model on six plants

Plants	Linear	Poly	RBF
	Acc	Acc	Acc
Arabidopsis	60	64	96
Maize	50	92	92
Wheat	60	96	96
Barley	60	64	95
Tomato	60	88	96
Soyabean	60	96	95.8

plants namely arabidopsis, tomato, soybean, and wheat whereas for other two remaining plants, i.e., barley and maize, the prediction accuracy was equal or below 95 %. However, when the same model was run only on rice proteins, the new model achieved 100 % accuracy during independent data test. This difference between the performances of both the method with rice and other plants indicate that there might be some species-specific feature in rice dependent method.

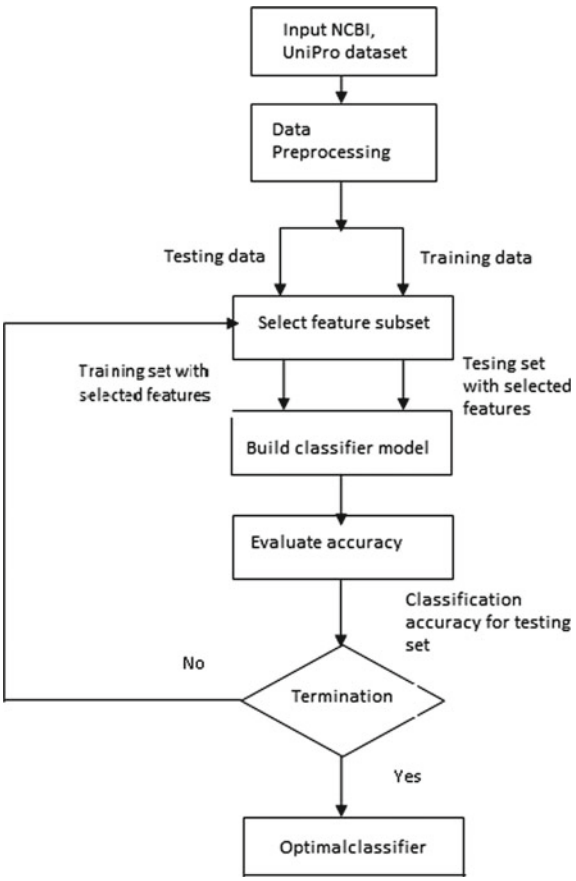

Fig. 2 Architecture of new model using SVM

6.4 Description of Architecture

The overall architecture of the methodology used for developing new method using SVM is depicted in the Fig. 2.

7 Conclusions

The use of computational tools and web databases has promoted the identification of various functional proteins. The different computational methods currently available are general ones and can be used for functional annotation of a given protein by determining their prediction accuracy. The sequencing of varieties of *oryza sativa indica* subspecies of *oryza sativa*, commonly used in Asian countries is yet to be completed and these newly sequenced proteins will have to be annotated. Different stress prediction tool for rice according to our knowledge is unavailable and the general methods are available but less accurate. Here, we have proposed a highly accurate prediction algorithm using SVM for identification of LTPs in *Oryza sativa*. Also in this work, we have proved the advantage of species-specific classifier over the general ones. This further substantiates that the new method using SVM will contribute significantly to the various annotation projects in rice. In our future work on LTPs, we plan to further elaborate the database of LTPs in rice and also study the effect of various other proteins with respect to this abiotic stress.

References

1. Krishnan, P., Ramakrishnan, B., Reddy, K. R., Reddy, V. R.: Chapter three-High-Temperature Effects on Rice Growth, Yield, and Grain Quality. Adv. Agron. 111, 87–206 (2011).
2. Kader, J. C.: Lipid-transfer proteins in plants. Annu. Rev. Plant. Biol. 47(1),627–654 (1996).
3. Wang, N. J., Lee, C. C., Cheng, C. S., Lo, W. C., Yang, Y. F., Chen, M. N., Lyu, P. C.: Construction and analysis of a plant non-specific lipid transfer protein database (nsLTPDB). BMC genomics. 13(Suppl 1) (2012).
4. Liu, Qiang, Yong Zhang, Shouyi Chen.: Plant protein kinase genes induced by drought, high salt and cold stresses. Chinese Sci Bull. 45(13), 1153–1157 (2000).
5. Li, W., Godzik, A.: Cd-hit: a fast program for clustering and comparing large sets of protein or nucleotide sequences. Bioinformatics. 22(13,1658–1659 (2006).
6. Vapnik, V.: The nature of statistical learning theory. Springer Science & Business Media. (2000).
7. Ma, J., Nguyen, M. N., Rajapakse, J. C.: Gene classification using codon usage and support vector machines. Computational Biology and Bioinformatics, IEEE/ACM Transactions on, 6(1),134–143 (2009).
8. Altschul, S. F., Madden, T. L., Schffer, A. A., Zhang, J., Zhang, Z., Miller, W., Lipman, D. J.: Gapped BLAST and PSI-BLAST: a new generation of protein database search programs. Nucleic acids res. 25(17), 3389–3402 (1997).
9. Schlkopf, B., Burges, C. J. Advances in kernel methods: support vector learning. MIT press (1999).

Load Balancing Challenges in Cloud Computing: A Survey

Rafiqul Zaman Khan and Mohammad Oqail Ahmad

Abstract Cloud computing has broadly been put into practice by business sector, however, there are several actual issues including load balancing, virtual machine migration, automated service provisioning, algorithm complexity, etc., that have not been completely resolved. Each of these are the main challenges of load balancing, that is likely to distribute the unwanted dynamic local workload smoothly to all the nodes in the entire cloud to gain a remarkable consumer fulfillment and resource utilizing ratio. It also makes sure that every computing resource is distributed proficiently and reasonably. This paper describes a thought of cloud computing along research challenges in load balancing.

Keywords Cloud computing · Load balancing · Challenges of load balancing · Goals of load balancing

1 Introduction

Cloud computing has grown to be incredibly favorite during the last couple of years. Due to the part of its service, it provides a flexible to retrieve data as well as an easy way to keep files, incredibly for making huge data sets and files accessible for the dispersing number of consumers to the entire world [1, 2]. Managing these types of large data sets call for several approaches to enhance and simplify operations and provide perfect levels of efficiency for the consumers [1].

Load balancing is a technique that distributes the workload all through various nodes in the presented workspace such that it makes sure no more nodes in the system is overloaded or idle for each moment of time (refer to Fig. 1). An efficient load balancing algorithm would clarify that each and every single node in the

R.Z. Khan · M.O. Ahmad (✉)
Department of Computer Science, Aligarh Muslim University, Aligarh, India
e-mail: oqail.jmu@gmail.com

R.Z. Khan
e-mail: rzk32@yahoo.co.in

D.K. Lobiyal et al. (eds.), *Proceedings of the International Conference on Signal, Networks, Computing, and Systems*, Lecture Notes in Electrical Engineering 396, DOI 10.1007/978-81-322-3589-7_3

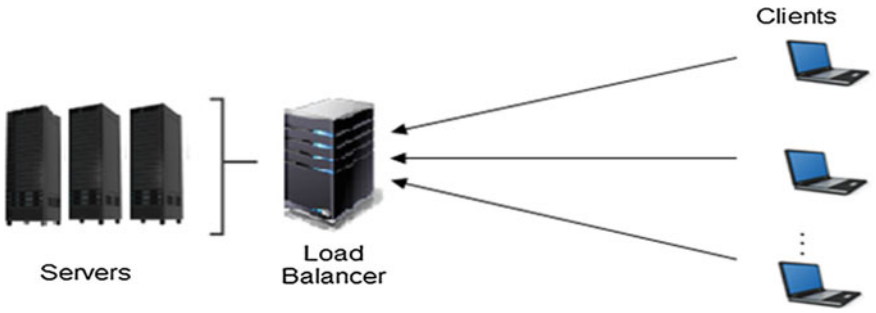

Fig. 1 Diagram for load balancing

system may have more or less identical amount of work. The accountability of the load balancing algorithm is that is really to manage the assignments which are put ahead to the cloud area for the unused services. Therefore, the entire accessible reactions time is enhanced and in addition it gives proficient resource use. Balancing the workload continue to be one of the significant worries in cloud computing since we are unable to figure out the quantity of demands that are released inside of every second in a cloud environment. The uncertainty is credited to the constantly varying tendency of the cloud. The fundamental consideration of load balancing in the cloud platform is in distributing and appointing the load dynamically throughout the nodes with a specific end goal to satisfy the consumer necessities and to give optimal resource use only by arranging the entire obtainable load to diverse nodes [3].

2 Cloud Load Balancing

Load balancing is the fact of dispersing the load all through several resources in every system. In this manner, load should to be distributed across the resources in a cloud-based construction modeling, so that each resource does around the identical quantity of task at every aspect of time. Elementary require is to deliver you some approaches to stabilize demands to give the choice of the application quicker [4]. Basically, load balancing method that makes each processor similarly busy as well as to complete the works around at the same time [5].

A diagrammatic representation of cloud load balancing shown in Fig. 2 and may be summarized as follows [6]:

- The consumer connects with the Internet and demands a service (e.g., a site).
- DNS puts the consumer with an exact open location which is linked to the total uptime technologies open for any activate the network.
- The consumer is linked to the nearby, native total uptime technologies node.

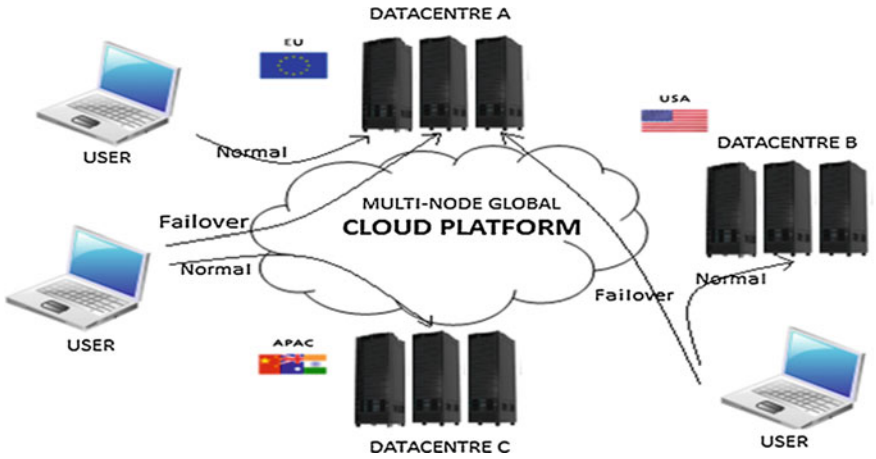

Fig. 2 Diagram for cloud load balancing

- Customer specified policy that allows the total uptime technology node to connect and decides which of the consumer's datacenter to send the user to.
- Users containing the desired application content they are directed to the customer's datacenter.
- Material is supplied to the consumer alternatively using direct server return, or through the nearby total uptime technologies cloud node. If a membership to progression is dynamic, material is optimized everywhere throughout the Internet back to the client.

2.1 Goals of Load Balancing

Goals of load balancing as discussed by the authors of [5, 7] include:

- Stability of the system remains on track.
- To have the capability to alter it as per any modifications or extend in system setup.
- Increase adoptability of the system to adjust to the modifications.
- Promote a fault tolerant system in case of performance, stamina under the partial failure of the system.
- To achieve tremendous improvement in performance.

2.2 Demand of Load Balancing

Load balancing is a technique such that it delegates to accomplish the task equally throughout every attainable node that is shown in the system. High-user fulfillment definitely is the aspect around it. Due to large number of client's and also their needs usually are growing time to time, the clouds will need to supply the products to the visitors with their personal at most fulfillment [3].

A desirable load balancing process guides to utilize of those available resources most positively, thus verifying no more node is over loaded or under loaded. Load balancing facilitates scalability, prevents difficulties as well as also minimizes the time period consumed to actually give the responds. A large number of load balancing algorithm has been developed during order to plan the load among most of the machines. But still so far at this time there is no this type of best load balancing algorithm has been introduced that will set aside the load smoothly all over the system [3].

2.3 Types of Load Balancing

Load balancing is classified as the current state of the system, like static and dynamic load balancing.

2.3.1 Static

Static load balancing usually call for previous knowledge related to the software and resources of the system. The choice to move the workload exactly should not rely on the present status of the system. Static load balancing relates to load balancing that distributes the workload derived exactly relating to a constant set of policies associated with qualities of the workload. Static load balancing are not defensive; thus every single system has at least one assignment allotted for itself [7]. Static algorithms usually do not take into consideration dynamic modifications at run-time [5].

Some static load balancing algorithms are Min–Min, Min–Max, and Round Robin algorithm.

2.3.2 Dynamic

In the course of the static load balancing, a lot more detail with regard to the system and tasks must be recognized prior to the execution. Each of these resources cannot be obtained in prior. A detailed survey of the system status as well as the tasks

Table 1 Static versus dynamic

Parameters	Static	Dynamic
Nature	Compile time	Run time
Performance	Less	More
Flexibility	More	Less
Implementation	Less	Difficult
Resource Utilization	Less	More
Communication Overhead	Less	More
Stability	More	Less
Adaptability	Less	More
Response Time	Easy	More
Reliability	Less	More
Processor thrashing	No	Considerable
Predictability	Easy	Difficult
Complexity	Less	More
Cost	Less	More

pretty boring technique in advance. Due to this fact, dynamic load balancing originated into the real world [5].

A dynamic load balancing does not take into consider the prior state of the system and no past understanding is required, i.e., it relies around the present status of the machine. It permits usual method to be relocated from heavily loaded machine to a lightly loaded machine dynamically to obtain rapid execution [5, 7]. In this conditions, the case communication over minds arises and turns into a lot more if a variety of processors enhance.

Some dynamic load balancing are active clustering, honey-bee foraging, biased random sampling, joint-idle queue, etc.

Various comparisons between static load balancing and dynamic load balancing are listed in Table 1 [8, 9].

2.4 Need of Load Balancing

Most people can equalize the work of a system by dynamically relocating the workload nearby to the system to faraway nodes or systems that are less widely used. Doing this enhances the client fulfillment, maximizing resource utilization, reducing reaction time, decreasing the set of amount of task refusals, as well as boosting the efficiency stability of the system. Additionally, green computing in the clouds can be achieved using load balancing. Some aspects with regards to it are [6]:

A. *Reduced Energy Absorption* Load balancing can easily cut down the capacity of power utilization by staying away from overheating of machines due to extreme workload.

B. *Minimizing Carbon Discharge* Energy absorption and carbon discharge are the two sections of the same stage. Both are specifically relative to one another. Minimizing energy utilization using load balancing which will automatically cut down carbon discharge and for that reason develop Green Computing.

3 Challenges for Load Balancing in Cloud Computing

In spite of the certainty, cloud computing has been broadly put into practice. Research in cloud computing is yet in its beginning phases, and many technical challenges continue to be uncertain in the scientific society and they are [1, 7].

3.1 Automated Service Provisioning

The core element related to cloud computing is flexibility; services may be assigned or delivered automatically. How then we would be able to utilize or discharge the resources of the cloud, just retaining the identical efficiency as traditional systems and utilizing ideal resources.

3.2 Spatial Distribution of the Cloud Nodes

A number of algorithms are formulated to be beneficial actually for an intranet in which communication waiting time are minor. Nonetheless, it is a test to layout a load balancing algorithm which can easily function with regards to divided nodes. This is because alternative aspects will have to be accepted into consideration like the network links speed amont most of the nodes, the length between the consumer and the task filtering nodes, and the ranges among the nodes concerned with delivering the service.

3.3 Virtual Machines Migration

Using virtualization, the whole machine are able to be seen like a file or group of files, to empty a physical machine, over loaded, it is achievable to swap a virtual machine inside physical machines. The most important goal is to disperse the load in a data center or group of data centers.

3.4 Algorithm Complexity

Load balancing algorithms are targeted to be much easier in conditions of application and implementation. The better execution barrier could possibly manage to much more challenging task that may reason few risky performance problems. Additionally, if the algorithms will need more detail and better connection for inspecting and to manage, waiting times may provokes additional issues and the affectivity will fall.

3.5 Energy Management

The advantages of energy management that proposes the usage of the cloud is the economy of scale. Power saving is the most important aspect that permits a worldwide economy where the pool of worldwide resources is going to be supported by minimal providers rather that every one possesses its private services.

4 Conclusion

In this paper, we have surveyed cloud load balancing, discussed it types and comparisons of static and dynamic load balancing, demand as well as its goals. We also take into consider some technical challenges continue to be unsolved in the scientific society, particularly challenges of load balancing. We desire this work may provide a much better guide to the critical issues that need to be addressed, while the design of load balancing algorithm in cloud computing.

References

1. Klaithem Al Nuaimi, Nader Mohamed, Mariam Al Nuaimi and Jameela Al-Jaroodi, "A Survey of Load Balancing in Cloud Computing: Challenges and Algorithms ", 2012 IEEE Second Symposium on Network Cloud Computing and Applications.
2. Mohammad Oqail Ahmad, Rafiqul Zaman Khan, "The Cloud Computing: A Systematic Review", International Journal of Innovative Research in Computer and Communication Engineering (IJIRCCE), Vol. 3, Issue 5, May 2015.
3. Foram F Kherani, Prof. Jignesh Vania, "Load Balancing in cloud computing", International Journal of Engineering Development and Research, Volume 2, Issue 1 | ISSN: 2321-9939.
4. Soumya Ray and Ajanta De Sarkar, "Execution Analysis Of Load Balancing Algorithms In Cloud Computing Environment", International Journal on Cloud Computing: Services and Architecture (IJCCSA), Vol. 2, No. 5, October 2012.

5. Ali M. Alakeel, “A Guide to Dynamic Load Balancing in Distributed Computer Systems”, IJCSNS International Journal of Computer Science and Network Security, VOL. 10 No. 6, June 2010.
6. http://totaluptime.com/solutions/cloud-load-balancing/cloud-load-balancing-101/.
7. Shoja, H.; Nahid, H.; Azizi, R., “A comparative survey on load balancing algorithms in cloud computing,” Computing, Communication and Networking Technologies (ICCCNT), 2014 International Conference on, vol., no., pp. 1, 5, 11–13 July 2014.
8. Firoj Ali and Rafiqul Zaman Khan, “The Study On Load Balancing Strategies In Distributed Computing System”, International Journal of Computer Science & Engineering Survey (IJCSES) Vol. 3, No. 2, April 2012.
9. GeethuGopinath P P, Shriram K Vasudevan, “An in-depth analysis and study of Load balancing techniques in the cloud computing environment.”, Procedia Computer Science 50 (2015) 427–432.

Physiological Modeling of Retinal Layers for Detecting the Level of Perception of People with Night Blindness

T. Rajalakshmi and Shanthi Prince

Abstract Human visual system (HVS) model concentrates on the evaluations of image quality as well as with the performance of the human observer in the process of visual recognition. Mathematical modeling of retina plays a vital role to produce better visual perception. The retina is responsible for detecting incoming light signal, and also proceeds to achieve with complex signal transformations. The main aim of this work is to develop an HVS (human visual system) model for detecting the perceptual level of people with night blindness. Mathematical modeling of photoreceptor, outer-plexiform and inner- plexiform layers is performed in this study considering the properties of compression and spatial properties in the processing of visual information. People with normal vision can visualize image clearly even in moonlight. The situation is not the same for a people with night blindness, they are unable to visualize image in dim light. In this work, it has been proved through physiological model that the perceptual level of people with night blindness is approximately same in day light vision where as it very poor in the case of people with night blindness.

Keywords Human visual system (HVS) · Spatial properties · Compression · Night blindness · Perception

T. Rajalakshmi (✉)
Department of Biomedical Engineering, SRM University,
Kattankulathur 603203, India
e-mail: rajalaksmi.t@ktr.srmuniv.ac.in

S. Prince
Department of ECE, SRM University, Kattankulathur 603203, India
e-mail: shanthi.p@ktr.srmuniv.ac.in

D.K. Lobiyal et al. (eds.), *Proceedings of the International Conference on Signal, Networks, Computing, and Systems*, Lecture Notes in Electrical Engineering 396, DOI 10.1007/978-81-322-3589-7_4

1 Introduction

Human retina is considered to be one of the most essential parts of the visual system. In view of retinal processing, optimal balance is required on data accuracy, processing on real time data, energy and structural complexity. The structure of retinal layer in HVS model is shown in Fig. 1. The first and foremost layer of retina is the photoreceptor layer which is responsible in acquiring information of the data visually and further compressing the luminance of the image using logarithmic compression technique. Photoreceptor layer includes two types of receptors namely the cones and the rods. Cone is responsible for photopic vision and is more sensitive to color. Rods are mainly achromatic. Central region of the retina are occupied by cones. Cones are mainly used in day light because of their low light illumination. The response of the cone gives rise to photopic vision. Visual response produced by rod at low level of illumination gives rise to scotopic vision. Photoreceptor layer receives the incoming light information and enhances the contrast value of an image. This contrast-enhanced image is then passed to the successive layers of retina.

Signals from the photoreceptor layer are transferred to the outer-plexiform layer which includes two types of cells namely, bipolar and horizontal cell layer. The main function of the outer-plexiform layer is to enhance the contour value of the incoming image. Bipolar cells are joined to the ganglion cells in the 'Inner-plexiform Layer' (IPL). Hence, through inner-plexiform layer finer details of the image are extracted. The main aim of this study is to develop HVS model for detecting the level of perception of people with night blindness. Night blindness is basically the inability to view scenes well at night or in poor light conditions. People suffering from night blindness will not see images clearly in night but they also take more time to adjust their eye from bright area to dim light. The role of vitamin A in vision under variable levels of light was enhanced to a greater level [1, 2]. The physiological mechanisms that give rise to night blindness are mainly due to genetic abnormalities of retina [3, 4]. Stationary night blindness is defined by the nonability of a person to see in the dark, during day time the vision is not affected [5, 6]. Steady illumination automatically leads to compression of the response amplitude [7]. There is no major work reported on compression properties, spatial and temporal properties of retina to detect the perceptual level of people with night blindness. In this work, the level of

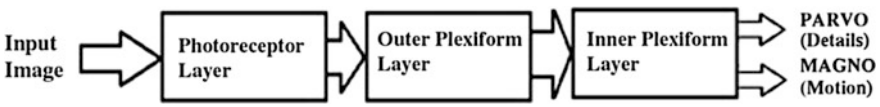

Fig. 1 Retinal layer in HVS model

perception of night blindness by physiological modeling of retinal functionalities including its luminance, compression properties, and spatial and temporal frequencies for visual processing has been evaluated.

2 Mathematical Modeling of Photoreceptor Layer

Modified version of Michaelis–Menten relation [8, 9] which include a local adaption effect and to have a normalized value of luminance ranging from of [0, $V_{\max}$] is considered for the study:

$$A(p) = \frac{C(p)}{C(p) + Co(p)} \cdot V_{\max} + Co(p). \tag{1}$$

$$Co(p) = S_0 \cdot L(p) + V_{\max}(1 - So). \tag{2}$$

In Eq. (1), the adjusted luminance value of the original image $A(p)$ of the photoreceptor p depends mainly on the current luminance value of the image $C(p)$ and also on the compression parameter value $Co(p)$, which is further linearly linked to the luminance value $L(p)$ of the neighboring photoreceptor p as shown in Eq. (2), [10]. In this work, luminance value $L(p)$ is computed by calculating spatial and temporal frequencies as shown in Eq. (5)

$$F_{\mathrm{h}}(f_{\mathrm{s}}, f_{\mathrm{t}}) = 1/[1 + \beta_{\mathrm{h}} + 2\alpha_{\mathrm{h}}(1 - \cos(2\pi f_{\mathrm{s}})) + j2\pi\tau_{\mathrm{p}} f_{\mathrm{t}}] \tag{3}$$

$F_{\mathrm{h}}(f_{\mathrm{s}}, f_{\mathrm{t}})$ is the horizontal cell output which has only low spatial frequencies content of the image is used for evaluating the local luminance value $L(p)$ [11]. Spatial frequency (f_{s}) is computed by applying Discrete Cosine Transform (DCT) to the input image and temporal frequency (f_{t}) is considered to be merely dc value since for this work a static image is considered. Equation (2) shows that the compression parameter value $Co(p)$ depends mainly on the luminance value $L(p)$. To enhance the flexibility and accuracy of the system, compression parameter S_0 is considered whose value ranges from [0, 1]. $V_{\max}$ Indicates the highest pixel value in an image and its value is 255, spatial cut-off frequency α_{h} is set at 7 and temporal constant τ_{p} is equated to 1 to minimize high frequency noise [12]. β_{h} is the gain of F_{h} is set to 0.7 to provide result [13]. In this study for computing the level of perception of a normal person and people with night blindness the static compression parameter value S_0 is adjusted between 0 and 1. Since the steady-state illumination depends on the compression properties, for people with normal vision the static compression value S_0 is equated to 0.9 and people with night blindness the static compression value S_0 is equated to 0. Results are analyzed for both day light image and moon light image.

3 Mathematical Modeling of Outer- and Inner-Plexiform Layers

Outer-plexiform layer is modeled using spatial temporal filter whose transfer function is given by the expression.

$$F_{\mathrm{OPL}}(f_s) = F_{ph}(f_s)[1 - F_h(f_s)]. \tag{4}$$

where,

$$F_{\mathrm{ph}}(f_s, f_t) = 1/[1 + \beta_{\mathrm{ph}} + 2\alpha_{\mathrm{ph}}(1 - \cos(2\pi f_s)) + j2\,\pi\,\tau_{\mathrm{ph}} f_t]. \tag{5}$$

$$F_h(f_s, f_t) = 1/[1 + \beta_h + 2\alpha_h\,(1 - \cos(2\pi f_s)) + j2\,\pi\,\tau_h f_t]. \tag{6}$$

As shown in [7], the spatial temporal filter is derived as a difference in the low-pass filter which models the photoreceptor network and a low-pass filter which model the horizontal cell network h of the retina. Response of the outer-plexiform is evaluated by calculating the difference between F_{ph} and F_h and denoted as B_{ON} and B_{OFF}. β_{ph} is the gain of photoreceptor and its value is equated to zero. β_h is the gain of horizontal cell layer in order to extract contour information alone its value is taken as zero. f_s and f_t are spatial and temporal frequencies, respectively. Spatial frequency is computed by applying DCT to the input image and since in this work only one single frame of image is considered the value for temporal frequency is equated to zero. τ_{ph} and τ_h are temporal frequency constants. Some of the parameters has been taken from [14, 15].

Contour contrast-enhanced image from the outer–plexiform layer is subjected as an input image to the inner-plexiform layer. Information from the bipolar cell is subdivided mainly into two main channels namely ON and OFF, each of the ON and OFF channel is independently enhanced using logarithmic transformation as shown in Fig. 2.

Photoreceptor layer is modeled using Michaelis–Menten law in a similar manner modeling of retinal parvo channel was also carried out in the proposed study [16]. Logarithmic transformation is basically used to expand the value of dark pixel values in an image and to compress the dynamic range of image. This in turn leads

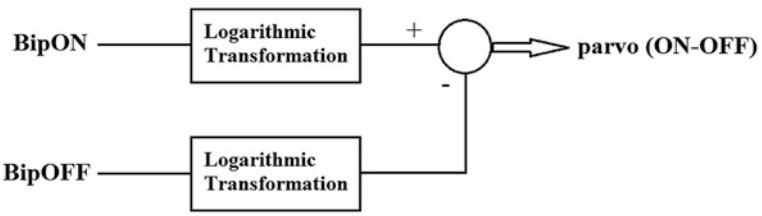

Fig. 2 Parvo channel modeling

to image contrast equalization. The difference of the two bipolar channels results in parvo (ON–OFF) output. Since the incoming information is about contours the parvo channel results in contour enhancement.

4 Methodology for Processing Night Blindness Vision

In the proposed work, physiological stages of retina were modeled through HVS. The flow diagram of the proposed retinal model to show the process involved in the visual perception of both the normal and night blind person is shown in Fig. 3.

Input image is fed to the photoreceptor layer where the image is processed for different compression parameter value S_0 In the photoreceptor layer, the image gets compressed and contrast value of the image is enhanced. The range of compression parameter is from 0 to 1. Since the steady illumination automatically leads to the compression properties [7]. In the proposed study for analysing the perceptual level of people with night blindness, the compression parameter value S_0 is checked for zero and with appropriate results it has been proved that the compression property is associated to level of perception of an image. The contrast-enhanced image is

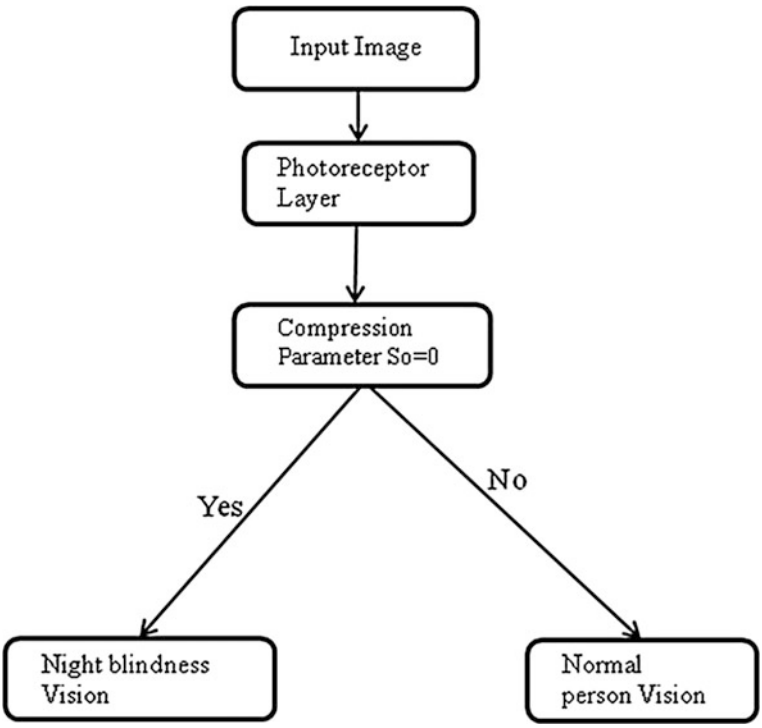

Fig. 3 Flow diagram for night vision processing in the proposed retina model

further processed through outer-plexiform and inner-plexiform layer for contour enhancement and extraction of finer detail of the image, respectively. Features like energy and intensity are extracted in all the successive layers of retina namely photoreceptor, outer-plexiform and inner-plexiform and the results are analysed.

5 Results

Photographs of natural images grabbed in both sunlight and moonlight are considered for the analysis to detect the level of perception of a normal person and people with night blindness. On an average of six to ten images were compiled for the study. Input images are fed to the photoreceptor layer of retina and processed to enhance the contrast value of image for different compression parameter values $S_0 = 0$ and $S_0 = 0.9$. Simulation results are shown Fig. 4 for both sunlight and moon light image. Simulation results showed the processed image of the retinal photoreceptor layer. Figure 4a, b shows the original sun light and moon light vision. Figure 4c, e shows the processed image for the values of compression parameters $S_0 = 0$ and $S_0 = 0.9$ during sun light, respectively. Figure 4d, f shows the processed image for the values of compression parameters $S_0 = 0$ and $S_0 = 0.9$ during moon light, respectively. It is proved through physiological modeling of retina in moon light; when the compression parameter value is 0 the image is not

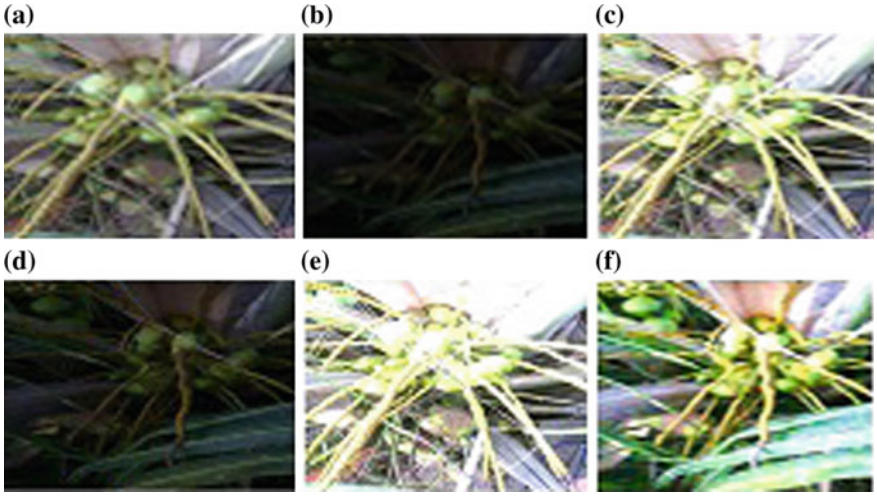

Fig. 4 Processed Image of photoreceptor layer. **a** Sun light image. **b** Moon light image. **c** Processed image during sunlight image for $S_0 = 0$. **d** Processed image during moonlight image for $S_0 = 0$. **e** Processed image during sunlight image for $S_0 = 0.6$. **f** Processed image during moonlight image for $S_0 = 0.9$

Table 1 Feature values of the processed image

Image texture feature		During sun light		During moon light	
		$S_0 = 0$	$S_0 = 0.9$	$S_0 = 0$	$S_0 = 0.9$
Photoreceptor	Energy	148400	196340	9864.5	90159
	Intensity	0.7548	0.9987	0.0502	0.4586
Outer-plexiform	Energy	194980	196590	43271	179680
	Intensity	0.9917	0.9999	0.2201	0/9139
Inner-plexiform	Energy	196350	196600	90453	192710
	Intensity	0.9987	1.0000	0.4601	0.9801

visualized clearly, where as the image looks clear when the compression parameter value is about 0.9. Hence, it observed that for both normal and people with night blindness to visualize an image in dim light compression properties plays a significant role. In the case of visual perception in sunlight both normal and people with night blindness visualize the same image for any value of compression parameter ranging from 0 to 1.

It is further observed that during sunlight good contrast enhancement occurs for a compression parameter value of $S_0 = 0.6$. Night blindness is basically the inability to perceive image in dim light. Hence, it is proved through this model that one of the reason for people with night blindness to perceive an image is that the compression parameter value is approximately zero. From the processed image, features like energy and intensity are extracted and the numerical values of the same are shown in Table 1.

It is observed from the tabulated results during sunlight the intensity value of the photoreceptor layer varies to a minimal level for the compression parameter values for $S_0 = 0.9$ and for $S_0 = 0$. As the image progresses to the outer-plexiform and inner-plexiform layer, the intensity level is approximately same. Similarly, energy level for a compression parameter value 0 is very low, when to 0.9, but in the inner-plexiform layer the energy level is approximately same for compression parameter values 0 and 0.9. Hence it is proved through the proposed retinal layer model people with night blindness can perceive image clearly like a normal person during day light vision. During moon light the energy and intensity value in all three successive layers of retina is very low for the compression parameter value 0. For $S_0 = 0.9$ the energy and intensity value is approximately same that of sunlight vision in the inner-plexiform layer. The proposed retinal layer model proves that during moonlight for people with night blindness the compression parameter value is approximately zero.

6 Conclusion

The knowledge in the study of mathematical modeling of human visual system for perception of night blindness has been limited. In this proposed study with appropriate results it has been proved that compression property is also responsible for night blindness. The proposed method is applied to different kinds of images and showed promising results. It is observed that during sunlight, the energy and intensity value for compression parameters $S_0 = 0$ and $S_0 = 0.9$ are approximately the same after processed through inner-plexiform layer. During moonlight, the situation is not the same that there is a drastic difference in the energy and intensity value for compression parameters $S_0 = 0$ and $S_0 = 0.9$. It is clearly proved that the perception of image is difficult for compression parameter value $S_0 = 0$. Hence, in the process of detecting the level of perception of a normal and people with night blindness this model proves with appropriate results that perceptual level of people with night blindness depends on the compression properties of retina. During moonlight for a people with night blindness the compression parameter value approximates to zero. The proposed work is a pilot study in future after development of optical corrective lens system the study will be extended for clinical analysis.

References

1. Dowling JE, Wald G.: Vitamin A deficiency and night blindness. Biochemistry, 44:648–661, (1958).
2. Wald G.: The molecular basis of visual excitation. Science. 162:230–239, (1968).
3. Carr RE.: The night-blindness disorders. International Ophthalmology Clinics, 9:971–1003, (1969).
4. Ripss H.: Night blindness revisited: from man to molecules. Investigations in Ophthalmology and Vision Science, 23:588–609, (1982).
5. Dryja TP, Hahn LB, Reboul T, Arnaud B.: Missense mutation in the gene encoding the alpha subunit of rod transducin in the Nougaret form of congenital stationary night blindness. Nat Genet 13: 358–360, (1996).
6. Muradov KG, Artemyev NO.: Loss of the effector function transducin-alpha mutant associated with Nougaret night blindness. J Biol Chem, 275: 6969–6974, (2000).
7. Viktor I. Govardoviskii et al.: Photoreceptor light adaptation. J Gen Phisiology, 116(6), 791–794, (2000).
8. W.H.A. Beaudot.: The Neural Information Processing in the Vertebrate Retina: A Melting Pot of Ideas for Artificial Vision. PhD Thesis in Computer Science, INPG, France, December 1 (994).
9. W.H.A. Beaudot.: Sensory coding in the vertebrate retina: towards an adaptive control of visual sensitivity. Network: Computation in Neural Systems 7(2), 317–3, (1996).
10. A. Benoit a, A. Caplier b, B. Durette b, J. Herault b.: Using Human Visual System modeling for bio-inspired low level image processing. Computer Vision and Image Understanding (114), pp. 758–773, (2010).

11. W.H.A. Beaudot, P. Palagi., J. Hérault.: Realistic Simulation Tool for Early Visual Processing Including Space, Time and Colour Data. International Workshop on Artificial Neural Networks, Barcelona, June (1993).
12. Al Lens, Sheila Coyne Nemeth, Janice K. Ledford.: ocular Anatomy and Physiology. SLACK Incorporated, Second edition, (2008).
13. Benoit, D. Alleysson, J. Herault, P. Le Callet.: Spatio-temporal tone mapping operator based on a retina model. Lecture Notes in Computer Science 5646, 12–22, (2009).
14. Y. Dan et al.: Efficient coding of natural scenes in the lateral geniculate nucleus: experimental test of a computational theory. Journal of Neuroscience 16, 3351–3362, (1996).
15. H.B. Barlow.: Redundancy reduction revisited. Computation in Neural Systems 12, 241–253, (2001).
16. S.M. Smirnakis, M.J. Berry, D.K. Warland, W. Bialek, M. Meister.: Adaptation of retinal processing to image contrast and spatial scale. Nature 386, 69–73, (1997).

An Improved Encryption and Signature Verification ECC Scheme for Cloud Computing

Shweta Kaushik and Charu Gandhi

Abstract Ensuring the security and efficient authentication of any information is a prime concern for a cryptographic technique. In cloud model, since data is outsourced over untrusted third party without any physical possession of that, increase the concern regarding the cloud data security. Public key cryptography technique in cloud system is useful only if there is proper authentication of transformation of public key to authenticated user only. On the other hand, ECC technique compared to this provides different ways of ECC cryptographic key management, encryption, decryption, and digital signature and its verification. The advantage of ECC over public key scheme is that, it provides the same security level for a smaller key size compared to public key scheme, thus, reducing the process time of any cryptographic operation over the data in its communication between different cloud communicating parties. In this paper, we present a new framework for cloud system which has a different way of encryption/ decryption using ECC over finite field and improve signature and verification scheme. The result shows that communication cost is less compared to other scheme and improved speedup for signature and verification.

Keywords Cloud computing · Elliptic curve discrete logarithm (ECDL) · Elliptical curve cryptography (ECC) · Security · Signature · Verification

1 Introduction

There are many digital signature algorithms that have been proposed successfully since the introduction of public key cryptography in 1970s [1, 2]. These mostly developed algorithms are generally related to two-number problems—factoring of

S. Kaushik (✉) · C. Gandhi
Department of Computer Science and Engineering,
Jaypee Institute of Information Technology, Noida, India
e-mail: shwetakaushik10@gmail.com

C. Gandhi
e-mail: charu.gandhi@jiit.ac.in

D.K. Lobiyal et al. (eds.), *Proceedings of the International Conference on Signal, Networks, Computing, and Systems*, Lecture Notes in Electrical Engineering 396, DOI 10.1007/978-81-322-3589-7_5

large prime number problem FAC [2] or discrete logarithm [3] problems. These approaches provide security as required but they are slow and less efficient. To overcome this inefficiency, new efficient approach elliptical curve cryptography [4, 5] introduces which utilize the concept of ECDL. This approach provides the improved security with reduced key size requirement and improved computation time. With the addition of digital signature and verification scheme, security is improved, which solves the confidentiality, integrity, authentication problem of data security also. In cloud computing, since owner's data is stored at cloud server with no physical access to that, increase the need for security requirements. Here, data owner requires that its data will be delivered to authenticated users only, without introduction of any vulnerabilities and malicious attacks from insider and outsider during its storage and transformation over the non-trusted network. During the encryption/ decryption using public key cryptography, sender requires two keys—private and public key. He uses private key as secret and encrypts the message M with that. Any receiver can decrypt it using its public key. Compared to this approach, in our proposed framework if two parties want to communicate a message M, then they must agree to use some elliptical curve equation Ep(a,b) and a random base point C on that elliptical curve, where p is a prime number. Sender needs to establish a private and public key pair and a special key which is specifically used for a particular receiver. Similarly, all users need to establish a private and public key pair and a special key specifically for a particular sender. With these keys only communication is done between two parties. In addition to this, sender also signs the message which is further verified by the receiver to confirm that received message is intact without any modification.

1.1 Cloud Computing

According to NIST [6] definition, cloud computing can be defined as a model for ubiquitous, convenient and on-demand access to services from a shared pool of resources (network, services, servers, application, etc.) on the Internet connection. This cloud model has five essential characteristics, i.e., on-demand self service, broad network access, resource pooling, rapid elasticity, and measured services, four deployment model, i.e., private, public, hybrid, community cloud, and three-service delivery model, i.e., Infrastructure as a Service (IaaS), Platform as a Service (PaaS), and Software as a Service (SaaS). Here, owner wants to share their data, information, or services with other users. To share this data, owner stores this at some remote location or servers, from where any user can access it without any interaction of owner after identification and authentication done by service provider. Since mostly data stored on the server is confidential and requires only authenticated user to access the data according to its accessibility criteria, there is a need for security concern to be taken care to secure the data from any malicious activity. To overcome this problem, owner encrypts the data before storing this over non-trusted cloud network and provides only authenticated users with decryption

key. To ensure the data integrity of its stored data, owner needs to sign the data and provide the user with its verification details. After receiving the data, user need to first decrypt this and then verify to know whether it received the required data without any modification or not. If it is correct, accepts it, else rejects this, and reports the data owner about it.

1.2 Algebraic Point Addition

Let A(*xa*,*ya*) and B(*xb*,*yb*) be two different point on elliptical curve Ep(*F*). **The algebraic sum of these two points C(*xc*,*yc*) can be defined as C = A + B**

$$m = \frac{yb - ya}{xb - xa} \bmod p \text{ if } A \neq B \text{ and}$$
$$m = \frac{3xa^2 + a}{2ya} \bmod p \text{ if } A = B$$
$$\text{Then } xc = m^2 - xa - xb \text{ and } yc\, m(xa - xb) - ya$$

For example: Let A = (3,10) and B = (9,7) in $E_{23}(1,1)$.

Now m = ((7 − 10)/(9 − 3)) mod 23 = 11

xc = (11^2 − 3 − 9) mod 23 = 17 and *yc* = (11(3−7) − 10)mod 23 = 20 thus, C = (17,20)

1.3 Algebraic Point Doubling

Let A(*xa*,*ya*) be a point on elliptical curve Ep(*a*,*b*) and P ≠ −P than 2P = (*xp*,*yp*) can be defined as

$$xp = \left(\frac{3xa^2 + a}{2ya}\right)^2 - 2xa \text{ and } yp = \left(\frac{3xa^2 + a}{2ya}\right)(xa - xp) - ya$$

For example: if A = (3,10) over the field $E_{23}(1,1)$ than 2A = (7,12).

1.4 Our Contribution

The main contributions of our work are described below

- We proposed a new approach for encryption and decryption using ECC over finite field.

- We also proposed a new efficient approach for digital signature and verification which increases the speedup compared to other schemes.
- We also prove the security of our scheme through justifying the performance, experimental results, concrete analysis, and comparison with other existing schemes also.

1.5 Paper Organization

This paper is further organized as—the new proposed scheme for secure and efficient encryption, and signature generation and its verification explained in Sect. 2. In Sect. 3, we describe the implementation detail of our proposed scheme with experimental evaluation. The security analysis of the proposed scheme such as its correctness and security attack consideration are explained in Sect. 4. Performance evaluation is examined in Sect. 5. Related work is presented in Sect. 6. We conclude our work in Sect. 7.

2 Proposed Scheme for Data Security

Both the Key Center (KC) and data owner agree to some data as

1. The elliptical curve equation for a particular file: (i) value of a and b and (ii) large prime number p.
2. A base point C, chosen from generated elliptical curve points.
3. The points generated for the defined elliptical curve computed from this equation (Table 1).

Key Generation (Ep(a,b) → A_1, A_2, B_1, B_2, D_U, U_D)

1. Data owner generates its key with the help of KC. It also selects a random number α which is less than order of elliptical curve such that $\alpha \in [1, p-1]$.
2. Data owner selects a point A from all generated points from this elliptical curve equation. He keeps α and A as his secret keys and generates public keys as $A_1 = \alpha C + A$ and $A_2 = \alpha A$.
3. Similarly, user also generates its own private and public keys with the help of KC. It selects a random number $\beta \in [1, p-1]$ and a random point B from the generated points. User keeps β and B as its private keys and generate public keys as $B_1 = \beta C + B$ and $B_2 = \beta B$.
4. Data owner and user now generates communication key specifically for each other as
   - Data owner communication key specifically for a particular user is $D_U = \alpha B_2$.
   - User communication key specifically for a data owner if $U_D = \beta A_2$.

Table 1 Meaning of notations used

Symbol	Meaning
M	Message to be communicate
H(M,Q)	Hashing function like SHA-1
E(*a*,*b*)	Elliptical curve
P	Prime number
PK_{DO}	Public key of data owner
SK_{DO}	Secret key of data owner
$Sign_{Key}$	Signature key of data owner
$Verify_{Key}$	Verification key
UID	User id
FID	File id
PK_{User}	Public key of user
SK_{User}	Secret key of user
C	Base point of elliptical curve
D_U	Data owner public key generated for specific user
U_D	User public key generated for specific data owner
γ	Secret number shared between user and data owner
α, β, *d*, *r*	Random number ϵ [1, p − 1]
E_1, E_2	Encrypted message
Y	Public key for verification
S	Count of key points generated from elliptical curve equation

Encryption (M, B_1, B_2, $U_D \rightarrow E_1$, E_2)

1. If data owner wants to share a message M with user, then encode all the characters of M to the points of elliptical curve. This encoding procedure is mutually agreed upon by both parties.
2. Each encoded character is encrypted to a pair of ciphertext as E1 = γC and $E_2 = M + U_D + \gamma B_1 + \alpha B_2$. Here γ is a random number.
3. After encryption of each character of the message, the ciphertext is again decoded into characters and communicate to service provider.

Decryption (E1, E_2, D_U, $\gamma \rightarrow$ M)

1. After receiving the ciphertext, first encode each character into elliptical point using the same encoding procedure as data owner did.
2. Then decrypt each encoded message character as: $M = E_2 - (\beta A_2 + \beta E_1 + \gamma B + D_U)$.
3. Decryption work properly as $E_2 = M + U_D + \gamma B_1 + \alpha B_2$ which is equivalent to service provider

$$M + \beta\alpha A + \gamma\beta C + \gamma B + \alpha\beta B. \quad (1)$$

And $\beta A_2 + \beta E_1 + \gamma B + D_U$ is equivalent to

$$\beta\alpha A + \beta\gamma C + \gamma B + \alpha\beta B. \quad (2)$$

From Eqs. 1 and 2, message (M) = (equation 1 − equation 2).

Signature (C → SignKey)

1. Choose a random number $r \in [1, p-1]$, keep this as secret and produce a public key as Y = rC.
2. Choose a random number $d \in [1, p-1]$ and compute Q = dC.
3. Convert message (M) and Q into e using a simple hash function such as SHA-1 where $e = h$(M,Q).
4. Generate the signature for the message as $s = d$ + re(mod p)
5. Send this signature key to user for the verification purpose.

Verification (SignKey, C → verification detail)

1. Compute z = sC – eY.
2. Compute $\bar{e}$ = h(M,z), where M is the received message by the user.
3. Signature is valid if $\bar{e}$ = e else reject the received message (Fig. 1).

Verification work properly as: z = sC − eY = (d + re)C − eY

$$z = dC + reC - eY = Q + eY - eY = Q$$
$$\bar{e}(M, z) = e(M, Q). \text{Thus, } \bar{e} = e \text{ verified.}$$

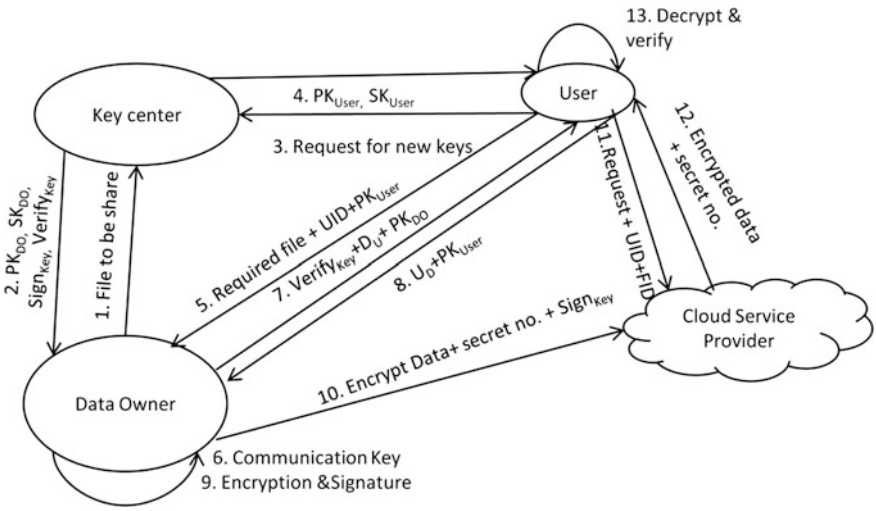

Fig. 1 Proposed framework

3 Implementation

We implement a working prototype of our proposed scheme using Java RMI in NetBeandIDE 7.4 on system with Intel core i3-2.53 GHz processor with 4 GB memory, 320 GB hard disk drive running on Windows 7. The complete scenario consists of four main functions, i.e., encryption, decryption, signature generation, and verification. Our data owner implements the two functions—encryption and signature generation to encrypt and sign the data before outsourcing it over non-trusted network. Service provider is responsible for implementing the secure identification and authentication process before transferring the data to user. User will implement the two functions—decryption and verification to get the original data and to verify the integrity of received data. We analyze the performance of our proposed scheme in terms of communication, storage, and computational complexity. Computational complexity of our scheme is compared with other existing scheme in terms of signature generation and verification speedup as shown in Table 3. Communication cost can be considered in between the service provider and user during request processing. The request sent by the user to service provider, which consist of O(1) and the response is sent by the service provider in terms of requisite file which is O(n). The communication between the user to KC, owner to KC, and user to owner requires only request and response for key generation and communication setup; communication cost is O(1) for all of them. All the entities in the proposed scheme need to store some amount of information which requires storage cost. Service provider needs to store the complete data, information, or service at their server, storage cost O(n). User and data owner only need to store some secret parameters such as their private key and communication key shared between them. Therefore, storage cost for them is O(1). Key center does not need to store any information, simply response to owner or user queries. Thus, no storage cost is required by key center.

We measure time required for the signature generation and its verification operations for the defined file size (including 1, 100, 200… 1000 kB). Figure 2 shows our result. From the result evaluation, we find that in all cases of file signature generation operation, the time for cryptographic operation is not more than 0.067 s (for a file size 100 kB) and verification operation it is not more than 0.042 s. We conclude from this concrete analysis that our proposed scheme is more efficient than already existing scheme in terms of speedup and communication cost.

4 Security Analyses

4.1 Correctness

The correctness of proposed scheme can be examined below

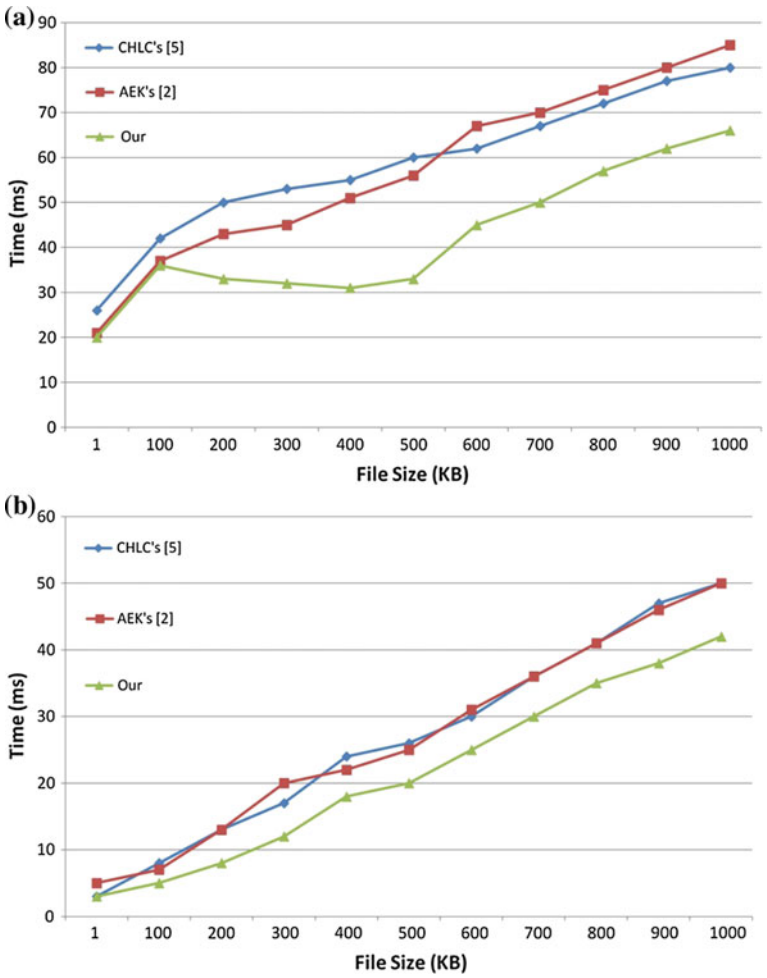

Fig. 2 Performance for file signature generation (**a**) and verification (**b**)

Theorem 1 *If signature algorithm runs correctly than verification algorithm can validate the signature (s,e) received.*

Proof

$$Z = sC - eY = (d + re)C - eY$$
$$Z = dC + reC - eY = Q + eY - eY = Q$$
$$\bar{e}(m, Z) = e(m, Q)$$

Theorem 2 *If encryption of each character is done properly using the correct keys, share between data owner and user, user will get the exact data after performing decryption.*

Proof

$$\begin{aligned} \mathrm{M} &= \mathrm{E}_2 - (\beta \mathrm{A}_2 + \beta \mathrm{E}_1 + \gamma \mathrm{B} + \mathrm{D}_\mathrm{u}) \\ &= \mathrm{M} + \beta\alpha\mathrm{A} + \gamma\beta\mathrm{C} + \gamma \mathrm{B} + \alpha\beta\mathrm{B} = \beta\alpha\mathrm{A} - \gamma\beta C - \gamma\mathrm{B} - \alpha\beta\mathrm{B} = \mathrm{M} \end{aligned}$$

4.2 Security Considerations

The security consideration of our proposed scheme is similar to other schemes. The difficulties linked with various attacks are related to the solution of the elliptic curve discrete logarithm problem (ECDL) [7]. Some possible way by which an attacker tries to breach our improved scheme can be summarized below

Attack 1: In this case, an adversary wants to know the secret key "d", used in signature, by knowing the public key Y. He will be confronted to ECDL problem as the base point C is chosen randomly from the generated points for a particular elliptical curve equation, which is different for each file. If the data owner chooses a same integer r to sign two different messages M_1 and M_2 then adversary may obtain the secret key d as

$$\begin{gathered} \mathrm{s}_1 = r + \mathrm{del}(\mathrm{mod}\,\mathrm{p}) \text{ and} \\ \mathrm{s}_2 = r + \mathrm{de}_2(\mathrm{mod}\,\mathrm{p}) \text{where } \mathrm{e}_1 = \mathrm{h}(\mathrm{M}_1, \mathrm{Q}) \text{ and } \mathrm{e}_2 = \mathrm{h}(\mathrm{M2,Q}) \\ \text{Therefore}, d = (\mathrm{s}_1 = \mathrm{s}_2)\,(\mathrm{e}_1 - \mathrm{ev}) - (\mathrm{mod}\,\mathrm{p}) \end{gathered}$$

Attack 2: In this case, an adversary aims to forge valid signature for a particular message M. Here, adversary first selects a random point z and computes e = h (M,z). By knowing this value of e and z adversary tries to find the value of s as

$$\begin{gathered} \mathrm{z} = \mathrm{sC} - \mathrm{eY} \\ \mathrm{z} + \mathrm{eY} = \mathrm{sC},\ \mathrm{s} = (\mathrm{z} + \mathrm{eY})/\mathrm{C} \end{gathered}$$

Here, value of Y and C are publically known and value of e and z are calculated by adversary. This method to find value of s is also confronted by ECDL problem as elliptical curve equation used here is unknown and it is difficult to know exactly this equation without applying brute force approach. Thus, it is infeasible to breach security.

Attack 3: In this case, an adversary tries to sign a message with different signature. In the proposed scheme, data owner encrypts the message using specific user's public key and a communication key shared between data owner and specific user only. By doing this, receiver is ensured that message is coming directly from the original sender because this is only the sender who knows the receiver's public key

for the communication. This will ensure that ciphertext received by the receiver possesses the features of confidentiality, integrity, and authentication.

Attack 4: In this case, an adversary tries to find out the value of secret number γ to know the relationship between plaintext and ciphertext. In the proposed scheme, data owner generates a new random number γ for each message. This random number is different for each character of a message. Due to random generation of this point, same character in the plaintext are not as same in ciphertext and also difference between characters in plaintext and ciphertext is not same. It will make linear cryptanalysis difficult for adversary.

5 Performance Evaluations

We compare our proposed signature and verification scheme with CHLC's scheme [8], ID's scheme [7], and AEK's scheme [9] in terms of signature and verification computations complexity and communication cost between two parties. To compare and describe the complexity of these schemes, we require Table 2 which provides the conversion of various operations units, respectively, to modular multiplication [10] time complexity. Here, the notation used T_{MUL}, T_{EXP}, T_{ADD} describe the time complexity requirements for modular multiplication, exponentiation, and addition, respectively, and T_{EC_MUL}, T_{EC_ADD}, T_H represents the time complexity for executing the elliptical curve multiplication, addition, and hash function, respectively.

Table 3 summarizes differences between the various schemes. From the information retrieved from Table 3, it can be stated that in both signature generation and signature verification, the number of modular multiplications required by our scheme is less than other scheme.

We can also calculate the speedup of our new proposed scheme in comparison with other scheme as in Table 3 by neglecting the time requirement of the hash function. Here, minimum time required related to signature generation and its verification is given by 1TEC_MUL + 1 TEC_ADD + 1TH $\cong$ 29.12 TMUL. To estimate our scheme, we use the following formula [7]:

$$\text{Speedup} = 100\% - \frac{\text{Time complexity of scheme} - 29.12}{\text{Time complexity of scheme}} \times 100\%$$

Therefore, in comparison to the techniques used in other schemes for signature generation and its verification phases with our scheme it can be stated that our scheme is more efficient. Our new scheme gives 97.07 and 50.11 % efficiency with

Table 2 Conversion of various operations to modular multiplication T_{MUL}

$T_{EXP} \cong 240T_{MUL}$
$T_{EC\_MUL} \cong 29\ T_{MUL}$
$T_{EC\_ADD} \cong 0.12\ T_{MUL}$
T_{ADD} is negligible

Table 3 Comparison between various schemes and our proposed scheme

Time complexity								
Scheme	Signature generation	In terms of T_{MUL}	Signature verification	In terms of T_{MUL}	No. of keys	Communication cost	Signature speedup (%)	Verification speedup (%)
CHLC's [8]	$2T_{EC\_MUL} + T_{EC\_ADD} + 2T_{ADD} + 2T_{MUL} + T_H$	$60.12T_{MUL} + T_H$	$3T_{EC\_MUL} + 2T_{EC\_ADD} + T_H$	$87.24T_{MUL} + T_H$	PK = 1, SK = 2	6|p|	48.44	33.38
ID's [7]	$T_{EC\_MUL} + T_{EC\_ADD} + T_{ADD} + T_{MUL} + T_H$	$30.12T_{MUL} + T_H$	$2T_{EC\_MUL} + 2T_{EC\_ADD} + T_H$	$58.24T_{MUL} + T_H$	PK = 1, SK = 1	3|p|	96.68	50
AEK's [9]	$2T_{EXP+} 3T_{MUL} + T_H$	$483T_{MUL} + T_H$	$4T_{EXP} + T_H$	$960T_{MUL} + T_H$	PK = 5, SK = 1	12|p|	6.63	3.1
Our scheme	$T_{EC\_MUL} + T_{ADD} + T_{MUL} + T_H$	$30T_{MUL} + T_H$	$2T_{EC\_MUL} + T_{EC\_ADD}T_H$	$58.12T_{MUL} + T_H$	PK = 1, SK = 1	2|p|	97.07	50.11

signature and verification, respectively, which is better than other stated schemes. From the estimation done in Table 3 it is clear that our scheme greatly improve the efficiency.

6 Related Works

Elliptic curve cryptography is researched widely from last many years in the field of computer science to provide the data security while using small key size and provide excellent security. In addition to this, elliptical curve scheme also support for secure key transformation [11] and authenticated session key management [12–14]. Researchers have proposed many variant for encryption, decryption, signature generation and its verification. AEK's [9] proposed a digital signature scheme, as shown in Table 3, by applying a variation of ELGamal scheme on elliptic curve. Security analysis of this scheme shows that it increases communication cost and reduces the speedup. While ID's [7] and CHLC's [8] scheme provides digital signature schemes based on identity of user to sign a particular message over elliptic curve. Security analysis, as in Table 3, of these two schemes shows that ID's scheme performance is better in comparison to CHLC's in both communication cost and speedup for signature generation and it verification. In [15] the author proposed a new scheme for encryption and decryption of data using elliptical curve and try to meet security requirements by using various public and private key for that. The generation of a secret number randomly for each message character does not provide any linear relationship between ciphertext and plaintext. In [16], the author proposed a progressive scheme which allows encryption to be done multiple times by using different key for each stage. On the other hand, decryption can be done only once by using a single decryption key. But this scheme require that owner should have a knowledge of service provider private key which is not possible as by knowing this an owner might also have a knowledge of other owner confidential data also.

7 Conclusions

In this paper, we present a secure and efficient cloud framework which utilizes the concept of ECC scheme. We have also proposed new algorithms for encryption, decryption, signature generation, and its verification. In the proposed work communicating parties such as data owner and user first need to agree upon an elliptical curve equation and a base point C on this elliptical curve. In order to establish a communication between these two parties both will select a key specifically for each other and communicate with the help of this and their public key. Use of this specific key for communication provides the confidentiality, integrity, and non-repudiation security requirements. Use of different secret number γ for encryption of each

message also makes the linear cryptanalysis difficult for attacker. Because of this secret number there is no direct relationship between plaintext and ciphertext. In addition to this, each character of a message is encoded to a point on elliptical curve using some encoding scheme, which is shared among owner and user only. This encoding scheme is different for each communicating parties. We also analyzed the efficiency and various security consideration and came to know that our proposed algorithms are more efficient and secure than other schemes [7–9]. Our proposed algorithm also increases the speedup for signature generation and verification compared to other scheme and reduces the communication cost also.

References

1. W. Diffie and M. E. Hellman, New directions in cryptography, IEEE Transactions on Information Theory, vol. IT-22, (1976), pp. 644–654.
2. R. Rivest, A. Shamir and L. Adeleman, A method for obtaining digital signatures and public key cryptosystems, Communication of the ACM, Vol. no 21, (1978), pp. 120–126.
3. T. ElGamal, A public key cryptosystem and a signature scheme based on discrete logarithms. IEEE Transaction on Information Theory, IT-31(4), 1985, pp. 469–472.
4. N. Koblizt, Elliptic curve cryptosystem, Mathematics of Computation 48(177), 1987, pp. 203–209.
5. V. S. Miller, Use of elliptic curves in cryptography, Advances in Cryptology-Proceedings of Crypto'85, LNCS, vol. 218, Springer, 1986, pp. 417–426.
6. Mell, Peter, and Tim Grance. "The NIST definition of cloud computing." (2011).
7. Shahril, Eddie, and Wan Daud Wan Suhana. "ID-Based signature scheme using elliptic curve cryptosystem." (2013).
8. Y. F. Chung, K. H. Huang, F. Lai, T. S. Chen, ID-based digital signature scheme on the elliptic curve cryptosystem, Computer Standards and Interfaces 29, 2007, pp. 601–604.
9. Abid, Ounasser, Jaouad Ettanfouhi, and Omar Khadir. "New digital signature protocol based on elliptic curves." arXiv preprint arXiv:1301.2335 (2013).
10. N. Koblizt, A. Menezes, S. Vanstone, The state of elliptic curve cryptography, Design, Codes and Cryptography 19, 2000, pp. 173–193.
11. Ch. Suneetha, D. Sravana Kumar and A. Chandrasekhar, "Secure key transport in symmetric cryptographic protocols using elliptic curves over finite fields", International Journal of Computer Applications, Vol. 36, No. 1 November 2011.
12. Kin Choong Yow and Amol Dabholkar, A Light-Weight mutual authentication and key-exchange protocol based of elliptical curve cryptography for energy-constrained devices, International Journal of Network Security & its Applications Vol. 2 No. 2 April 2010.
13. Mohsen Machhout eat.al., coupled FPGA/ASIC implementation of elliptic curve crypto-processor, International Journal of Network Security & its Applications Vol. 2 No. 2 April 2010.
14. K. R. Chandrasekhara Pillai and M P Sebastian, "Elliptic Curve based authenticated session Key establishment protocol for High Security Applications in Constrained Network environment" International Journal of Network Security & its Applications (IJNSA), Vol. 2, No. 3, July 2010.
15. Kumar, D. Sravana, C. H. Suneetha, and A. Chandrasekhar. "Encryption of data using Elliptic Curve over finite fields." arXiv preprint arXiv:1202.1895 (2012).
16. Zhao, Gansen, et al. "Trusted data sharing over untrusted cloud storage providers." Cloud Computing Technology and Science (CloudCom), 2010 IEEE Second International Conference on. IEEE, 2010.

Implementing a Web-Based Simulator with Explicit Neuron and Synapse Models to Aid Experimental Neuroscience and Theoretical Biophysics Education

Aadityan Sridharan, Hemalatha Sasidharakurup, Dhanush Kumar, Nijin Nizar, Bipin Nair, Krishnashree Achuthan and Shyam Diwakar

Abstract In this paper, we implemented a virtual laboratory of neurons and synapses via dynamical models on a web-based platform to aid neurophysiology and computational neuroscience education. Online labs are one of the best alternatives to many universities confronting socio-economic issues in maintaining infrastructure for good laboratory practice. The neural network virtual laboratory was implemented using HTML5 and JQuery, which allowed users to access the lab as a browser-based app. The simulator allows reconstructions of population code and biophysics of single neuron firing dynamics and hence will allow experimentalists to explore its use for hypothesis-based predictions. Such tools as educational aids allow an interrelationship of cognitive, social, and teaching presence. We found students could easily reproduce the common voltage and current clamp protocols on such models without significant instructor assistance and the platform was developed to allow further extensions like raster plots, network computations using extensions to code modules. With new technologies, we foresee a potential redesign of the use of such virtual labs for large-scale modeling as teaching and learning tools in blended learning environments.

Keywords Neuron simulator · Neurophysiology · Pedagogy · Virtual laboratory · ICT

A. Sridharan · H. Sasidharakurup · D. Kumar · N. Nizar · B. Nair · S. Diwakar (✉)
Amrita School of Biotechnology, Amrita Vishwa Vidyapeetham (Amrita University), Clappana (P.O.) Kollam, Kerala, India
e-mail: shyam@amrita.edu

A. Sridharan
Amrita School of Arts & Sciences, Amrita Vishwa Vidyapeetham (Amrita University), Clappana (P.O.) Kollam, Kerala, India

K. Achuthan
Amrita School of Engineering, Amrita Vishwa Vidyapeetham (Amrita University), Clappana (P.O.) Kollam, Kerala, India

D.K. Lobiyal et al. (eds.), *Proceedings of the International Conference on Signal, Networks, Computing, and Systems*, Lecture Notes in Electrical Engineering 396, DOI 10.1007/978-81-322-3589-7_6

1 Introduction

Several studies have been proposed on the circuit and neuronal properties bringing computational neurosciences as a mainline hypothesis-making study [1–4]. Computational reconstruction of brain circuits allows hypothetical exploration of its properties, behavior, and functions that may not be feasible via experimentation [5]. Existing studies and tools add to the repertoire of simulators that are capable to simulate spiking behavior and mechanisms at the single neuron and circuit level [6–8].

In a previous attempt, we had built Hodgkin-Huxley model of squid axon [9, 10] as a virtual laboratory for students to study the basic neuronal behavior. Hodgkin-Huxley model is considered as the classical neuronal model for teaching basic neurophysiology and its mathematical form for computational neuroscience. The pedagogical goal of virtual labs was to allow self-learning of some neurophysiology protocols, reconstruct electro-responsiveness properties and characteristics of ionic conductances [10–12]. However, single neuron model was not sufficient for explaining synaptic and network properties and for building simpler network models to hypothesize circuit properties. Consequently, open source implementations were also crucial to get student community contributions. With advances in computing technology, it is suggested that simulation of large-scale brain circuits may be possible [5]. For advanced experimental design, hypothesis making tools such as brain models have become pertinent and hence teaching basic mathematical models in neuroscience has become essential. Several tools are already available including the NEURON [13] and GENESIS [8] for modeling and simulation of detailed neurons and networks.

In this paper, a client-based spiking neural network simulator has been designed and implemented using HTML5 and Jquery. This implementation allows user to understand the behavior of a single neuron allowing data fits from electrophysiological studies. The simulator allows reconstructing passive properties of the neural membrane including membrane resistance, membrane capacitance [2, 14], and active properties including ion channel kinetics, pharmacological effects, frequency–current and voltage–current relationships [14–16].

2 Materials and Methods

2.1 Neuronal Biophysics

Our single neuron model was an extension based on the Hodgkin-Huxley (HH) neuron model [10, 17], since students had shown learning improvements based on the virtual lab model in our previous study. Neuronal biophysics models active ion channels via state-based equations and the membrane as a resistance–capacitance model [18] (Fig. 1).

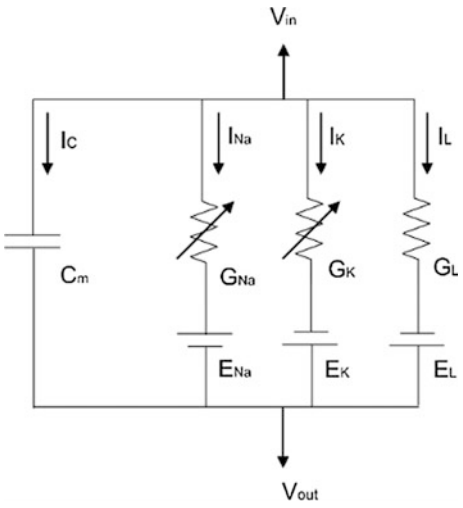

Fig. 1 Electrical equivalent of Hodgkin-Huxley neuron

Explicit implementation of neuron model and total membrane current flowing across the membrane (I_m) was computed using

$$I_m = I_c + I_i \tag{1}$$

Capacitive current

Capacitive current was modeled (I_c) as the rate of change of charge 'q' across the membrane.

$$I_c = \frac{\mathrm{d}q}{\mathrm{d}t} \tag{2}$$

The behavior of single neuron was modeled as

$$C_m \frac{\mathrm{d}V}{\mathrm{d}t} + I_i = I_m \tag{3}$$

Ionic current—Activation and inactivation states

Ionic current (I_i) was modeled as three individual Hodgkin-Huxley style ionic currents: sodium current (I_{Na}), potassium current (I_{K}), and leakage current (I_{leak}) also referred as chloride current.

$$I_{\mathrm{Na}} = g_{\mathrm{Na}} m^3 h (V - E_{\mathrm{Na}}) \tag{4}$$

$$I_{\mathrm{K}} = g_{\mathrm{K}} n^4 (V - E_{\mathrm{K}}) \tag{5}$$

$$I_{\text{leak}} = g_{\text{cl}}(V - E_{\text{cl}}) \tag{6}$$

where, g_{K} and g_{Na} denotes the maximum conductance for sodium and potassium channels, E_{K} and E_{Na} denotes the reversal potential of potassium and sodium channels (reversal potential of individual ion channels were calculated from Nernst equation; [14], 'n' is the gating variable for potassium channel (dimensionless number, its value ranges from 0 to 1). n denotes the probability of finding one activation particle in its open/permissive state and $(1 - n)$ denotes the probability of being closed or nonpermissive state (current flow will be zero in this state) similarly for m and h. The state transition between open and closed for a gating particle was given by first-order kinetics. Replacing the neuron model, total ionic current, the sum of individual ionic currents was modeled as a Hodgkin-Huxley (HH) neuron [9]

$$I_i = m^3 h g_{\text{Na}}(V - E_{\text{Na}}) + n^4 g_{\text{K}}(V - E_{\text{K}}) + g_L(V - E_L) \tag{7}$$

The Hodgkin-Huxley model for squid axon was

$$C_m \frac{\mathrm{d}V}{\mathrm{d}t} + m^3 h g_{\text{Na}}(V - E_{\text{Na}}) + n^4 g_{\text{K}}(V - E_{\text{K}}) + g_L(V - E_L) = I_m \tag{8}$$

The excitatory and inhibitory synapses for the network simulator were AMPAergic and GABAergic and were modeled using exponential alpha functions [19].

2.2 Simulation Input

Students were allowed to voltage and current clamp the neuron model to study electro-responsiveness properties as seen in experiments. Voltage clamp technique was simulated on the neuron model to study the kinetics of voltage-activated ion channels responsible for neuronal excitation (Na^+, K^+, fast gates, slow gates, etc.). Pharmacology conditions were implemented on the tool by accessing the conductance property of the respective ion channels.

2.3 Web-Based Neuron and Neural Network Simulator

To be easily accessible and for web-based access, we used HTML5 and Java Script to implement the mathematical simulator of excitable neuronal membrane of squid axon. Simulator (see Fig. 2a, b) uses Hodgkin-Huxley equations and provides full access to Hodgkin-Huxley parameters, membrane properties, various ionic concentrations, pharmacological effects, stimulus parameters and voltage clamp protocol.

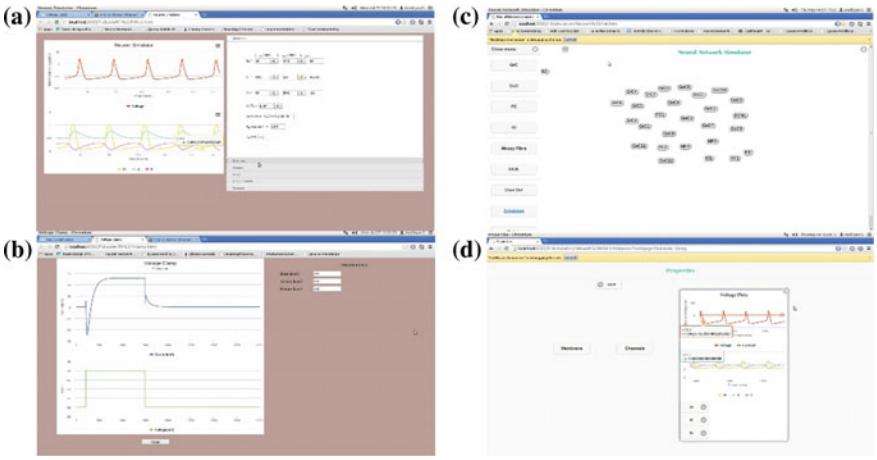

Fig. 2 Single neuron and network simulator GUI. **a** Neuronal simulator under current clamp, **b** single neuron simulation on voltage clamp, **c** network simulator demonstrating a low-scale cerebellum input layer. **d** Characteristics of neuron in the network mode

The neuron simulator was scaled up into a network simulator (see Fig. 2c) that acts as a network of H-H neurons. GUI displays properties and characteristics of each neuron. Electro-responsiveness of neuron was analyzed by plotting its firing characteristics. Change in the number of spikes, spike latency, and behavior of ionic currents were analyzed from the plot (see Fig. 3).

To analyze the effect of neural network simulator on user adaptability and learning ability, a survey-based analysis was conducted among them. The online neuron simulator lab was used for analyzing user feedback. For this study, we selected 100 undergraduate and postgraduate students who undertook a neurophysiology course in their curriculum. The students were subjected to a questionnaire based pretest regarding basic knowledge in various neurophysiology experiments. The questions were same as in the online virtual labs [10] and individual performance report was calculated. After that, these students were asked to perform any two virtual neurophysiology experiment of their choice without the help of an instructor. After completing two experiments, a posttest was conducted with same set of questions as in the pretest. The individual performance was noted and tabulated for further analysis.

To test the role of simulation-based experiments in education, another set of questions was also posed to student users to analyze their interest in neural network simulator. The question asked were (1) would you support usage of neural network simulator in classroom education? (2) With the neural network simulator, could you manage to learn an experiment without the help of an instructor? (3) Do you think neural network simulator can be used as a supplementary tool to learn concepts in an interesting way? (4) Did the neural network simulator help you to make

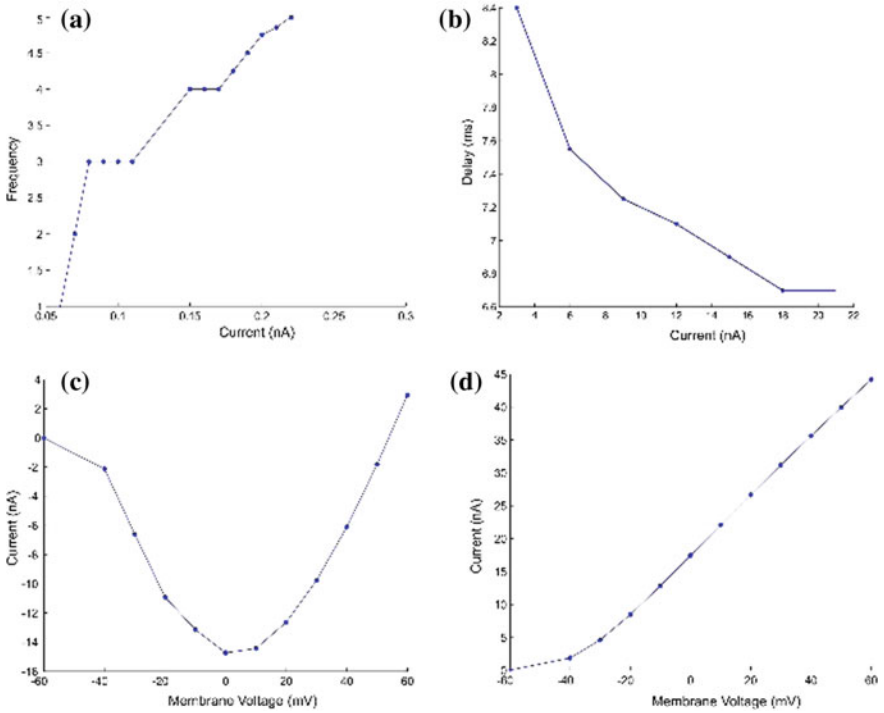

Fig. 3 Electro-responsiveness of a neuron via current clamp protocol—user reconstructions. **a** Frequency versus injected current, **b** first spike latency versus injected current, **c** I_{Na} versus voltage, **d** I_K versus voltage

experimental calculations and results interpretation easier? Individual scores were noted and tabulated for further analysis.

2.4 Architecture, Design, and Implementation

Architecture of the simulator consisted of a GUI (see Fig. 4), JS source code (DOM), and a Web Server. GUI was developed in HTML5. When a web request reaches the server, the JS source code (DOM) with GUI is loaded into the client browser. Architecture used to design the simulator was explained in Fig. 4. The main advantage of using client-only architecture was that the UI at the client side depended on the web server for initial loading of the simulator and for some predefined libraries. Since the client-based standalone applications execute fully on client machine, the server was not overloaded with additional communication operations/scientific computations. Preloading of HighCharts UI was used to avoid backend streaming issues while plotting the simulated data. Since 3000 ms of

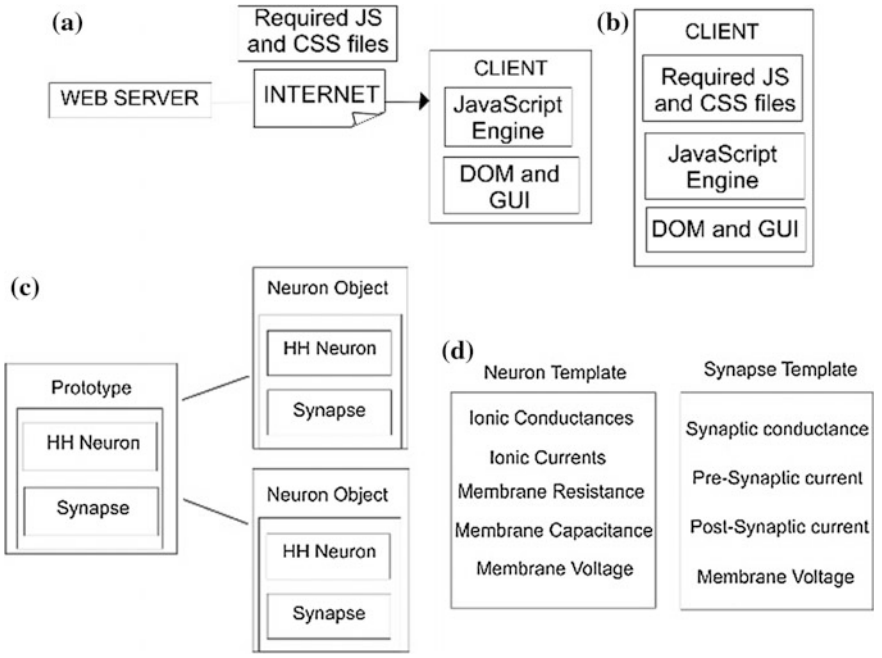

Fig. 4 Architecture used to build the simulator. **a** Neuron simulator server-client architecture, **b** neuron simulator stand-alone architecture, **c** client-side object instantiation, **d** neuron and synapse class templates

simulation was sufficient to simulate functionalities of neuron model, we limited the total simulation time to 3000 ms and this helped avoid data overflow issues. Upcoming versions of neuron simulator have been intended to overcome these restrictions by parallel multiple thread architecture for multicore multithread models used in Servo like browsers [20].

3 Results

3.1 Student's Examination Scores Improved After Performing Simulation-Based Neural Network Experiments

The statistics of student's marks for each question in pretest and posttest showed that, in posttest, 40 % of the students were able to score above 90 % marks whereas the same users did not score as much in their pretest evaluations. All participants scored above 70 % in the posttest improving the class average from the pretest

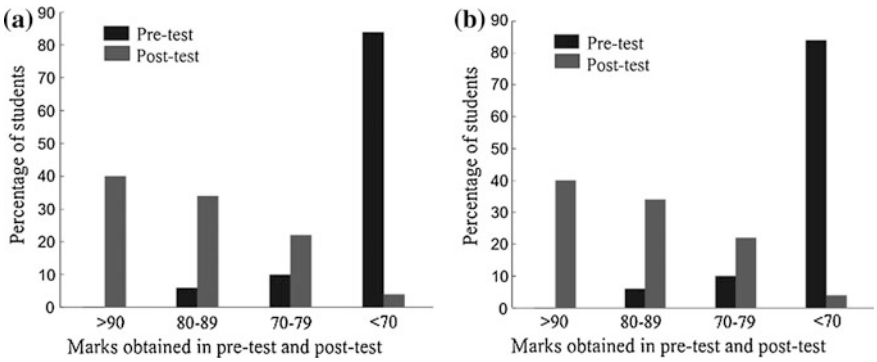

Fig. 5 Performance rate and feedback analysis. **a** User performance in pre- and postsimulation examinations. **b** Feedback analysis of student usage

scenario. Overall results suggested that student's performance increased after they engaged on simulation-based neural network experiments (see Fig. 5a).

In addition, we analyzed student's response for another set of questions given to know the effect of simulation-based experiments in education (see Fig. 5b). From the participants, 88 % of them specified that they support usage of neural network simulator in classroom education. Among 100 students, 78 % of them supported that, with the neural network simulator, they could manage to learn an experiment without the help of an instructor. 82 % of them reported that neural network simulator can be used as a supplementary tool to learn concepts in an interesting way. 85 % of them suggested that neural network simulator helps them to make experimental calculations and their interpretation of outputs easier. Results showed that a significant percentage of students adapted to blended learning environment.

4 Discussion and Conclusion

The network simulator was developed with the goal of online and offline usage to study theoretical biophysics and neural dynamics. We find such virtual lab tools useful to allow students to explore developing the skillsets needed in neurophysiology. The network simulator allows multiple neurons to be configured and run on an offline basis and to simulate small-scale network dynamics. The neurons in such model were individually configured and modeled as cerebellar neurons. Such capability allows students to explore models of neurophysiological studies and will replace our existing virtual simulator at http://vlab.amrita.edu.

With online version, we tested the user behavior on the simulator. We are yet to test the capability on teachers. Student feedback indicated that student examination scores improved after practicing on the simulator and the responses indicated the role of such tools as supplementary learning environments. Further testing of such

methods, to scale for large number of neurons and with spatial configurations, will allow usage of this simulator as hypothesis testing tool. The modeling of DOM and JS-based multicore multithread environments will further allow expansion of realistic brain-like microcircuit models.

Acknowledgments This work derives direction and ideas from the Chancellor of Amrita University, Sri Mata Amritanandamayi Devi. The authors would like to thank Harilal Parasuram, Chaitanya Medini, Asha Vijayan, Rakhi Radhamani, Priya Chelliah for their contributions in this work. This work was partially funded by the Sakshat project of NME-ICT, Ministry of HRD, Government of India and by research for a cause initiative by Embracing the World, M.A. Math.

References

1. Purves, D., Augustine, G.J., Fitzpatrick, D., Hall, W.C., LaMantia, A.-S., McNamara, J.O., Williams, M.S.: Neuroscience. (2004).
2. Eric Kandel, Thomas Jessell, James Schwartz, Steven Siegelbaum, A.J.H.: Principles of Neural Science, Fifth Edition, http://www.mhprofessional.com/product.php?isbn=0071390111, (2000).
3. Gerstner, W., Naud, R.: Neuroscience. How good are neuron models? Science. 326, 379–380 (2009).
4. Gutkin, B., Pinto, D., Ermentrout, B.: Mathematical neuroscience: from neurons to circuits to systems. J Physiol Paris. 97, 209–219 (2003).
5. Markram, H.: The blue brain project. Nat. Rev. Neurosci. 7, 153–60 (2006).
6. Hines, M.L., Carnevale, N.T.: The NEURON simulation environment. Neural Comput. 9, 1179–1209 (1997).
7. Ray, S., Deshpande, R., Dudani, N., Bhalla, U.S.: A general biological simulator: the multiscale object oriented simulation environment, MOOSE. BMC Neurosci. 9, P93 (2008).
8. Bower, J.M., Beeman, D., Hucka, M.: The GENESIS Simulation System, (2003).
9. Touretzky, D., Albert, M., Daw, N., Ladsariya, A., Bonakdarpour, M.: HHsim: Graphical Hodgkin-Huxley Simulator, http://www.cs.cmu.edu/~dst/HHsim/, (2004).
10. Diwakar, S., Parasuram, H., Medini, C., Raman, R., Nedungadi, P., Wiertelak, E., Srivastava, S., Achuthan, K., Nair, B.: Complementing Neurophysiology Education for Developing Countries via Cost-Effective Virtual Labs: case Studies and Classroom Scenarios. J. Undergrad. Neurosci. Educ. 12, A130–9 (2014).
11. Hodgkin, A.L., Huxley, A.F., Katz, B.: Measurement of current-voltage relations in the membrane of the giant axon of Loligo. J Physiol. 116, 424–448 (1952).
12. RINZEL, J.: Mechanisms for Nonuniform Propagation Along Excitable Cables. Ann. N. Y. Acad. Sci. 591, 51–61 (1990).
13. Hines, M.L., Carnevale, N.T.: The NEURON simulation environment. Neural Comput. 9, 1179–209 (1997).
14. Hillle, B.: Ion Channels of Excitable Membranes, http://www.sinauer.com/ion-channels-of-excitable-membranes.html, (2001).
15. D'Angelo, E., Filippi, G. De, Rossi, P., Taglietti, V.: Synaptic excitation of individual rat cerebellar granule cells in situ: evidence for the role of NMDA receptors. J Physiol. 484 (Pt 2, 397–413 (1995).
16. D'Angelo, E., De Filippi, G., Rossi, P., Taglietti, V., Filippi, G. De: Ionic mechanism of electroresponsiveness in cerebellar granule cells implicates the action of a persistent sodium current. J. Neurophysiol. 80, 493–503 (1998).
17. Hodgkin, A.L., Huxley, A.F.: Quantitative description of nerve current. E. J. Physiol. 117, 500–544 (1952).

18. Dayan, P., Abbot, L.F.: Theoretical Neuroscience: Computational and Mathematical Modeling of Neural Systems. MIT Press (2005).
19. Medini, C., Nair, B., D'Angelo, E., Naldi, G., Diwakar, S.: Modeling spike-train processing in the cerebellum granular layer and changes in plasticity reveal single neuron effects in neural ensembles. Comput. Intell. Neurosci. 2012, 359529 (2012).
20. Anderson, B., Bergstrom, L., Herman, D., Matthews, J., McAllister, K., Goregaokar, M., Moffitt, J., Sapin, S.: Experience Report: Developing the Servo Web Browser Engine using Rust. 1–6 (2015).

On Intuitionistic Fuzzy Soft Sets and Their Application in Decision-Making

B.K. Tripathy, R.K. Mohanty and T.R. Sooraj

Abstract Molodtsov introduced soft set theory as a new mathematical approach to handle uncertainty. Hybrid models have been found to be more useful than the individual components. Following this trend fuzzy soft sets (FSS) and intuitionistic fuzzy soft sets (IFSS) were introduced. Recently, soft sets were introduced by Tripathy and Arun (Int J Reasoning-Based Intell Syst 7(3/4):244–253, 2015) [6] using the notion of characteristic function. This led to the redefinitions of concepts like complement, intersection, union of IFSS, Null and absolute IFSS. In this paper, we follow the approach of Tripathy et al. in redefining IFSS and present an application of IFSS in decision-making which substantially improve and is more realistic than the algorithms proposed earlier by several authors.

Keywords Soft sets · Fuzzy sets · FSS · IFSS · Decision-making

1 Introduction

The notion of fuzzy sets introduced by Zadeh [9] in 1965 is one of the most fruitful models of uncertainty and has been extensively used in real-life applications. Molodtsov [5] introduced the concept of soft sets in 1999. Subsequently, many new operations on soft sets were introduced by Maji et al. [3, 4]. As mentioned in the abstract, hybrid models obtained by suitably combining individual models of uncertainty have been found to be more efficient than their components. Several such hybrid models exist in literature. Following this trend, Maji et al. [2] put

B.K. Tripathy (✉) · R.K. Mohanty · T.R. Sooraj
School of Computing Science and Engineering, VIT University,
Vellore, Tamil Nadu, India
e-mail: tripathybk@vit.ac.in

R.K. Mohanty
e-mail: rknmohanty@gmail.com

T.R. Sooraj
e-mail: soorajtr19@gmail.com

D.K. Lobiyal et al. (eds.), *Proceedings of the International Conference on Signal, Networks, Computing, and Systems*, Lecture Notes in Electrical Engineering 396, DOI 10.1007/978-81-322-3589-7_7

forward the concept of FSS by combining the notions of fuzzy set and soft set. Tripathy and Arun [6] defined soft sets through their characteristic functions. This approach has been highly authentic and helpful in defining the basic operations like the union, intersection, and complement of soft sets. Similarly, it is expected that defining membership function for FSSs will systematize many operations defined upon them as done in [8]. Extending this approach further, we introduce the membership functions for IFSS in this paper. Many of soft set theory have been discussed by Molodtsov in [5]. Maji et al. discussed an application of soft sets in decision-making problems [4]. This study was further extended to the context of FSSs by Tripathy et al. in [7], where they identified some drawbacks in [3] and took care of these drawbacks while introducing an algorithm for decision-making. In this paper, we have carried this study further using IFSS instead of FSS in handling the problem of multi-criteria decision-making. Atanassov introduced the concept of IFSS [1]. Later Maji et al. [2] has defined FSS and operations on it. In this paper, we follow the definition of IFSS provided by Tripathy et al. [8]. The major contribution in this paper is introducing a decision-making algorithm which uses IFSS and we illustrate the suitability of this algorithm in real-life situations. Also, it generalizes the algorithm introduced in [7] while keeping the authenticity intact.

2 Definitions and Notions

A soft universe (U, E) is a combination of a universe U and a set of parameters E. Elements of U are denoted by x and those of E are denoted by e. By $P(U)$ and $I(U)$ we denote the set of all subsets of U and the set of all fuzzy subsets of U, respectively.

Definition 2.1 (*Soft Set*) We denote a soft set over (U, E) by (F, E), where

$$F : E \rightarrow P(U) \tag{1}$$

Definition 2.2 (*Fuzzy soft set*) We denote a FSS over (U, E) by (F, E) where

$$F : E \rightarrow I(U) \tag{2}$$

3 Intuitionistic Fuzzy Soft Sets

In this section, we describe the main notions used and the operations of IFFSs. We denote the set of all IF subsets of U by IF (U).

Definition 3.1 A pair (F, E) is called an IFSS over (U, E), where F is a mapping given by

$$F : E \rightarrow IF(U) \tag{3}$$

We denote $\mu^a_{(F,E)}(x)$ as the degree of membership of the element x in the IFSS (F, E) with respect to parameter a and $v^a_{(F,E)}(x)$ as the degree of nonmembership of the element x in the IFSS (F, E) with respect to parameter a.

Let (F, E) and (G, E) denote any two IFSSs on (U, E). Then

Definition 3.2 We say that (F, E) is an intuitionistic fuzzy soft subset of (G, E) iff

$$\mu^a_{(F,E)}(x) \leq \mu^a_{(G,E)}(x) \quad \text{and} \quad v^a_{(F,E)}(x) \geq v^a_{(G,E)}(x) \tag{4}$$

Definition 3.4 The complement of (F, E) in (U, E) is denoted by $(F, E)^c$ such that and clearly $\forall x \in U$ and $\forall e \in E$,

$$\mu^a_{(F,E)^c}(x) = v^a_{(F,E)}(x) \text{ and } v^a_{(F,E)^c}(x) = \mu^a_{(F,E)}(x) \tag{5}$$

Definition 3.5 For any two IFSSs (F, E) and (G, E), their intersection is IFSS (H, E) and $\forall a \in E$, $\forall x \in U$, we have

$$\mu^a_{(H,E)}(x) = \min\left\{\mu^a_{(F,E)}(x), \mu^a_{(G,E)}(x)\right\} \quad \text{and}$$

$$v^a_{(H,E)}(x) = \max\left\{v^a_{(F,E)}(x), v^a_{(G,E)}(x)\right\} \tag{6}$$

Definition 3.6 For any two IFSSs (F, E) and (G, E), their union is IFSS (H, E) and $\forall a \in E$, $\forall x \in U$, we have

$$\mu^a_{(H,E)}(x) = \max\left\{\mu^a_{(F,E)}(x), \mu^a_{(G,E)}(x)\right\} \quad \text{and}$$

$$v^a_{(H,E)}(x) = \min\left\{v^a_{(F,E)}(x), v^a_{(G,E)}(x)\right\} \tag{7}$$

4 Application of IFSS in Decision-Making

Molodtsov discussed several applications of soft set in [5]. Later on Tripathy et al. [8] redefined the concept of IFSS. In this paper, we discuss an application of IFSS in decision-making problems.

Consider the case of a football team manager who wants to buy a new player from the transfer market. Before the manager selects a player, he needs to consider the attributes (parameters) of that particular player. Few parameters of a player can be discipline, loyalty, overall attributes, nationality, transfer fee, etc. If there is one or more parameters like "transfer fee," the values of those parameters affect the decision inversely. We call these parameters as negative parameters. Here, if the

value of the parameter "Transfer fee" increases then the interest of managers will decrease.

We prioritize the parameters by multiplying with priority values given by the team manager. The manager has to give the priorities for each parameter. When a parameter value does not affect the manager's decision then the priority will be 0 (zero). If priority value is not given for one or more parameters then the value of the priority is assumed to be 0 by default and that parameter can be eliminated from further computation. To get even more reduction in computation we can keep only one object if there are some objects with same values for all parameters.

The manager's priority value will be multiplied by the parameter values to obtain the priority table. In this paper, three different Tables 2, 3, and 4 are computed separately for the membership, nonmembership, and the hesitation values. The comparison tables for membership, nonmembership, and hesitation values can be obtained by taking the difference of row sum of an object with others in respective priority table.

Table 1 IFSS (F, E)

U	e_1		e_2		e_3		e_4		e_5	
p_1	0.2	0.5	0.1	0.9	0.2	0.7	0.1	0.8	0.8	0.2
p_2	0.7	0.2	0.3	0.3	0.6	0.2	0.3	0.5	0.3	0.6
p_3	0.4	0.2	0.2	0.5	0.3	0.7	0.1	0.4	0.4	0.6
p_4	0.5	0.4	0.6	0.2	0.6	0.4	0.6	0.3	0.6	0.3
p_5	0.5	0.3	0.4	0.2	0.4	0.3	0.3	0.2	0.3	0.6
p_6	0.2	0.4	0.4	0.4	0.5	0.3	0.4	0.2	0.3	0.4

Table 2 Priority table for membership values

U	e_1	e_2	e_3	e_4	e_5	Row sum
p_1	0.12	0	0.06	−0.05	0.16	0.29
p_2	0.42	0	0.18	−0.15	0.06	0.51
p_3	0.24	0	0.09	−0.05	0.08	0.36
p_4	0.3	0	0.18	−0.3	0.12	0.3
p_5	0.3	0	0.12	−0.15	0.06	0.33
p_6	0.12	0	0.15	−0.2	0.06	0.13

Table 3 Priority table for nonmembership values

U	e_1	e_2	e_3	e_4	e_5	Row sum
p_1	0.3	0	0.21	−0.4	0.04	0.15
p_2	0.12	0	0.06	−0.25	0.12	0.05
p_3	0.12	0	0.21	−0.2	0.12	0.25
p_4	0.24	0	0.12	−0.15	0.06	0.27
p_5	0.18	0	0.09	−0.1	0.12	0.29
p_6	0.24	0	0.09	−0.1	0.08	0.31

In decision table, the score of each object can be obtained by calculating row sum in all comparison tables. The object having highest score will be more suitable to customer's requirement and subsequent values are the next choices. If more than one object is having the same highest value in the score column then the object having higher value under the highest priority column is selected and will continue like this. In this paper, we improved the algorithm provided by Tripathy et al. [8] with the help of score, which gives more precise result.

$$\text{Score} = \mu(1 + h) \tag{8}$$

Equation (8) reduces to only membership score in case of a FSS.

4.1 Algorithm

1. Input the IFSS (F, E) in tabular form.
2. Input the priority given by the customer for every parameter. For negative parameters, the priority value must have to lie in the interval (−1, 0).
3. Multiply the priority values with the corresponding parameter values to get the priority tables for membership, nonmembership, and hesitation values.
4. Compute the row sum of each row in all of the priority tables.
5. Construct the respective comparison tables by finding the entries as differences of each row sum in priority tables with those of all other rows.
6. Compute the row sum for each row in all of the comparison tables to get the membership, nonmembership, and hesitation values for decision table.
7. The decision table can be constructed by taking the row sum values in comparison tables and compute the score using (8).
8. The object having highest value in the score column is to be selected.

The example we consider is as follows:

Let U be a set of players given by $U = \{p_1, p_2, p_3, p_4, p_5, p_6\}$ and E be the parameter set given by E = {Loyalty, Overall attributes, Discipline Transfer fee, Distance}. Consider an IFSS (F, E) which describes the "selection of player," given in Table 1.

Table 4 Priority table for hesitation values

U	e_1	e_2	e_3	e_4	e_5	Row sum
p_1	0.18	0	0.03	−0.05	0	0.16
p_2	0.06	0	0.06	−0.1	0.02	0.04
p_3	0.24	0	0	−0.25	0	−0.01
p_4	0.06	0	0	−0.05	0.02	0.03
p_5	0.12	0	0.09	−0.25	0.02	−0.02
p_6	0.24	0	0.06	−0.2	0.06	0.16

The priority given by the manager for all parameters, respectively, are 0.6, 0.0, 0.3, −0.5, 0.2. The priority table [8] can be obtained by multiplying the values in Table 1 with respective parameter priority values given by the user. This way Tables 2, 3, and 4 are obtained for membership, nonmembership, and hesitation values, respectively.

The respective comparison tables are constructed by finding the entries as differences of each row sum in priority tables with those of all other rows and compute row sum in each of the table (Tables 5 , 6 and 7).

Using the formula (8), the decision table can be formulated (Table 8).

Decision-Making The manager should go for the player p_2 which has highest score. The ordering of players are p_2, p_1, p_3, p_4, p_6, p_5.

Table 5 Comparison table for membership values

P_i	P_j						
	p_1	p_2	p_3	p_4	p_5	p_6	Row sum
p_1	0	−0.22	−0.0.7	−0.01	−0.04	0.16	−0.18
p_2	0.22	0	0.15	0.21	0.18	0.38	1.14
p_3	0.07	−0.15	0	0.06	0.03	0.23	0.24
p_4	0.01	−0.21	−0.06	0	−0.03	0.17	−0.12
p_6	0.04	−0.18	−0.03	0.03	0	0.2	0.06
p4	0.16	−0.38	−0.23	−0.17	−0.2	0	–0.82

Table 6 Comparison table for nonmembership values

P_i	P_j						
	p_1	p_2	p_3	p_4	p_5	p_6	Row sum
p_1	0	0.1	−0.1	−0.12	−0.14	−0.16	−0.42
p_2	−0.1	0	−0.2	−0.22	−0.24	−0.26	−1.02
p_3	0.1	0.2	0	−0.02	−0.04	−0.06	0.18
p_4	0.12	0.22	0.02	0	−0.02	−0.04	0.3
p_6	0.14	0.24	0.04	0.02	0	−0.02	0.42
p_1	0.16	0.26	0.06	0.04	0.02	0	0.54

Table 7 Comparison table for hesitation values

P_i	P_j						
	p_1	p_2	p_3	p_4	p_5	p_6	Row sum
p_1	0	0.12	0.17	0.13	0.18	0	0.6
p_2	−0.12	0	0.05	0.01	0.06	−0.02	−0.12
p_3	−0.17	−0.05	0	−0.04	0.01	−0.17	−0.42
p_4	−0.13	−0.01	0.04	0	0.05	−0.13	−0.18
p_6	−0.18	−0.06	−0.01	−0.05	0	−0.18	−0.48
p_1	0	0.12	0.17	0.13	0.18	0	0.6

Table 8 Decision table

Houses	Membership score	Nonmembership score	Hesitation score	Score
p_1	−0.18	−0.42	0.6	–0.288
p_2	1.14	−1.02	−0.12	1.0032
p_3	0.24	0.18	−0.42	0.1392
p_4	−0.12	0.3	−0.18	–0.0984
p_6	0.06	0.42	−0.48	0.0312
p_1	−0.82	0.54	0.6	–1.312

5 Conclusion

In this paper, we discussed the membership function and operations of IFSS which was introduced by Tripathy et al. in 2015. With this new definition Tripathy et al. redefined many concepts associated with IFSSs and established some of their properties. The application to decision-making provided by Maji et al. had many flaws. In this paper, we discuss an application of IFSS which is more efficient and realistic.

References

1. Atanassov K.: “Intuitionistic Fuzzy Sets”, Fuzzy Set Systems, Vol. 20, (1986), pp. 87–96.
2. Maji P.K., Biswas R. and Roy A.R.: “Fuzzy Soft Sets”, *Journal of Fuzzy Mathematics*, 9(3), (2001), pp. 589–602.
3. Maji P.K, Biswas R. and Roy A.R: An Application of Soft Sets in a Decision Making Problem”, *Computers and Mathematics with Applications*, 44, (2002), pp. 1007–1083.
4. Maji P.K., Biswas R. and Roy A.R.: “Soft Set Theory”, Computers and Mathematics with Applications, 45, (2003), pp. 555–562.
5. Molodtsov D.: “Soft Set Theory—First Results”, Computers and Mathematics with Applications, 37, (1999), pp. 19–31.
6. Tripathy B.K. and Arun K.R.: “A New Approach to Soft Sets, Soft Multisets and Their Properties”, International Journal of Reasoning-based Intelligent Systems, Vol. 7, no. 3/4, 2015, pp. 244–253.
7. Tripathy B.K., Sooraj T.R, Mohanty RK, “A New Approach to Fuzzy soft set theory and its applications in decision making” accepted for presentation at ICCIDM2015.
8. Tripathy B.K., Mohanty RK, Sooraj T.R and K.R. Arun, “A New Approach to Intuitionistic Fuzzy Soft Set Theory and its Application in Decision Making”, Proceeding of ICICT 2015, 9–10th oct, Udaipur (2015).
9. Zadeh L.A.: “Fuzzy sets”, Information and Control, 8, (1965), pp.338–353.

CheckPDF: Check What is Inside Before Signing a PDF Document

Bhavya Bansal, Ronak Patel and Manik Lal Das

Abstract Over the years, digital document signing, particularly PDF (Portable Document Format) document, has gained increasing demand in many applications. The PDF file has a flexible logical structure; therefore, an attacker can take advantage of it to create a polymorphic PDF file which contains the actual document and another hidden object. The polymorphic PDF can be interpreted correctly by both PDF parser and image parser. As a result, when a signer signs the polymorphic PDF content by seeing the original content of the PDF file, the attacker gets the intended content signed by the signer without the signer's knowledge. In this paper, we present a detailed illustration on how a fraudulent document be signed by a legitimate signer with different versions of PDF Reader without his/her knowledge. We provide a countermeasure by which any one can detect the presence of any objects in the PDF file while opening the file with a PDF Reader.

Keywords Digital signature · Polymorphic PDF file · Dali attacks

1 Introduction

Digital signatures [1] are being used widely for authenticating digital documents or identifying the source of the documents. In order to sign a document digitally, the signer uses his/her private key and signs the document. Anyone who has the corresponding public key can verify the digital signature. After introduction of the RSA algorithm [1], several digital signature schemes have been proposed in literature relying on some computationally hard problems. It has been a common

B. Bansal · R. Patel · M.L. Das (✉)
DA-IICT, Gandhinagar, India
e-mail: maniklal_das@daiict.ac.in

B. Bansal
e-mail: bhavyabnsl07@gmail.com

R. Patel
e-mail: ronak0314@gmail.com

D.K. Lobiyal et al. (eds.), *Proceedings of the International Conference on Signal, Networks, Computing, and Systems*, Lecture Notes in Electrical Engineering 396, DOI 10.1007/978-81-322-3589-7_8

practice in electronic commerce applications that service provider and service consumer, both can legally bind transaction details by signing documents digitally. Many applications rely on digital document signing such as insurance payment receipts, digital contracts, tender documents, copyright agreements, e-subscription, and so on. Generally speaking, signing documents digitally not only makes the application user friendly, but also makes it cost effective and paperless service execution. Nevertheless, some precaution must be taken while signing content digitally, as the content may have malicious objects [2–4]. It has been observed that most of times people sign a PDF (portable document format) document with a common misconception that the PDF document [5, 6] is safer than other document types. We note that a PDF file can be a powerful malicious content bearer [7–11]. An attacker can make a polymorphic PDF file and then can provoke a legitimate signer to sign the polymorphic PDF file that contains some hidden object. The main reason for polymorphic nature of the PDF file is that the PDF file has a flexible logical structure in which an attacker can create a file that can be interpreted by a PDF parser (e.g., Adobe reader) and an image parser. As a result, when a signer signs the polymorphic PDF file, the attacker gets the other object (e.g., image) signed by the signer without her/his knowledge. This type of attack is known as Dali attacks [12]. The objective of the attack is as follows.

A dishonest party (say, attacker) creates a polymorphic file which combines a PDF file and a TIFF (tagged image file format) file. The original content in the polymorphic PDF file needs to be signed and the TIFF file is the fraud document which attacker wants to get it signed without signer's knowledge.

The attacker creates a file that displays the original content while opening it with a PDF reader and the content of the fraud object is not displayed in it. When a victim signs the PDF content and sends it back to the requester (attacker), the requester obtains the hidden document signed by the victim signer. For example, a company CEO requires to sign a sell order of goods which values at $500,000. The order is prepared by his manager in a PDF document. The manager prepares the polymorphic PDF document that shows the original sell order of $500,000 and another image document with sell order amount $200,000,000 in a way that when the manager opens the PDF document with a conventional PDF reader (e.g., Adobe [5] or Foxit [13] reader) he can only see the original order which states about $500,000 value. The CEO opens the PDF document and sees that everything is perfect as it shows the order value $500,000 and related statements. The CEO digitally signs the PDF and handover it to his manager. Now, the manager has got the CEO's signature on the order of $500,000 and on the order $200,000,000 as well. The manager now gets the signed order of $200,000,000 and proceeds further to execute it. The CEO can come to know this business deal at a later time, if he audits all the files on his own; otherwise, the CEO will remain unaware of this malpractice.

Our Contributions We present a detailed illustration of how a PDF document signing can suffer with polymorphic attacks. We briefly sketch out the logical structure of PDF and TIFF file. Then, we give a detailed step-wise illustration of

how the polymorphic PDF attacks can be performed on a target PDF document using both Adobe and Foxit Reader. We provide a countermeasure to resist the attacks on polymorphic PDF document demonstrated in the paper.

Organization of the Paper The remainder of the paper is organized as follows. Section 2 gives some preliminaries that make the paper self content. Section 3 explains the attacks on polymorphic PDF document. Section 4 provides our observation and discusses on suggested countermeasure to resist the attack. We conclude the paper with Sect. 5.

2 Preliminaries

2.1 PDF File Structure

PDF file structure is a hierarchy of different objects logically connected to each other. Broadly, the PDF file structure consists of four components [5]: Objects, File Structure, Document Structure, and Content Streams. The Objects include boolean, numeric, string, array, name, dictionary, stream, and null type. The file structure determines how objects are accessed and updated inside the PDF file. Each PDF file is composed of a header, a body, a cross-reference table (Xref), and a trailer. We note that a PDF reader reads the document from end to beginning, because it needs to encounter Xref table first and then can find any objects without scanning the whole document. The document structure specifies how objects are used to represent several parts of the PDF document, such as pages, images, fonts, animations, etc. It describes the hierarchy of the objects in the body of the PDF file. The stream objects that contain a sequence of instructions describe the appearance of the page and the graphical entity. Figure 1 depicts the PDF file structure.

Header - %PDF-1.4

Body
7 0 obj.<</Metadata 4 0 R/Pages 3 0 R/Type/Catalog/PageLabels 1 0 R>>.endobj.

8 0 obj.<</CropBox[0 0 612 792]/Parent 3 0 R/Contents 11 0 R/Rotate 0/MediaBox[0 0 612 792]/Resources 9 0 R/Type/Page>>.endobj.

Cross Reference Table (Xref)

.. xref..6 9..0000000016 00000 n..0000000626 00000 n..0000000703 00000n
..0000000830 00000 n..

Trailer
trailer..<</Size 6>>..startxref..116..%%EOF..

Fig. 1 PDF file structure

Nowadays, PDF document reading, editing, and signing are a common practice in many applications. Adobe Reader [5, 6] and Foxit Reader [13] are two standard PDF readers widely used in practice.

2.2 The TIFF File Structure

Tagged Image File Format (TIFF) [14] is a file format used for storing images. It was originally created by the company Aldus and now adopted by Adobe System. TIFF file structure envelops the entire image data in structures called as Image File Directories (IFDs). An IFD is a two-dimensional array that specifies the image parameters such as resolution, pallets, colors. In TIFF structure, IFDs can be placed anywhere and therefore, the document must contain the pointer to the first IFD. This pointer is grouped into the first 8 bytes of the TIFF header and these bytes represent as

(i) The first two bytes identify the TIFF format and byte order.
(ii) The next two bytes form what is called as magic number, used to identify the TIFF format.
(iii) Last 4 bytes are offset to the first IFD.

The TIFF file structure, header, and IFDs are depicted in Figs. 2, 3 and 4, respectively.

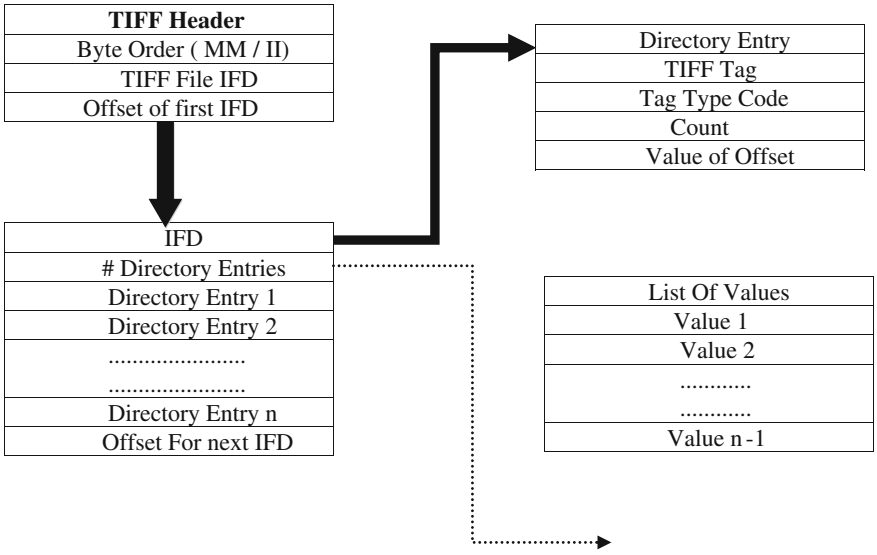

Fig. 2 TIFF FILE structure

Length	Value
2	**Byte Order** (0x49,0x49) for little endian ('I', 'I') (0x4D,0x4D) for Big endian ('M', 'M')
2	**TIFF ID** Always (0x00 , 0x2A)
4	**Offset to 0th IFD** From the start of the TIFF header

Fig. 3 TIFF file header structure

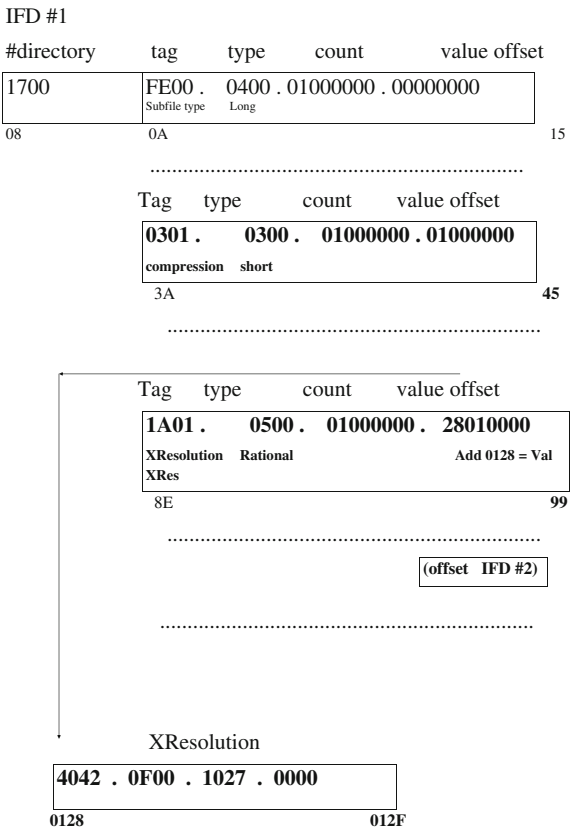

Fig. 4 IFD structure

3 A Step-Wise Illustration of the Attack on Polymorphic PDF Document Signing

The process consists of three phases—setup, sign, and extract, as explained below.

3.1 Setup

The setup phase has the following steps:

(i) A PDF file, named *original.pdf*, is created. Suppose that the file shows a sell order of $200,000, to be signed by the company CEO.
(ii) A TIFF file, named *fraud.tif*, is created with a order value $500,000. Suppose that the manager of the company wants to get the fraud document signed by the CEO while signing the original.pdf. We note that the header of the PDF file can be placed anywhere within the first 1024 bytes of the file.
(iii) A polymorphic file, named *polymorphic.tif*, is created by copying the whole contents of the *original.pdf* file and pasting it after the first 8 bytes of the *fraud.tif* file. In order to make the polymorphic file compatible with Adobe/Foxit reader that should show the content of the original.pdf, the manager adds the trailer of *original.pdf* file at the end of the polymorphic file.
(iv) Because of insertion of the *original.pdf* into the TIFF file after the first 8 bytes, the pointers in the *polymorphic.tif* file gets shifted, therefore, these need to be pointed to the correct locations so that the image reader can read the extracted image file from the polymorphic file.

3.2 Signing the Document

The polymorphic file needs to be manipulated so as to make the file compatible with image reader. Following steps illustrate how the forged document gets signed by the target signer without his/her knowledge.

(i) *Modify the header* The last 4 bytes of sequence `4949.2A00.0800.0000` in the TIFF file are the offset to the first IFD. It is important to note that the address `0800.0000` corresponds to `1700.FE00.0400.0100`. To fix this problem in the polymorphic file, the attacker has to find the sequence `1700.FE00.0400.0100` in the polymorphic file, which will point to the 1781 h location. Now, the attacker should change the header of the polymorphic file to `4949.2A00.8117.0000` (note that 1781 h in big-endian becomes 8117 h). The structure of the new position of IFD is shown in Fig. 5.

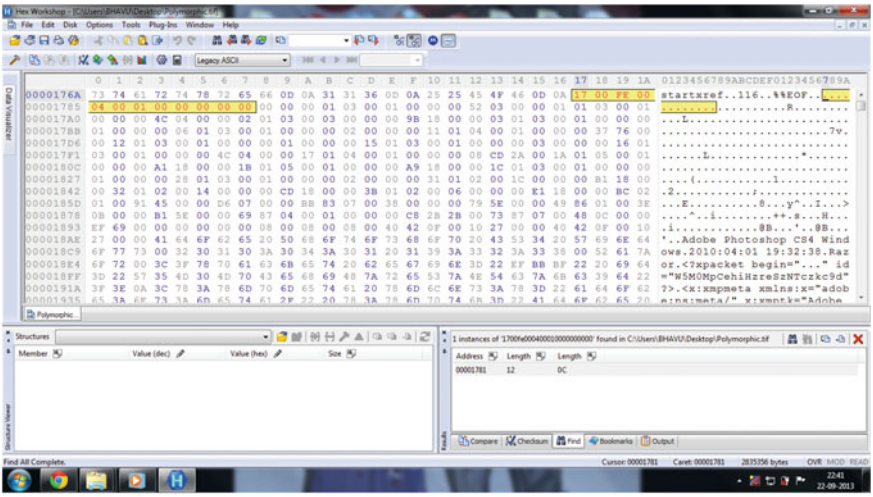

Fig. 5 New position of IFD

(ii) *Modifying the parameters* In order to make the file compatible with an image parser, there are some changes to be made in the TIFF parameters. One can use any standard tool for making the necessary changes of the TIFF file. The parameters that require changes are BitsPerSample, X-resolution, Y-resolution, and strip offsets. The changes are being indicated (see the column 1 and column 3) in Fig. 6.

(iii) *Change the extension of the polymorphic file* The polymorphic file, *Contract.pdf.tif*, needs to be changed to *Contract.pdf*, so that Adobe/Foxit reader can open the file without any error message.

Contract.tif	Attribute	Contract.pdf.tif
4949	Byte order	4949
2A00	Magic Number	2A00
0800.0000	Offset IFD #1	8117.0000
0201.0300.03000000.22010000	Bits Per Sample Offset	0201.0300.03000000.9B180000
1101.0400.01000000.BE5E0000	Strip Offsets	1101.0400.01000000.37760000
1A01.0500.01000000.28010000	Offset XResolution	1A01.0500.01000000.A1180000
1B01.0500.01000000.30010000	Offset YResolution	1B01.0500.01000000.A9180000
3101.0200.1C000000.38010000	Software	3101.0200.1C000000.B1180000
3201.0200.14000000.54010000	Date/Time	3201.0200.14000000.CD180000
3B01.0200.06000000.68010000	Artist	3B01.0200.06000000.E1180000
BC02.0100.91450000.6E010000	Too	BC02.0100.91450000.D6070000
BB83.0700.38000000.00470000	RichTIFFPTC	BB83.0700.38000000.795E0000
4986.0100.3E0B0000.38470000	Photoshop	4986.0100.3E0B0000.B15E0000
7387.0700.480C0000.76520000	ICC Profile	7387.0700.480C0000.EF690000

Fig. 6 Modified TIFF parameters in the polymorphic file

(iv) *Open the polymorphic file with Adobe/Foxit* The victim opens the polymorphic file (*Contract.pdf* that shows the original content, while hiding the fraud content inside it.

(v) *Sign the PDF file* The target victim signs the PDF document using a standard digital signature algorithm (e.g., RSA [1]) supported by Adobe/Foxit. Once the *Contract.pdf* is signed, it is saved as *Contract.pdf.pkcs7*. After that, the signed file is sent to the manager (acting as the attacker). The manager now has victim's signature on both original content and fraud content.

(vi) The manager changes the file extension to *Contract.tif*. Now, the fraud document has signature of the victim.

4 Observation and Countermeasure

Observation We have experimented the phases explained in Sect. 3 with Foxit and Adobe reader. With Foxit reader (version 6) and Adobe reader (version 9), the attacker can successfully get a fraud document signed by the victim signer without his/her knowledge. We then experimented the phases in Adobe reader (version 11). While opening the polymorphic file in Adobe reader (version 11), a generic error message "…could not open the file as it not supported or damaged…" is displayed. However, the error message does not provide any specific reasons (e.g., hidden object). Instead, the Adobe reader gives an impression that the file might have been corrupted, though it is not. User, while opening the file, should get some specific message whether the file is really corrupted, has some hidden objects, or malicious, etc.

Countermeasure The main reason of the attack explained in Sect. 3 is due to the flexible structure of PDF and TIFF file. The header in PDF file format can be placed anywhere within the first 1024 bytes of the file. As in TIFF file format, the 4 bytes offset in the header can be placed anywhere in the file. In the polymorphic file, the PDF header is placed after first 8 bytes of the TIFF file. While opening the file, if the PDF parser detects an image file header before the PDF header, then it should display a message saying that the file contains another object. The pseudocode of the suggested defense mechanism is given in Algorithm 1.

Algorithm 1 Hidden Object Detection in PDF file

DESCRIPTION: Open the PDF file with any PDF parser. If the file contains any other object in it, it displays an appropriate message.

```
PDF_FLAG = FALSE; TIF_FLAG = FALSE; pattern_1 = "25 50 44 46"; pattern_2 = "49 49 2A 00"
Input the PDF file hex content in a text file: "Sample"
Sample stores all bytes of the input PDF file
Search for PDF Header within the first 1024 bytes of the input file: "Sample"
Rabin_Karp(Sample, pattern_1)
if PDF Header Found then
    PDF_FLAG = TRUE
end if
Search for TIFF Header within the first 1024 bytes of the input file: "Sample"
Rabin_Karp(Sample, pattern_2)
if TIFF Header Found then
    TIF_FLAG = TRUE
end if
if PDF_FLAG && TIF_FLAG == TRUE then
    WARNING: The PDF file contains hidden object...
else
    MESSAGE: File scanning is over. No hidden objects...
end if
return
```

We used Rabin–Karp algorithm [15] to search the pattern in the polymorphic file. The Hex content of the polymorphic file is stored in a text file: "Sample". The algorithm reads from the text file line by line and searches for the pattern supplied in the argument; if found, the algorithm returns the position of the pattern in the text file. The search continues until 1024 bytes of the text file have been read. In order to detect for a hidden object in the PDF file the approach is to search the file structure if there are more than one headers. If so, the file might have some other objects and it should show an appropriate message to the user while opening the file. By seeing a message, the user/signer would get enough information and may stop the signing process of the document. The proposed algorithm can also be used to check for other files. In that case, one has to replace the pattern_2 value with the pattern of the file he is looking for. We note that one could have a dictionary look up collecting a list of headers of various commonly used files that could be hidden in a PDF file to form a polymorphic file. Each time a pdf reader tries to open a specific pdf file he could check whether the hex data of that particular file has suspicious hex codes as mentioned in Fig. 7, thus, producing a warning message that the pdf file might contain a hidden object.

PDF :		25 50 44 46
EXE :		4D 5A
TIFF :		49 20 49
	or	49 49 2A 00
	or	4D 4D 00 2A
	or	4D 4D 00 2B
PNG :		89 50 4E 47 0D 0A 1A 0A
JPEG/JPE :		FF D8 FF E0
	or	FF D8 FF E2
	or	FF D8 FF E3
JAR :		50 4B 03 04
	or	5F 27 A8 89
	or	4A 41 52 43 53 00
	or	50 4B 03 04 14 00 08 00
DOC :		D0 CF 11 E0 A1 B1 1A E1
	or	0D 44 4F 43
	or	CF 11 E0 A1 B1 1A E1 00
	or	DB A5 2D 00
	or	EC A5 C1 00
GIF :		47 49 46 38
DOCX/ODT :		50 4B 03 04
	or	50 4B 03 04 14 00 06 00
RTF :		7B 5C 72 74 66 31
Zip:		37 7A BC AF 27 1C
JS :		4A 53

Fig. 7 List of some commonly used file signatures

5 Conclusion

We discussed how an attacker can create a polymorphic PDF file that contains the actual document and a hidden object (e.g., image) in it which would be interpreted correctly by both PDF parser and image parser. Once a signer signs on a polymorphic PDF file, the attacker obtains the intended document signed by the victim signer. We demonstrated the detailed steps with Foxit reader (ver. 6.0) and Adobe reader (ver. 9.0). Adobe reader (ver. 11) does not show any specific reason for the error message. Instead, it displays a generic message like "could not open…file is corrupted…", which may occur without having any hidden objects in it. We have suggested a countermeasure, which displays a proper error message while opening a polymorphic PDF file with a PDF parser. The limitation of the proposed countermeasure is that matching the first bytes of the file against a set of known signatures, while there are a number of file formats that lack a reliable signature, e.g., HTML [16]. A notable example is the signature used for the JPG format. While the signature is correct according to the specification of the format, several JPG interpreters will allow slightly malformed signatures. Such a malformed signature will bypass the check in PDF parser and still be rendered correctly in a viewer.

References

1. R. Rivest, A. Shamir, L. Adleman. A Method for Obtaining Digital Signatures and Public-Key Cryptosystems. In: Communications of the ACM, 21(2):120–126, 1978.
2. A. Alsaid and C. J. Mitchell. Dynamic Content Attacks on Digital Signatures. In: Information Management and Computer Security, 13(4):328–336, 2005.
3. F. Buccafurri. Digital Signature Trust Vulnerability: A New Attack on Digital Signatures. In: Information Systems Security Association Journal, 2008.
4. P. Laskov and N. Srndic. Static Detection of Malicious JavaScript-bearing PDF Documents. In Proceedings of the Annual Computer Security Applications Conference, pp. 373–382, 2011.
5. PDF Reference. Adobe Portable Document Format Version 1.7. Adobe, November 2006.
6. Adobe Supplement to ISO 32000. Adobe, June 2008.
7. D. S. Popescu. Hiding Malicious Content in PDF Documents. In: Journal of Mobile, Embedded and Distributed Systems, 3(3):102–127, 2011.
8. D. Stevens. Malicious PDF Documents Explained. In: IEEE Security and Privacy, 9(1):80–82, 2011.
9. C. Smutz and A. Stavrou. Malicious PDF Detection using Metadata and Structural Features. In Proceedings of the Computer Security Applications Conference, pp. 239–248, 2012.
10. X. Lu, J. Zhuge, R. Wang, Y. Cao, Y. Chen. De-obfuscation and Detection of Malicious PDF Files with High Accuracy. In Proceedings of Hawaii International Conference on System Sciences, pp. 4890–4899, 2013.
11. N. Srndic and P. Laskov. Detection of Malicious PDF files based on Hierarchical Document Structure. In Proceedings of the Annual Network and Distributed System Security Symposium, 2013.
12. F. Buccafurri, G. Caminiti, G. Lax. The Dali Attack on Digital Signature. In: Journal of Information Assurance and Security, 3(3):185–194, 2008.
13. Foxit Reader Stack Overflow Exploit. http://www.exploit-db.com/foxit-reader-stack-overflow-exploit-egghunter/, [Accessed January 2015].
14. TIFF Revision 6.0, Adobe Systems, 1992. http://partners.adobe.com/public/developer/en/tiff/TIFF6.pdf [Accessed January 2015].
15. R. M. Karp and M. O. Rabin. Efficient Randomized Pattern-Matching Algorithms. In: IBM Journal of Research and Development, 31(2):249–260, 1987.
16. J. Magazinius, B. K. Rios, A. Sabelfeld. Polyglots: Crossing Origins by Crossing Formats. In Proceedings of the ACM Conference on Computer and Communications Security, pp. 753–764, 2013.

Kinematic Analysis of a Two-Wheeled Self-Balancing Mobile Robot

Animesh Chhotray, Manas K. Pradhan, Krishna K. Pandey and Dayal R. Parhi

Abstract This paper describes the development of a two-wheeled self-balancing robot and its kinematic analysis. The system architecture consists of two co-axial wheeled rectangular structure powered by a pair of DC motors. Two separate motor drivers are controlled by pulse width modulated voltage signals received from the Arduino microcontroller board. The attitude determination of the robotic platform can be accomplished by an IMU sensor, which is a combination of accelerometer and rate gyro. After mechanical system design, the velocity decomposition of the two wheels and robot body are analyzed to establish the kinematic model. In this model, local position of the robot is mapped according to the global coordinates. Finally, the kinematic constraints are established for fixed standard wheels of the two-wheeled robot.

Keywords Two-wheeled self-balancing robot · Kinematic model · Kinematic constraints

1 Introduction

Current considerable research on human–robot interaction in the public domain with real-time responses results in the development of two-wheeled mobile robots. These robots have better potential for use in indoor environments as personal

A. Chhotray (✉) · M.K. Pradhan · K.K. Pandey · D.R. Parhi
Robotics Laboratory, Department of Mechanical Engineering, National Institute of Technology, Rourkela, Sundergarh 769008, Odisha, India
e-mail: chhotrayanimesh@gmail.com

M.K. Pradhan
e-mail: manas.pradhan141@gmail.com

K.K. Pandey
e-mail: kknitrkl@yahoo.in

D.R. Parhi
e-mail: dayalparhi@yahoo.com

D.K. Lobiyal et al. (eds.), *Proceedings of the International Conference on Signal, Networks, Computing, and Systems*, Lecture Notes in Electrical Engineering 396, DOI 10.1007/978-81-322-3589-7_9

assistance, tour guidance, surveillance, and as cleaning robots in households. It is much easier to make a two-wheeled robot with tall structure than the bipedal structure without compromising the ability to turn on the spot with greater agility. Rather these robots offer higher levels of mobility and maneuverability than their four-wheeled counterparts due to the ability to negotiate with tight corners and corridors.

This leads the research on two-wheeled self-balancing robot to be accelerated over the last decade in many control and robotic research centers [1–3]. These robots have two co-axial differential drive wheels mounted on either side of an intermediate rectangular body. The center of mass lies above the wheel axles, which actively stabilizes the robot, while traversing over steep hills or slopes. Two-wheeled robots also have smaller footprints and can spin on the spot about a single axis in various terrains. These robots are characterized by their capacity to balance on their two wheels by overcoming the inherent dynamics of the system. This additional maneuverability allows easy navigation on various terrains. These capabilities of two-wheeled robots have the potentiality to solve numerous challenges in society and industry.

Many researchers have discussed several kinematic analysis approaches for various types of robots with a different number of wheels [4, 5]. The kinematic analysis establishes a relation between robot geometry, system behavior, and control parameters in an environment. In this analysis, robot velocity is generated after considering the speed of the wheels, rotation angle, and geometric parameters from the robot configuration [6–8].

2 Mechanical Systems Design

For the robot to be able to balance successfully, it is essential that the sensors provide reliable information about the inclination of the robotic platform and its angular velocity. This is also, of course, to ensuring that the control system, motor drivers, and motors themselves are properly designed. The design process here is completed in several phases. At first 3D sketches of the rectangular body structure with wheels is created through CATIA as shown in Fig. 1. The wheels are placed parallel to each other and driven by two separate motors. As power source battery are placed as high as possible above the wheel axis to get better stability, the power transmission from the motor shaft to the wheel axis is achieved by gear chain assembly.

In the next phase to enable stabilizing control, the two-wheeled robot is equipped with appropriate actuators and sensors, which are connected with each other through microcontroller and motor drivers. An Arduino microcontroller board is having ATmega328 controller and six analog inputs with fourteen digital input or output pins from which six can be used as PWM outputs. The microcontroller sends a suitable signal to PWM generator to generate commands of required force for the DC motor of the two wheels. The sensor used here is an IMU sensor called

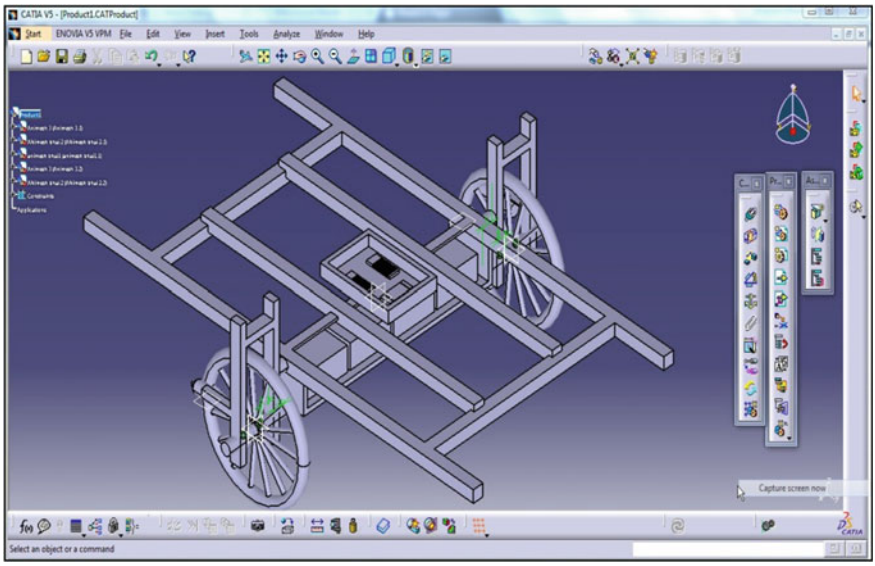

Fig. 1 CAD model of the Lab-built two-wheeled mobile robot

MPU6050 which contains 3-axis accelerometer and a 3-axis gyroscope in a single chip. It is very accurate and captures *X*, *Y*, *Z* axis values simultaneously. Gyroscope measures the rate of change of angular orientation, i.e., the angular velocity with respect to a reference frame. Accelerometers are used to find the rate of change of linear velocity that the body experiences when a force is applied on it. Also two separate motor drivers of 6–16 V, 20 A capacity are used to control the direction and speed of the wheels through motors. These drivers can be interfaced with the microcontroller and receive digital signals as pulse width modulation to control motor velocity.

3 Kinematic Model of Two-Wheeled Mobile Robot

Kinematics is the most basic study to understand the mechanical behavior of the robot. While designing appropriate mobile robots for performing desired tasks and to create suitable control software for any instance of robot hardware, prior knowledge of proper kinematic model is highly essential. Also, Robotic direction cannot be measured instantaneously; rather it is integrated over time. Also, slippages of wheels add some inaccuracies to the motion. Therefore, to get precise robot position is always an extremely challenging task. Since each wheel contributes to robot motion and both are coupled together on robot chassis, their individual constraints combine to figure the overall constraints affecting final robot

motion. Hence, to formulate the kinematic model the actual model is simplified with the following assumptions.

1. The Robot must be considered as a rigid body irrespective of joints and degrees of freedom due to wheel and steering assembly.
2. The plane of operation should be treated as horizontal.
3. Robot motion is pure rolling without slipping, skidding, or sliding between wheel and floor.
4. There should not be any friction for rotation around contact points.
5. Steering axes must be orthogonal to the surface.
6. During motion, the wheel and the horizontal plane is get in touch with a single point.

The understanding of the robot motion starts with analyzing the individual contribution of each wheel toward the whole robot motion. Also the effect of constraints like lateral skidding cannot be overlooked. As the wheels are tied together according to the robot chassis geometry, their constraints are also combined to affect the overall motion. Therefore, while describing a robot's navigation as a function of its geometry and wheel behavior, we have to introduce notations for its motion in a global reference frame and local reference frame as in Fig. 2. In the kinematic analysis of a two-wheeled differential robot the position of the robot is described by a local reference frame as $\{X_L, Y_L\}$ in a global reference frame $\{X_G, Y_G\}$. If the angle of orientation of the robot is θ then its complete location in the global reference frame is given by

$$\xi_G = \begin{bmatrix} x \\ y \\ \theta \end{bmatrix} \tag{1}$$

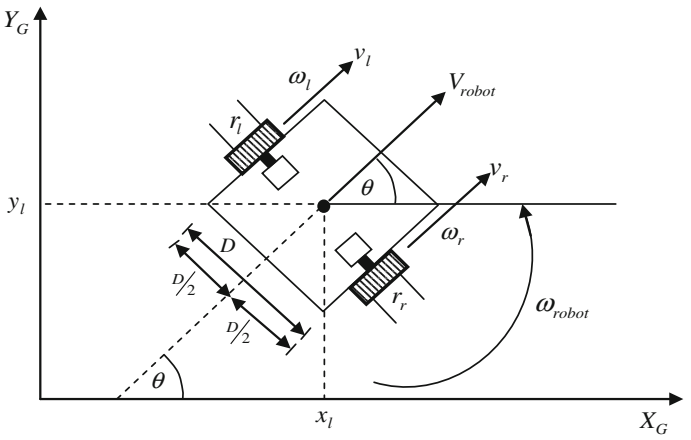

Fig. 2 Two-wheeled differential robot kinematics

Mapping between two frames can be established by considering the rotational matrix as

$$R(\theta) = \begin{bmatrix} cos(\theta) & \sin(\theta) & 0 \\ -\sin(\theta) & \cos(\theta) & 0 \\ 0 & 0 & 1 \end{bmatrix} \tag{2}$$

Therefore, the local position of the robot can be mapped with respect to global coordinates as

$$\dot{\xi}_l = R(\theta)\dot{\xi}_G = R(\theta) \cdot \begin{bmatrix} \dot{x} \\ \dot{y} \\ \dot{\theta} \end{bmatrix} = \begin{bmatrix} \cos(\theta)\dot{x} + \sin(\theta)\dot{y} \\ -sin(\theta)\dot{x} + \cos(\theta)\dot{y} \\ \dot{\theta} \end{bmatrix} \tag{3}$$

Let us consider a two-wheeled robot with two independently driven wheels mounted on the same axis as in Fig. 1. The movement of robot is described by both translation of center and orientation of centroid. The above two action can be accomplished by controlling the wheel speeds of left and right wheels. Robot linear velocity $V_{\text{robot}}(t)$ and angular velocity $\omega_{\text{robot}}(t)$ are functions of the linear and angular velocities of its right wheel, $v_r(t)$, $\omega_r(t)$ and left wheel, $v_l(t)$, $\omega_l(t)$, respectively. The distance between the two wheels is taken as D and the right and left wheel radius are taken as r_r, r_l respectively. The rotation angle of the wheel about its horizontal axis is denoted by φ_r and φ_l accordingly.

The robot velocities can be expressed as

$$V_{\text{robot}} = \frac{v_r + v_l}{2},\ \omega_{\text{robot}} = \frac{v_r - v_l}{D} \tag{4}$$

The kinematic equation can be written in global coordinate or initial frame as

$$\begin{bmatrix} \dot{x}(t) \\ \dot{y}(t) \\ \dot{\theta}(t) \end{bmatrix} = \begin{bmatrix} \cos(\theta) & 0 \\ \sin(\theta) & 0 \\ 0 & 1 \end{bmatrix} \begin{bmatrix} V_{\text{robot}} \\ \omega_{\text{robot}} \end{bmatrix} \tag{5}$$

And in according to local coordinate it is

$$\begin{bmatrix} \dot{x}_l(t) \\ \dot{y}_l(t) \\ \dot{\theta}_l(t) \end{bmatrix} = \begin{bmatrix} r/2 & r/2 \\ 0 & 0 \\ -r/D & r/D \end{bmatrix} \begin{bmatrix} \omega_l(t) \\ \omega_r(t) \end{bmatrix} \tag{6}$$

4 Wheel Kinematic Constraints

The primary step of a kinematic model is to find out the number of constraints that are affecting the motion of each wheel. By assuming that the wheels always remain vertical with pure rolling condition and a single point contact the analysis become

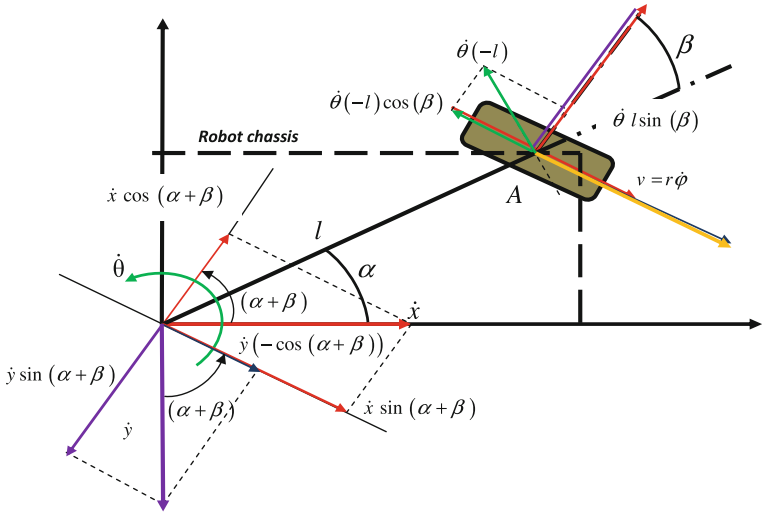

Fig. 3 Fixed standard wheel kinematic constraints

quite simplified. Here in local coordinate, velocity in *Y* axis is always zero; since the possible motion for wheel is to move back and forth along wheel plane and rotate around its contact point with the ground plane as in Fig. 2.

Hence from Fig. 3 the kinematic constraints for a two-wheeled robot having fixed standard wheels can be derived as.

1. Rolling Constraints

$$[\sin(\alpha+\beta) - cos(\alpha+\beta)(-1)cos\beta]R(\theta)\dot{\xi}_l - r\dot{\varphi} = 0 \tag{7}$$

2. Sliding Constraints

$$[\cos(\alpha+\beta)\ \sin(\alpha+\beta)\ l\sin\beta]R(\theta)\dot{\xi}_l = 0 \tag{8}$$

5 Conclusions

The two-wheeled mobile robot can be a better alternative than multi-wheeled and humanoid robots to work in indoor environments like narrow corridors and tight corners. The kinematic analysis establishes the relation between position and orientation of the robot in local reference frame to that of global reference frame. A relation for both linear and angular velocity of the robot has been derived taking

the left and right wheel velocities and robot dimensions. Finally, the kinematic constraints like rolling and sliding constraints are established for fixed standard wheels of the two-wheeled robot.

References

1. Grasser, F., D'arrigo, A., Colombi, S., Rufer, A. C.: JOE: a mobile, inverted pendulum. Industrial Electronics, IEEE Transactions, 49, 107–114 (2002).
2. Anderson, D.P.: nBot Balancing Robot. Retrieved March 1, (2007) http://www.geology.smu.edu/∼dpa-www/robo/nbot.
3. Ooi, R. C.: Balancing a two-wheeled autonomous robot. University of Western Australia, 3, (2003).
4. Morin, P., Samson, C.: Motion control of wheeled mobile robots. In Springer Handbook of Robotics, 799–826. Springer Berlin Heidelberg (2008).
5. Alves, S. F., Ferasoli Filho, H., Rosario, J. M., Rincón, L. K., Yamasaki, R. A.: Conceptual Bases of Robot Navigation Modeling, Control and Applications (2011).
6. Siegwart, R., Nourbakhsh, I. R., Scaramuzza, D.: Introduction to autonomous mobile robots. MIT press (2011).
7. Deepak, B. B. V. L., Parhi, D. R.: Kinematic Analysis of Wheeled Moblie Robot. Automation and Systems Engineering, 5(2) (2011).
8. Novak, G., Seyr, M.: Simple path planning algorithm for two-wheeled differentially driven (2wdd) soccer robots. WISES, 4, 91–102 (2004).

Program Code Understandability and Authenticating Code Predicting Systems: A Metric-Based Approach

Pooja Jha and K. Sridhar Patnaik

Abstract Software metrics have always been an area of research proposing abundant process metrics for quantifying the internal process attributes helpful in predicting the quantified degree of process attributes determined externally. But, the research lacks when question arises about defining metrics for understandability of program code as well as justification of the forecasting systems. Identification of some probable problems with metric reliability and legitimacy is the main concern of this paper. Further, two new metrics: PPCU and EPCU for better program code understandability have been proposed. The research shows effects of quantifying program code on understandability of programmers by postulating certain assumptions. Different aspects of program code understandability can be problematical for a program to some extend affecting the desirable properties of the software. This expansion of work can be treated as a part of future work as far as code understandability is concerned.

Keywords Program code understandability · Metric · Shapiro–Wilk test · Wilcoxon rank-sum tests

1 Introduction

Utilization of software metrics for community of software evolution is increasing for its credible methods to assess, observe, model, and analyze software evolution process [1]. Process metrics for measuring internal process model attributes is always subject of motivation [2]. Besides structural process understandability, many other quality facets influencing understandability exists. Mendling et al. [3] stresses on existence of diminutive knowledge in modeling contributing to an "excellent" process model based on individual understandability. Melcher and

P. Jha (✉) · K. Sridhar Patnaik
Department of Computer Science and Engineering,
Birla Institute of Technology, Ranchi 835215, India
e-mail: pooja.jha.ism@gmail.com

K. Sridhar Patnaik
e-mail: kspatnaik@bitmesra.ac.in

D.K. Lobiyal et al. (eds.), *Proceedings of the International Conference on Signal, Networks, Computing, and Systems*, Lecture Notes in Electrical Engineering 396, DOI 10.1007/978-81-322-3589-7_10

Seese [4] linked reliability and legitimacy of metrics for structural process understandability. This paper attempts to develop prediction system for better code understandability. The remaining of the paper is organized as follows: Sect. 2 discusses the associated work in this area. Some of the definitions and comments and criticism of existing work are covered in Sects. 3 and 4. Section 5 presents program code understandability. Section 6 deals with experimental evaluation and results. Section 7 presents the conclusions with future scope.

2 Related Work

Evaluation-based studies [5] on factors affecting software understandability have been studied and understandability about documentation, structure, components, source code and data is the factor of prime importance. Thereby, a model integral of understandability has been proposed. Empirically, a summarized result in evaluating the relative importance of COCOMO II model drivers [6] aided in understandability prediction. Al-Ja'afer and Sabri [7] worked on tool AUTOMARK++, for assessing the design excellence of Java programs based on CK and LK metrics. Rachel Harrison et al. [8] demonstrated utility of metrics in overall appraisal of the system by use of six properties of metrics for object-oriented design (MOOD). A novel metric set for estimating the testing efforts for object-oriented programs was proposed in [9]. Quality metrics [10] have always been area of interest. Researchers have suggested quality factors for multidimensional model for data warehouse like maintainability, simplicity, completeness, consistency etc. Vanderfeesten et al. [11] proposed CC metric and confirmed that the correlation between CC and SCORE is not significant. The influence of content-related factors on process understandability was inspected by Mendling and Strembeck [12].

3 Measurement and Prediction of Program Code

The domain of process quantification has always been stimulated by the works and consequences of software measurement. Fenton and Pfleeger [13] suggested two main types of measurement; one is **Measurement system**, generally applicable for reviewing an existing attribute by mathematically portraying one or more of its qualities and the other is **Prediction system**, applicable in envisaging some traits in future is based on an experimental model with allied forecasted measures.

4 Annotations and Analysis of Previous Work

Information related to current research in the literature, crucial for imitation and extension of the works is unavailable. Also, sometimes promising factors are changed concurrently and nonscientifically. Many times, only Pearsons correlation

coefficients for measuring linear correlation is recommended and generally only linear regression models for analyzing potential relations between metrics and process understandability are used. Above all, the prevalent factor to criticize is the lack of validity and reliability in these methods.

Some of the questions that arise after going through the literature are:

(1) Does there exist additional significant aspects of program understandability?
(2) How diverse is the foundation of understanding from different programmers perspective of coding?
(3) How can *total process understandability* be figured out?

5 Measuring Program Code Understandability

Aspects of Program Code Understandability: The research aims to incorporate the various aspects of software code understandability necessary for validity of content requirement for metrics. We used aspects rank, coincidence, elitism, and replication as identified by Mendling et al. [3]. Below, we discuss some of the definitions that will be undertaken.

Definition 1 (*Activity period*) For a particular program code t it is defined as the phase between a certain instance in time when t becomes functional and till it terminates. Next, four important aspects of software program coding understandability: *rank*, *coincidence*, *elitism,* and *replication* are discussed.

Definition 2 (*Rank*) The queries regarding program rank, the relations $r\exists$, $r\nexists$, $r\forall \subseteq R \times R$ were used, added with following meanings:

- $(r_1, r_2) \in r\nexists \Leftrightarrow$ No program instance exists for which coding phase of program r_1 ends prior to coding phase of program r_2 initiates.
- $(r_1, r_2) \in r\nexists \Leftrightarrow$ A program instance exists for which coding phase of program r_1 ends prior to coding phase of program r_2 initiates.
- $(r_1, r_2) \in r\forall \Leftrightarrow$ A program instance exists such that, rank of program r_1 ends prior to rank of program r_2 initiates.

Definition 3 (*Coincidence*) The queries regarding program code coincidence, the relations $c\exists$, $c\nexists$, $c\forall \subseteq R \times R$ with the following meanings are used.

- $(c_1, c_2) \in r\nexists \Leftrightarrow$ No program module exists for which programs r_1 and r_2 coding phase coincide or overlap.
- $(c_1, c_2) \in c\nexists \Leftrightarrow$ A program module exists for which coding phase of programs r_1 and r_2 coincide or overlap.
- $(c_1, c_2) \in c\forall \Leftrightarrow$ for each program module, coding rank of programs r_1 and r_2 must coincide at least once.

Definition 4 (*Elitism*) The queries regarding program code elitism or exclusiveness, the relations $e\exists$, $e\nexists$, $e\forall \subseteq R \times R$ were used added with the following meanings:

- $(e_1, e_2) \in e\nexists \Leftrightarrow$ No program module exists for which coding phase of programs r_1 and r_2 executed.
- $(e_1, e_2) \in e\nexists \Leftrightarrow$ A program module exists for which coding phase of programs r_1 and r_2 both are executed.
- $(e_1, e_2) \in e\forall \Leftrightarrow$ for each program module, coding rank of programs r_1 and r_2 are mutually executed.

Definition 5 (*Replication*) The queries regarding code replication, the relations rep_1, rep_2, rep_3, rep_4 $\subseteq R$ with the subsequent meanings are used.

- $r \in \text{rep}_1 \Leftrightarrow$ for every program module, code r is accomplished exactly.
- $r \in \text{rep}_2 \Leftrightarrow$ for every program module, code r is accomplished not once or exactly once, both cases really occur.
- $r \in \text{rep}_3 \Leftrightarrow$ for every program module, code r is accomplished not once or exactly once or more than once. There might be presence of a coding module for which r is accomplished not once and another one for which r is accomplished more than once.
- $r \in \text{rep}_4 \Leftrightarrow$ for every program module, code r is accomplished at least once. There might be presence of a program module for which r is accomplished greater than once.

Definition 6 (*Personal program coding understandability*) The program coding metric in understandability $U_a(p, s)$ of code a of program p by programmer s is proposed as the ratio of the standard deviation of the program code to the mean of Euclidean metric given by Eq. 1

$$U_a(p, s) = \frac{\text{Standard Deviation of Prog Code}}{\text{Mean of Euclidean metric}} \tag{1}$$

Definition 7 (*Estimated program coding understandability*) The estimated program coding understandability $\tilde{U}_a p(a, s)$ of code a inside of program p and programmers S is defined as the mean of personal program coding understandability of p by the subject of S.

$$\tilde{U}_a p(a, S) = \frac{\sum \tilde{U}_a p(a, S), a \in \{r, c, e, \text{rep}\}}{|s|} \tag{2}$$

Moreover, the true expected values of the random variables for the different aspects of program code understandability are determined for its confidence and the width of these intervals may be reduced for more complex codes. In the mean time, the assurance of the true expected value will be rising.

Definition 8 (*Upper limit of programs*) The maximum or upper limit $|P_{a,\max(p)}|$ of probable various codes $a \in \{r, c, e, \text{rep}\}$ for a program p having n programs is

$$|P_{c,\max(p)}| = |P_{c,\max(p)}| = n(n-1) \tag{3}$$

$$= |P_{e,\max(p)}| = \frac{n(n-1)}{2} \tag{4}$$

$$= |P_{\text{rep},\max(p)}| = n \tag{5}$$

Hypothesis 1 The metric, referred as personal program coding understandability $\tilde{U}_a p(a, s_i)$ of a program p are distributed normally and it takes different values. Definition given in Eq. 2 can be used for predicting the probable value of that variable.

Hypothesis 2 The different characteristic of understandability about program code results in dissimilar values $\tilde{U}_a p(a, s_i)$ of a program p. Therefore, it becomes crucial to measure every facet for obtaining overall program code understandability as well as, existence of other characteristics of process understandability.

6 Experimental Assessment and Results

6.1 Investigational Design

In the investigational process, we assign 30 java programs to be developed by about 15 novice programmers to test their understandability about the programming language. Based on their attempt to develop, the *Euclidean Metric* was computed to know the degree of association with best code. This is given as in Eq. (6).

$$d = \sqrt{\sum_{i=1}^{v} (p1_i - p2_i)^2} \tag{6}$$

where the difference between two programmers' scores are squared and summed for v programs. For instance, the distance between coding of third program for programmers p1 and p2 is given as: $d = \sqrt{(p1_3 - p2_3)^2}$. The research comprises of 30 programs, $P_{r,\max}(p)$ = 870, $P_{c,\max}(p) = P_{e,\max}(p)$ = 435, and $P_{\text{rep},\max}(p)$ = 30 are calculated from Eqs. 3, 4, and 5.

7 Results

Tables 1 and 2 show the metric and statistical values calculated for the same, respectively. The personal program coding understandability (PPCU) values of various programmers are depicted in Fig. 1.

Table 1 A sample metric values for different programs

Metric types	Program number						
	P1	P2	P3	P4	…	…	P30
Total lines	14	35	34	40	…	…	57
Avg line length	21	83	41	26	…	…	15
Code lines	13	78	35	36	…	…	20
Comment lines	12	28	39	36	…	…	41
White space lines	11	15	40	31	…	…	39
Code(comment + white space) ratio	15	60	37	27	…	…	22
Code/comment ratio	20	15	28	31	…	…	33
Code/total lines ratio	14	24	40	24	…	…	39

Table 2 Statistical values calculated for different metrics

Metric types	Min	Max	Mean	Median	Stan.deviation
Total lines	13	57	1.13	26	12.02
Avg line length	14	83	1.36	26	16.38
Code line	13	78	1.16	24	16.21
Comment lines	11	56	1.3	28	11.23
White line space	11	60	1.33	29	11.42
Code/(comment + whitespace) ratio	14	60	1.23	33	12.06
Code/comment ratio	13	60	0.933	27	12.84
Code/total lines ratio	14	83	1.33	35	14.04

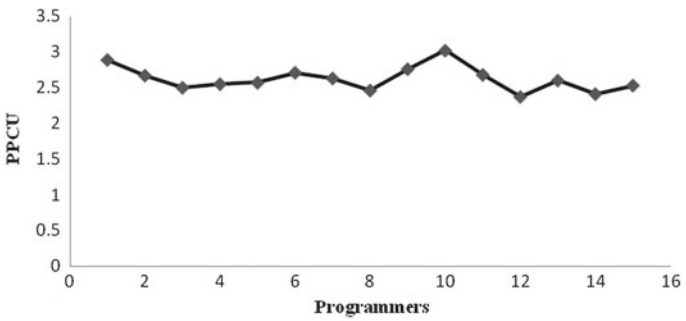

Fig. 1 Personal program coding understandability

Table 3 Shapiro–Wilk test for Hypothesis 1

Parameters	Value
Mean	43.23
Standard deviation	3.93
Variance	15.51
Kurtosis	0.533
Calculated Shapiro–Wilk statistic (W)	0.868
Calculated Shapiro–Wilk p-value	0.031
Critical value of W (5 % significance level)	0.881

Regarding Hypothesis 1 Shapiro–Wilk test [14] is conducted for every program under survey for first hypothesis test (stated above), the null hypothesis is rejected as data is not normally distributed as p-value is <0.005. Again, the calculated value of W is less than its critical value, thereby, the null hypothesis is again rejected. We also computed confidence intervals at 95 % for the estimated program understandability values of the various programmers (Table 3).

Table 4 shows the same. Figure 2 depicts the EPCU.

Regarding Hypothesis 2 Wilcoxon rank-sum tests were selected for testing our second hypothesis (stated above), as these tests do not require normally distributed data. As calculated value of W is less than the critical value of W the null hypothesis is rejected. Also, the result is found to be significant as p-value is <0.005 and the z-score is found to be -3.4

Table 4 Estimated process understandability values and 95 % confidence intervals for the different programmers

Programmer	$\tilde{U}_a p(a,s)$	Standard deviation	Mean of Euclidean metric
S1	2.89	110.95	38.43
S2	2.67	107.51	40.25
S3	2.50	100.48	40.26
S4	2.55	116.42	45.65
S5	2.57	112.31	43.78
S6	2.71	117.12	43.19
S7	2.63	108.79	41.36
S8	2.46	103.73	42.09
S9	2.76	117.63	42.689
S10	3.02	132.71	43.92
S11	2.68	134.49	50.14
S12	2.37	93.06	39.21
S13	2.60	111.92	43.05
S14	2.41	127.87	53.1
S15	2.53	104.6	41.34

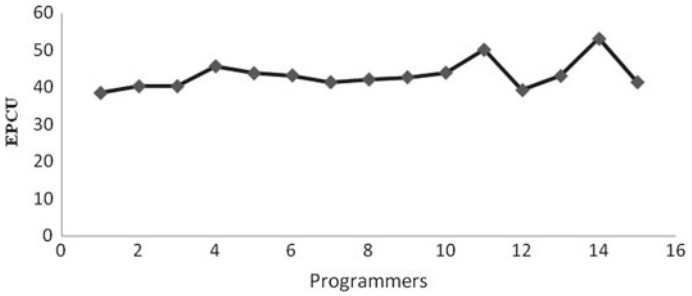

Fig. 2 Estimated program coding understandability

8 Conclusions and Future Work

The paper highlights work on measuring program code understandability and fundamentals about measurement and prediction systems through tangible and comprehensive definitions. The research supports our hypotheses but asking only limited questions can cause values for program understandability vary from the actual values. In future, additional research with larger program codes and more programmers and to test whether the effect of different values for the different aspects of program code understandability becomes even more obvious can be explored. Further, there might be other aspects of program code understandability which are not within the scope of this research.

References

1. W.Li, J.Talburt: Empirically Analysing Object-Oriented Software Evolution. J.of Object-Oriented Programming, Vol.11, pp 15–19 (1998).
2. Joachim Melcher, Detlef Seese: Process measurement: Insights from software mea-surement on measuring process complexity, quality and performance. Research report, Universit at Karlsruhe (TH), Institut AIFB (2008).
3. Jan Mendling, Hajo A. Reijers, Jorge Car-doso.: What makes process models understand-able? In Gustavo Alonso, Peter Dadam, and Michael Rosemann, editors, Business Process Management: Proceedings of the 5th Interna-tional Conference BPM 2007, vol.4714, LNCS, pp 48–63 (2007).
4. Joachim Melcher, Detlef Seese.: Towards validating prediction systems for process under-standability: Measuring process understandabil-ity. In Viorel Negru, Tudor Jebelean, Dana Petcu, and Daniela Zaharie, editors: Proceedings of the 10th International Symposium on Symbolic and Numeric Algorithms for Scientific Computing (SYNASC 2008), pp 564–571 (2008).
5. Jin-Cherng Lin, Kuo-Chiang Wu: A Model for Measuring Software Understandability, Proceedings of The Sixth IEEE International Conference on Computer and Information Technology (2006).
6. Malik, A., Boehm, B.,Brown, A. W.: Predicting Understandability of a Software Project Using COCOMO II Model Drivers. 23rd International Forum on COCOMO and

Systems/Software Cost Modeling and ICM Workshop 3, October 27–30, Los Angeles, USA (2008).
7. Jubair Al-Ja'afer, Khair Eddin Sabri.: Automark ++ a Case Tool to Automatically Mark Student Java Programs, The International Arab Journal of Information Technology, Vol. 2, No. 1 (2005).
8. Harrison, R.: An evaluation of the MOOD set of object-oriented software metrics, IEEE Transactions on Software Engineering, Vol. 24, Issue: 6, pp491 – 496 (1998).
9. Periyasamy, K.: A New Metrics Set for Evaluating Testing Efforts for Object-Oriented Programs, Technology of Object-Oriented Languages and Systems(TOOLS-30), Proceedings of IEEE, August, pp.84–93 (1999).
10. Manuel Angel Serrano,Coral Calero, Houari A. Sahraoui, Mario Piattini.: Empirical studies to assess the understandability of data warehouse schemas using structural metrics, Software Quality J, pp 79–106 (2008).
11. Irene Vanderfeesten, Hajo A. Reijers, Jan Mendling, Wil M. P. van der Aalst, Jorge Car-doso.: On a quest for good process models: The cross-connectivity metric. In Zohra Bellahs 'ene and Michel L eonard, editors, Advanced Information Systems Engineering: Proceedings of the 20th International Conference (CAiSE 2008), vol.5074 of LNCS, pp 480–494 (2008).
12. J. Mendling, M. Strembeck,: Influence factors of understanding business process models: in Business Information Systems: Proceedings of the 11th International Conference (BIS 2008), ser. Lecture Notes in Business Information Processing, W. Abramowicz and D. Fensel, Eds., vol. 7, pp. 142–153 (2008).
13. N. E. Fenton, S. L. Pfleeger, Software Metrics: A Rigorous and Practical Approach, 2nd ed. International Thomson Computer Press (1996).
14. S. S. Shapiro, M. B. Wilk.: An analysis of variance test for normality (complete samples), Biometrika, vol. 52, no. 34, pp 591–611 (1965).

Fuzzy Sliding Mode-Based STATCOM for Stability and Reactive Power Compensation in DG-Based Power System

Asit Mohanty, Meera Viswavandya, Sthitapragyan Mohanty and Pragyan Paramita

Abstract The objective of the paper is to study the reactive power regulation and stability study of an isolated wind-fuel cell hybrid power system. A Fuzzy sliding mode-based STATCOM controller has been considered for compensating reactive energy in a wind-diesel-fuel cell-based remote hybrid power system. For detailed analysis and simulation, a transfer function small signal model of the hybrid power system has been considered. A double-fed induction generator-based wind turbine and fuel cell are the main constituents of hybrid system with a diesel generator as backup. The system performance is studied with a random variation of loads and wind power input. Further the system performance is improved and analyzed with the incorporation of Fuzzy sliding mode-based STATCOM controller.

Keywords Wind-diesel-fuel cell · Voltage stability · Reactive power · Fuzzy sliding mode controller

1 Introduction

According to demand, distributed energy resources either operate in scattered manner or in grid inter connection mode [1]. Complexity of centralized control in the interconnected power system leads to decentralized control as it improves the system performance. It is in isolated mode and decentralized system issues like

A. Mohanty (✉) · M. Viswavandya · S. Mohanty
College of Engineering & Technology Bhubaneswar, Bhubaneswar, India
e-mail: asithimansu@gmail.com

M. Viswavandya
e-mail: mviswavandya@rediffmail.com

S. Mohanty
e-mail: msthitapragyan@gmail.com

P. Paramita
VSSUT Burla, Sambalpur, India
e-mail: pragyanmohanty.design@gmail.com

D.K. Lobiyal et al. (eds.), *Proceedings of the International Conference on Signal, Networks, Computing, and Systems*, Lecture Notes in Electrical Engineering 396, DOI 10.1007/978-81-322-3589-7_11

voltage irregularities and reactive energy imbalances happen repeatedly and are consequently taken care of [2] FACTS devices always play an important role and are utilized for overall compensation of the reactive energy of the hybrid power network. They not only stabilize the system voltage but also helps in angle stability studies [3]. Issues like stability improvement and reactive power management are the most important aspects in hybrid power system and should be addressed with a lot of care. Imbalance in these issues occur due to the wide variation of load and irregular availability of renewable energy sources and it leads to unwanted voltage variations with fluctuations in other system parameters [3].

Before the FACTS devices, mechanically switched capacitors and reactors were generally used to improve the steady-state power flow in regulating the system voltage as well as voltage along the lines but static compensators. Nowadays compensators like SVC, STATCOM, UPFC are regularly utilized for stability improvement of the hybrid power network. The STATCOM compensator gives rise to shunt compensation which is exactly same in its working as SVC but unlike SVC it carries voltage-based source converter (VSC) in place of shunt-operated capacitors and reactors. STATCOM has been an active FACTS device, that manages not only the voltage magnitude but also angle (phase) in a short period of time. This compensator also possesses capability to increase the network damping as well as the terminal voltage profile of the discussed hybrid power system. STATCOM in comparison to the conventional SVC always has more reactive current output at small voltage and has quicker response. The device is a better choice in comparison to SVC as it has better stability control capability, lower harmonics with smaller size, etc.

STATCOM is basically made of three-phase inverter (with a pulse-width modulation-based inverter) with silicon-controlled rectifiers, MOSFETs, and IGBTs. It is also having a DC capacitor for providing DC voltage to the inverter. The device consists of a reactor having the output of the inverter connected to the AC supply side and having number of filter elements for filtering purpose that includes high frequency components. A three-phase voltage has been generated through the inverter from the DC side capacitor and is synchronized with the AC supply. The inductor linked with the device makes contact of the voltage with the AC supply side. Basic controls in STATCOM are AC voltage management of power system, i.e., hybrid power system, and is done by managing reactive power between the STATCOM device and different components of hybrid power system. Another aspect of this reactive power management is that, the DC voltage generated across the capacitor, through which the real power flows from the STATCOM to the hybrid power system, has been controlled. PI-based controllers always provide balancing controls at the same time, whenever the AC and DC regulators are designed. The fixed parameters of PI controllers are not adequate for providing negative damping for any system parameters with all sorts of loading conditions. The compensation technique of STATCOM has been used in this paper with linear configuration. The hybrid power system equations have been linearised around an operating point and small signal transfer function-based equations have been developed for this particular problem. In the linearised hybrid system model When

STATCOMs are finely tuned to respond the small-scale and large-scale disturbances. Many times the PI controllers are used in STATCOMs to designate internal controllers for distribution and enable them to mitigate voltage flicker. SVC and STATCOM devices use PI controllers frequently and are cited in many papers. But in this paper STATCOM as a compensator has been proposed. Vital controls which are possible through the voltage-controlled STATCOM are voltage magnitude and phase angle. The proposed compensator goes through a wide range of operating conditions with numerous disturbances like wind power, fuel inputs, and load variation and despite all these disturbances, this controller provides reliable and optimum damping characteristics. Due to certain demerits and limitations, the PI controller fails to achieve good results. To overcome this, Fuzzy Sliding Mode Controller (FSMC) is employed to achieve and ensure the stability of the controller [4–9].

2 Detailed Mathematical Modeling

For the performance and dynamics of the isolated wind-diesel-fuel cell hybrid system, a small signal model of DFIG-based wind turbine is considered working in hybrid with synchronous generator-based diesel generator as back up. The system parameters are mentioned in Appendix.

2.1 Modeling of Fuel Cell

Fuel cell as shown in Fig. 2 generally consists of three main elements that are reformer, stack, and power conditioner. As the electrical, chemical, and thermodynamic processes are complex and offer nonlinear behavior, the systems become complicated models. It is difficult to estimate the parameters of such models, but for fuel cell connected with full controlled inverters with large capacitors, energy storage devices, the voltage or the reactive power has been assumed to be controlled by controlled inverters.

In a typical isolated hybrid system the entire generations like wind, fuel cell, and diesel act together and close to the load and the total power output is pumped to the common bus, i.e., point of common coupling (PCC) and all the loads are connected to the bus bar as receivers of power as shown in Fig. 1. Basic aim behind this arrangement is to find out a reactive power-balanced equation. The system inputs (generations) and the outputs go through a small change prompting the system load bus voltage to change accordingly (Fig. 2).

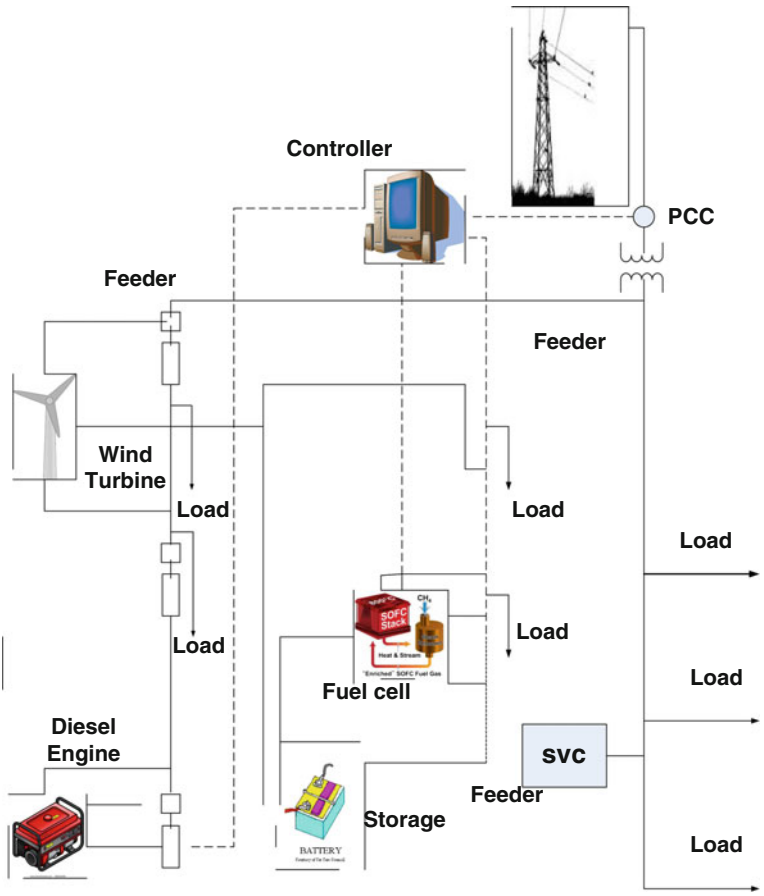

Fig. 1 Standalone wind-diesel-fuel cell hybrid system

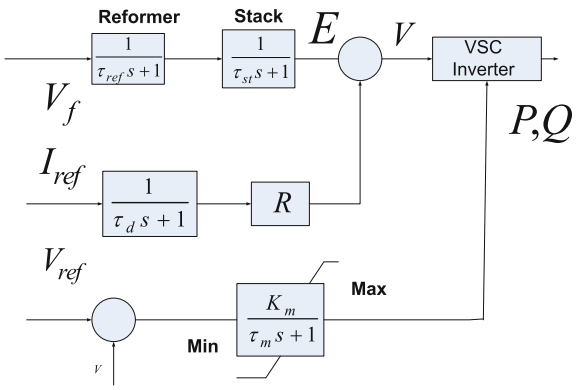

Fig. 2 Transfer function of fuel cell

The balanced equation of reactive power of Synch Gen, Fuel Cell, IG, STATCOM, and Load is expressed as

$$\Delta Q_{\mathrm{FC}} + \Delta Q_{\mathrm{SG}} + \Delta Q_{\mathrm{COM}} = \Delta Q_{\mathrm{L}} + \Delta Q_{\mathrm{IG}}$$

Reactive balanced equation of wind-diesel-fuel cell system

$$\Delta Q_{\mathrm{FC}} + \Delta Q_{\mathrm{SG}} + \Delta Q_{\mathrm{COM}} - \Delta Q_{\mathrm{L}} - \Delta Q_{\mathrm{IG}}$$

$$\Delta Q_{\mathrm{FC}} + \Delta Q_{\mathrm{SG}} + \Delta Q_{\mathrm{COM}} - \Delta Q_{\mathrm{L}} + \Delta Q_{\mathrm{IG}} = \frac{\mathrm{d}}{\mathrm{d}t}(\Delta E_{\mathrm{m}}) + D_{\mathrm{V}}\Delta V$$

$$\Delta V(S) = \frac{K_{\mathrm{V}}}{1 + ST_{\mathrm{V}}}[\Delta Q_{\mathrm{SG}}(S) + \Delta Q_{\mathrm{COM}}(S) + \Delta Q_{\mathrm{FC}}(S) - \Delta Q_{\mathrm{L}}(S) - \Delta Q_{\mathrm{IG}}(S)]$$

The synchronous generator equation is given by

$$Q_{\mathrm{SG}} = \frac{(E_q^{'} V\cos\delta - V^2)}{X^{'}d} \quad \text{and} \quad \Delta Q_{\mathrm{SG}} = \frac{V\cos\delta}{X^{'}d\Delta E^{'}q} + \frac{E^{'}q\cos\delta - 2V}{X^{'}d\Delta V} \tag{1}$$

$$\Delta Q_{\mathrm{SG}}(s) = K_{\mathrm{a}}\Delta E_q^{'}(s) + K_{\mathrm{b}}\Delta V(s) \quad K_{\mathrm{a}} = V\cos\delta \Big/ X^{'}d$$
$$K_{\mathrm{b}} = E^{'}q\cos\delta - 2V \Big/ X^{'}d$$

$$(1 + \mathrm{ST_G})\Delta E^{'}q(s) = K_{\mathrm{e}}\Delta E_{\mathrm{fd}}(s) + K_{\mathrm{f}}\Delta V(s) \tag{2}$$

$$T_{\mathrm{G}} = \frac{X_d^{'}T_{do}}{X_d}, \quad K_{\mathrm{e}} = \frac{X_d^{'}}{X_d} \quad \text{and} \quad K_{\mathrm{f}} = \frac{(X_d - X_d^{'})\cos\delta}{X_d} \tag{3}$$

This reactive power required for the DFIG changes with the different input conditions like input wind speed or wind energy.

2.2 Small Signal Model of Induction Generator (DFIG)

Reactive power needed by induction generator at constant slip is given by

$$\Delta Q_{\mathrm{IG}} = \frac{2V_t^0 X_{\mathrm{T}}}{((1-s)R_2^{'}/S - R_{\mathrm{T}})^2 + X_T^2} + \frac{-2(V_t^0)^2 X_T R_Y}{\{2R_Y(P_{1W} - P) + (V_t^0)^2\}(R_Y^2 + X_T^2)}\Delta P_{1W} X_{\mathrm{T}}$$
$$= X_1 + X_2^{'} \quad \text{and} \quad R_{\mathrm{T}} = R_1 + R_2^{'}$$

2.3 STATCOM Controller

The STATCOM is made of voltage source converter with a coupling transformer and DC capacitor. The management of the reactive current is made possible by the variation of δ (phase angle) and α (angle of fundamental output voltage).

The reactive power injected by the system bus is

$$Q + V^2B - KV_{\mathrm{dc}}VB\cos(\delta - \alpha) + KV_{\mathrm{dc}}VG\sin(\delta - \alpha) = 0 \tag{4}$$

$$\Delta Q_{\mathrm{STATCOM}}(S) = K_J\Delta\alpha(S) + K_K\Delta V(S) \tag{5}$$

$$K_k = KV_{\mathrm{dc}}B_{\sin\alpha} \quad K_L = KV_{\mathrm{dc}}B_{\cos\alpha} \tag{6}$$

$$\underline{x} = \left[\Delta I_{\mathrm{dr}}^{\mathrm{ref}},\ \Delta I_{\mathrm{dr}},\ \Delta V,\ \Delta\delta,\ \Delta E_{fd},\ \Delta V_a,\ \Delta V_f,\ \Delta E_q^{'}\right]^T \quad \underline{u} = [\Delta V_{\mathrm{ref}}] \quad \underline{w} = [\Delta Q_L]$$

The state-space representation of the wind-diesel system is written as $\dot{x} = Ax + Bu + Cw$ and X, U, W = state, control, and disturbance vectors.

3 Proposed Control Design

3.1 Objective Function and Optimization

PI-based controllers for STATCOM operation and DC voltage regulator have been tuned for optimum results.

The main aim behind optimization is always to damp out the power system oscillations. This has been found out by maximizing the damping ratio of poorly damped values. Indices like IAE, ISE, and ISTE have been utilized for calculation of performance index.

$$\mathrm{IAE} = \int_0^\infty |V_{\mathrm{t}}(t)|\mathrm{d}t, \quad \mathrm{ISE} = \int_0^\infty V_t^2(t)\mathrm{d}t, \quad \mathrm{ISTE} = \int_0^\infty tV_{\mathrm{t}}^2(t)\mathrm{d}t$$

3.2 Fuzzy Sliding Mode Controller

Fuzzy Sliding Mode Controller has been used to find out the stability of the controller occurring in nonlinear as well as linear systems. Sliding Mode Controller has been represented in Fig. 3 and is a Variable Structure Controller. This combines a number of continuous functions that can connect a plant state to a control surface. The switching existing with several functions is influenced by plant state and is represented by switching function. The sliding surface as well as switching never

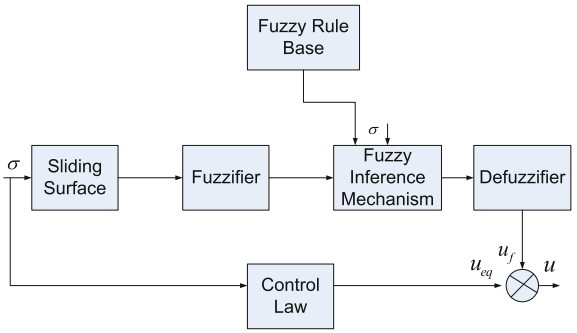

Fig. 3 Fuzzy sliding mode controller

Table 1 Optimal parameters

System	PI	SMC	FSMC
Kp	65	35	31
Ki	13,500	6000	5100
IAE	961.2	897.7	607.8
ITSE	24.4	23.3	10.67
ITAE	15.92	11.45	8.19
Rise	0.0943	0.0345	0.355
Overshoot	0.0198	0.0180	0.0126

depends upon operating point and therefore, converter dynamics offer good robustness (Table 1).

$$\dot{x} = f(x,t) + B(x,t)u$$

$x \in R^n$ Represents the state variable having dimension n. $u \in R^m$ is defined as the controller force. x_d is known as the reference state trajectory. The error between that of reference and system is given by $X = x_d - x$, where $s(x) = 0$. It denotes the sliding surface existing in the space of the error state. The minimum requirement, i.e., $s(x)\,\dot{s}(x)\langle 0$ has been satisfied, then X always moves toward the sliding surface

$$\frac{\partial s}{\partial x}\left(\dot{x}_d - \dot{x}\right) = \frac{\partial s}{\partial x}\dot{x}_d - \frac{\partial s}{\partial x}\left(f(x,t) + B(x,t)u\right) = 0$$

$$u_{eq} = \left[\frac{\partial s}{\partial x}B(x,t)\right]^{-1}\left(\frac{\partial s}{\partial x}\dot{x}_d - \frac{\partial s}{\partial x}\left(f(x,t)\right)\right)$$

$$u = u_{eq} + \left[\frac{\partial s}{\partial x}B(x,t)\right]^{-1} u_{sw},\; u_{sw} = Q_{\mathrm{sgn}}(s)\; Q = \mathrm{diag}[q_1, q_2, q_3, \ldots, q_n]$$

For determination of the required sliding surface $\sigma(x)$ the modified equation is given by

Table 2 PI controller values at diff slips

Hybrid system	CONST SLIP		VARIABLE	
	Kp	Ki	Kp	Ki
STAT(FSMC)	31	5100	29	4900
STATCOM(SMC)	35	6000	33	5878
STATCOM(PI)	48	7800	45	7890
No controller	65	13500	60	13120

Table 3 Comparison with FSMC

Del	PI controller		FSMC	
	Dev	Settling	Dev	Settling
V	0.05	0.5	0.048	0.475
QSG	0.52	0.5	0.515	0.48
QIG	0.0052	0.42	0.0051	0.4
$E_{q'}$	0.01	0.61	0.009	0.6
Alpha	4.1	0.55	3.4	0.52
Efd	0.049	0.64	0.048	0.6

$$\sigma(x) = \left(\frac{\mathrm{d}}{\mathrm{d}x} + k_i\right)^{q_n - 1} er(x),\ v(x) = \frac{\sigma^T(x)\sigma(x)}{2},\ u(t) = u_{eq}(t) + u_f(t)$$

The values that are given to the input of the fuzzy controller for calculation of u_f of sliding surface σ and $\dot{\sigma}$ (derivative) membership values $\mu_p(\sigma)$ and $\mu_N(\sigma)$ $\mu_p(\dot{\sigma})\mu_N(\dot{\sigma})$ (Tables 2 and 3).

4 Simulation and Results

The said wind-diesel-fuel cell hybrid system is simulated with varying load inputs and disturbances and is analyzed under various operating conditions. During simulation it is studied how different controllers perform under various circumstances and how far they contribute in minimization of voltage deviation and enhance reactive power management as well as improves voltage stability in the hybrid power system. The hybrid model's performance has been examined under normal operating condition and random load variation (±5 %). The controller performance and the deviation of system voltage profile are also studied. Detailed analysis with and without controller has been carried out and improvements have been noticed with the introduction of STATCOM controller as shown in Fig. 4. Further studies with random wind and fuel input are carried out to examine the effects upon the system and to testify the robustness of the controller. Further the system performance is examined with Fuzzy sliding mode-based STATCOM controller (Fig. 5).

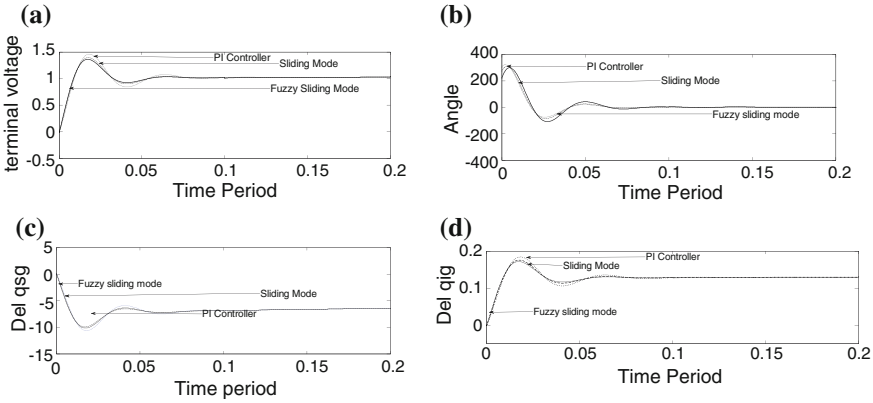

Fig. 4 **a–d** Showing the deviations of parameters with variation of loads

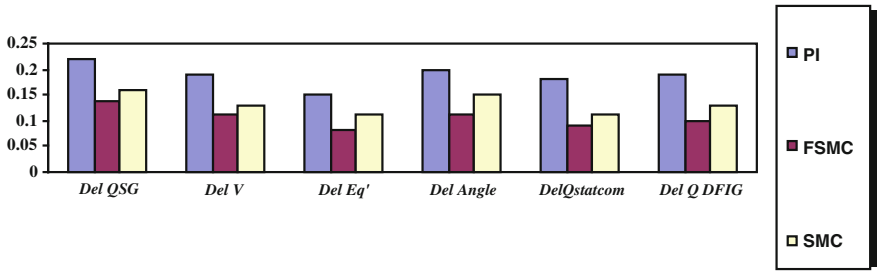

Fig. 5 Chart showing peak deviation

5 Conclusion

The reactive power management with dynamic stability of standalone wind-diesel-fuel cell hybrid power system has been thoroughly inspected with STATCOM controller. The compensator shows its robustness with simplicity in operation and is quite adaptable in its nature with numerous wind inputs and load variation. A comparison has been drawn between the system parameters with the proposed Fuzzy sliding mode controller and traditional PI and PID controllers. It is noticed that the time taken for settlement of different parameters indicating the voltage stability of the standalone wind-diesel-fuel cell hybrid power system improves noticeably with Fuzzy sliding mode-based STATCOM controller.

Appendix

Parameters of hybrid power system

Hybrid system		Wind-diesel-fuel cell	
Wind turbine		2.5 M V A	
Diesel Engine(Synchronous)		2.5 M V A	
Fuel cell		2.5 KW	
Base energy		3 M V A	
Synchronous generator		2.5 M V A	
$X_{\mathrm{d}}^{'}$	0.29 pu	X_{d}	1.56 pu
T_{e}	0.55 pu		27.8
K_{f}	0.5 pu	T_{a}	0.05
K_{a}	40	T_{do}	4.49 s
Generator(Doubly fed IG)	P_{IN}		1.67 M V A
L_{ss}	3.07	L_m	2.9 pu
$Q_{\mathrm{DFIG}}{}^{\mathrm{pu}}$	0.125	$I_{\mathrm{d}r}$	0.4 pu
Load Input	Q_L (pu)		0.2 pu
H_{r}	0.62 s	$\mathrm{T_S}$	0.08 s
$\mathrm{Pf}_{\mathrm{synchronous\ gen}}$	0.95	V_{ref}	1 pu

References

1. Kundur, P.: *Power system stability and control. The EPRI power system engineering series.* New York: McGraw-Hill Inc. (1994).
2. Hingorani, NG.,GyugyiN,:*UnderstandingFACTS, Concepts and Technology of Flexible AC TransmissionSystem,* NewYork, *IEEEPowerEngineering Society*, 2000.
3. Mohanty Asit., Viswavandya Meera., Ray Prakash., Patra Sandeepan: Stability Analysis and Reactive Power Compensation Issue in a Micro grid with a DFIG based WECS. *International journal of Electrical power and energy systems;* Elsevier Science, 2014.
4. Utkin, V. I.: *Sliding Mode in Control Optimization*, New York: Springer Verlag, 1992.
5. Soltanpour, M. R., Fateh, M. M,: *Sliding mode robust control of robot manipulators in the task space by support of feedback linearization and back stepping control*, World Applied Sciences Journal, vol. 6, no. 1, pp. 70–76, 2009.
6. Utkin, V. I.: *Variable Structure Control Systems with Sliding Mode,* IEEE Trans. Automat. Contr., Vol. AC-22, pp. 210–222, April 1977.
7. Palm, R.: *Sliding mode fuzzy control*, Proc. of IEEE International Conference on Fuzzy Systems, vol. 1, pp. 519–526, 1992.
8. Lhee, C. G.: *Sliding-like fuzzy logic control with self tuning the dead zone parameters,* Proc. of IEEE International Fuzzy Systems Conference, vol. 1, pp. 544–549, 1999.
9. Utkin, V. I.: *Sliding Modes and Their Application to Variable Structure Systems*, MIR Publishing Inc, Moscow, 1978.

ANFIS-Based Controller for DFIG-Based Tidal Current Turbine to Improve System Stability

Asit Mohanty, Meera Viswavandya, Sthitapragyan Mohanty and Pragyan Paramita

Abstract This paper presents ANFIS-based control for DFIG-based Tidal Current Turbine for stability improvement of offshore hybrid power system. The small signal transfer function models of DFIG-based tidal turbines are considered and an ANFIS control is proposed in order to improve the stability of converter lying in both grid end and generator end. The simulink model has been created in MATLAB and after proper simulation the effectiveness of the compensator is achieved.

Keywords Stability analysis · Tidal-diesel-wind hybrid system · ANFIS

1 Introduction

Nonconventional energy sources are intermittent and nonpredictable though they are widely available in the nature. Hybrid energy sources often unite multiple energy sources to a great extent to face energy crisis as shortfall due to one source is fulfilled by other source. Practically, standalone hybrid systems occur near the place of consumption and can be interconnected to the main grid. The combination of two or more renewable sources forms a hybrid system where the inadequacy or shortfall of generation of power of one source is met by the other source. [1–2]. Tidal-wind-diesel offshore hybrid system is rapidly becoming a popular choice. The wind power is always an unpredictable energy source. The much needed electrical energy of the tidal turbine is extracted from water. Generally, tidal currents are variable in nature and quite fluctuating, but it is comparatively stable when it is considered with respect to wind. There are lots of similarities between wind and

A. Mohanty (✉) · M. Viswavandya · S. Mohanty
College of Engineering & Technology Bhubaneswar, Bhubaneswar, India
e-mail: msthitapragyan@gmail.com

P. Paramita
VSSUT Burla, Odisha, India

D.K. Lobiyal et al. (eds.), *Proceedings of the International Conference on Signal, Networks, Computing, and Systems*, Lecture Notes in Electrical Engineering 396, DOI 10.1007/978-81-322-3589-7_12

tidal system as far as the electrical side layout and modeling approaches are concerned. Water currents in case of tidal turbine are having lower speed in comparison to air density. On the contrary, tidal turbines have high torque and lower rotational speed in comparison to wind turbines. [3–5].

Integration of tidal energy source to the main grid becomes more feasible because the source is more reliable and predictable. There exists enormous scopes, where it is very difficult to connect places with the main grid and therefore offshore wind and tidal energy sources become popular there. In future, the applications of such devices will increase as remote areas like small islands with limited grid connectivity and technical limitations can utilize these sources in standalone ways. Hybrid system with multiple energy sources becomes complex in operation and its stability is endangered. Unstable hybrid sources make the power delivery uncertain as there is complete mismatch between the power generated and the power to be delivered at the load. Therefore, enhancement and improvement of stability becomes essential to save the entire system from sudden collapse and to improve the power quality of the system. Impact of tidal current and wind energy sources is analyzed and its impact on the stability of the hybrid power system is discussed after proper simulation in MATLAB environment.

ANFIS control [5–9] basically covers both adaptive control and neuro-fuzzy control which are two advanced methods for time-varying and nonlinear processes. The ANFIS control begins with adaptive control of linear systems, nonlinear systems and also covers related control issues. Neural network and fuzzy model are described as general structures getting an approximating nonlinear functions and dynamic processes. Comparing the two methods neuro-fuzzy model can be proposed as a promising technology for the system control and also the adaptive control of nonlinear processes.

2 System Configuration and Its Mathematical Modeling

The hybrid system with its state-space representation has been devised to carry out proper study on the small signal modeling of a SMIB for tidal current turbine. The tidal turbine consisting of DFIG with PI and ANFIS-based PI controllers are simulated with MATLAB. Through small signal stability studies, the power systems show their synchronism under small disturbances and is analyzed with small variation in loading conditions. The stability analysis has been done by finding out the eigenvalues of the system and plotting the pole zeros on the complex plane.

Generally to get fixed speed, Squirrel Cage induction generator (SCIG) has been preferred to other turbines for dynamic behavior. The main parameters that are chosen for SCIG system have been rotor speed, stator voltage, turbine speed, and electrical torque. For the variable wind speed operation, the doubly fed induction

generator (DFIG) has been considered and preferred. The dynamic behavior of this system gets simulated using MATLAB/SIMULINK. The main parameters of DFIG-based turbine system are rotor speed, turbine speed, electrical torque, and d-axis flux.

The offshore wind and marine current hybrid generation system is an interconnected network with undersea cable. From the main grid, i.e., point of common coupling, i.e., PCC, power has been transported to the grid by the help of offshore step-up transformer and HVDC line. Stability analysis has been performed on the hybrid system with marine current generator and wind turbine generator with FACTS-based controllers. FACTS devices improve reactive power and thereby

Table 1 Eigenvalues of tidal-wind-diesel offshore system with **a** No Controller, **b** PI Controller, **c** ANFIS Controller

(a) No controller		
Eigenvalue	Damping	Frequency
−3.83e − 02	1.00e + 00	3.83e − 02
−4.84e + 00	1.00e + 00	4.84e + 00
−1.18e + 1 + 3.06e + 1*i*	3.59e − 01	3.28e +01
−1.18e + 01 − 3.06e + 1*i*	3.59e − 01	3.28e + 01
−4.44e + 01	1.00e + 00	4.44e + 01
−1.45e + 02	1.00e + 00	1.45e + 02
−6.14e + 02	1.00e + 00	6.14e +02
−7.96e + 04	1.00e + 00	7.96e + 04
(b) PI controller-based DFIG		
Eigenvalue	Damping	Frequency
−3.83e – 02	1.00e + 00	3.83e − 02
−4.84e + 00	1.00e + 00	4.84e + 00
1.09e + 1 + 3. 06e + *i*	3.36e − 01	3.25e + 01
−1.09e + 01 − 3. 06e + 1*i*	3.36e − 01	3.25e + 01
−1.18e + 1 + 3.06e + 1*i*	3.59e − 01	3.28e + 01
−1.18e + 01 − 3.06e + 1*i*	3.59e − 01	3.28e + 01
−4.44e + 01	1.00e − 00	4.44e + 01
−1.45e + 02	1.00e + 00	1.45e + 02
(c) ANFIS controller-based DFIG		
Eigenvalue	Damping	Frequency
−4.55e – 02	1.00e + 00	4.55e − 02
−8.59e – 01	1.00e + 00	8.59e − 01
−1.40e + 00	1.00e + 00	1.40e + 00
−5.01e + 00	1.00e + 00	5.01e + 00
−2.01e + 01	1.00e + 00	2.01e + 01
−2.06e + 01	1.00e + 00	2.06e + 01
−1.16e + 01 + 3.08e + 1*i*	3.52e − 01	3.29e + 01
−1.16e + 01 − 3.08e + 01*i*	3.52e − 01	3.29e + 01

improve the overall stability of the hybrid system. Linear model of the whole system has been modeled for reducing complexity of the calculation (Figs. 1 and 2). The eigenvalues of the described system have been depicted in Table 1a, b, c.

Tidal energy generation is one of the most important renewable energy sources for generation of electric power in standalone sites. Like wind turbine, the tidal turbine configuration uses doubly fed induction generators (DFIG) or direct drive permanent magnet synchronous generators (DDPMSG) because of their robust characteristics. The efficiency of tidal current turbine is commendable as it utilizes the same technology like wind energy system. The tidal stream is predictable to some extent which makes the system very effective and useful. We know that tidal stream and tidal barrage are mainly used for generating energy from the tides. The main difference between the two is that, tidal stream uses the kinetic energy of moving water and tidal barrage uses the potential energy in height, respectively.

The power delivered by the tidal turbine is

$$p_T = \frac{1}{2}\rho.A.C_{pt}(\lambda, \beta).v_t^2,$$

where ρ is the density of water, A is the swept turbine area, C_{pt} is equal to power coefficient of turbine, and V_t is the water flow velocity

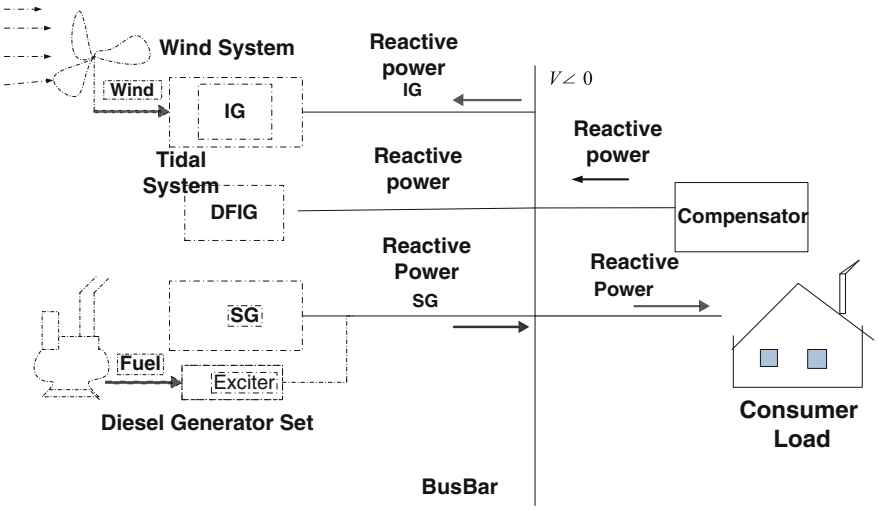

Fig. 1 Block diagram showing tidal-wind-diesel offshore hybrid system

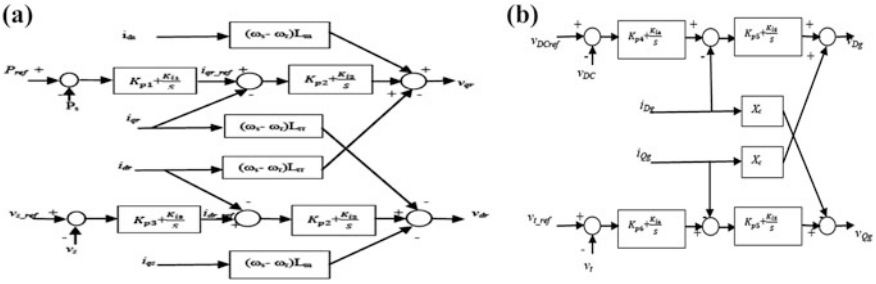

Fig. 2 **a** Converter (generation end). **b** Converter (grid end)

$$T_m = \frac{0.5\rho \prod R^2 C_p v_{\text{tide}}^3}{w_t}$$

$$2H_t \frac{\mathrm{d}w_t}{\mathrm{d}t} = T_m - T_e - D_m\omega$$

$$\omega_t = \frac{\omega}{p}$$

$$V_{\text{ds}} = -R_s i_{\text{ds}} + X^{'} i_{qs} + e_d$$

$$V_{qs} = -R_s i_{qs} + X^{'} i_{\text{ds}} + e_q$$

$$\frac{\mathrm{d}e_d}{\mathrm{d}t} = -\frac{1}{T_0}(e_d + (X - X^{'})i_{qs} + s\omega_s e_q - \omega_s \frac{L_m}{L_{rr}} v_{qr}$$

$$\frac{\mathrm{d}e_q}{\mathrm{d}t} = -\frac{1}{T_0}(e_q + (X - X^{'})i_{\text{ds}} + s\omega_s e_d - \omega_s \frac{L_m}{L_{rr}} v_{\text{dr}}$$

$$e_d = \frac{\omega_s L_m}{L_{rr}}\psi_{qr} \text{ and } e_q = \frac{\omega_s L_m}{L_{rr}}\psi_{\text{dr}}$$

$$\dot{x} = Ax + Bu$$

$$x = [w_t,\ \beta,\ v_{DC},\ \theta_{tr},\ e_d,\ e_q,\ V_{DC},\ x_1,\ x_2,\ x_3,\ x_4,\ x_5,\ x_6,\ x_7,\ x_8]^T$$

$$\Delta\dot{x} = A\Delta x + B\Delta u$$

$$\Delta x = [\Delta w_t,\ \Delta\beta,\ \Delta v_{DC},\ \Delta\theta_{tr},\ \Delta e_d,\ \Delta e_q,\ \Delta V_{DC},\ \Delta x_1,\ \Delta x_2,\ \Delta x_3,\ \Delta x_4,\ \Delta x_5,\ \Delta x_6,\ \Delta x_7,\ \Delta x_8]^T$$

3 Adaptive Neuro-Fuzzy Inference System

Adaptive neuro-fuzzy system ANFIS method as shown in Fig. 3 is a process for modeling the system with fuzzy inference system. For getting out the membership functions, the fuzzy inference system (FIS) achieves all the data (input and output) with certain prescribed methodology for designing ANFIS-based DFIG turbine in tidal turbine. The input variables like error e and change in error Δe have been fed to the ANFIS controller with seven linguistic values. The values of ANFIS-based

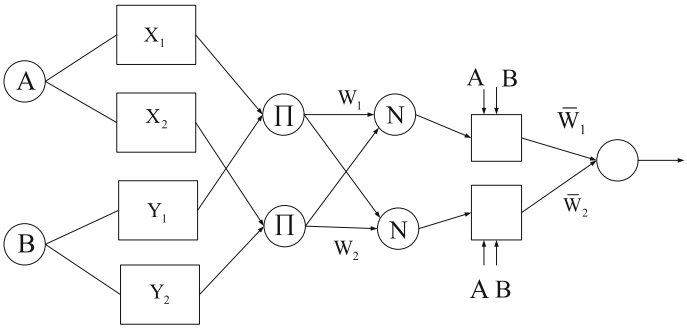

Fig. 3 Simplified ANFIS structure

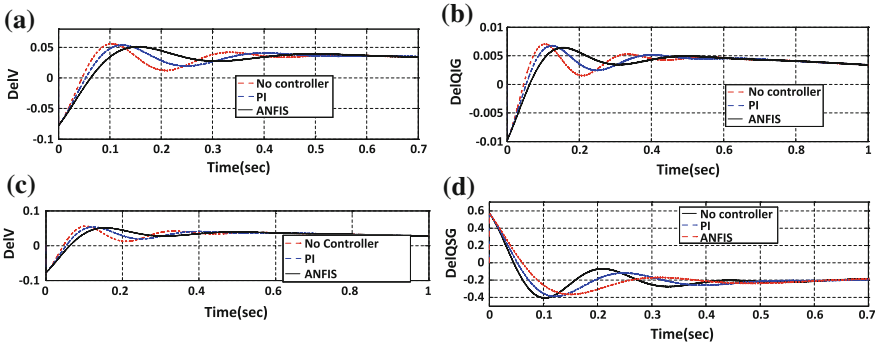

Fig. 4 **a**, **b**, **c**, **d**-Comparative results of Tidal-wind-diesel hybrid system

DFIG controller are large positive (LP), medium positive (MP), small positive (SP), zero (ZE), small negative (SN), medium negative (MN), large negative (LN).

A. ANFIS Architecture

For example, 2 inputs $(x \,\&\, y)$ with 1 output (z)ANFIS

$$\text{if } x = A_1 \text{ and } y = B_1 \text{ then } f_1 = p_1 x + q_1 y + r_1$$
$$\text{if } x = A_2 \text{ and } y = B_2 \text{ then } f_2 = p_2 x + q_2 y + r_2$$

ANFIS architecture adaptive nodes

$$O_{1,i} = \mu_{A_i}(x) \qquad i = 1,\ 2$$
$$O_{1,i} = \mu_{B_{i-2}}(x) \qquad i = 3,\ 4$$

$\mu_{A_i}(x)$ and $\mu_{B_i}(x)$ any membership function $\mu_{A_i}(x) = \frac{1}{1 + [\frac{(x - c_i)^2}{a_i^2}]^{b_i}}$ $\{a_i,\ b_i,\ c_i\}$. The parameter of premise fixed-type node with multiplication functions $O_{2,i} = w_i = \mu_{A_i}$

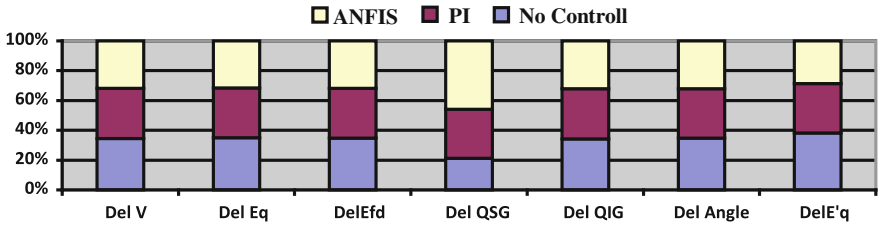

Fig. 5 Timings of settlement of parameters

$(x) \times \mu_{B_i}(x) \quad i = 1, 2$—are the strength of a rule-normalized fixed nodes $O_{3,i} = \bar{w}_i = \frac{w_i}{w_1 + w_2} \quad i = 1, 2$ firing strength after having normalization with adaptive nodes $O_{4,i} = \bar{w}_i f_i = \bar{w}_i(p_i x + q_i y + r_i)$ $\{p_i, q_i, t_i\}$ all the consequent parameters Summation function $O_{5,1}$ = overall output = $\sum_i \bar{w}_i f_i$

4 Simulation Results & Discussion

Parameter variation results of DFIG-based tidal turbine with ANFIS controller are noticed. The tidal system has been simulated number of times with different input conditions. Taking a variable step load change of (1–5) % and variable input parameters like wind and hydro energy, the changes of all existing system parameters are noticed and plotted as shown in Figs. 4 and 5. Parameters like settling period and maximum overshoot are minimum in case of ANFIS in contrast to traditional PI. ANFIS provides better damping but it has some drawbacks like creation of membership function, making of rules and suitability of scaling factors which are achieved by trial and error method. Eigenvalues of the DFIG-based tidal turbine has been calculated for (a) No controller, (b) Proportional Integral type Controller & ANFIS-based controller for detailed analysis of the voltage stability and reactive power management of the whole system. Hybrid system, where ANFIS ANFIS-based controller is used for DFIG tidal turbine, makes the system more comparatively stable and robust than the conventional PI controller.

5 Conclusion

In this particular problem, an ANFIS-governed DFIG tidal turbine is used in the offshore hybrid system and issues of reactive power and voltage stability are discussed. The parameters are properly tuned to achieve better results from the eigenvalue analysis, it is concluded that the neuro-fuzzy controller-based system is

more stable and robust than the conventional one. Final outcome shows small settling duration with better overshoots. ANFIS controller-based hybrid system is robust and more reliable.

References

1. Hamed H. Aly, El-Hawary M. E.: *An Overview of Offshore Wind Electrical Energy Systems*, 23rd Annual Canadian IEEE Conference on Electrical and Computer Engineering, Calgary, Alberta, Canada, May 2–5, 2010.
2. Yazhou Lei, Alan Mullane, Gordon Lightbody, Yacamini Robert,: *Modeling of the Wind Turbine with a Doubly Fed Induction Generator for Grid Integration Studies*, IEEE Transaction on Energy Conversion, Vol. 28, No. 1, March 2006.
3. Hamed H. H. Aly, and El-Hawary, M. E.: *Small Signal Stability Analysis of Tidal In-Stream Turbine Using DDPMSG with and without Controller*, 5th IEEE Annual Electrical Power and Energy Conference, Winnipeg, Canada, 2011.
4. Wu, F., Zhang, X.-P., Ju P.:, *Small signal stability analysis and control of the wind turbine with the direct-drive permanent magnet generator integrated to the grid*, Journal of Electric Power and Engineering Research, 2009.
5. Wu, F., Zhang, X.-P., Ju, P.,: *Small signal stability analysis and optimal control of a wind turbine with doubly fed induction generator*, IET Journal of Generation, Transmission and Distribution, 2007.
6. Kundur, Prabha.,: *Power System Stability and Control*, McGraw-Hill, Inc. USA, 1994.
7. Khutia, SR., panda S, Sidhartha.,: ANFIS approach for SSSC controller design for the improvement of transient stability performance. Math Comput Model 57:289–300, 2013.
8. Roger Jang., Jyh-Shing., *ANFIS: Adaptive-Network-Based Fuzzy Inference System,* IEEE Trans. Syst. Man and Cyber., 23, (3), pp. 665–685, 1993.
9. Mohanty Asit., Viswavandya Meera., Ray Prakash., Patra Sandeepan: Stability Analysis and Reactive Power Compensation Issue in a Micro grid with a DFIG based WECS. *International journal of Electrical power and energy systems;* Elsevier Science, 2014.

Design of Reversible Floating Point Adder for DSP Applications

A.N. Nagamani, C.K. Kavyashree, R.M. Saraswathy, C.H.V. Kartika and Vinod Kumar Agrawal

Abstract Motivation for the study of technologies implementing reversible computing methods are that they offer a potential way to improve the energy efficiency of computers beyond the fundamental von Neumann-Landauer limit. Several implementations of floating-point unit in reversible logic have been suggested; and it has been found that the floating point addition is the most frequently used operation. In this paper, we present a reversible 16-bit floating-point adder that closely follows the IEEE-754 specification for binary floating-point arithmetic. The implementation of the floating-point adder using carry-lookahead adder and Brent-Kung adder structures have been designed and its performance parameters such as quantum cost, depth, garbage outputs, ancilla inputs, and delay have been compared. The proposed design has been extended to 32-bit to compare with existing works.

Keywords Reversible computing · Floating-point adder · Single precision · Double precision

A.N. Nagamani (✉) · C.K. Kavyashree · R.M. Saraswathy · C.H.V. Kartika
Department of ECE, PES Institute of Technology, Bangalore, India
e-mail: nagamani@pes.edu

C.K. Kavyashree
e-mail: kavyashree.ck@gmail.com

R.M. Saraswathy
e-mail: saraswathy31@gmail.com

C.H.V. Kartika
e-mail: kartikachv@gmail.com

V.K. Agrawal
Department of ISE, PES Institute of Technology, Bangalore, India
e-mail: vk.agrawal@pes.edu

D.K. Lobiyal et al. (eds.), *Proceedings of the International Conference on Signal, Networks, Computing, and Systems*, Lecture Notes in Electrical Engineering 396, DOI 10.1007/978-81-322-3589-7_13

1 Introduction

In recent years, reversible logic has received great attention due to its ability to reduce the power dissipation which allows higher density and higher speeds on the chip. Reversible logic is different as the inputs and the outputs have a one-to-one relation, and hence the input can be determined from the output, resulting in no loss of information. This conforms with Landauer's principle [1].

The conventional computational units in a computer work with integers only. Although an exact representation of numeric values is provided by integers it has two major drawbacks: the inability to represent fractional values and limited dynamic range; these two problems are solved by floating-point arithmetic. A floating-point unit is a part of a computer system specially designed to carry out operations on floating-point numbers. Floating-point numbers are represented using IEEE-754 standard. Floating-point addition is the most commonly used operation [2]. In this paper, RCViewer+ [3] has been used as a viewer/analyzer for the reversible circuits.

The paper has been structured as follows: Sect. 2 'basic reversible gates', which explains the basic gates used in the design of reversible circuit. Section 3 'design and methodology' which outlines the algorithm used and all the modules used to construct the adder. Section 4 consists of comparison and results.

2 Basic Reversible Gates

One of the major advantages of reversible gates is that more than one operation can be implemented in a single unit of reversible gate. The quantum gate library used to create the basic reversible gates includes controlled-V, controlled-V+, CNOT, and NOT, each with a quantum cost of 1. Some of the most commonly used reversible gates are described as follows:

NOT gate is the simplest reversible gate with a quantum cost of 1. It is a 1 * 1 gate mapped as $(P) = (\overline{P})$. **Feynman gate** [4], also known as CNOT gate is a 2 * 2 gate mapped as $(A, B) = (A, A \oplus B)$. Its quantum cost is 1. Feynman gates are mainly used for fan-out purpose. **Fredkin gate** [5] is a 3 * 3 gate with a quantum cost of 5. It is mapped as $(A, B, C) = (A, \overline{A}\, B \oplus AC, \overline{A}\, C \oplus AB)$. It is also known as Controlled SWAP gate. **Toffoli gate** [6] is a CCNOT gate that is mapped as $(A, B, C) = (A, B, AB \oplus C)$. It is a 3 * 3 gate with quantum cost 5. **Peres gate** [7, 8] gate is a 3 * 3 gate with a quantum cost of 4. It is mapped as $(A, B, C) = (A, A \oplus B, AB \oplus C)$.

2.1 Optimization Parameters for Reversible Gates

Garbage Output refers to the number of additional outputs added so as to make the number of inputs and outputs equal. In certain cases, these become mandatory to attain reversibility. **Ancilla input/constant inputs** are the constant inputs to a reversible circuit that are always maintained constant at 1 or 0 in order to obtain the required logical function. **Quantum cost** is the cost of the circuit in terms of the number of primitive 2 * 2 gates used. **Gate level/depth** is the minimum number of levels in the reversible logic circuit where functions on disjoint input lines are performed simultaneously in the same level. **Delay** [9] of a circuit is the sum of the maximum delay of individual gates in each level. **Gate count** simply refers to the number of basic reversible gates used in the circuit.

3 Design and Methodology

In this paper, floating point adder is designed using reversible logic. A 16-bit (half precision) and also a 32-bit (Single precision) floating-point adder is designed.

According to IEEE-754 standard, a 16-bit number is split as 1 bit for sign, 10 bits for mantissa, and 5 bits for exponent. And a 32-bit number is split as 1 bit for sign, 23 bits for mantissa, and 8 bits for exponent. The design of proposed adder follows the block diagram in Fig. 1 with the modules replaced by their reversible counterparts. The adder has been designed using carry-lookahead adder (CLA) and Brent Kung. The performance parameters of the proposed design are determined and are compared with the existing design.

Algorithm

Consider the two numbers $A = 4.625$ and $B = 33.5$ representing the numbers in the IEEE floating-point format. We get $A = 0100010010100000$ and $B = 0101000\ 000110000$.

Step 1 We send the exponents of both inputs to a comparator. The output is sent to a decision box, which sends the mantissa of the number with smaller exponent to the barrel shifter. It is found that 10100 > 10001, i.e., exponent of B > exponent of A.

Step 2 The exponents are next sent into a subtractor, the output of which serves as another input for the barrel shifter. The result obtained from subtraction is 00011.

Step 3 Barrel shifter performs the required amount of shift and passes the value into the adder. The mantissa of A becomes 0010010100 (10 bit mantissa) 000 (GRN bits).

Step 4 From Step 1, the larger exponents mantissa are sent in as the second input for the adder. Sign to 2's complement unit is incorporated into the adder. Adding the newly obtained mantissa of A and B using the 10 bit adder, we get Output = 0011000100 and Output sign = 0.

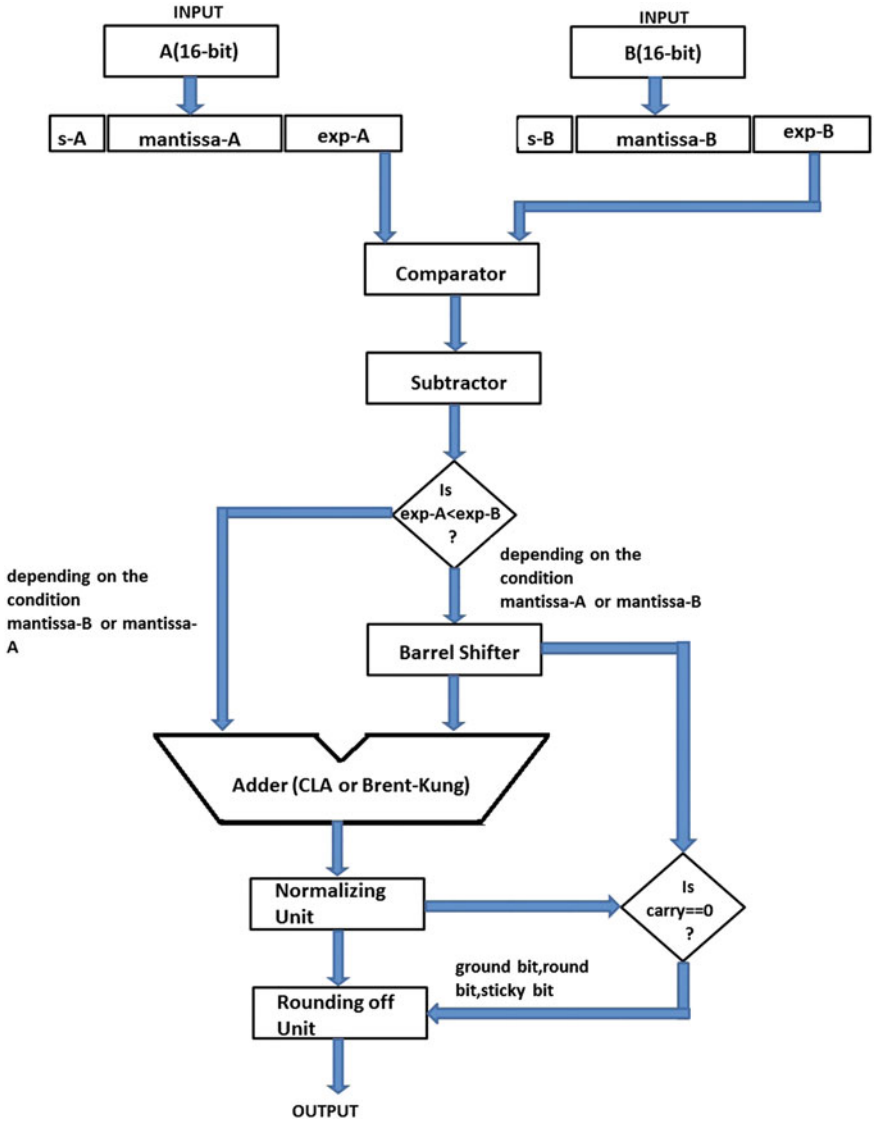

Fig. 1 Block diagram of floating-point adder

Step 5 The result of the adder is sent into the normalizing unit. The carry obtained from the adder in the above case is 0. Hence output is already in the normalized form. **Step 6** The result of this normalizing unit is then given to the rounding off unit which produces the final output G+R+N = 0. So, no additional bit is added to the LSB. Thus, the output obtained would be, Output = 0101000011000100 = 38.125.

3.1 Proposed Designs

The circuit consists of a comparator, subtractor, barrel shifter, adder, normalizing unit, and a rounding off unit.

3.1.1 Comparator

The comparator has been designed using [10] as the reference. The exponent of the 16-bit number is represented using 5 bits where the exponent ranges from −14 to 15 (Fig. 2). The real exponent of the number would be as follows (for 5 bits): Exponent $= 2^{(5\text{ bit exponent}-15)}$ Comparison of two exponents is done by first comparing its corresponding bits one at a time. The one bit comparator can be designed using a peres gate. Assuming the 2 inputs to be A and B and E represents 'Equal to', G 'Greater than', and L 'Less than', we get

$$E[i] = \overline{(A[i] \oplus B[i])} = A[i] \oplus (\overline{B[i]}) \text{ and } G[i] = A[i] \cdot (\overline{B[i]}) \tag{1}$$

$$L = \overline{(E \oplus G)} \tag{2}$$

A group 'Equal to' and group 'Greater than' bit can be used to represent the comparison output for a group of bits and is computed as follows:

$$E[i:k] = E[i:j] \cdot E[j-1:k] \tag{3}$$

$$G[i:k] = G[i:j] + E[i:j]G[j-1:k] \tag{4}$$

The final G and E bits are E = E[4:0] and G = G[4:0].

3.1.2 Subtractor

Subtractor unit designed in this paper consists of two submodules namely 2′s complement generator and 5-bit CLA adder. CLA adder has been used, since for 5-bit input both CLA and Brent-Kung have same depth and CLA has less quantum cost (Fig. 3).

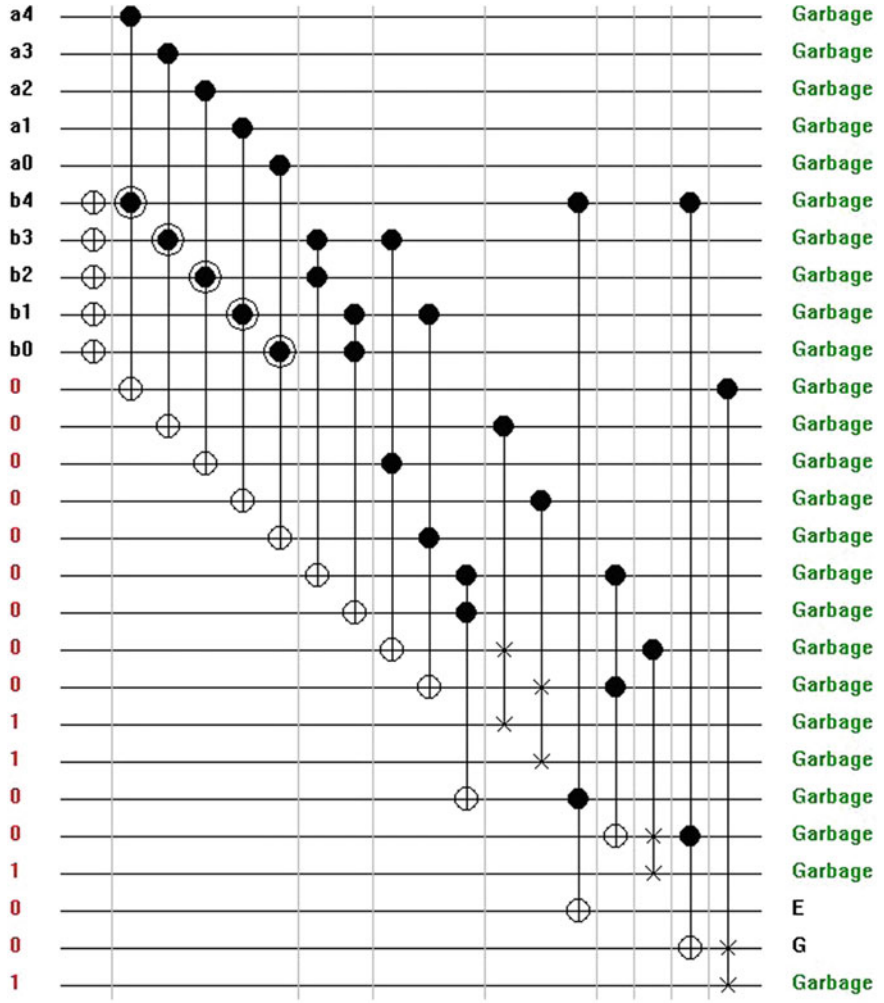

Fig. 2 The quantum diagram for comparator used in the 16-bit adder design

3.1.3 Barrel Shifter

A barrel shifter is the most commonly used shifter in any digital signal processor unit. The barrel shifter used here is a reversible 10-bit input and 13-bit output logarithmic barrel shifter. It is a universal shifter. The barrel shifter has been designed using [11] as the basis. It has four levels of shifts, which allows a shift up to 10. The shift is limited to 10 as the input is 10-bit and any shift beyond will produce the same result as the 10-bit shift. The shifter used is more efficient compared to [12]. The last three extra bits in the output account for the guard bit,

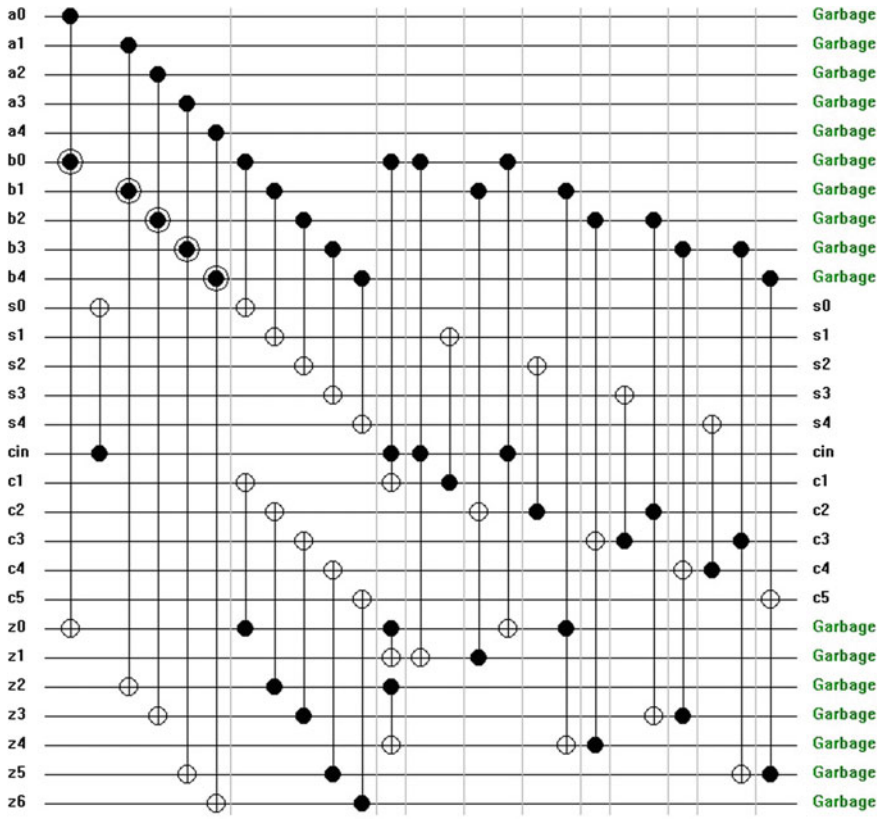

Fig. 3 The quantum diagram for adder/subtractor used in the 16-bit adder design

the round bit, and the sticky bit. These three are used for rounding off and are given as the input to the rounding off unit.

3.1.4 Adder

The half-precision (16-bit) floating-point adder uses a 10-bit adder for adding the mantissa of the input. The adder proposed is a 10-bit adder [13] that takes in input in the sign-magnitude format, where the sign bit is obtained from the number in IEEE-754 format. The sign of the inputs are compared and decision to either add or subtract the magnitude is made.

The input is then converted to its 2′s complement form before performing conventional integer addition (10-bit) on it. A peres gate can be used to compute the generate and propagate bits. Two different adders structures namely CLA and

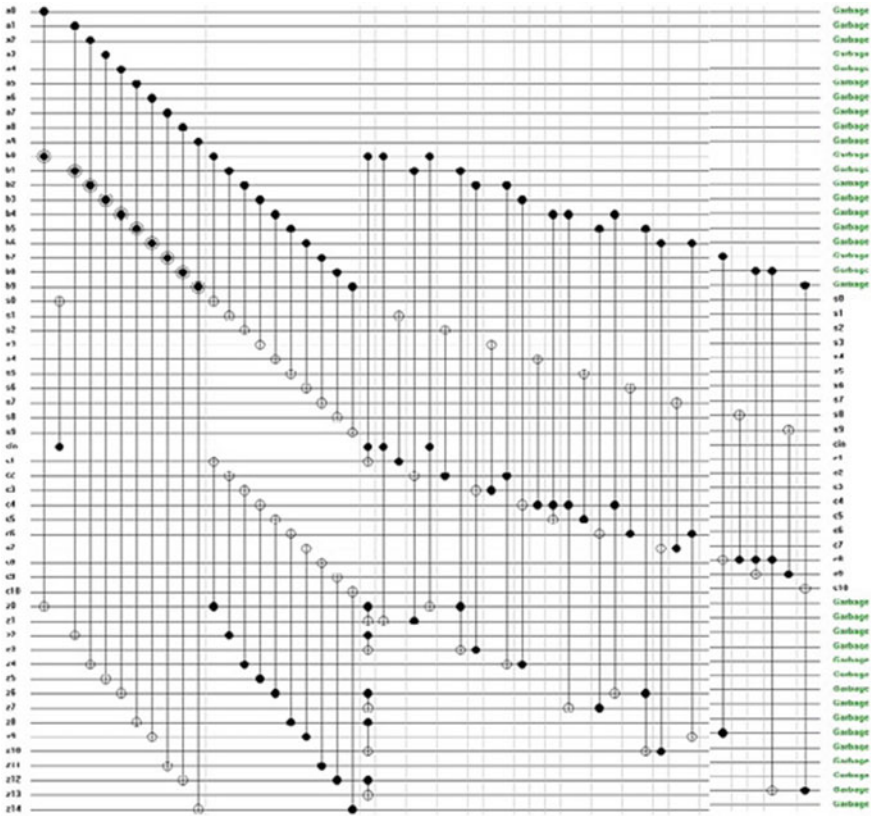

Fig. 4 The quantum diagram for CLA used in the 16-bit adder design

Brent-Kung are used to compute the group generate and propagate bits. To design CLA [14] P_i and G_i bits are generated using peres gate. Feynman is used to generate copies of P_i and G_i to calculate sum and carry. From the generated P_i and G_i, carry (c_{i+10}) and sum (S_i) are calculated using Toffoli and Feynman gate (Fig. 4).

In CLA, sum and carry are calculated as shown below We know that, carry propagation (P_i) and carry generation G_i are given by

$$P_i = a_i \oplus b_i \text{ and } G_i = a_i \cdot b_i \tag{5}$$

Therefore, sum S_i and carry C_{i+1} given by

$$S_i = P_i \oplus c_i \tag{6}$$

$$c_{i+1} = G_i \oplus P_i c_i \tag{7}$$

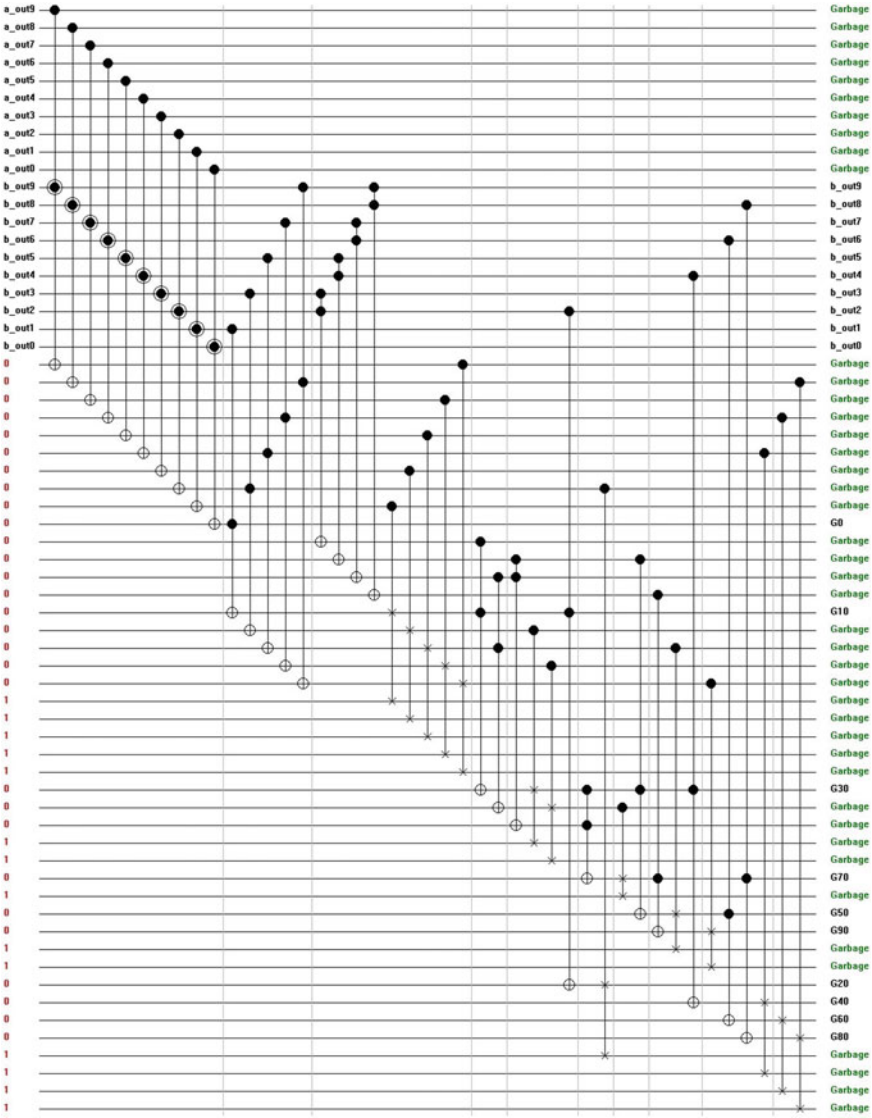

Fig. 5 The quantum diagram of Brent-Kung adder unit used in the 16-bit adder design

By expanding Eqs. (6) and (7), we get the sum and carry as (Fig. 5)

$$c_n = G_{n-1} \oplus P_{n-1}(G_{n-2} \oplus \cdots \oplus P_{n-2}P_{n-3}\ldots P_0C_0), \text{ and} \tag{8}$$

$$S_n = P_n \oplus G_{n-1} \oplus P_{n-1}(G_{n-2} \oplus \cdots \oplus P_{n-2}P_{n-3}\ldots P_0C_0) \tag{9}$$

In Brent-Kung adder, the individual propagate and generate bits are computed as $p[i] = A[i] \oplus B[i]$ and $g[i] = A[i] \cdot B[i]$, which is the same as CLA adder. However, the group generate and propagate is computed using the following formulae:

$$P[i:k] = P[i:j] \cdot P[j-1:k] \tag{10}$$

$$G[i:k] = G[i:j] + P[i:j]G[j-1:k] \tag{11}$$

Brent-Kung is a parallel prefix adder and hence the delay obtained during the computation is reduced. The logic depth in a Brent-Kung adder is $2\log n - 1$, which is lesser than that in conventional addition. The final sum is computed using the following equation:

$$\text{Sum}[i] = p[i] \oplus G[i-1:0] \text{ and Carry} = G[9:0] \tag{12}$$

The sum thus obtained is in its 2′s complement form and has to be converted to the sign-magnitude form. This can be done by comparing the sign of the inputs and the carry thus obtained.

3.1.5 Normalizing Unit

This unit is used to make sure that there are no overflows and that the number is in standard format. The carry from the adder is used as an input to the barrel shifter. The barrel shifter then gives an appropriate output of mantissa, and a corresponding change in the exponent is made using a 5-bit CLA adder.

3.1.6 Rounding off Unit

'Round to nearest even' technique has been used in this paper to round off the intermediate result to a more appropriate result. According to IEEE-754 standard [15], there are three types of mode for rounding off and one of these is 'Round to nearest even'. In this mode, the inexact results are rounded to the nearer of two possible result values. If neither of the possibilities are nearer, then the even alternative is chosen. This form of rounding is also called 'round to even'. Round to

nearest produces more accurate results as it is unbiased and as a result it does not favor errors of any particular sign.

The guard bit, round bit, and sticky bit [16] are taken as the input from the normalizing unit. An OR operation is performed on these bits and the result is added to the least significant bit of our result to produce the rounded-off result. Reversible OR function are implemented as a cascade of peres gates, each operating as a two-input OR gate.

4 Results and Conclusion

Table 1 shows comparison of the proposed designs with the existing designs and it can be found that Brent-Kung adder has lesser depth and delay than the carry-lookahead adder. However, this decrease in delay comes with an increase in Quantum cost. It can be noted that in the 16-bit adder the delay is reduced by 45 % in the Brent-Kung adder when compared to the carry-lookahead adder. Similarly, the reduction in delay was 64 % in the Brent-Kung adder designed for single precision. Single precision design is extended for double precision and performance parameters are tabulated.

The design of the adder in the reference has not been compared with the proposed design for delay and depth as it has not been mentioned. However, the inherent properties of Brent-Kung and carry-lookahead adder makes it more efficient in terms of delay when compared to the ripple carry adder presented in the reference.

From Table 2 it is evident that Brent-Kung adder is found to be efficient compared to CLA with 21.92 % reduction in the quantum cost, 69.30 % reduction in garbage output, and 70.59 % reduction in ancilla inputs.

Hence, the analysis gives rise to a conclusion that proposed adder design in this paper has better performance parameters when compared to existing works and is suitable for design of low-power digital signal processors.

Table 1 Comparison of parameters calculated for the proposed design and existing work

Parameters			
Floating point adder design	Quantum cost	Ancilla input	Garbage outputs
Ripple carry adder (32-bit) [17]	7458	2646	2926
Proposed adder (32-bit) using Brent-Kung	5823	778	898
Proposed adder (32-bit) using CLA	5341	622	76

Table 2 Parameters for comparison

Floating point adder using Brent-Kung							
Size	Modules	Quantum cost	Gate count	Ancilla inputs	Depth	Garbage outputs	delay (in Δ)
16-bit	Adder/subtractor (5-bit)	119	44	14	21	24	77
	Barrel shifter	759	157	99	34	103	170
	Comparator	95	24	17	9	25	40
	Adder unit (10-bit)	485	141	87	50	98	167
	Adder (10-bit)(for rounding off unit)	243	53	44	11	54	50
	Total	2603	624	390	184	437	771
32-bit	Adder/subtractor (8-bit)	191	62	22	31	38	115
	Barrel shifter	1672	340	181	87	192	427
	Comparator	161	39	29	11	43	50
	Adder unit (23-bit)	1278	355	228	86	253	331
	Adder (23-bit)(for rounding off unit)	634	135	113	15	136	74
	Total	5823	1337	778	352	898	1559
16-bit	Adder/subtractor (5-bit)	119	44	14	21	24	77
	Barrel shifter	759	157	99	34	103	170
	Comparator	95	24	17	9	25	40
	Adder unit (10-bit)	412	152	58	62	81	209
	Adder (10-bit)(for rounding off unit)	170	64	15	21	34	92
	Total	2457	646	332	206	400	855
32-bit	Adder/subtractor (8-bit)	191	62	22	31	38	115
	Barrel shifter	1672	340	181	87	192	427
	Comparator	161	39	29	11	43	50
	Adder unit (23-bit)	1037	368	150	118	197	463
	Adder (23-bit) (for rounding off unit)	393	148	35	47	80	206
	Total	5341	1363	622	416	786	1823

References

1. R. Landauer, "Irreversibility and heat generation in the computational process," IBM Journal of Research and Development, 5, pp. 183–191,1961.
2. A. Malik, "Seok-Bum Ko, Effective implementation of floating-point adder using pipelined LOP in FPGAs," Electrical and Computer Engineering, 2005. Canadian Conference on, vol., no., pp. 706–709, 1-4 May 2005.
3. RCViewer+, http://ceit.aut.ac.ir/QDA/RCV.htm.
4. R. Feynman, "Quantum Mechanical Computers," Optics News, Vol. 11, pp. 11–20, 1985.
5. E. Fredkin and T. Toffoli, "Conservative logic," Int'l J. Theoretical Physics, Vol. 21, pp. 219–253, 1982.
6. T. Toffoli., Reversible Computing", Tech memo MIT/LCS/TM-151, MIT Lab for Computer Science 1980.

7. Shefali Mamataj, Dibya Saha, Nahida Banu, "A Review of Reversible Gates and its Application in Logic Design", American Journal of Engineering Research (AJER), e-ISSN:2320-0847, p-ISSN:2320-0936 Volume-03, Issue-04, pp-151-161.
8. Peres, "Reversible Logic and Quantum Computers", Physical review A, 32:3266–3276, 1985.
9. Nabila Abdessaied, Robert Wille, Mathias Soeken, "Rolf Drechsler, Reducing the Depth of Quantum Circuits Using Additional Circuit Lines".
10. James E. Stine, "Michael J. Schulte, A Combined Twos Complement and Floating-Point Comparator".
11. Saurabh Kotiyal, Himanshu Thapliyal and Nagarajan Ranganathan, "Design of A Reversible Bidirectional Barrel Shifter", 2011 11th IEEE International Conference on Nanotechnology, August 15–18, 2011.
12. Ravish Aradhya H.V, Lakshmesha J, Muralidhara K.N, "Design optimization of Reversible Logic Universal Barrel Shifter for Low Power applications", International Journal of Computer Applications (0975 8887) Volume 40 No. 15, February 2012.
13. Haridimos T. Vergos, Giorgos Dimitrakopoulos, "On Modulo 2n + 1 Adder Design", IEEE transactions on computers, VOL. 61, NO. 2, February 2012.
14. Lafifa Jamal, Md. Shamsujjoha, Haz Md. Hasan Babu, "Design of Optimal Reversible Carry Look-Ahead Adder with Optimal Garbage and Quantum Cost", International Journal of Engineering and Technology Volume 2 No. 1, January, 2012.
15. Prof. W. Kahan, "Lecture Notes on the Status of IEEE Standard 754 for Binary Floating-Point Arithmetic", Lecture Notes on the Status of IEEE 754, October 1997.
16. David J. Kuck, Douglass S. Parker, JR., Ahmed H. Sameh, "Analysis of Rounding Methods in Floating-Point Arithmetic", IEEE transactions on computers, VOL. C-26, NO. 7, July 1977.
17. Michael Nachtigal, Himanshu Thapliyal, Nagarajan Ranganathan, "Design of a Reversible Floating-Point Adder Architecture", 2011 11th IEEE International Conference on Nanotechnology, August 15–18, 2011.

Navigation of Mobile Robot Using Type-2 FLC

Krishna Kant Pandey, Anish Pandey, Animesh Chhotray and Dayal R. Parhi

Abstract We know that, developing control algorithm for local navigation (environment are unknown) is one of the weak point in mobile robotics research. To achieve maximum accuracy with local navigation problem, an enormous amount of research has been carried out. Control in local environment offers comprehensive nontrivial processes such as; refining topography maps, precisely stirring along composite, wavy routs upholding a given alignment of the robot elements in space. The AI techniques used for these applications are proven to be effective and proper when applied to a range of engineering systems. The hallmark of this paper rectifies the application of a Type-2 fuzzy towards navigation, path generation and obstacle avoidance for an autonomous mobile robot. A noble self-learning capability and reasoning ability is the advantage of type 2 fuzzy over others intelligent algorithms. Thus, type 2 fuzzy-based heuristics is offered, which results in a significant increase in the process of finding optimal solution for target search and path planning.

Keywords Type-2 fuzzy · Mobile robot · Navigation · Obstacle avoidance

1 Introduction

In recent time, mobile robotics explains collective assumptions of modernistic and automated science. Everyday we notice its application throughout our surroundings. Researches on mobile robotics are totally based on our organizational needs.

K.K. Pandey (✉) · A. Pandey · A. Chhotray · D.R. Parhi
Dept. of Mechanical Engineering, National Institute of Technology, Rourkela 769008, India
e-mail: kknitrkl@yahoo.in

A. Pandey
e-mail: anish06353@gmail.com

A. Chhotray
e-mail: chhotrayanimesh@gmail.com

D.R. Parhi
e-mail: dayalparhi@yahoo.com

D.K. Lobiyal et al. (eds.), *Proceedings of the International Conference on Signal, Networks, Computing, and Systems*, Lecture Notes in Electrical Engineering 396, DOI 10.1007/978-81-322-3589-7_14

For example; cleaning surfaces, agricultural science, medical science, hazard backgrounds astronomical survey, military, smart shipping, communal robotics, and entertainment. Also, to maintain accuracy without any difficulty for the test of chemical in laboratory or in toxic environment, robots are being regularly used [1]. In robotics research, requirement for real integral equipment to carry out precious scientific tasks is devolved repeatedly [2]. On the other hand, researchers spend maximum time, to determine specific hardware arrangement (wheel arrangements) for autonomous robotic system [3]. In present time, researchers offer various mobile robotic stages and stages have capability to assent research work [4] focusing on organizational platform, such as quest and rescue operation, safety applications and social interface or cybernetics soccer. Presently, almost every major engineering organization have artificial intelligence (AI) research laboratories, and somewhere these laboratories are engaged in mobile robotics research.

Previously, the emphasis of the robotic research was incorporated with large and medium types of systems. But, presently advancement in sensor design [5] and computational control technology through microcontrollers, the focus has been put on the manufacturing of smaller and lower cost robots [6]. Thus, through a large number of low-cost robots, we have to arrange a cheap experimental platform (e.g., swarm robotics [7] tasks) and also create ideal research environment for students in technical institute. With such stimulus in mind, we analyze and assessing work which is based on type-2 fuzzy algorithm (navigation and path planning algorithm). Consequently, the preference continuing with Webots software (A 3D physics-based simulation platform) solutions. Since, it is easy-to-learn as well as easy to implement with programming strategy [8]. In addition, the simplicity of Webots to easily build, transform and expand platform to platform with reference to robotics research [9]. Further, to explore the application of Webots and its flexibility when interrelating with different sensors.

1.1 Algorithm Flexibility to Interact with Environmental Setup

To test the performance of T-2 fuzzy algorithm, an environmental scenario of 0.5 m by 0.5 m (length and width respectively) have been setup, with the height of wall is 0.05 m (Fig. 1a). To carry out this test, 11 IR sensors and 5 ultrasonic sensors are mounted on the robot body (Fig. 1b).

Red and yellow circle (Fig. 1b) shows the IR sensors and blue circle on robot body (Fig. 1b) shows the Ultrasonic sensors. The IR sensors ray (Fig. 2 Red lines) are used for detection and avoidance of an obstacles, whereas ultrasonic sensors ray (Fig. 2 Black lines) are used to detects the range of Target inside the environment. The specification of IR and Ultrasonic sensors are given in Table 1 with measuring

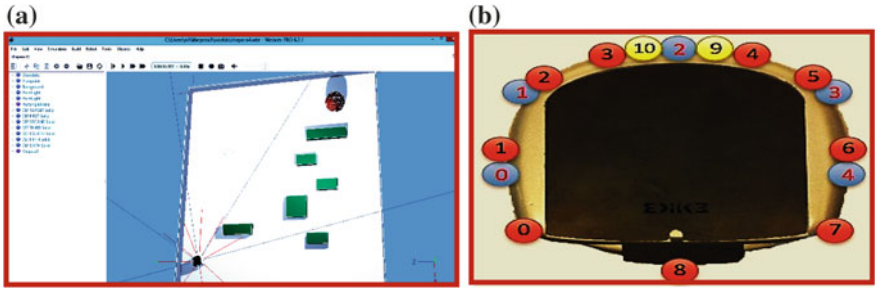

Fig. 1 **a** Khepera III complete environmental set-ups on webots simulation platform. **b** Position of sensors on the robot body (*Red* and *Yellow circle* indicate the position of IR sensors whereas *Blue circle* indicate the position of ultrasonic sensors)

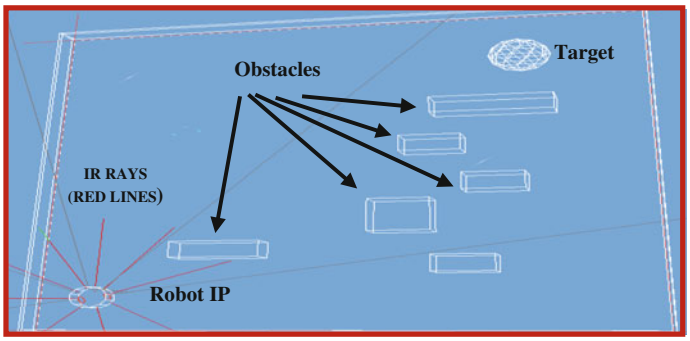

Fig. 2 Simulation environmental scenarios for mobile robot navigation on Webots platform

Table 1 Khepera-III mobile robot specifications

Processor	DsPIC 30F5011 at 60 MHz
RAM	4 KB on DsPIC
Speed max	0.02– 0.5 m/s
Sensors	11 IR sensors (Range 30 cm), 5 ultrasonic sensors (Range 4 m)
Power	Li-polymer battery pack (1350 m Ah)
Size diameter	Diameter 130 mm, height 70 mm
Weight	690 g approx.
Payload	2000 g approx.

range. The control algorithm is dived into two stages. First one; if obstacle detected by the IR sensorns during navigation then avoide the obstacles. Second, if IR reading found no obstacle on the path than move toward the target. At the same time, both algorithms are activated but primary condition is to avoid the obstacle on its path.

2 Architecture of the Type 2 Fuzzy for Current Analysis

Type-2 fuzzy, presented by Zadeh, has the capability to hold mobile uncertainties of amorphous environments [10, 11]. T2 FLC uses surplus aspect of uncertainty to control output. To deal with the bigger computational problem, Mendel et al. presented the Interval T2 (IT2) fuzzy methodology [12]. A number of investigators worked in current years on the way for signifying advantageous cretic of the IT2 FLC over the T1. Yet, the design and optimization of IT2 FLC and its succeeding unfounded decision to the unique T1 FLC are quiet an open question [13].

2.1 Mathematical Design of Control Algorithm

T-2 fuzzy logic creation is the arrangement of five components in sequence manner such as; fuzzification, rule base, interface engine, type reducer and defuzzification (Fig. 3). A T-2 fuzzy logic system based on type-2 fuzzy sets and used to characterize the inputs and outputs of the FL system. In this paper, we have put emphasis on the T-2 fuzzifier as it is fast to characterize and, thus, suitable for the T-2 FLS real world job. Fuzzification plots the crispy input into a fuzzy logic set, which has a non-zero membership function. Hence, fuzzifier maps the crisp input into a type-2 fuzzy sets. The inference stage calculate the fuzzy output sets from fuzzy input sets and rules. Further, fuzzy output is stored in type reducer stage and converted into reduced type-1 sets. After following the type reducer, type-1 set is defuzzified in the defuzzifier stage and crisp output has been created for navigation. In 2002 Mendel and John [14] proposed the work and had shown that a T-2 fuzzy set '$\hat{C}$' can be given as follows:

$$\hat{C} = \sum_{i=1}^{n} \hat{C}_k^i \tag{1}$$

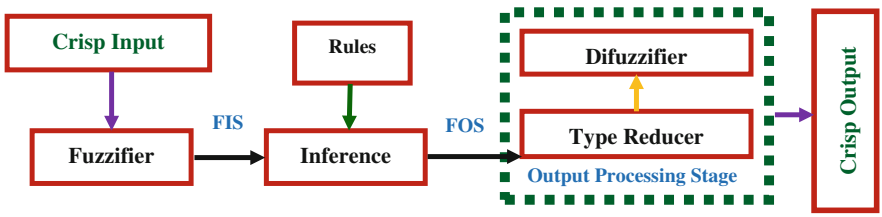

Fig. 3 Type-2 fuzzy logic system

where $\hat{C}$ is an inserted T-2 fuzzy logic set, which can be given as:

$$\hat{C}_k^i = \sum_{D=1}^{Z} \left[F_{N_D}(v_D^i)/v_D^i \right]/N_D \tag{2}$$

where $v_D^i \in J_{N_D} \subseteq U = [0, 1]$

$\hat{C}_k^i$, has 'n' element, as it holds exactly single element from J_{N_1}, J_{N_2}, … J_{N_n} namely v_1^i, v_2^i, … v_n^i each with its related secondary grade namely $F_{N_1}(v_1^i)$, $F_{N_2}(v_2^i), F_{N_n}(v_n^i)$.

$\hat{C}_k^i$ is inserted in $\hat{C}$, and there is a total of $S = \prod_D^n G_D$ inserted sets $\hat{C}_k^i$, where G_D is the discretization level of v_D^i at each N_D. Based on these condition control algorithm has to be evaluated. The control algorithm contains much of the rules. Here, some of the rules has to be given as:

If Front IR Reading is Near and Side IR Reading is Near THAN Output = Left.

If Front IR Reading is Near and Side IR Reading is Far THAN Output = Left.

These rules has to be more clarified from crisp input to crisp output due to the presence of type reducer [15] and Defuzzification both at the same processing time (stage of output processing). The performance of the fuzzy controllers is compared using a wall-following IR based mobile robot in noisy environments (Fig. 4). It is experimentally confirmed that the IT2 FLC can handle well the active uncertainties in the sensual inputs due to the unstiffening and smoothing of the control algorithm by the T-2 fuzzy arrays.

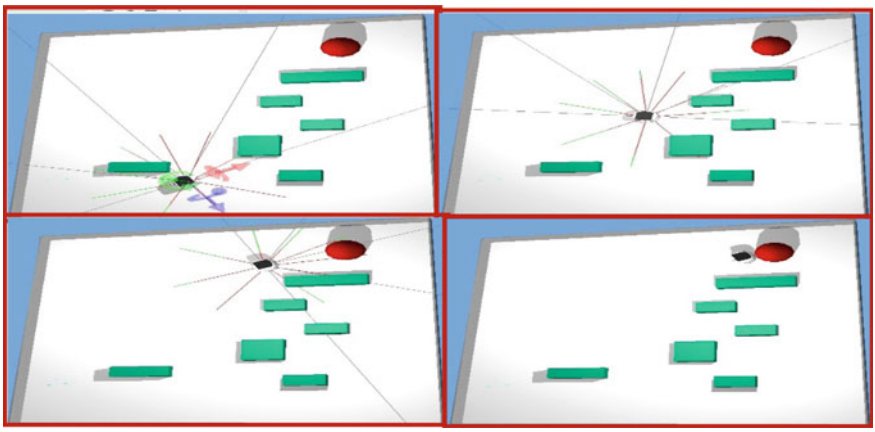

Fig. 4 Navigation using current analysis in an unknown environment

3 Experimental Set-up

In this investigation, the robot movement counted very slowly (about 658 stages from initial position to target position). Table 2 represents some of the stages with distance (distance of robot from the target in x and y direction), orientation (θ) and number of stages, respectively. Form Fig. 4, it can be seen that the IR readings are stable (red line) with scenario limits. Further, green lines represent the contact between IR ray and obstacle while robot moving on its path. Minimum issues occur during the 90^0 turning, as the IR beam cone has an opening of nearly 45^0 (see Fig. 2).

To show the success rate of the existing control algorithm and reliability of the methodology, two real-time experiments are conducted using Webots simulation software (Fig. 4). Khepera III mobile robot has been used for experimental validation (Fig. 5b). To compare the experimental and simulation results, we have proposed the same experimental environment as compared to simulation environment (Fig. 5a). Further, Table 2 represents the simulation experimental data for navigation (two cases taken) using Type 2 fuzzy control algorithm. Due to large number of data, we have only shown some of the stages. Figure 6 has shown the path planning using current analysis.

It is possible to observe nearly divergence in some readings mainly at the end of the stage, due to the IR position reading error (Fig. 7 path) stored throughout the

Table 2 Presents the data related to robot navigation

S. No.	Stages	'*X*' direction		'*Y*' direction		Orientation (degree)		Distance between robot and target	
		*P-I	P-II	P-I	P-II	P-I	P-II	P-I	P-II
1	0	0.04010	0.04010	0.04010	0.04010	0	0	0.380	0.380
2	66	0.16325	0.16623	0.08664	0.08765	31.68	31.62	0.256	0.251
3	132	0.18001	0.18112	0.07754	0.07762	−39.70	−39.64	0.247	0.246
4	198	0.19243	0.19452	0.06723	0.06754	−37.12	−37.06	0.243	0.244
5	264	0.20036	0.20125	0.06156	0.06173	−35.46	−35.44	0.241	0.241
6	330	0.25613	0.25626	0.06421	0.06471	30.82	31.39	0.205	0.203
7	396	0.34176	0.34229	0.16910	0.16876	65.14	65.20	0.078	0.078
8	462	0.36441	0.36721	0.24623	0.24710	116.30	116.36	0.0046	0.0045
9	528	0.35951	0.36562	0.24112	0.24231	−7.62	−7.67	0.0030	0.0031
10	594	0.35911	0.36001	0.24710	0.24731	−176.06	−176.01	0.0023	0.0024
11	658	0.36221	0.36213	0.24313	0.24431	12.26	12.31	0.0015	0.0017

*P = Represents the cases (two cases taken to validate the movement of robot) to calculate the graph (Fig. 7)

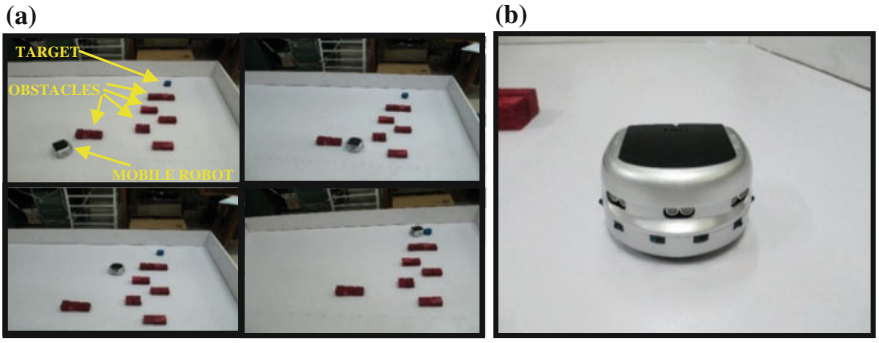

Fig. 5 **a** Real time environmental set-ups for mobile robot navigation and different position of the Khepera-III robot inside the environment. **b** Khepra-III mobile robot for experimental verification

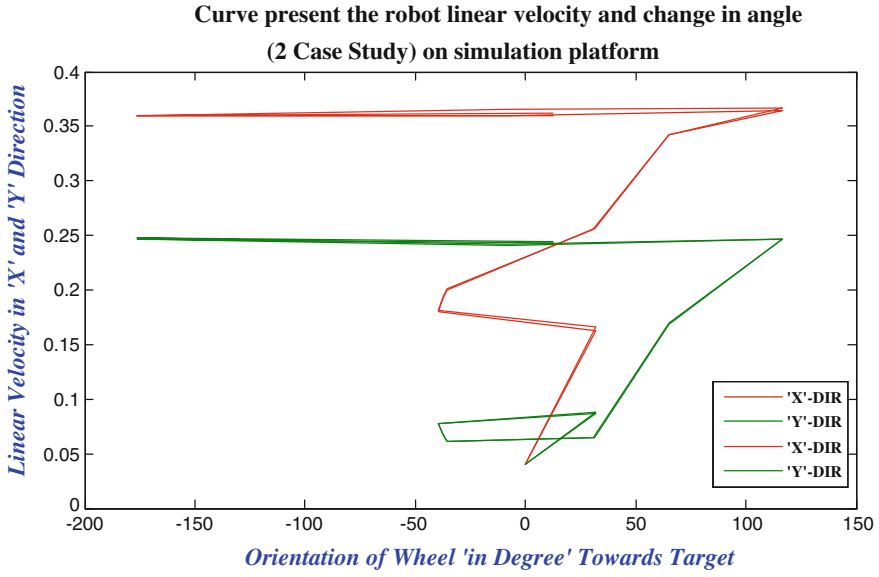

Fig. 6 Curve presents the velocities of wheel versus change in angle on simulation platform (data from Table 2)

motion. It can be observed that, the type 2 fuzzy control algorithm with IR sensors offers a higher flexibility related to other systems.

The robot also followed the path effectively with the help of motor driver components by using developed control algorithms. Initial position (IP) of the robot (in X and Y direction) and position of the target (in X and Y direction) on Webots simulation platform is given by Fig. 8.

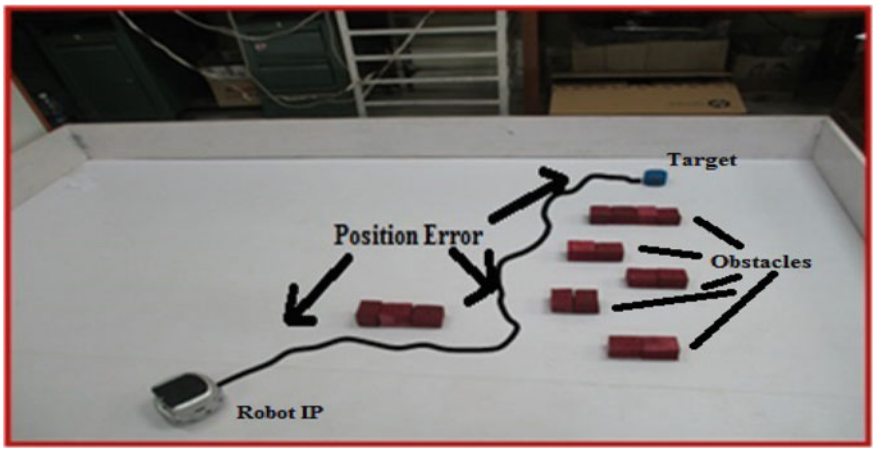

Fig. 7 Investigational results for navigation of mobile robot shown by Fig. 3 on Webots platform

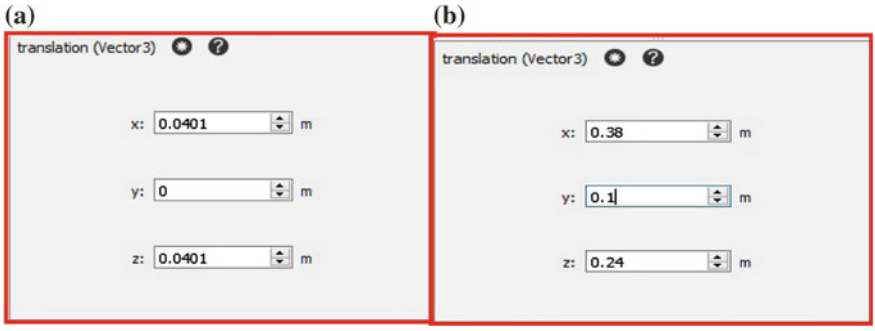

Fig. 8 a Initial position (IP) of the robot in *X*, *Y* and *Z* direction on Webots platform. **b** Position of the target in *X*, *Y* and *Z* direction on Webots platform

4 Conclusions

This paper evolves a methodology for designing a type-2 fuzzy logic control algorithm for autonomous robot navigation and path planning. In addition, also explains how it can be advanced using type 2 fuzzy sets. Accordingly, several simulation experiments have been carried out using Webots simulation environment. In order to measure its performance, robustness and mutability under noisy environment, simulation results have been compared with real-time experiments. Experiments confirm that the T2-FLC is robust for path planning, obstacle avoidance, wall following and navigation, etc. The end results is that autonomous control algorithm is designed to give the scholars what the mobile robots needs when navigated inside local environment. To navigate freely inside noisy environment,

few restrictions, few criticisms, and a compact set of applications have been presented. As future work, it will be considered to advance a T2-FLS algorithm, merging with other AI technique as well as implement into multi robot navigation.

References

1. Hilder, J. A., Owens, N. D. L., Neal, M. J., Hickey, P. J., Cairns, S. N., Kilgour, D. P. A., Timmis, J., Tyrrell, A. M.: Chemical Detection Using the Receptor Density Algorithm, IEEE Transactions on Systems, Man, and Cybernetics—Part C: Applications and Reviews, Vol. 42. (2012) 1730–1741.
2. Dogramadzi, S., Giannaccini, M. E., Harper, C., Sobhani, M., Woodman, R., Choung, J.: Environmental Hazard Analysis—A Variant of Preliminary Hazard Analysis for Autonomous Mobile Robots, Journal of Intelligent and Robotic Systems: Theory and Applications, (2014) pp. 1–45.
3. Hofbaur, M., Kob, J., Steinbauer, G., Wotawa, F.: Improving robustness of mobile robots using model-based reasoning, Journal of Intelligent and Robotic Systems: Theory and Applications, Vol. 48. (2007) 37–54.
4. Lee, S. J., Jung, S.: Object handling control among two-wheel robots and a human operator: An empirical approach, International Journal of Control, Automation and Systems, Vol. 11. (2013) 346–353.
5. Kim, Y., Choi, H. Y., Lee, Y. C.: Design and Preliminary Evaluation of High-Temperature Position Sensors for Aerospace Applications, IEEE Sensor Journal, Vol. 14. (2014) 4018–4025.
6. Di Paola, D., Gasparri, A., Naso, D., Lewis, F. L.: Decentralized dynamic task planning for heterogeneous robotic networks, Autonomous Robots, Vol. 38. (2014) 31–48.
7. Parhi, D. R., Pothal, J. K., Singh, M. K.: Navigation of Multiple Mobile Robots Using Swarm Intelligence, IEEE-World Congress on Nature & Biologically Inspired Computing, (2009) 1145–1149.
8. Olivier, M.: Cyberbotics Ltd - WebotsTM: Professional Mobile Robot Simulation, International Journal of Advanced Robotic Systems, (2004) 40–43.
9. Cervera, E., Martinet, P., Marin, R., Moughlbay, A. A., Del Pobil, A. P., Alemany, J., Esteller, R., Casan, G.: The Robot Programming Network, Journal of Intelligent & Robotic Systems, Vol. 37. (2014) 137–156.
10. Zadeh, L. A.: The Concept of a Linguistic Variable and its Approximate Reasoning - II, Information Sciences, (1975) 301–357.
11. Karnik, N. N., Mendel, J. M.: Type-2 Fuzzy Logic Systems, IEEE Transaction on Fuzzy Systems, Vol. 7 (1999).
12. Mendel, J. M.: Uncertain Rule-Based Fuzzy Logic Systems: Introduction and New Directions, Prentice-Hall, Upper Saddle River, NJ, 2001.
13. Mendel, J. M.: A Quantitative Comparison of Interval Type-2 and Type- 1 Fuzzy Logic Systems: First Results, Proceeding of FUZZY-IEEE, Barcelona, Spain, (2010) 404–411.
14. Mendel, J., John, R.: Type-2 fuzzy sets made simple, IEEE Transaction- Fuzzy System, Vol. 10. (2002) 117–127.
15. Nie, M., Tan, W.W.: Towards an efficient type-reduction method for interval type-2 fuzzy logic system, Proceeding of Fuzzy-IEEE Hong Kong, (2008) 1425–1432.

Analysis of the Complexity of Brain Under Mobile Phone Radiation Using Largest Lyapunov Exponent

C.K. Smitha and N.K. Narayanan

Abstract The changes in complexity of brain while using two types of mobile phones are analyzed using Electroencephalogram (EEG) signals in this paper. Largest Lyapunov Exponent (LLE) of the data set prepared with EEG record of 35 subjects with and without phone is analyzed using non parametric Mann-Whitney U test. The test is significant in 8 electrodes for data set with phone-1 and is significant for one electrode for the data set with phone-2. Symmetry of brain using asymmetry index is analyzed for further verification and found within allowable range. It is concluded that there is no significant change in complexity of brain while using mobile phone.

Keywords EEG · Mobile phone radiation · Largest lyapunov exponent · Asymetryindex Mann-Whitney U test

1 Introduction

The concern about the effect of electromagnetic radiation on human brain increases due to wide spread use of mobile phones. A number of studies [1–7] show some adverse effects and some others [8–13] ascertain that there is no clear evidence to link the relationship between the changes in the human body and mobile phone radiation.

For any changes in the cellular level, mutation of cells are to take place and mutation is initiated by ionizing radiation. Frequency of ionizing radiation is greater

C.K. Smitha (✉)
Department of Electronics and Instrumentation Engg, College of Engineering, Vadakara 673105, Kerala, India
e-mail: smi_c_k@yahoo.com

N.K. Narayanan
Department of Information Technology, Kannur University, Kannur 670567, Kerala, India
e-mail: nknarayanan@gmail.com

D.K. Lobiyal et al. (eds.), *Proceedings of the International Conference on Signal, Networks, Computing, and Systems*, Lecture Notes in Electrical Engineering 396, DOI 10.1007/978-81-322-3589-7_15

than the frequency of visible light (>8×10^{14} Hz). The frequency range of electromagnetic field (RF-EMF) generated by mobile phones are very much less than that of visible light. So as per basics of physics, electromagnetic radiations from mobile phone are not able to produce any effect on human tissue. We choose EEG signal for the analysis of the effect of mobile phone radiation on brain, since the variations in the electrophysiological characteristics of the brain can easily measure using EEG. A set of non linear differential equations can be used to describe the bio-physical process underlying the EEG generation. Being chaotic in nature, the attractor dimension is suitable for the evaluation of changes in EEG. We tried to investigate the variation in brain due to mobile phone radiation using Largest Lyapunov Exponent (LLE).

It is learnt from the review of literature that LLE is not used for the analysis of the effects of mobile phone radiation. Various nonlinear measures specifically fractal dimension [14–19], and entropies [20–22] were used for the analysis of signal complexity of EEGs with and without radiation from mobile phone in the previous work by same authors. The results showed that, there were some changes in single electrodes but the effect is not prominent while analyzing the signals in 21 electrodes. So in this paper we studied the effect of mobile phone radiation on the brain by analyzing the LLE of signals in 21 electrodes of the EEG data set.

The paper is outlined as follows: The methods of feature extraction and analysis included in Sect. 2. Results obtained and the discussions of the result are detailed in Sect. 3 and conclusion in Sect. 4.

2 Methods

The scalp record of electrical activity of the brain is the electroencephalogram (EEG). EEGs were recorded with 21 scalp electrodes placed as per conventional 10–20 system of electrodes.

2.1 Data Acquisition

35 healthy individuals of different age groups (39.8 + 11.8) were participated in this study. EEGs were recorded from EEG Lab under Neurology Department of Malabar Institute of Medical Sciences Hospital Calicut using Galelio N.T machine. EEGs of the volunteers were recorded at rest and by keeping mobile phones near to the right ear for 5 min each with two types of mobile phones. The phone-1 was a GSM with SAR 1.3 W/Kg and phone-2 was a CDMA phone with SAR 0.987 W/Kg. During the procedure, the volunteers were instructed to lie down and relax. EEGs were taken initially at rest and then the phone is switched on (in talking mode) and kept near the right ear. The subjects were unaware of the instant of switching of mobile phone.

2.2 Preprocessing

Visual inspection and filters are used to eliminate unwanted signals or artifacts in EEG. 50 Hz line frequencies are eliminated using a notch filter and denoising was done by wavelet algorithm using threshold filtering [23]. The SNR obtained is 12–17 dB using this method.

2.3 Feature Extraction

Lyapunov exponent is one of the best attractor dimensions in the case of a chaotic signal. The Lyapunov exponent [24–29] measures the rate of convergence or divergence of adjacent trajectories in phase space. Quantitatively, the separation of two trajectories with initial distance ΔZ_0 is represented in phase space as

$$|\Delta Z(t)| \approx e^{\lambda t}|Z_0| \tag{1}$$

where λ is the Lyapunov exponent. Positive Lyapunov exponent represents diverging trajectories and a chaotic system. The features of all the electrodes were calculated using MATLAB software and statistical analysis is done using the Mann Whitney U test in SPSS software. The statistical method used is discussed in the next section.

2.4 Statistical Test—Mann Whitney U Test

A hypothesis test [30, 31] is a method of making decisions using data from a scientific study. The Mann Whitney U test is a non parametric test compares samples from two groups based on the median. The test statistic (U static and p value) is calculated and the null hypothesis is rejected at the given level of significance if the p-value is less than the required significance.

Symmetry of significant electrode pairs was analyzed using asymmetry index which is discussed in the next section.

2.5 Asymmetry Index—Analysis of Left-Right Symmetry of Brain

The normality of the EEG signals is verified using left right symmetry. Visual inspection of EEG signals was used for the analysis of the status of the brain by EEG technicians. EEG waves are classified as abnormal, if the difference of signal

in pairs of electrodes is greater than 50 %. Coefficient of Variance (C V), the ratio of mean to standard deviation [32] of the feature is taken as the asymmetry index. The asymmetry index of pairs of channels was compared.

3 Results and Discussions

3.1 Verification of SAR

We verified the SAR of the mobile phone specified by manufacturers by using FDTD (Finite Difference Time Domain) method of simulation The value of SAR obtained is less than the prescribed value by the manufacturers of the phone. The prescribed value for GSM phone (Phone-1) is 1.3 W/Kg and for CDMA phone is 0.987 W/Kg. Maximum value of SAR obtained by method of FDTD simulation is 1.12 W/Kg for GSM phone and 0.84 W/Kg for CDMA phone.

3.2 Analysis of Feature

The typical plot of Lyapunov exponent against the number of iterations for a subject for example is shown in Fig. 1. The average values of the feature with phone-2 are greater and feature with phone-1 are less than the feature at rest.

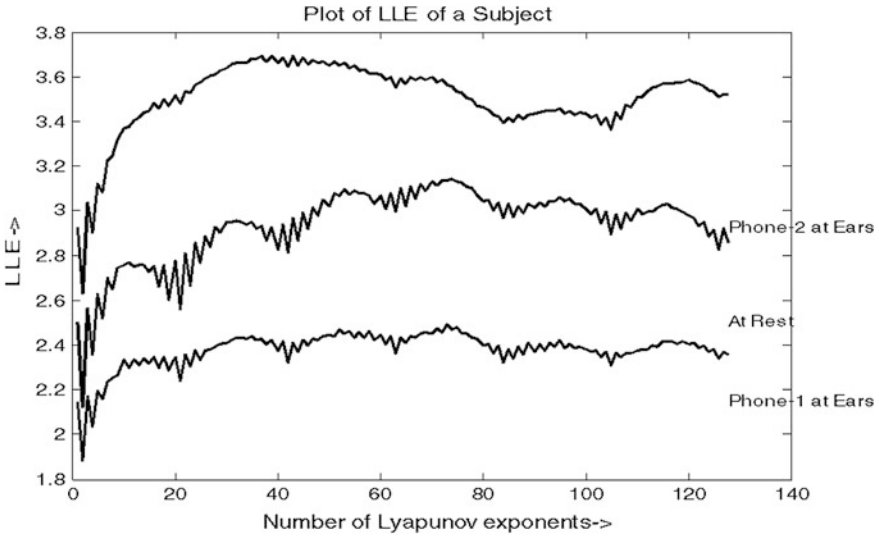

Fig. 1 Plot of LLE of a subject for different conditions. The plot at the *top* is for EEG data with phone-2, 2nd plot from the *top* is for data at rest and 3rd plot is for data with phone-1

Table 1 The percentage change in asymmetry index with respect to the *left side*

At rest	−1.5	2.1	8.1	1.1	−1.3	2	−3.6	2.9
Ph-1 at ears	−3.6	−3.4	2.5	3.8	8.5	2.4	5.1	3.3
Ph-2 at ears	−4.1	0.2	9.3	−2	4.9	1	−0.4	1.6

3.3 Statistical Analysis

Thirty samples with a length of 256 points are selected from signals of each electrode of the data set, largest Lyapunov exponent is calculated and analysed statistically. Gaussianity/Normality is checked using box plot to select the appropriate test for statistical analysis. Since data are not symmetrically distributed, non parametric non linear, two independent sample test named Mann Whitney U test is used for the analysis. On analyzing the result of Mann Whiteny U test for the data set with phone-1, the p values (0.002, 0.008, 0.004, 0.032, 0.004, 0.019, 0.008 and 0.021) obtained for signals in electrodes Fp1, F7, F3, C4, T5, P3, O1 and O2 are less than the confidence interval 0.05. So the null hypothesis is rejected and the alternate hypothesis is accepted which depicts that the median of the sample with phone-1 is different from that of the median at rest. Similarly the test statistics shows that the test is significant in electrode Fp1 (p value = 0.004) while comparing the data at rest with data with phone-2.

To study the impact of this difference, the variation of feature in pair of electrodes is assessed using asymmetry index to check the variation in symmetry of two hemispheres of brain. Channels in left hemisphere of head are odd numbered and right hemisphere is even numbered. The pair of channels are Fp1-Fp2, F3-F4, F7-F8, C3-C4, T3-T4, T5-T6, P3-P4 and O1-O2. Asymmetry index of pair of these significant electrodes (Fp1-Fp2, F7-F8, F3-F4, C3-C4, P3-P4, T5-T6 and O1-O2) are analysed. The percentage change in asymmetry index in the significant electrodes (Fp1-Fp2, F7-F8, F3-F4, C3-C4, P3-P4, T5-T6 and O1-O2) is tabulated in Table 1. The difference in asymmetry index changes from—4.1–9.3 %.

4 Conclusions

The statistical test is significant in 8 electrodes for GSM phone and in one electrode for CDMA phone using LLE as feature. It is concluded that the data set of features whereas using mobile phone-1 is different from that of the data set at rest in Fp1, F7, F3, C4, T5, P3, O1, O2 and is different in Fp1 whereas using phone-2. The statistical analysis is significant for those electrodes having an increase of 1.5 % or more, but as far as the EEG is considered, the EEG signal with 50 % change in a pair of electrodes is treated as abnormal.

The difference in asymmetry index changes from—4.1–9.3 %. The difference in asymmetry index is not greater than 50 % in any of the electrode pairs while using LLE as feature. Here all the magnitudes of asymmetry indexes in all pairs are much less than the prescribed limit. So the effect of radiation from two types of mobile phone cannot produce any measurable effect on the brain.

The measured value of the potential in an electrode is the sum of the potential of a group of neurons comes under that particular electrode. The change in feature parameter shows the variations in EEG signal while using the mobile phone, which demonstrates transformation in the activities of the brain due to radiation. The change in EEG signals is due to activation or in activation of group of neurons comes under each electrode. Since this value is within the limit, it can be concluded as there is no activation of neurons took place due to radiation from mobile phones.

Acknowledgments The data set was prepared solely for this research purpose, from the MIMS Hospital Calicut without any financial assistance. We thank Director, Management of the Hospital for the consent to use Lab facility and also thank Dr. Ashraf and staff members of Neurology Department of the Hospital, for helping with their EEG expertise.

References

1. Hardell, L., Hallquist, A., Mild, H.: Cellular and cordless telephones and the risk for brain tumors. Fur. J. Cancer Prev., Vol.11.(2002) 377–386.
2. Min Kyung Chu, Hoon Geun Song, Chulho Kim and Byung Chu Lee.: Clinical features of headache associated with mobile phone use: a cross-sectional study in university students. BMC Neurology. Vol 11:115. (2011) 1–7.
3. Ashok Agarwal, Fnu Deepinder, Rakesh K. Sharma, Geetha Ranga, and Jianbo Li: Effect of cell phone usage on semen analysis in men attending infertility clinic: an observational study. American Society for Reproductive Medicine, Elsevier Inc., (2008) 124–128.
4. James C Lin.: Cellular Telephone Radiation and EEG of Human Brain. IEEE Antennas and Propagation Magazine. Vol 45, No-5 (2003).
5. H. D'Costa, G.Trueman, L Tang, U. Abdel-rahman, U. Abdel-rahman, K Ong and I Cosic.: Human brain wave activity during exposure to radiofrequency field emissions from mobile phones. Australasian Physical & Engineering Sciences in Medicine Vol. 26, Number 4. 2003.
6. Eleni Nanou, Vassilis Tsiafakis, E. Kapareliotis.: Influence of the Interaction of a 900 MHz Signal with Gender On EEG Energy: Experimental Study on the Influence of 900 MHz Radiation on EEG. The Environmentalist, Vol. 25. Springer Science. (2005) 173–179.
7. Hie Hinkirikus, Maie Bachmann et al.: Non-Thermal Effect of Microwave Radiation on Human Brain. The Environmentalist, Vol.25.Springer Science. (2005), 187–194.
8. IARC/A/WHO (2011) Classifies radiofrequency electromagnetic fields as possibly carcinogenic to humans. Press Release.
9. Ghosn, Rania, Thuroczy György, Loos Nathalie, Brenet-Dufour Valérie, Liabeuf Sophie, De Seze Rene.: Effects of GSM 900 MHz on Middle Cerebral Artery Blood Flow Assessed by Transcranial Doppler Sonography. Radiation Research, Vol.178, No.6. (2013) 543–550.
10. N., Perentos, Croft, RJ., Mc Kenzie, I., Cosic.: Comparison of the effect of continuous and pulsed mobile phone like RF exposure on human EEG. Australian Physical and Engineering Science in Medicine. Vol. 30, No 4. (2008) 274–280.

11. Michael H.Repacholi, Alexander Lerchl, Martin Rosli, Zenon Sienkiewicz.: Systematic Review of Wireless Phone Use and Brain Cancer and Other Head Tumors. Bioelectromagnetics, (2011) 187–207.
12. Myoung-Soo Kwon, Jaaskelaine Satu K, Toivo, Tim Hamlainen, Heikki.: No effects of mobile phone electromagnetic field on auditory brainstem response. Bioelectromagnetics, Vol.31, No.1, (2010) 48–55.
13. Hirose Hidek Sasaki, Atsush Ishii Nana, Sekijima Masaru, Iyam Takahiro, Nojima Toshio, Ugawa, Yoshikazu.: 1950 MHz IMT-2000 field does not activate microglial cells in vitro. Bioelectromagnetics, Vol.31, No.2. (2010)104–112.
14. C. K., Smitha, N. K., Narayanan.: Effect of mobile phone radiation on brain using EEG analysis by Higuichi's fractal dimension method. Proc. SPIE 8760, International Conference on Commu nication and Electronics System Design, 87601C (2013).
15. C. K., Smitha, N. K., Narayanan.: Study of Brain Dynamics under Mobile Phone Radiation Using Various Fractal Dimension Methods. Proce. of International Conference on Signal processing, image processing and pattern recognition. (2013) 288–292.
16. C. K., Smitha, N. K., Narayanan.: Effect of Mobile Phone Radiation on EEG Using Various Fractal Dimension Methods. International Journal of Advancements in Research & Technology, Volume 2, Issue5, (2013).
17. C. K., Smitha, N. K., Narayanan.: Effect of Mobile Phone Radiation on EEG. Proce. of third International Conference on Advances in Computing and Communications, Kochi. (2013).
18. C. K., Smitha, N. K., Narayanan.: Brain Dynamics under Mobile Phone Radiation Using Various Fractal Dimension Methods. International Journal of Imaging and Robotics, Vol. 13, Issue Number 2. (2014)166–180.
19. C. K., Smitha, N. K., Narayanan.: Analysis of Fractal Dimension of EEG Signals under Mobile Phone Radiation. The Proce. of IEEE international Conference on Signal Processing, Informatics, Communication and Energy Systems (2015) 1–5.
20. C. K., Smitha, N. K., Narayanan.: Interaction of Mobile Phone radiation with Brain. The Proce. of 14th Biennial International Symposium on Antenna and Propagation, CUSAT, Cochin, Vol -1. (2014) 57–60.
21. C. K., Smitha, N. K., Narayanan.: Analysis of the Effects of Mobile Phone Radiation on Brain using Approximate entropy. The proce. of Joint International Conferences on ITC 2015. McGraw-Hill Education. (2015) 208–215.
22. C. K., Smitha, N. K., Narayanan.: Entropy Analysis to Study the Effects of Mobile Phone Radiation on Brain, Proce. of the International Conference on Information and Communication Technology Research. Abudhabi (2015) 251–254.
23. Abdullah Al Jumah.: Denoising of an Image Using Discrete Stationary Wavelet Transform and Various Thresholding Techniques" Journal of Signal and Information Processing. Vol. 4. (2013) 33–41.
24. Saeid Sanei and J.A. Chambers.: EEG Signal Processing. John Wiley and Sons (2007).
25. AlanWolf, Jack B swif, Harry L. swinney and John A Vastano.: Determining Lyapunov exponent from time series, Physica D 65 North-Holland. (1985) 285–317.
26. Michael T. Rosenstein, James J. Collins and Carlo J. De Luca.: A practical method for calculating largest Lyapunov exponents from small data sets, Physica D 65 North-Holland (1993) 117–134.
27. Elif Derya Übeyl, Nan Guler.: Statistics over Lyapunov Exponents for Feature Extraction: Electroencephalographic Changes Detection Case. World Academy of Science, Engineering and Technology 2. (2007) 624–628.
28. Pengjian Shang, Xuewei Li., Santi Kamar.: Chaotic analysis of traffic time series. Chaos, Solitons and Fractals Vol. 25. (2005) 121–128.
29. Marc W Slutzky, Predrag Cvitanovic and David J Mogul.: Deterministic Chaos and Noise in Three In Vitro Hippocampal Models of Epilepsy. Annals of Biomedical Engineering, Vol. 29. pp 1–12.
30. Irwin Miller and John E Freund.: Probability and Statistics for Engineers. 4th Edn, Prentice Hall, (1985).

31. A Stuart and MG Kendall.: Statistical Inference and Statistical Relationship The theory of Statistics Vol-2. Hafers Press (1986).
32. Kenneth Hugdahl,: Symmetry and asymmetry in the human brain, European Review, Vol 13, Supp. No. 2. UK (2005).

A Review of Bio-Inspired Computing Methods and Potential Applications

Amrita Chakraborty and Arpan Kumar Kar

Abstract The domain of bio-inspired computing is increasingly becoming important in today's information era. More and more applications of these intelligent methods are being explored by information scientists for different contexts. While some studies are exploring the application of these algorithms, other studies are highlighting the improvement in the algorithms. In this study, we identify five more popular algorithms and briefly describe their scope. These methods are neural networks, genetic algorithm, ant colony optimization, particle swarm optimization, and artificial bee colony algorithms. We highlight under what context these algorithms are suitable and what objectives could be enabled by them. This would pave the path for studies conducted in the future to choose a suitable algorithm.

Keywords Bio-inspired computing · Neural networks · Genetic algorithm · Ant colony optimization · Particle swarm optimization · Artificial bee colony

1 Introduction

The domain of bio-inspired computing is gradually getting prominence in the current times. Algorithms from bio-inspired computing are gradually gaining prominence since these algorithms are more intelligent and can learn. Further, these algorithms have the capability to generate information based on the changes in the

A. Chakraborty (✉)
Electronics & Telecommunication Engineering, Jadavpur University, Kolkata 700032, India
e-mail: amrita.chakraborty2@gmail.com

A.K. Kar
Information Systems Area DMS, Indian Institute of Technology Delhi, New Delhi 110016, India
e-mail: arpan_kar@yahoo.co.in

D.K. Lobiyal et al. (eds.), *Proceedings of the International Conference on Signal, Networks, Computing, and Systems*, Lecture Notes in Electrical Engineering 396, DOI 10.1007/978-81-322-3589-7_16

ecosystem that is generating data. The subsequent sections are subdivided in the following: first we identify the different types of popularly used algorithms among bio-inspired algorithms. Subsequently we explore the scope of these algorithms in specific context. Then based on the applications and scope of the algorithms, we try to provide insights on the potential applications for future research directions. We do not attempt to explore the scope or performance centric issues for the current study. Further the comparison through empirical validation is also beyond the scope of our current study, which has been built through the review of literature.

2 Review of Algorithms

This section is subdivided into independent reviews of multiple algorithms. All of these algorithms try to replicate the way biological organisms and entities operate to achieve high efficiency, even if sometimes the actual optimization is not achieved. After the review of algorithms, we focus on the scope of applications.

2.1 Neural Networks

Neural Networks [11] are often defined as adaptive nonlinear data processing algorithms that combine multiple processing units connected in a network in different layers. These networks are characterized by being self-adapting, self-organizing, and with the potential to learn based on inputs and feedbacks from the ecosystem within which it is operating. These neural networks try to replicate the way the neurons in any organism are coded to take inputs and through operations in a black box, to provide an output. The difference of outputs from desired results is sent back as feedback to improve the processing systems.

While there are different approaches with which neural networks are implemented, probably the simplest implementation is that of a perceptron network where there is a feedback to improve upon the output and there is often a single layer that provides the internal operations. Perceptron networks can be used both for linear and nonlinear systems [22]. Further such a network could also have multiple inputs and multiple layers [2]. Also developments in neural networks have seen applications of probabilistic and approximation-based algorithms to accommodate imprecise or incomplete information to improve outcome [13, 24]. Also, the way information as processed was segregated into linear and nonlinear neural networks in the same way as the individual information processing nodes operated within the network [11, 20]. Recent literature [23] highlights how deep, shallow, unsupervised, supervised, and reinforcement-based approaches are used to train the

networks based on data availability. However, neural networks can be combined with other algorithms and methods, based on the needs of the problem to provide improved predicting capabilities to the system [14, 23].

2.2 Genetic Algorithm

Genetic algorithm [12] was introduced to accommodate the way nature uses powerful computational techniques to obtain a highly suitable solution. It is an evolutionary search heuristic that mimics the process of natural selection. It is used to solve a variety of single and multi-objective problems that are combinatorial in nature and NP hard [1, 4]. For using this algorithm, a problem solution is defined in terms of the fitness function where the fitness of the potential solution is an indicator of its suitability. This fitness may be represented by integers, vectors, matrices, linked lists, or other data structure based on how the problem is tackled. A coding mechanism may transfer the data structure to the fitness function. Fitness could be either a maximization or a minimization function, based on objective. To address this situation, four basic operators were defined in genetic algorithm literature [3, 21]. For a new candidate solution to be produced, a pair of pre-optimized solutions are modified by using these operators. By using the operators, a "child" solution is obtained through crossover and reproduction where typically the new candidate solution shares many of the characteristics of its "parents". However in the mutation operator, a specific fitness driver may be changed to enhance the fitness of the candidate solution abruptly. This is done to avoid local optimality and challenges associated with intermediate levels [19, 25].

2.3 Ant Colony Optimization

Ant colony optimization [6, 7] is a heuristic search algorithm, for solving combinatorial optimization problems. It is based on the indirect communication of simple agents (called ants here) foraging for information, mediated by artificial pheromone trails. The trails serve as a distributed numerical information for the agents to construct solutions based on probabilistic search experience. The results are obtained in a reasonable amount of search time.

In this algorithm, the solution is often attempted in a sequence of iterative steps [5]. Candidate solutions are developed from a sample of solutions using a parametric probability distribution. For doing so, a group of ants is selected and a pool of decision variable is defined in the problem. The ants select the design variables for creating the candidate solutions. As the ants explore the candidate solutions, a

local updation of the solution is done based on its optimality. These candidate solutions are used to modify the value of the trails based on the local updation in such a way to select the higher quality solutions in the subsequent sampling for candidate solutions by the same group of ants. The candidate solutions created in the initial phase therefore pave the path for optimality.

2.4 Particle Swarm Optimization

Particle swarm optimization is a heuristic algorithm inspired from the collective group behavior of animals such as fish schooling, insect swarming, or birds flocking, whereby the group attempts to meet the collective objective of the group based on the feedback from the other members. It is used for problems where the function to be optimized is discontinuous, non-differentiable with too many nonlinearly related parameters [8]. Assumption for this algorithm is that the collective intelligence of the group is more than the sum of individual intelligence of its members. This algorithm operates in a sequence of few iterative steps [8, 9]. Each particle or member in the swarm (say a bird or fish) tries to sense a potential solution at any point of time. It communicates a signal proportional to the suitability of the candidate solution to the other particles in the swarm. Each swarm particle or member can therefore sense the strength of the signal communicated by the other members, and thus the suitability of the candidate solution based on a fitness function [9]. When a particle or member tries to focus on a more suitable candidate solution from among the locally available candidate solutions, based on different learning mechanisms [26, 27], a new movement direction is identified along with an inertial influence to gradually guide the particles toward an optimal solution wherever possible. Application of this algorithm could be in multi-criteria decision problems, searching, constraint-based optimization problems, deterministic optimization problems, scheduling problems, thresholding, and maximization/minimization problems.

2.5 Artificial Bee Colony Algorithm

The artificial bee colony algorithm [10, 15] is a metaheuristic-based optimization algorithm which searches for an optimal numerical solution among a large number of alternatives while trying to solve NP hard problems [16]. This approach is based on the foraging behavior of the honey bee swarm. The behavior of honey bees based on the communication, task allocation, nest site selection, reproduction, mating, floral foraging, and pheromone laying and navigation behaviors of the swarm has been used in modification of this algorithm [15, 16, 26].

In this algorithm [15, 16], first the vectors of the population are initialized as a potential food source. Employed bees search for new food sources with a random stimulus initially. Subsequently, once a food source is identified (a candidate solution), the fitness of the same is identified and computed. In the next phase, if a new food source is subsequently discovered (a new candidate solution) by "employed bees" with a greater fitness, the new source is adopted else and the new one is rejected. Employed bees share the fitness information with the onlooker bees who choose their food source based on the probability of the food occurring. If bees are unable to improve the fitness of the food source, their solutions are rejected.

3 Discussion on the Scope of Applications

In this section, we highlight the potential scope of applications based on the evidences in published literature. However, due to lack of page constraints, we are brief in our discussion. Neural networks [11, 14, 23, 24] have been used extensively for the generation of association rules, classification problems, detection problems, pattern recognition, nonlinear regression, feature selection, missing data prediction, time series prediction, data normalization, principal component analysis, and probabilistic prediction. Genetic algorithms [1, 3, 21] have been used for searching among alternatives, maximization/minimization problems like the traveling salesman problem, sorting problems, multi-objective decision-making, multi-criteria decision-making, and constrained optimization problems. Ant colony optimization [17, 18] is extended to be able to tackle mixed variable optimization problems and continuous optimization problems for selection-, searching-, and optimization-based problems. Application of particle swarm optimization [5–7] could be in multi-criteria decision problems, searching, constraint-based optimization problems, deterministic optimization problems, scheduling problems, thresholding, and maximization/minimization problems. Artificial Honey Bee algorithm [9, 15, 16] has predominantly been used in literature as a single objective numerical value optimizer. Further it has been used for searching, routing problem, assignment problem, allocation problem, and maximization or minimization problems.

4 Conclusion

While these algorithms have witnessed a lot of attention from information scientists in recent years, the understanding within the domain is far from being mature. Except for a few these algorithms which are selected for discussion here, literature presents a lot of debate on the convergence and stability of these algorithms. The focus of this paper is not to highlight how these algorithms may be used for solving real-life problem through scientific notation, but to provide initial food for thought for understanding the scope and objective for these algorithms, and then choose one

based on the scope of the research problem and explore it in greater depth. Such an exploration would require a detailed break down and coding of the individual systems (say the fitness functions or computational units) for the algorithm chosen for solving the research problem.

References

1. Aytug, H., Khouja, M., & Vergara, F. E. (2003). Use of genetic algorithms to solve production and operations management problems: a review. International Journal of Production Research, 41(17), 3955–4009.
2. Bounds, D.G., Lloyd, P.J., Mathew, B., & Waddell, G. (1988). A multilayer perceptron network for the diagnosis of low back pain. IEEE International Conference on Neural Networks, 481–489.
3. Colin, R.R., & Jonathan, E.R. (2002). Genetic algorithms-Principles and perspectives.
4. Dimopoulos, C., & Zalzala, A. (2000). Recent developments in evolutionary computation for manufacturing optimization: problems, solutions, and comparisons. IEEE Transactions on Evolutionary Computation, 4(2), 93–113.
5. Dorigo, M., & Blum, C. (2005). Ant colony optimization theory: A survey. Theoretical computer science, 344(2), 243–278.
6. Dorigo, M., & Birattari, M. (2010). Ant colony optimization. In Encyclopedia of machine learning (pp. 36–39). Springer US.
7. Dorigo, M., Birattari, M., & Stützle, T. (2006). Ant colony optimization. Computational Intelligence Magazine, IEEE, 1(4), 28–39.
8. Floreano, D., & Mattiussi, C. (2008). Bio-inspired artificial intelligence: Theories, methods, andtechnologies. Cambridge: MIT Press.
9. Gandomi, A. H., Yun, G. J., Yang, X. S., & Talatahari, S. (2013). Chaos-enhanced accelerated particle swarm optimization. Communications in Nonlinear Science and Numerical Simulation, 18(2), 327–340.
10. Gao, W. F., & Liu, S. Y. (2012). A modified artificial bee colony algorithm. Computers & Operations Research, 39(3), 687–697.
11. Grossberg, S. (1988). Nonlinear neural networks: Principles, mechanisms, and architectures. Neural networks, 1(1), 17–61.
12. Holland, J. H. (1975). Adaptation in natural and artificial systems: An introductory analysis with applications to biology, control, and artificial intelligence.
13. Hornik, K. (1991). Approximation capabilities of multilayer feedforward networks. Neural networks, 4(2), 251–257.
14. Kar, A.K. (2015). A hybrid group decision support system for supplier selection using analytic hierarchy process, fuzzy set theory and neural network. Journal of Computational Science, 6, 23–33.
15. Karaboga, D. (2005). An idea based on honey bee swarm for numerical optimization (Vol. 200). Technical report-tr06, Erciyes University, engineering faculty, computer engineering department.
16. Karaboga, D., Gorkemli, B., Ozturk, C., & Karaboga, N. (2014). A comprehensive survey: artificial bee colony (ABC) algorithm & applications. Artificial Intelligence Review, 42(1), 21–57.
17. Liao, T., Socha, K., Montes de Oca, M., Stutzle, T., & Dorigo, M. (2014). Ant colony optimization for mixed-variable optimization problems. Evolutionary Computation, IEEE Transactions on, 18(4), 503–518.
18. Liao, T., Stützle, T., deOca, M.A.M., & Dorigo, M. (2014). A unified ant colony optimization algorithm for continuous optimization. European J. of Operational Research, 234(3), 597–609.

19. Mitchell, M., Forrest, S., & Holland, J. H. (1992). The royal road for genetic algorithms: Fitness landscapes and GA performance. European Conf. on artificial life (pp. 245–254).
20. Oja, E. (1992). Principal components, minor components, and linear neural networks. Neural Networks, 5(6), 927–935.
21. Reeves, C. (2003). Genetic algorithms. Handbook of Metaheuristics, 57, 55–82.
22. Sadegh, N. (1993). A perceptron network for functional identification and control of nonlinear systems. IEEE Transactions on Neural Networks, 4(6), 982–988.
23. Schmidhuber, J. (2015). Deep learning in neural networks: An overview. Neural Networks, 61, 85–117.
24. Specht, D. F. (1990). Probabilistic neural networks. Neural networks, 3(1), 109–118.
25. Srinivas, M., & Patnaik, L. M. (1994). Adaptive probabilities of crossover and mutation in genetic algorithms. IEEE Transactions on Systems, Man and Cybernetics, 24(4), 656–667.
26. Yang, X. S., Cui, Z., Xiao, R., Gandomi, A. H., & Karamanoglu, M. (Eds.). (2013). Swarm intelligence and bio-inspired computation: theory and applications. Newnes.
27. Zhan, Z. H., Zhang, J., Li, Y., & Shi, Y. H. (2011). Orthogonal learning particle swarm optimization. IEEE Transactions on Evolutionary Computation, 15(6), 832–847.

An Effective Task Scheduling Approach for Cloud Computing Environment

Jyoti Gupta, Md. Azharuddin and Prasanta K. Jana

Abstract Cloud computing is one of the fastest growing technologies which delivers online services to a consumer on pay-per-use basis. Recently, the concept of multi-cloud environment has been evolved in the recent years in which workloads are distributed among the data centers of multiple clouds. However, task scheduling in a multi-cloud environment is more challenging as the resources of the data centers belonged to the clouds are heterogeneous in nature. In this paper, we propose an efficient task scheduling algorithm for multi-cloud environment. We perform extensive simulation of the proposed algorithm on benchmark data and compare the results with the existing algorithms. We show that the algorithm performs better than the existing algorithms in terms of make span and resource utilization.

Keywords Cloud computing · Task scheduling · Makespan · Resource utilization

1 Introduction

Cloud computing has emerged as one of the fastest growing technologies in the field of information technology. It can be described as delivering many aspects of computing to the end users as a web service with the help of virtualized resources [1]. The benefits of cloud computing are high scalability, reliability, multi-tenancy, lower cost in procuring resources, ease of access to data, and many more [1–3]. In the recent years, multi-cloud environment has been evolved to provide the customer

J. Gupta · Md. Azharuddin (✉) · P.K. Jana
Department of Computer Science and Engineering, Indian School of Mines, Dhanbad 826004, India
e-mail: jyoti.cse.iit@gmail.com

Md. Azharuddin
e-mail: azhar_ism@yahoo.in

P.K. Jana
e-mail: prasantajana@yahoo.com

D.K. Lobiyal et al. (eds.), *Proceedings of the International Conference on Signal, Networks, Computing, and Systems*, Lecture Notes in Electrical Engineering 396, DOI 10.1007/978-81-322-3589-7_17

services. This is due to the fact that there is no data center which have unlimited resource capacity. In this environment, customer services are provided by sharing workload among the data centers that belong to multiple clouds. However, as the resources are heterogeneous in nature, scheduling tasks among clouds is the most challenging problem.

In this paper, we address the following task scheduling problem in a multi-cloud environment as discussed by Li et al. [4]. We assume a set of k applications $A = \{A_1, A_2, A_3, \ldots, A_k\}$ in which each application A_i is a set of tasks $T = \{T_1, T_2, T_3, \ldots, T_n\}$ where k and n are two nonnegative integers. We also consider a set of m clouds, $C = \{C_1, C_2, C_3, \ldots, C_m\}$ where $0 < m < n$. Execution time of each task is different on different clouds. The problem is to allocate all the tasks to the set of clouds so that the makespan is minimized and better resource utilization can be achieved.

We propose an efficient algorithm that minimizes the total execution time and at the same time maximizes the resource utilization. Here we categorize the complete set of tasks into three categories—long tasks, medium tasks, and small tasks on the basis of a threshold value which is calculated based on the execution time of the tasks on different clouds. The long tasks are scheduled based on minimum execution time. We schedule the second and third group tasks on the basis of other threshold value which is based on utilization of the resources. We perform extensive experiments on the proposed algorithm and compare the results with existing algorithms namely, CMMS, and CMAXMS [5] using benchmark datasets [6]. The experimental results show the effectiveness of the proposed algorithm.

Many task scheduling algorithms [3–8] have been developed for cloud computing that have focused either on minimizing the makespan or maximizing the resource utilization. Min-Min algorithm [5] is very well known for giving the minimized makespan whereas Max-Min algorithm (CMAXMS) [5] is known for resource utilization. Minimum completion time (MCT) and minimum execution time (MET) are two immediate mode heuristics proposed by Armstrong et al. [9]. Maheswaran et al. proposed three heuristics, one for batch mode-sufferage heuristic and two for immediate mode algorithms namely, switching algorithm and k-percent best algorithm [10]. Recently another two algorithms, namely Cloud List Scheduling (CLS) and Cloud Min-Min Scheduling (CMMS) have been proposed in [4]. They are developed to minimize makespan only. Note that Panda et al. [11] have also proposed threshold-based task scheduling, however it has the following differences over the algorithm in [11]. It calculates threshold value for categorizing tasks from the ETC (expected time to compute) matrix differently from that of [11]. It is also a hybrid of batch mode and immediate mode heuristics, whereas the algorithm in [11] is a batch mode heuristic. Our algorithm uses minimum time execution for scheduling tasks of group, whereas algorithm in [11] uses Min-Min scheduling algorithm. Other papers can be seen in [12–14].

2 Proposed Algorithm

The basic thought of the proposed algorithm is as follows. We schedule the tasks having larger execution time on a cloud which takes minimum time to execute. As a result the small tasks do not affect the makespan greatly even if they are executed on low end servers. In order to implement this idea, we categorize the whole set of tasks into two subsets G_1 and G_2 based on a threshold value (Th_{task}). Here, G_1 is the set of the tasks having average execution time on clouds greater than Th_{task} and G_2 is the set of tasks having average execution time on clouds less than Th_{task}. The threshold is calculated on the basis of the following equation

$$\text{Th}_{\text{task}} = \frac{\sum_{i=1}^{n} \sum_{j=1}^{m} TC_{i,j}}{m \times n} \tag{1}$$

where $TC_{i,j}$ represents the execution time of task T_i on cloud C_j.

Next, we divide the group G_1 into two subgroups G_{11} and G_{12} by applying the same process. Now, we have three groups $G_{11,}$ G_{12}, and G_2 which are referred here as long task, medium task, and small task group, respectively. To this end, we apply Minimum execution time algorithm on the tasks belonging to $G_{11.}$ Once all the tasks belonging to G_{11} complete their execution, we schedule the tasks of the groups G_{12} and then G_2. Before scheduling G_{12} and G_2, we check for the clouds which have been extensively used by G_{11}. To implement this, we calculate a new threshold value for clouds, called Th_{cloud}. Now we schedule the tasks of G_{12} and G_2 by ignoring the clouds having average utilization greater than the Th_{cloud}. In this way, proper utilization of each resource can be done. The threshold value for cloud is calculated based on the following equation

$$\text{Th}_{\text{cloud}} = \frac{\sum_{i=1}^{m} \text{RU}_i}{m} \tag{2}$$

where RU_i represents the resource utilization of ith cloud.

In the proposed work, we use some terminologies to describe the pseudocode which are: ETC(*i, j*): Expected time to compute *i*th task on *j*th cloud; *TET*: Total execution time; *task_flag*(*i*): Shows to which group task falls; *cloud_flag*(*i*): For cloud availability, 0–for not available and 1–for available. The pseudocode of the proposed main algorithm is shown in Fig. 1 which calls the other procedures as given in Fig. 2.

Time Complexity

We consider *n* number of tasks and *m* number of available clouds. The algorithm is broadly divided into two parts: calculating threshold and scheduling tasks. The algorithm calculates the threshold value for tasks as well as clouds. The procedure for finding threshold, CALCULATE-TASK-THRESHOLD (ETC, *n, m*) and CALCULATE-RESOURCE-THRESHOLD (ETC, *cloud_timer, n, m*) takes $O(nm)$

Algorithm: Main

```
Input: ETC matrix
Output: Task mapping and corresponding makespan and resource utilization
for i = 1, 2, …, m
    Set cloud_timer(i) = 0; cloud_flag(i) = 1
Call CALCULATE-TASK-THRESHOLD (ETC, n, m)
for i = 1, 2, …, m
     if task_execution_avg(i) > task_threshold
       task_flag(i) = 1
     else
       task_flag(i) = 2
for i = 1, 2, …, n
     if task_flag(i) =1
        (no_task_above_threshold = no_task_above_threshold +1)
remain_task_threshold=TASK-THRESHOLD(ETC, no_task_above_threshold , m)
for i = 1,2, …, n
     if  task_flag(i)= 1
         if(task_execution_avg(i) > remain_task_threshold)
           task_flag(i) = 11
         else
             task_flag(i) = 12
Call SCHEDULE_TASK(ETC, task_flag,11,n,m)
Call RESOURCE_THRESHOLD(ETC, cloud_timer, n, m)
for i = 1, 2, …, n
     Call SCHEDULE_TASK(ETC, task_flag, 12, n, m)
     Call RESOURCE_THRESHOLD(ETC, cloud_timer, n, m)
for i = 1, 2, …, n
     Call SCHEDULE_TASK(ETC, task_flag, 2, n, m)
     Call  RESOURCE_THRESHOLD(ETC, cloud_timer, n, m)
```

Fig. 1 Pseudocode of proposed algorithm

time. For Scheduling of tasks of group G_{11}, G_{12} and G_2, algorithm calls SCHEDULE-TASK (ETC, *task_flag, k, n, m*) procedure which takes $O(nm)$ time. So, the overall time complexity of proposed algorithm is $O(nm)$ time.

3 Experimental Results

The proposed algorithm has been simulated with two benchmark data sets. The simulation has been performed on Intel(R) Core(TM) i5-3230 M CPU @2.60 GHz (4 CPUs), ~ 2.6 GHz with operating system Windows 8.1 using C programming and MATLABR2013a. To evaluate the performance of the proposed algorithm, we compare the results with other two task scheduling algorithms Min-Min and CMAXMS [5]. Two data sets are 512 × 16 and 1024 × 32 by Braun et al. [6] in which the first one has 512 tasks to be scheduled on 16 clouds and the second one

```
PROCEDURE 1: TASK_THRESHOLD (ETC, n, m)
TET = 0
for i = 1, 2, …, n
    task_time(i) = 0
    for j = 1, 2, …, m
        task_time(i) = task_time(i) + ETC(i,j)
        TET = TET + task_time(i)
        task_execution_avg(i) = task_time(i)/m
task_threshold = TET/(m*n)
```

```
PROCEDURE 2: SCHEDULE-TASK(ETC, task_flag, k, n, m)
for i = 1, 2, …, n
    minimum = 999999
    if task_flag(i) = k
        for j=1, 2, …, m
            if (minimum > ETC(i, j) AND cloud_flag(j) = 1)
                resource_selected = j
                minimum= ETC(i,j)
                cloud_timer[resource_selected] = cloud_timer[resource_selected]
                + minimum
```

```
PROCEDURE 3: RESOURCE -THRESHOLD (ETC, cloud_timer, n, m)
max_cloud_timer = cloud_timer(1)
for j = 2, …, m
    if max_cloud_timer < cloud_timer(j)
        max_cloud_timer = cloud_timer(j)
for j = 1, 2, …, m
    resource_factor(j)=cloud_timer(j) / max_cloud_timer
    resource_factor_sum = resource_factor_sum + resource_factor(j)
resource_threshold = resource_factor_sum/m
for j = 1,2, …, m
    if resource_factor(j) > resource_threshold
        cloud_flag(j) = 0
    else cloud_flag(j) = 1
```

Fig. 2 Procedures called by the main algorithm

has 1024 tasks to be scheduled on 32 clouds. Expected time to compute for all the tasks is considered in milliseconds (ms). The comparison of makespan is presented in the Figs. 3 and 4 for 512 × 16 and 1024 × 32 datasets, respectively. The observation shows that the proposed algorithm outperforms the previous two algorithms, i.e., min-min and max-min.

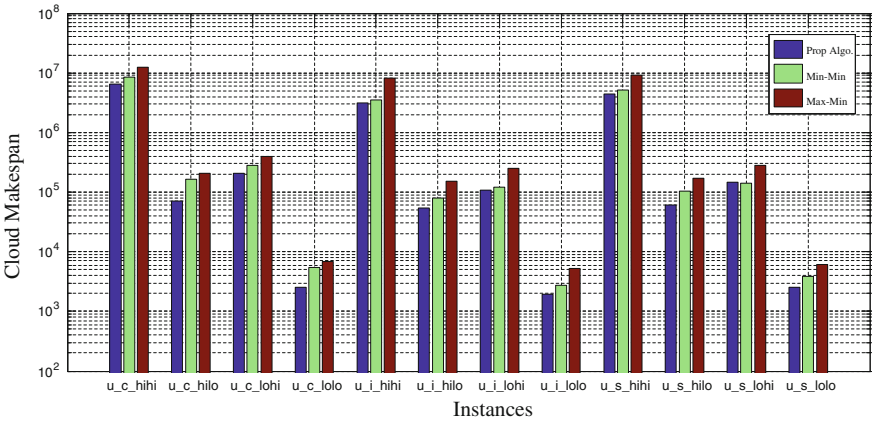

Fig. 3 Comparison of makespan using 512 × 16 benchmark data set

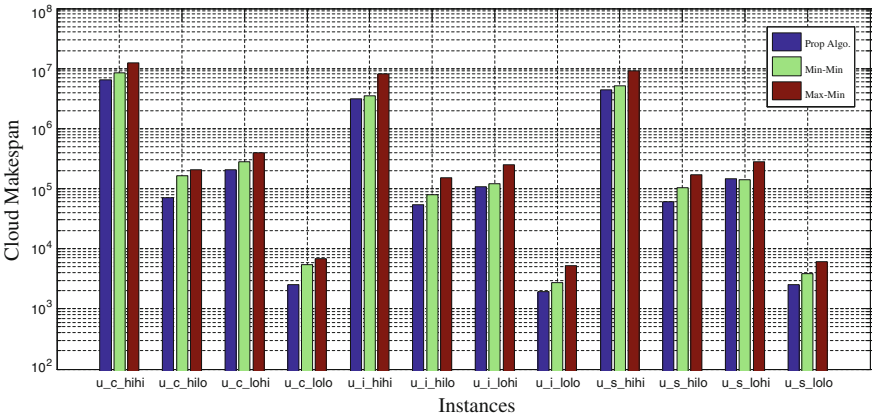

Fig. 4 Comparison of makespan using 1024 × 32 benchmark data set

4 Conclusion

We have presented an efficient task scheduling algorithm for multi-cloud environment which considers two parameters namely, makespan and resource utilization. The proposed algorithm has been simulated extensively on benchmark data sets. However, results for only two benchmark data sets namely, 512 × 16 and 1024 × 32 have been shown due to space limitation. The results have shown that the proposed algorithm outperforms the existing algorithms in terms of makespan and resource utilization.

References

1. Buyya R, Yeo CS, Venugopal S, Broberg J, Brandic I. Cloud computing and emerging IT platforms: vision, hype and reality for delivering computing as the 5th utility. *Future Gen. Computer Systems*. (25) 599–616 (2009).
2. Tsai J, Fang J, Chou J. Optimized task scheduling and resource allocation on cloud computing environment using improved differential evolution algorithm. *Comput. Oper. Res*. (40) (12) 3045–3055 (2013).
3. Y. Zhang, A. Sivasubramaniam, J. Moreira and H. Franke. 2001. Impact of workload and system parameters on next generation cluster scheduling mechanisms. *IEEE Transaction on Parallel and Distributed Systems.* (12) (9) 967–985 (2001).
4. J. Li, M. Qiu, Z. Ming, G. Quan, X. Qin and Z. Gu. 2012. Online optimization for scheduling preemptable tasks on IaaS cloud system. *J. of Parallel Distr. Comp*. (72) 666–677 (2012).
5. O. H. Ibarra and C. E. Kim. Heuristic algorithms for scheduling independent tasks on non-identical processors. *J. of the Assoc. for Computing Machinery*. (24)(2) 280–289 (1977).
6. Braun TD et al. A comparison of eleven static heuristics for mapping a class of independent tasks onto heterogeneous distributed computing systems. *J. Parallel Distri. Comp.,* (61) (6) 810–837 2001.
7. G. Ming and H. Li. 2012. An improved algorithm based on Max Min for cloud task scheduling. *Recent Advances in Computer Science and Information Engineering, Lecture Notes in Electrical Engineering*. (125) 217–223 (2012).
8. Li J, QiuM, Niu JW, ChenY, Ming Z. Adaptive resource allocation for preemptable jobs in cloud systems. In Proc. of 10th *IEEE intl. conf. ISDA*, Cairo, 31–36 (2010).
9. R. Armstrong, D. Hensgen and T. Kidd. The relative performance of various mapping algorithms is independent of sizable variances in run-time predictions. *In Proc. of 7th IEEE Heterogeneous Computing Workshop*, IEEE, Orlando, FL, 79–87 (1998).
10. M. Maheswaran et al. Dynamic mapping of a class of independent tasks onto heterogeneous computing systems. *J. of Parallel and Distributed Computing*. (59) 107–131 (1999).
11. Panda S K and Jana P K. Efficient task scheduling algorithms for heterogeneous multi-cloud environment. *Journal of Super Computing* (71) (4) 1505–1533 (2015).
12. Xiaomin zhu et al. Real-Time tasks oriented energy-aware scheduling in virtualized clouds. *IEEE Transactions on Cloud Computing*. (2) (2) 168–180 (2014).
13. Durao F, Carvalho JFS, Fonseka A, Garcia VC. A systematic review on cloud computing. J. Supercomputer. (68) (3)1321–1346 (2014).
14. Smanchat S, Viriyapant K. Taxonomies of workflow scheduling problem and techniques in the cloud. *Future Generation Computer Systems*. (52), 1–12 (2015).

Construct-Based Sentiment Analysis Model

Smriti Singh, Jitendra Kumar Rout and Sanjay Kumar Jena

Abstract Expression of opinions is basic human nature. With the advent of various online platforms, this expression has largely taken digital form. More often than not, it is in the interest of enterprises and individuals to know the sentiment of these opinions, be them in the form of reviews, blogs or articles. Given the humungous amount of this data, it becomes essential to analyze it programmatically and with accuracy. The paper looks at various methods of doing this and also suggests one which takes into account the sentence constructs and the way the sentences are framed. One of the primary concerns is also to detect and handle negations and contradictions occurring in the sentences.

Keywords Opinion mining · Sentiment analysis · Natural language processing

1 Introduction

Starting with a movie review polarity dataset, containing 5331 positive and 5331 negative processed sentences shown in Table 1, which were manually tagged as positive or negative. The sentences are first POS-tagged using HMM and Viterbi method. A dictionary-based approach is used using SentiWordNet. SentiWordNet is a device that is generally utilized as a part of sentiment mining, and is focused

S. Singh (✉) · J.K. Rout · S.K. Jena
National Institute of Technology, Rourkela, Sundargarh 769008, Odisha, India
e-mail: smritisingh22@gmail.com

J.K. Rout
e-mail: jitu2rout@gmail.com

S.K. Jena
e-mail: skjena@nitrkl.ac.in

D.K. Lobiyal et al. (eds.), *Proceedings of the International Conference on Signal, Networks, Computing, and Systems*, Lecture Notes in Electrical Engineering 396, DOI 10.1007/978-81-322-3589-7_18

Table 1 The movie review dataset

Total number of tweets	10,662
Number of positive tweets	5331
Number of negative tweets	5331

around an English lexical lexicon called WordNet [1]. We extract individual sentiment scores and summate them to get overall polarity of a sentence. This method gives unsatisfactory results and thus we move on to machine learning-based approaches. We start with two baseline methods to find the sentiment of a test sentence, using the Naiye bayes method and the K-nearest neighbour method.

1.1 Naive Bayes Method

The Naive Bayes classifier, based on Bayes theorem is a simple probabilistic classifier with strong and naive independence assumptions, i.e. the occurrences of entities are independent of each other. It is commonly used in email spam detection and sorting, sentiment detection, categorization of electronic content. This classifier is very efficient even though it is outperformed by techniques, such as max entropy, support vector machines, etc, since it is less computationally intensive (both in terms of CPU and memory usage). It requires a small amount of training data also the training time is significantly smaller as opposed to alternative methods [4]. The method assigns a score of negativity and positivity to each word based on the frequency of its occurrence in a positive or a negative context, respectively. To score a document 'd' for a class 'c' having words 'w', conditional probability:

$$P(c|d) = \text{argmax}[P(c) * \prod_{i=1}^{n} P(w_i|c)] \tag{1}$$

We choose the label with the highest probability.

Sentiment Calculation The method assigns a positivity and a negativity score to each word in the sentence based on the frequency of its occurrence in a negative or positive context. The prior probability $P(c)$ of a class c: (c could be positive or negative)

$$P(c) = \text{no. of words in } 'c'/\text{total no. of words in the corpus} \tag{2}$$

In general, sentiment value associated with each word(w) = [pos_score(w)− neg_score(w)]. The sentiment of the whole sentence is calculated as the summation of sentiment values of its of its constituent word.

Table 2 A comparision of Naive Bayes and K-NN method on move

Training set data size (%)	Test set data size (%)	Naive Bayes (%)	K-NN algorithm (%)
90	10	79.00	68.07
80	20	77.90	67.35
70	30	76.60	67.14

1.2 K-NN Method

K-NN is a lazy algorithm that determines the sentiment of a sentence by checking the sentiment of *k*-sentences which are the closest neighbours of the given sentence (the distance metric being the number of matching words) and taking the sentiment which majority of these neighbours have. *K* was chosen to be five for our experiment. A comparison of the two methods is shown in Table 2.

Drawbacks in these two methods are that each word is considered independent of the other, while words affect each other.

The rest of the paper is organized as follows: Sect. 2 discusses the work previously done with relation to *n*-gram model. Section 3 describes the proposed construct-based model in details. Section 4 describes the detailed algorithm used as well the results obtained. Section 5 concludes the work done, highlighting the contributions and suggests directions for possible future work.

2 Related Work

The unigram model assumes that all good words in a sentence can occur independently of any other words in the sentence [7]. In basic sentences with sentiment heavy words, or where words qualify their sentiments individually, this method works fine. Example"I disliked the movie.", "The book is nice.", etc. However, the method fails to give good results if the works are related and change the sentiments of other words, as happens when we use a negative word in a sentence. Example: "I did not like the movie."

n-gram: A slightly improvised version of the *n*-gram model is to use a bigram, where we take words in groups of two [3, 7]. This improves the accuracy level slightly but doesn't give any impressive result. Tri-gram method completely fails giving bad accuracy for the dataset we use. A combination of bi-gram and uni-gram model using Nave Bayes method works better than other methods. Table 3 depicts some of the comaprative results.

But we conclude that using an *n*-gram model does not provide a solution to our problems such as negation words and sentiment neutralisers. Thus, we model a construct-based method discussed in the next segment to solve our issue.

Table 3 *n*-gram method

# of Training Sentences (Total = 5330)	70 % (3730)	80 % (4265)	90 % (4800)
Unigram	76.32	71.79	77.04
Bi-gram	77.53	73.49	78.42
Unigram + Bi-gram	78.91	73.07	79.85

3 The Construct-Based Model

As a human reader, it comes to us naturally to determine the overall opinion or sentiment of a sentence. Sentence opinion is a function of the opinions of the individual constituents of a sentence. Classifying sentiment on the basis of individual words can give misleading results because atomic sentiment carriers can be modified (weakened, strengthened, or reversed) based on lexical, discoursal or paralinguistic contextual operators [8].

Past attempts to deal with this phenomenon include writing heuristic rules to look out for negatives and other changing words [6], combining the scores of individual positive and negative word frequencies [12], and training a classifier on a set of contextual features [11].

Several rules govern the polarity of words or group of words in a sentence [5, 9, 10]. In Neviarouskaya et al. 2010 [5], six composition rules were defined, i.e. domination, neutralization, sentiment reversal, aggregation, propagation, and intensification. Our model is an extension of the same idea. We propose to model these rules in a construct-based model for polarity determination. We use the basic Naive Bayes classification method as the classifier.

The proposed essential rules that have been implemented in our model are as follows:

1. *Parts of Speech that provide sentiment information* Certain Parts of Speech are better indicators of opinions than the others. The sentiment is mainly determined by the order in which these certain parts of speech occur in a sentence. In this process, we skim over words that do not provide any useful information about the sentiment of a sentence. Thus, in our model, we determined those parts of speeches and calculated polarity for the ones that are indicative and contributors of sentiments in a sentence, such as, adjective, noun, verb, and adverb.
2. *Neutraliser* If a compound sentence has connecting words such as "but," "nevertheless," "still," we observe that the sentence part following the connector has a domination over the sentiment of the overall sentence. Hence, during calculations, we neutralize to sentence polarity till the point we observe the connecting word and do the calculations following it. Example: "The phone is costly but it has amazing features." This is applicable only when the words are used as conjunctions. For example, But is a three-lettered word is not a valid example for this construct.

3. *Intensifier* The rule of intensification is applied to strengthen or weaken a sentiment polarity. Examples of intensifiers are words such as "very" and "extremely." These are valence shifters which have the ability to increase or decrease the sentiment polarity of a word. We divide them into two categories: Incrementors and Decrementors, where Incrementors intensify and decrementors weaken the sentiment score of the corresponding word(s) they refer to. As an example, the sentence "I am extremely happy." will have the (positive score of happy) > (positive score of extremely happy). We have a list of pre-determined opinion incrementors and decrementors which have the ability to intensify or diminish the word sentiment polarity. Examples of decrementors would be reduced, decreased, etc.
4. *Negation* Once individual word sentiments are determined as per the methods described in the previous sections, the next step is to determine how to use these values to handle negations. As a human, in the case of occurrence of a negation, we can easily determine, what it is, that is being negated. Our model tries to simulate this behaviour to handle the analysis of sentiments in the sentence and any negations that may occur. The main problem with handling simple sentences with negation is to determine the scope of effect of the negative word. Traditional methods include reversing polarity till the end of sentence. Some other methods include, scope of negation being words between negation and first punctuation mark [7]. The works described in [2, 3] suggest scope of negation to be next five words.
   The approach aims at inverting sentiments in the vicinity of the negation words. In our proposed model, we determine this vicinity in terms of, what we call, the depth of negation. In a crude sense, depth of negation is the number of words around the negator whose polarity should be flipped. While calculating this depth, we noticed certain sentence constructs that occur frequently in negative sentences. Example negation sentence phrases and their corresponding POS tags:

"do not buy": VB−NEG−VB	"be not worth": VB−NEG−JJ
"would not recommend": MD−NEG−VB	"not the good": NEG−DT−JJ
"not very impressed": NEG−RB−JJ	"not bad": NEG−JJ
"not a good choice": NEG−DT−JJ−NN	

5. *Delimiter* A delimiter determines the extent or the vicinity till which the negation word will have polarity reversal effect. If we observe a delimiter, we finalize that as our effect scope. Some delimiters include Coordinating conjunction words and Wh-determiners/pronouns. Examples of delimiters are "when," "whenever," "whether," "because," "unless," "until," "since," and "hence."

4 Experimentation and Results

Suppose a sentence *s* is given, we perform two sub-tasks:

1. Subjectivity classification: This determines whether *s* is a subjective or an objective sentence.
2. Sentence-level sentiment classification: This determines whether it expresses a positive or negative opinion, if *s* is subjective.

Construct-based model features:

- Naive Bayes unigram model.
- Identify POS that provide no sentiment information and those that do:
  Provides No Sentiment Information = [‘CD’, ‘DT’, ‘EX’, ‘FW’, ‘IN’, ‘LS’, ‘NNP’, ‘NNPS’, ‘PDT’, ‘POS’, ‘PRP’, ‘PRP$’, ‘RP’, ‘SYM’, ‘TO’, ‘WP’, ‘WRB’].
  Provides Sentiment Information = [‘JJ’, ‘JJR’, ‘JJS’, ‘NN’, ‘NNS’, ‘RB’, ‘RBR’, ‘RBS’, ‘UH’, ‘VB’, ‘VBD’, ‘VBG’, ‘VBN’, ‘VBP’, ‘VBZ’].
- Identifying negation breakers.
- Delimiters = [‘CC’, ‘WDT’, ‘WP$’].
- Identifying default positive POS: [‘MD’].
- Identifying sentiment incrementors and decrementors:
  e.g.: {‘rising’,’extremely’,’slightly’,’increased’,’increasing}
  {‘reduced’,’compensated’,’lessened’,’trivialised’,’decreased’,’trivialized’}.
- Identifying the negation scope.
  #TextAfterNEG in the form of ordered list of words. (Known patterns were identified).
  #output: whether the condition is followed and if yes, we keep count of the depth of negation from point of occurrence.
  # More than one negation phrase is handled properly.

The snapshot of ordered list is shown in Fig. 1.
The results obtained are shown in the Fig. 2.

Fig. 1 Snippet of ordered list of words

```
suffixstructure = {
                  'RB':
                          {
                              'JJ':{}
                          },
                  'DT':
                          {
                              'JJ':{},
                              'RB':
                                  {
                                      'NN':{}
                                  }
                          },
                  'VB': {},
                  'NN': {},
                  'JJ': {}
```

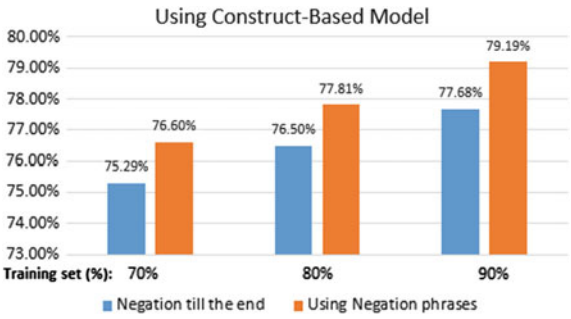

Fig. 2 Result obtained using construct-based model

5 Conclusion and Future Work

The construct-based model, given a set of five constructs (rules), could attain an accuracy of **79.19 %**, so as we expand the domain to more such constructs, the accuracy can then be increased further. Thus, future work would involve incorporating more such composition rules from grammar that affect the sentence polarity.

References

1. Esuli, A., Sebastiani, F.: Sentiwordnet: A publicly available lexical resource for opinion mining. In: Proceedings of LREC. vol. 6, pp. 417–422 (2006).
2. Grefenstette, G., Qu, Y., Shanahan, J. G., Evans, D. A.: Coupling niche browsers and affect analysis for an opinion mining application. In: RIAO. pp. 186–194 (2004).
3. Hu, M., Liu, B.: Mining and summarizing customer reviews. In: Proceedings of the tenth ACM SIGKDD international conference on Knowledge discovery and data mining. pp. 168–177. ACM (2004).
4. Huang, J., Lu, J., Ling, C. X.: Comparing naive bayes, decision trees, and svm with auc and accuracy. In: Data Mining, 2003. ICDM 2003. Third IEEE International Conference on. pp. 553–556. IEEE (2003).
5. Neviarouskaya, A., Prendinger, H., Ishizuka, M.: Recognition of affect, judgment, and appreciation in text. In: Proceedings of the 23rd International Conference on Computational Linguistics. pp. 806–814. Association for Computational Linguistics (2010).
6. Niu, Y., Zhu, X., Li, J., Hirst, G.: Analysis of polarity information in medical text. In: AMIA Annual Symposium Proceedings. vol. 2005, p. 570. American Medical Informatics Association (2005).
7. Pang, B., Lee, L., Vaithyanathan, S.: Thumbs up?: sentiment classification using machine learning techniques. In: Proceedings of the ACL-02 conference on Empirical methods in natural language processing-Volume 10. pp. 79–86. Association for Computational Linguistics (2002).
8. Polanyi, L., Zaenen, A.: Contextual valence shifters. In: Computing attitude and affect in text: Theory and applications, pp. 1–10. Springer (2006).
9. Poria, S., Cambria, E., Winterstein, G., Huang, G. B.: Sentic patterns: Dependency-based rules for concept-level sentiment analysis. Knowledge-Based Systems 69, 45–63 (2014).

10. Sangiorgi, P., Augello, A., Pilato, G.: An approach to detect polarity variation rules for sentiment analysis. In: Proc of WEBIST 2014–10th international conference on web information systems and technologies, 3–5 April (2014).
11. Wilson, T., Wiebe, J., Hoffmann, P.: Recognizing contextual polarity in phrase-level sentiment analysis. In: Proceedings of the conference on human language technology and empirical methods in natural language processing. pp. 347–354. Association for Computational Linguistics (2005).
12. Yu, H., Hatzivassiloglou, V.: Towards answering opinion questions: Separating facts from opinions and identifying the polarity of opinion sentences. In: Proceedings of the 2003 conference on Empirical methods in natural language processing. pp. 129–136. Association for Computational Linguistics (2003).

Part II
Methodologies for Systems Design

Effect of Delay Approximation Using Pade Technique on Controller Performance Designed for a SOPDT Model

Pradeep Kumar Juneja, Nidhi Jain, Mayank Chaturvedi and Sameer Kumar Singh

Abstract Second order plus dead time model approximates many processes in the chemical, metallurgical, paint, paper, oil refineries and petroleum industries. PID controller is commonly used to control an industrial process. In the present analysis, various PID controllers based on Skogestad and Internal Model Control principles with different closed loop constants have been designed for a selected Second Order plus Dead Time model. The selected model is approximated using different approximation techniques. Significant time response characteristics of closed loop responses for the designed controllers are compared and analyzed for set-point tracking of the controller.

Keywords SOPDT · Dead time · Steady state · Transient state · Padè approximation · IMC tuning technique

1 Introduction

To produce a control algorithm which works suitably in real environment for any design procedure, process model, inputs, control objectives and uncertainty bounds of the model must be quantified. Tuning methods are dependent on the process model. The input is to be decided conferring to their significance. The specifications

P.K. Juneja
Department of Electronics & Communication Engineering,
Graphic Era University, Dehradun, India
e-mail: mailjuneja@gmail.com

N. Jain · M. Chaturvedi (✉) · S.K. Singh
Department of Electrical Engineering, Graphic Era University,
Dehradun, India
e-mail: mayankchaturvedi.geit@gmail.com

N. Jain
e-mail: er.nidhijain2013@gmail.com

S.K. Singh
e-mail: sam.ideal@gmail.com

D.K. Lobiyal et al. (eds.), *Proceedings of the International Conference on Signal, Networks, Computing, and Systems*, Lecture Notes in Electrical Engineering 396, DOI 10.1007/978-81-322-3589-7_19

of the system are designed to deliver optimum performance [1]. The set of equations that predicts the behavior of the system, with the knowledge of the input is the model of that process [2].

The industrial process generally have inherent time delay. The dead time in the process may be due to the transportation lag. The delay in any part of the system causes an increase in overall delay of the system. The presence of time delay in the process causes complexity and difficulty in analysis. The system with time delay are difficult to analyze and can be classified as first order plus dead time (FOPDT), second order plus dead time (SOPDT) and other higher order system with dead time [3, 4]. The second order plus dead time model's transfer function can be defined as:

$$G(s) = \frac{K\mathrm{e}^{-\theta s}}{(1+\tau_1 s)(1+\tau_2 s)} \tag{1}$$

where, K is the process gain and τ_1, τ_2 are the time constants and θ is the time delay [4, 5]. The time delay present in the process can be approximated by various approximating techniques such as Taylor's approximation, Padè's approximation etc. [6, 7]. The simplest pole zero approximation is the 1/1 Padè approximation:

$$e^{-\theta s} = \frac{1-\frac{\theta s}{2}}{1+\frac{\theta s}{2}} \tag{2}$$

For Second order Padè approximation is:

$$\mathrm{e}^{-\theta s} = \frac{1-\theta s/2+\theta^2 s^2/12}{1+\theta s/2+\theta^2 s^2/12} \tag{3}$$

PID controller is the first choice of the control engineers for most of the chemical industries and various other industries until today in spite of innovations in predictive and advanced control techniques. The high cost to benefit ratio, robust nature and easy maintenance are the major causes which makes it widespread [8, 9].

Many PID controller tuning methods have been proposed till date, these methods have their own advantages, disadvantages and limitations [10]. Skogestad presented analytic rules for PID controller tuning that are simple and still result in good closed loop behavior. For a large number of SISO process in industries, the Internal Model Control (IMC) design procedure is shown to lead to PID controllers. These PID controllers have only one tuning parameter i.e. the closed loop time constant (τ_c) [11–13].

2 Methodology

In the present analysis, process which can be modeled as SOPDT is taken under consideration. Then this SOPDT model is approximated using Padè first order and second order approximation. Various PID controllers based on Skogestad and

Internal Model Control tuning techniques with different values of closed loop time constant τ_c. The selected SOPDT process model [14] is given as:

$$G(s) = \frac{e^{-2s}}{(10s+1)(s+1)} \tag{4}$$

The delay can be approximated by first order Padè approximation as:

$$GP_1(s) = \frac{-s+1}{10s^3+21s^2+12s+1} \tag{5}$$

The delay can be approximated by second order Padè approximation as:

$$GP_2(s) = \frac{s^2-3s+3}{10s^4+41s^3+64s^2+36s+3} \tag{6}$$

These IMC controllers are designed for different selected closed loop time constant (τ_c = 1, 5 and 8). All the designed controllers are subjected to the step input and the behavior of the controller is investigated. The behavior of different controllers is compared for the set point tracking, on the basis of the performance evaluation and time specifications.

3 Results and Analysis

Tuning parameters for PID controllers are designed using Skogestad and IMC tuning methods for the selected SOPDT process. Simulation is performed to compare closed loop response of the selected process with various controllers Time response characteristics have been compared to analyze set point tracking capabilities of the controllers.

Figure 1 shows the comparison between selected model and its Padè approximated models using Skogestad tuning technique which shows second order Padè approximated model gives better settling time as compare to selected process model and first order Padè approximated model. Figure 2 shows the comparison between selected model and its Padè approximated models using IMC (τ_c = 1) tuning technique. Figure 3 shows the comparison between selected model and its Padè approximated models using IMC (τ_c = 5) tuning technique. The comparison between selected model and its Padè approximated models using IMC (τ_c = 8) tuning technique is shown by Fig. 4.

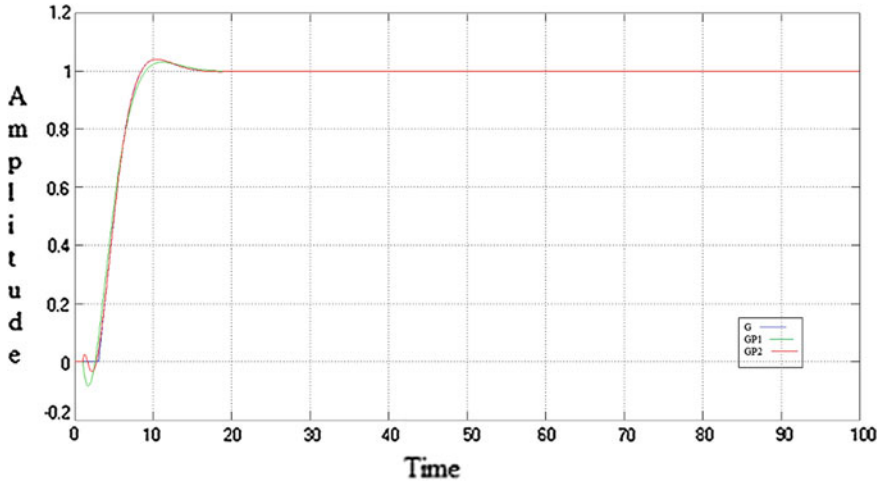

Fig. 1 Comparison of selected, first and second order Padè approximated model using Skogestad

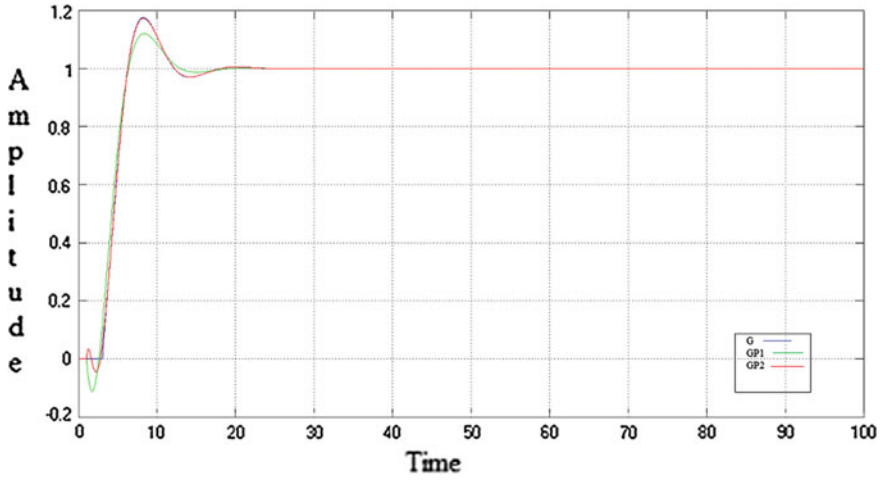

Fig. 2 Comparison of selected, first and second order Padè approximated model using IMC ($\tau_c = 1$)

Table 1 shows the comparison of time response characteristics for the selected and approximated models for the controller designed using different tuning techniques.

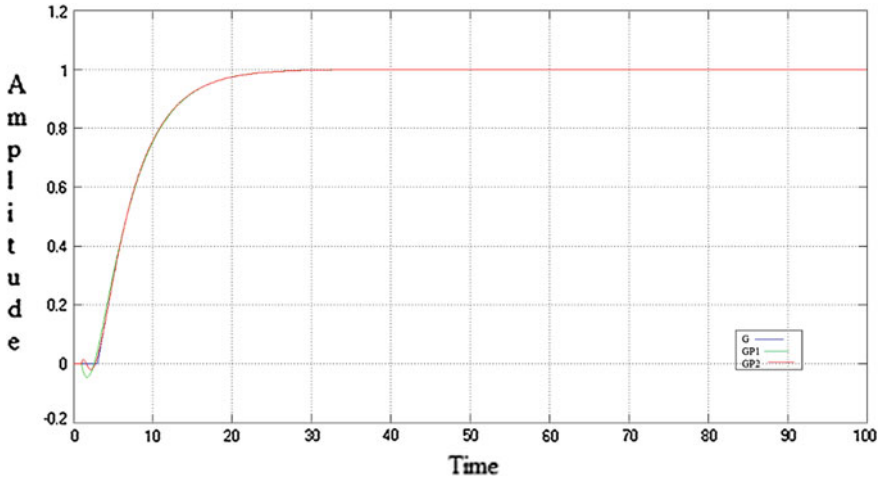

Fig. 3 Comparison of selected, first and second order Padè approximated models using IMC ($\tau_c = 5$)

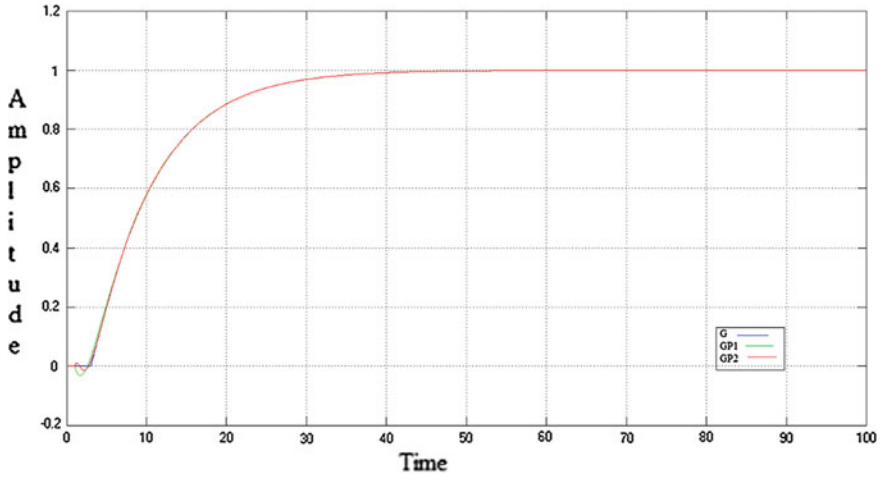

Fig. 4 Comparison of selected, first and second order Padè approximated models using IMC ($\tau_c = 8$)

Table 1 Comparison of time response characteristics

Process	Tuning technique	Rise time	Settling time	% Overshoot
G	Skogestad	3.8	12.1	4.05
	IMC1	2.5	14.8	17.5
	IMC5	10.3	20.2	0
	IMC8	17.1	32.5	0
GP_1	Skogestad	4.28	12.1	3.05
	IMC1	2.79	10.9	12
	IMC5	10.5	20	0
	IMC8	17.3	32.3	0
GP_2	Skogestad	3.86	12	4.05
	IMC1	2.58	14.7	17.3
	IMC5	10.3	20.1	0
	IMC8	17.1	32.4	0

4 Conclusion

In the present analysis, the delay of the selected SOPDT process model have been approximated using Padé's first and second order approximation method. PID controllers have been designed using IMC and Skogestad tuning techniques for the selected SOPDT model and its approximated models. The closed loop step responses have been compared for set point tracking capability of the selected SOPDT process model as well as approximated process models.

- Rise time is minimum in case of IMC tuning method with closed loop time constant 1, settling time is minimum in case of Skogestad tuning technique and maximum percentage overshoot is least for controller designed using IMC tuning method $\tau_c = 5$ and 8, for the selected SOPDT process model.
- In case of first order Padé approximated process model, rise time and settling time is minimum for controller designed using IMC tuning method with $\tau_c = 1$, while maximum percentage overshoot is least for controller designed using IMC tuning method $\tau_c = 5$ and 8.
- Rise time is minimum in case of IMC tuning method with closed loop time constant 1, settling time is minimum in case of Skogestad tuning technique and maximum percentage overshoot is least for controller designed using IMC tuning method $\tau_c = 5$ and 8, for the second order Padé approximated process model.

Controller designed using IMC tuning method with closed loop time constant equal to one, for Padé first order approximated process model exhibits the optimum response when comparing all the controllers designed using IMC ($\tau_c = 1$, 5 and 8) and Skogestad tuning methods for all the process models viz. selected SOPDT process model, Padé first order and second order approximated process model.

References

1. Hughes, T. A.: Measurement and Control Basics. Research Triangle Park, N. C. IV edition, (2007).
2. Bequette, B. W.: Process Control: Modelling, Design and Simulation. Prentice Hall, (2003).
3. Rao, C. V. N., Rao A. S. and Padama Sree, R.: Design of PID Controllers for Pure Integrator Systems with Time Delay. Int. J. Applied Science and Engineering, (2011) 241–260.
4. Chaturvedi, M., Juneja, P.: Effect of dead time approximation on controller performance designed for a second order delayed model. Proceedings ICAES 2013, CEERI, Pilani, (2013) 313–315.
5. Chaturvedi, M., Juneja, P. K., Chauhaan, P.: Effect of Implementing Different PID Algorithms on Controllers Designed for SOPDT Process. Proceedings of the ICACCI 2014, GCET Greater Noida, (2014) 853–858.
6. Seborg, D. E.: Process Dynamics and control. 2nd edition, John Wiley & sons Asia PTE. LTD, (2007).
7. Chauhaan, P., Juneja, P. K., Chaturvedi, M.: Controller Design and Its Performance Analysis for a Delayed Process Model. Proceedings of the ICACCI 2014, GCET Greater Noida, (2014) 859–862.
8. Panda, R. C., Yu, C. C., Huang, H. P.: PID tuning rules for SOPDT systems: Review and some new results. ISA Transactions 43, (2004) 283–295.
9. Visioli, A.: Research trends for PID controllers. Acta Polytechnica, Vol. 52, No. 5, (2012) 144–150.
10. Micheal, Foley M. W., Julien R. H., Copeland B. R.: A comparison of PID controller tuning methods Can. J. Chem. Eng. 83, (2005) 712–722.
11. Skogestad, S.: Simple Analytic Rules for Model Reduction and PID Controller Tuning. J. Process Control 13, (2003) 291–309.
12. Morari, M., Skogestad, S., Rivera, D. F.: Implications of internal model control for PID controllers. Proceedings of American Control Conference, (1984) 661–666.
13. Chien, L., Fruehauf, P. S.: Consider IMC tuning to Improve Controller Performance. Chem. Eng. Progress, 86 (10), 33–41 (1990).
14. Dos Santos, J., Barros, P.: A Simple Identification Technique for Second-Order plus Time-Delay Systems. Proceedings of the 9th International Symposium on Dynamics and Control of Process Systems (DYCOPS 2010), Leuven, Belgium, (2010) 188–193.

Neuro-Fuzzy Controller Design for MIMO Boiler Turbine Process

Sandeep Kumar Sunori, Shweta Shree, Ajay Kumar Maurya and Pradeep Juneja

Abstract The plant selected for control system analysis is a 2 × 2 MIMO system with high multivariable interaction having two manipulated variables, the position of the governor valve and the fuel flow rate and two controlled variables, generated electric power and the steam pressure. A neuro-fuzzy controller has been designed using ANFIS in MATLAB for a boiler turbine plant. This technique is a hybrid of neural network and fuzzy logic techniques.

Keywords Relative gain array · Boiler turbine · Multivariable process · Neuro-fuzzy controller

1 Introduction

In boiler turbines, the chemical and thermal energy is transformed to electricity. It is a highly complex, multivariable, time delayed, and nonlinear process. In a typical boiler turbine plant, a header collects all the steam which is generated from number of boilers which is then distributed to several turbines through header. The steam flow is directly proportional to power generation which is the key parameter to be controlled. The other parameter to be controlled is the drum pressure. The ultimate objective is to meet the load demand of electric power [1].

The ANFIS (Adaptive Neuro-Fuzzy Inference System) approach combines the advantages and avoids the drawback of fuzzy logic and neural network approaches

S.K. Sunori (✉) · S. Shree
Graphic Era Hill University, Bhimtal Campus, Nainital, India
e-mail: sandeepsunori@gmail.com

A.K. Maurya
Debre Tabor University, Debra Tabor, Ethiopia

P. Juneja
Graphic Era University, Dehradun, India
e-mail: mailjuneja@gmail.com

D.K. Lobiyal et al. (eds.), *Proceedings of the International Conference on Signal, Networks, Computing, and Systems*, Lecture Notes in Electrical Engineering 396, DOI 10.1007/978-81-322-3589-7_20

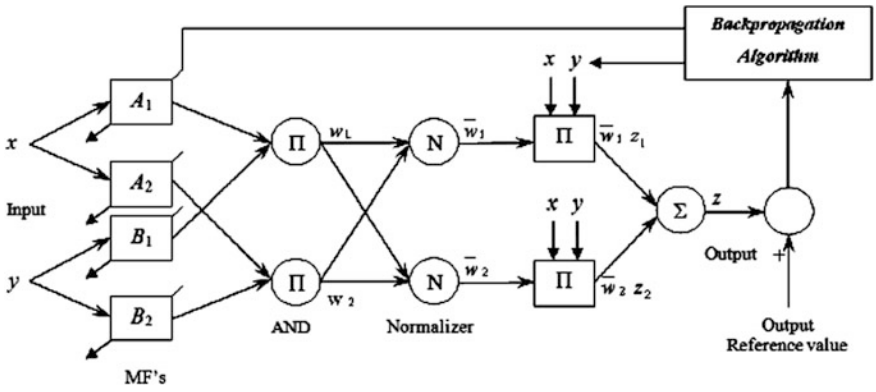

Fig. 1 Schematic of ANFIS [3]

[2]. The main advantage of this technique is that it auto tunes the membership functions without any need of human operator.

The Fig. 1 reveals the schematic of an ANFIS with x and y as the two inputs and z as the output. A_1, A_2 are representing the two fuzzy sets for input x and B_1, B_2 are representing the two fuzzy sets for input y. The fuzzy model used by ANFIS is the Sugeno fuzzy model. In this figure, fixed nodes and adaptive nodes are indicated by circles and squares respectively.

Here, $\overline{wi} = \frac{wi}{w1+w2}, i = 1, 2$

The types of neuro-fuzzy systems are cooperative neuro-fuzzy system, concurrent neuro-fuzzy system, and hybrid neuro-fuzzy system [4]. Omar Shahin et al. observed robustness and satisfactory performance of the boiler turbine system employing adaptive wavelet neural network. Discrete Lyapunov stability theorem was used here to determine the learning rates [5]. Speed control of gas turbine system was proved to be outstanding with adaptive fuzzy PID controllers as compared to conventional PID controllers [6]. The hybrid of neural network and fuzzy logic approaches has been reported to be very effective to design controllers. It shows an improved performance and robustness [7]. Demetri Psaltis et al. introduced a modified back propagation algorithm and proposed various learning architectures like general learning architecture, indirect learning architecture, and specialized learning architecture [8].

2 Plant Model and Its Multivariable Analysis

The process has two manipulated variables, the governer valve position (GV) and the fuel flow rate (FR). The variables to be controlled are the electric power (EP) and the steam pressure (SP). Equation 1 shows the model of an industrial boiler turbine process [9] that will be used to design the controller.

$$\begin{bmatrix} \text{EP} \\ \text{SP} \end{bmatrix} = \begin{bmatrix} \dfrac{68.81\,\mathrm{e}^{-2s}}{984\,s^2+94\,s+1} & \dfrac{(-23.58\,s-2.196)\,\mathrm{e}^{-8s}}{372\,s^2+127\,s+1} \\ \dfrac{\mathrm{e}^{-2s}}{6889\,s^2+166\,s+1} & \dfrac{2.194\,\mathrm{e}^{-8s}}{6400\,s^2+160\,s+1} \end{bmatrix} \begin{bmatrix} \text{GV} \\ \text{FR} \end{bmatrix} \tag{1}$$

Before designing the controller for the considered plant the suitable pairing between manipulated and control variables is done by determining the relative gain array (RGA) [10].

$$\text{Mathematically, RGA} = K^{*}\left(K^{T}\right)^{-1} \tag{2}$$

where the operator '*' represents element by element multiplication. Now, for the considered plant the steady-state gain matrix is given below,

$$[k] = \begin{bmatrix} 0.6 & -2.1 \\ 0.1 & 0.9 \end{bmatrix} \tag{3}$$

Using relations (2) and (3), the RGA for this plant comes out as,

$$\text{RGA} = \begin{bmatrix} 0.985 & 0.015 \\ 0.015 & 0.985 \end{bmatrix} \tag{4}$$

This RGA suggests that the suitable pairing is u_1–y_1 and u_2–y_2.

3 Controller Design

First of all, the control of the considered boiler turbine plant is attempted employing a normal fuzzy logic controller based on manual tuning of membership functions and rules whose simulink model is shown in Fig. 2. But, it results in unstable responses for both the outputs as depicted in Fig. 3. So it fails in taking desired control action.

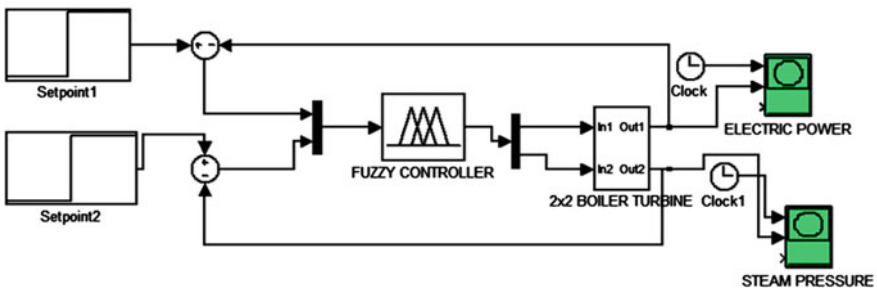

Fig. 2 Fuzzy controller model

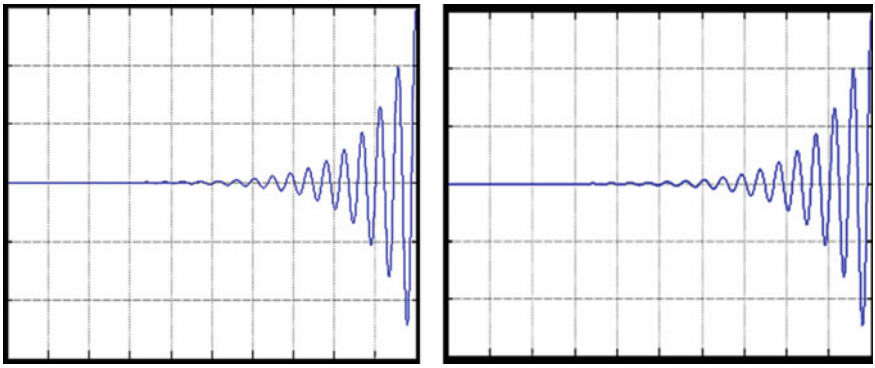

Fig. 3 Responses of fuzzy controller for electric power (*left*) and steam pressure (*right*)

Now, the control of same plant will be attempted with a neuro-fuzzy controller based on ANFIS tool. The simulink model of ANFIS-based controller for the considered boiler turbine plant is depicted in Fig. 4. It contains two controllers namely neuro-fuzzy controller1 with two inputs, 'time' and 'electric power(EP) error' and one output, governer valve (GV) position and neuro-fuzzy controller2 with two inputs, 'time' and 'steam pressure (SP) error' and one output, 'fuel flow rate'.

The initiated seven triangular membership functions for the input, 'time' are designated as ES (extremly small), VS (very small), S (small), M (medium), L (large), VL (very large), EL (extremly large). The initiated seven triangular membership functions for the inputs, 'EP error' and 'SP error' are designated as,

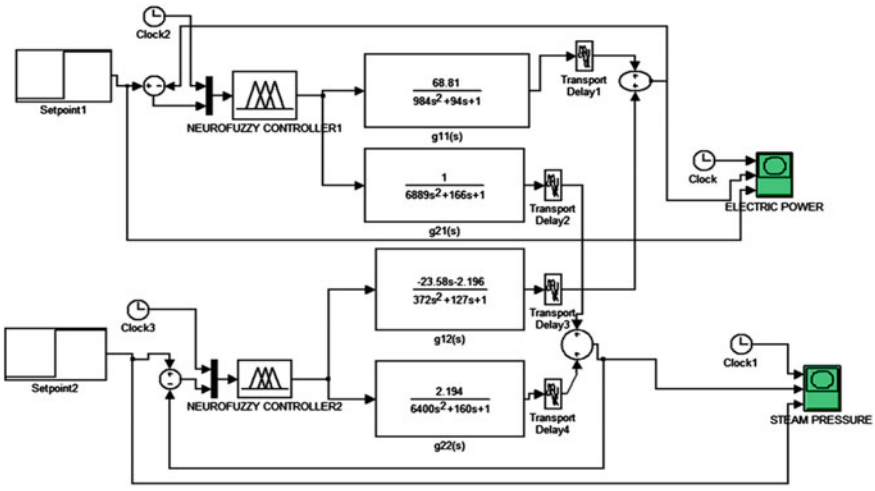

Fig. 4 Simulink model of Neuro-Fuzzy controller

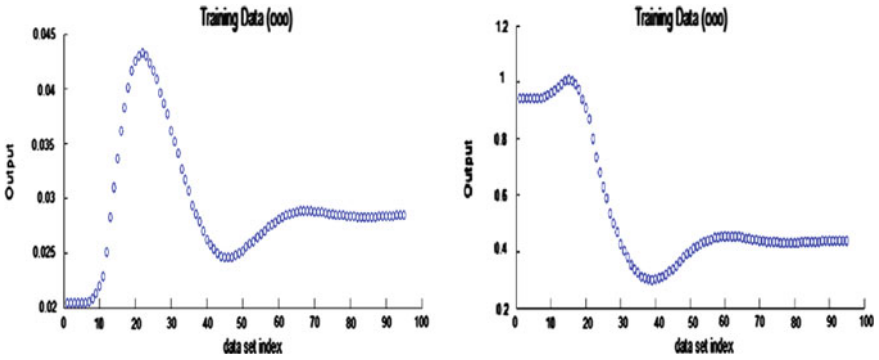

Fig. 5 Training data for controller1 (*left*) and controller2 (*right*)

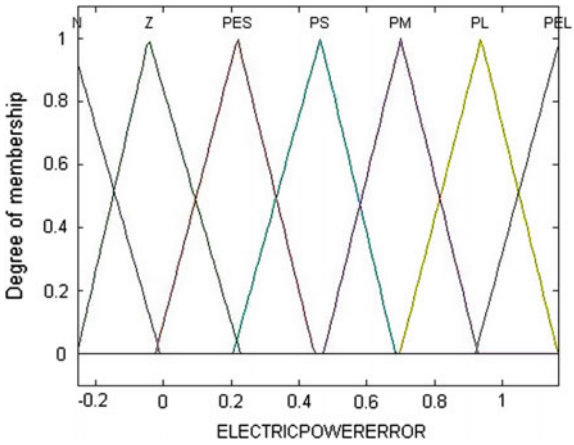

Fig. 6 Tuned membership functions for electric power error

N (negative), Z (zero), PES (positive extremly small), PS (positive small), PM (positive medium), PL (positive large), PEL (positive extremly large).

So, total number of rules is $7 \times 7 = 49$. The final output is the summation of these outputs. Before training, the output corresponding to each rule is zero, so the net output is also zero. Now the two ANFIS are trained by an input/output training data with 100 samples for both. The training data is depicted in Fig. 5. The number of training epochs are fixed at 100. The tuned membership functions for inputs are shown in Figs. 6 and 7.

Now, the set-point tracking responses of this designed neuro-fuzzy control system is depicted in Figs. 8 and 9.

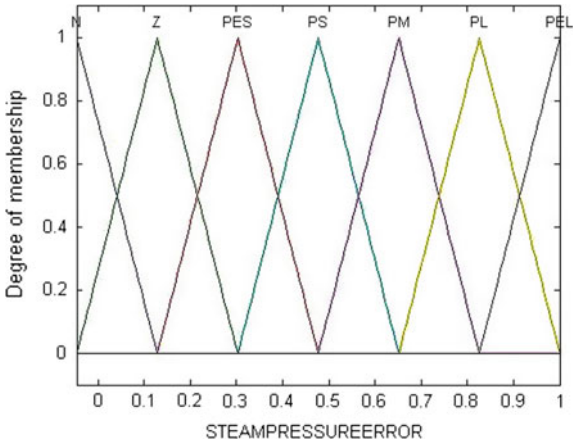

Fig. 7 Tuned membership function for steam pressure error

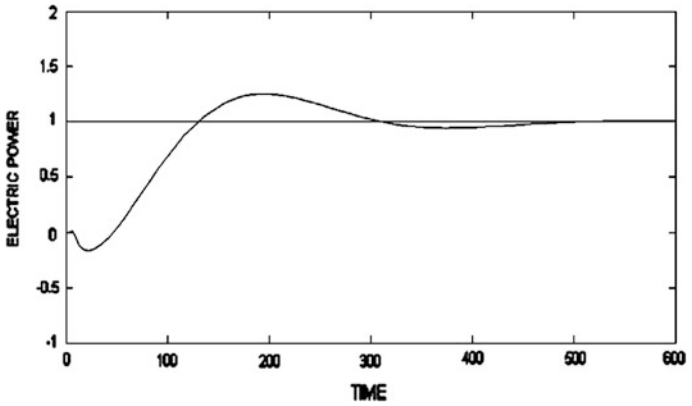

Fig. 8 Set-point tracking for electric power

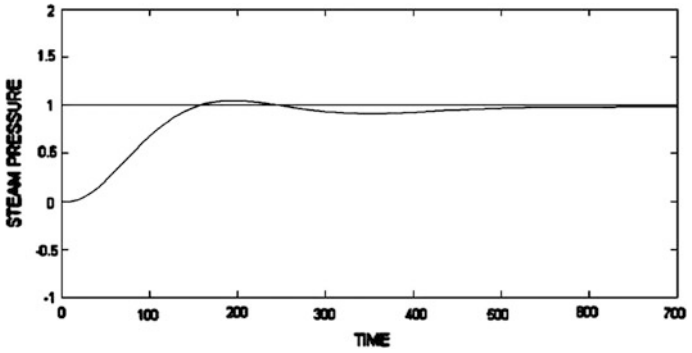

Fig. 9 Set-point tracking for steam pressure

4 Conclusion

In the present work, initially a normal fuzzy control system was designed for a 2×2 boiler turbine plant using manual tuning of membership functions and rules but it failed to take desired control action. Then the control of the two outputs of this plant was successfully accomplished using ANFIS-based controller and an excellent set-point tracking performance was observed.

References

1. M. Sarailoo, B. Rezaie and Z. Rahmani, MLD Model of Boiler Turbine System based on PWA Linearization approach, International Journal of Computer Science and Engineering, 2 (4), pp. 88–92, 2012.
2. Gurpreet S. Sandhu and Kuldip S. Rattan, Design of a Neuro Fuzzy Controller, IEEE International Conference, Vol. 4, pp. 3170–3175, 1997.
3. Boumediene Allaoua, Abdellah Laoufi, Brahim Gasbaoui and Abdessalam Abderrahmani, Neuro-Fuzzy DC Motor Speed Control Using Particle Swarm Optimization, Leonardo Electronic Journal of Practices and Technologies, Issue 15, pp. 1–18, 2009.
4. D. Nauck, F. Klawon and R. Kruse, Foundations of Neuro-Fuzzy Systems, J. Wiley & Sons, 1997.
5. Omar Shahin, Mohammad El-Bardini and Nabila M. El-Rabaie, Control Scheme of a BoilerTurbine using Adaptive Wavelet Neural Network, Journal of Engineering Sciences, AssiutUniversity, Vol. 39, No. 6, pp. 1387–1401, 2011.
6. Saeed Balochian and Soheil Vosoughi, Design and Simulation of Turbine Speed Control System based on Adaptive Fuzzy PID Controller, Advances in Mechanical Engineering and its Applications(AMEA), Vol. 1, No. 3, 2012.
7. Mouloud Azzedine Denai and Sid Ahmed Attia, Fuzzy and Neural Control of an Induction Motor, Int. J. Appl. Math. Comput. Sci., Vol. 12, No. 2, pp. 221–233, 2002.
8. Demetri Psaltis, Athanasios Sideris and Alan A. Yamamura, A Multilayered Neural Network Controller, IEEE International Conference on Neural Networks, San Diego, California, pp. 17–21, 1987.
9. Zhang Hua Guang and Lilong Cai, Multivariable Fuzzy Generalized Predictive Control, Cybernetics and Systems: An International Journal, Taylor & Francis, pp 33:69–99,2002.
10. Babatunde A. Ogunnaike and W. Harmon Ray, Process Dynamics, Modeling and Control, Oxford University Press, 1994.

Predictive Control System Design for Lime Kiln Process

Sandeep Kumar Sunori, Vimal Singh Bisht, Mohit Pant and Pradeep Juneja

Abstract MPC is a computer-based technique that requires the process model to anticipate the future outputs of that process. An optimal control action is taken by MPC based on this prediction. The MPC is so popular since its control performance has been reported to be best among other conventional techniques to control the multivariable dynamical plants with various inputs and outputs constraints. In this work, the control of lime kiln process with two manipulated variables namely the fuel gas flowrate, and the percent opening of the induced draft damper and two controlled variables namely front-end temperature and back-end temperature has been attempted using MPC technique. Lime kiln process is very complex and nonlinear multivariable process. A linearized model obtained using Taylor series expansion around operating point has been used.

Keywords Model predictive control · Lime kiln · Nonlinear process

1 Introduction

Limekiln is a long rotating cylinder with single which has a little inclination to the horizontal as shown in Fig. 1. The lime kiln converts lime mud ($CaCO_3$) into lime (CaO). This process is called calcination process. The chemical equation of this reaction is [1]:

$$CaCO_3 + \text{heat} \rightarrow CaO + CO_2.$$

The MPC calculates an objective function [2] on the basis of predicted values of the output samples up to a fixed prediction horizon, and then determines the discrete

S.K. Sunori (✉) · V.S. Bisht · M. Pant
Graphic Era Hill University, Bhimtal Campus, Nainital, India
e-mail: sandeepsunori@gmail.com

P. Juneja
Graphic Era University, Dehradun, India

D.K. Lobiyal et al. (eds.), *Proceedings of the International Conference on Signal, Networks, Computing, and Systems*, Lecture Notes in Electrical Engineering 396, DOI 10.1007/978-81-322-3589-7_21

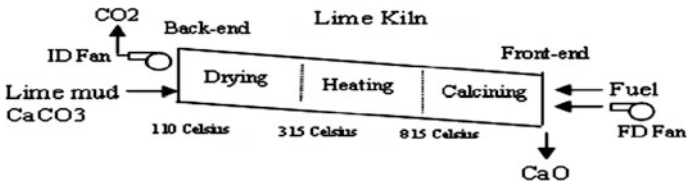

Fig. 1 Lime kiln process [1]

moves of the input manipulated variables in such a way that the objective function is minimized. The MPC strategy is elaborated in Fig. 2.

The MPC takes control actions at regularly spaced intervals which are called control intervals [3]. As shown in figure, the controller predicts the output values at sampling instant t. After having completed the prediction calculations it sends move $u(t)$ to the plant. The plant then operates with this constant input until the next sampling instant. At this sampling instant $t + 1$, the controller again does prediction over prediction horizon in the same way and again determines the new optimal control moves over the control horizon and this cycle repeats indefinitely. Thus we see that both prediction and control horizons are receding.

Goran Stojanovski and Mile Stankovski presented a case study of two-level control system for tunnel kiln in which MPC and fuzzy control techniques were employed [4]. Jarrensivu et al. successfully operated an intelligent supervisory level kiln control system at the Wisaforest pulp mill in Finland [5]. The design of knowledge base for an expert system for rotary lime kiln was reported by Zhu and Zhang [6].

The PLCs were used by Bharadwaja for intelligent control of lime kiln process [7]. The improvement of 20–30 % was reported in the quality of clinker using distributed control system for cement production [8].

Fig. 2 MPC strategy [3]

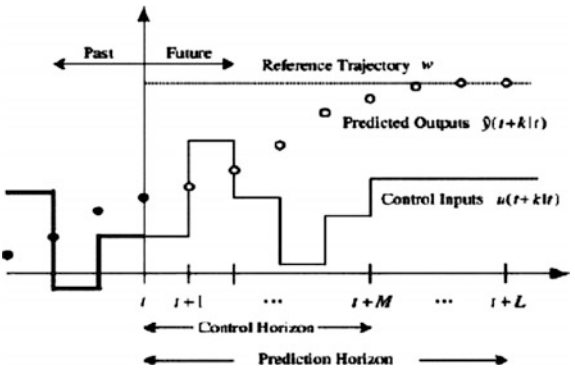

2 MPC Controller Design

In this work two temperatures are controlled in the kiln:the front-end temperature (T_{fe}), and the back-end temperature (T_{be}). The process has two manipulated variables: the fuel gas flowrate (F) and the percent opening of the induced draft damper (vp). Figure 3 shows the model of an industrial lime kiln that will be used to design a MPC based control system.

The open-loop step response of this plant model is shown in Fig. 4.

It clearly indicates that the pairing ID damper opening → front-end temperature exhibits an inverse response which makes the controlling process difficult.

$$\begin{bmatrix} T_{fe} \\ T_{be} \end{bmatrix} = \begin{bmatrix} \frac{0.6}{3s+1} & \frac{-2.1}{(6s+1)(5s+1)} \\ \frac{0.1}{(10s+1)(s+1)} & \frac{0.9}{(7s+1)(10s+1)} \end{bmatrix} \begin{bmatrix} F \\ vp \end{bmatrix}$$

Fig. 3 Transfer function of lime kiln process

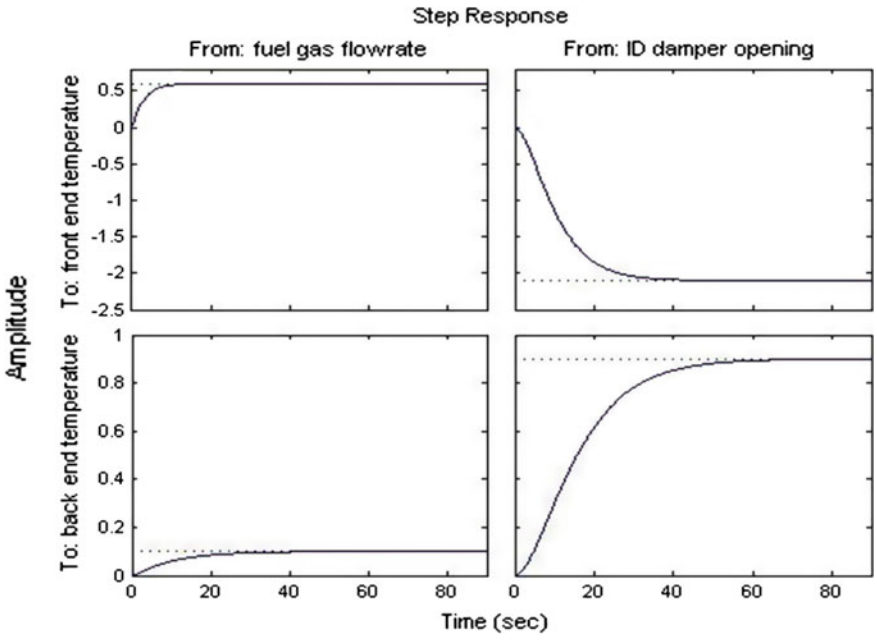

Fig. 4 Open loop step response

Now this plant is to be controlled by an MPC controller with set points for controlled variables front-end temperature and back-end temperature equal to 1500 and 230 °F, respectively. The consequences of varying MPC controller settings will be investigated.

3 Results and Analysis

The following plots in Figs. 5 and 6 depict the set point tracking response of MPC with control horizon (CH) equal to 1, 2, and 5, respectively, keeping prediction horizon fixed at 10 [9].

Figures 5 and 6 clearly indicate that settling time of responses is very large with control horizon equal to 1 hence set point tracking is worst in this case. The responses are almost similar with control horizon value of 2 and 5.

Figure 7 shows the controller response with control horizon value of 2 and prediction horizon value of 4, i.e., control horizon(CH) to prediction horizon(PH) ratio, (M/P) =0.5

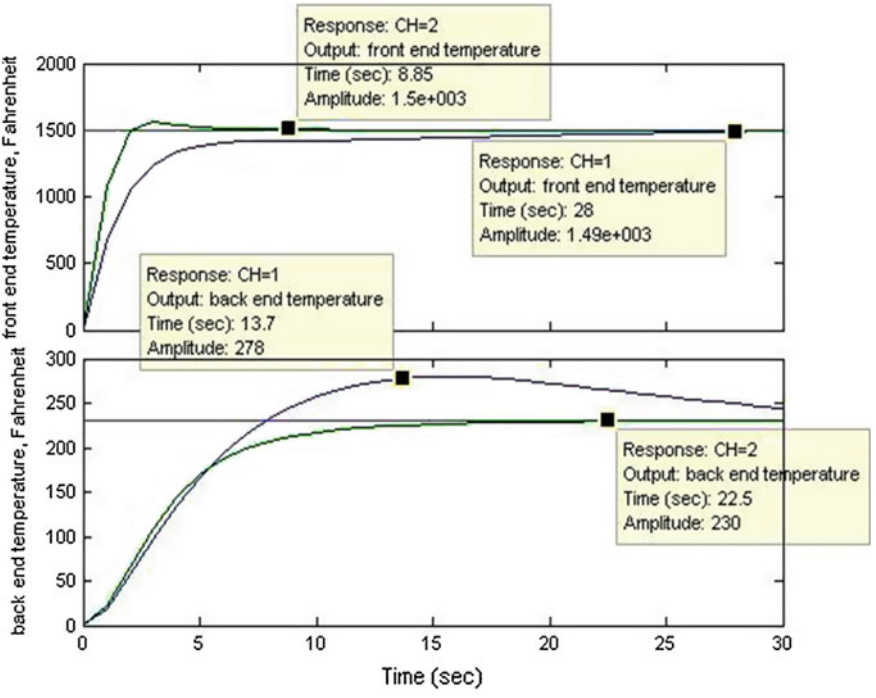

Fig. 5 Set point responses with control horizon (CH) value of 1 and 2

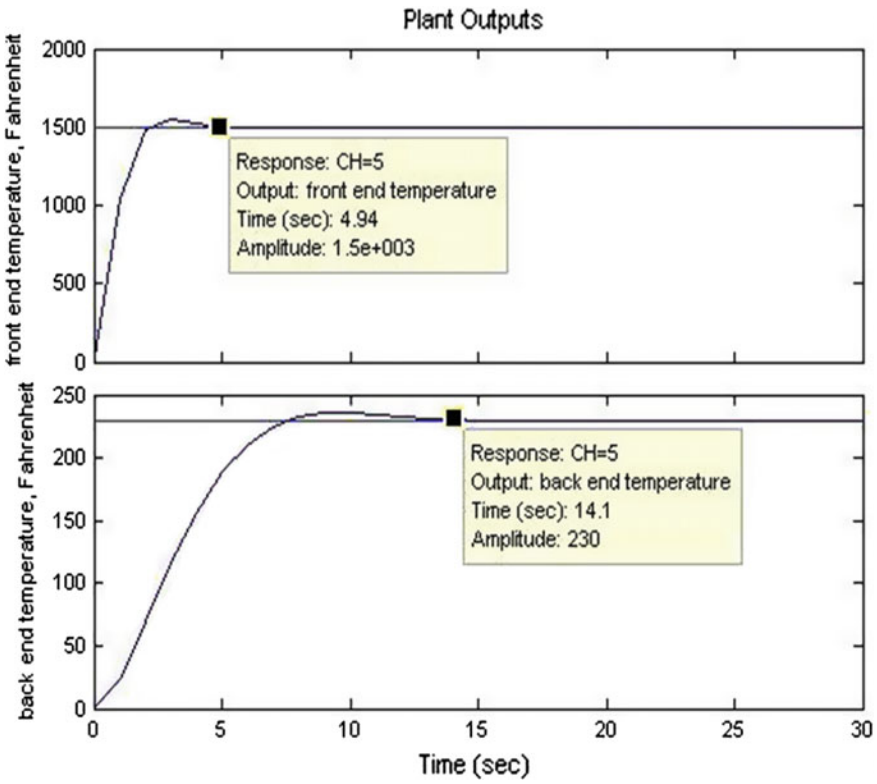

Fig. 6 Set point responses with control horizon (CH) value of 5

The comparison of Figs. 7 and 6 reveals that the same value of M/P ratio results in identical set point tracking response.

Figure 8 compares the calculated moves in the two manipulated variables for respective rate weights of 0.1 and 0.8. It is clearly observed that the increase in the value of input rate weight results in decrease in the required value of discrete moves in manipulated variable, i.e., decrease in the amount of control effort required for set point tracking.

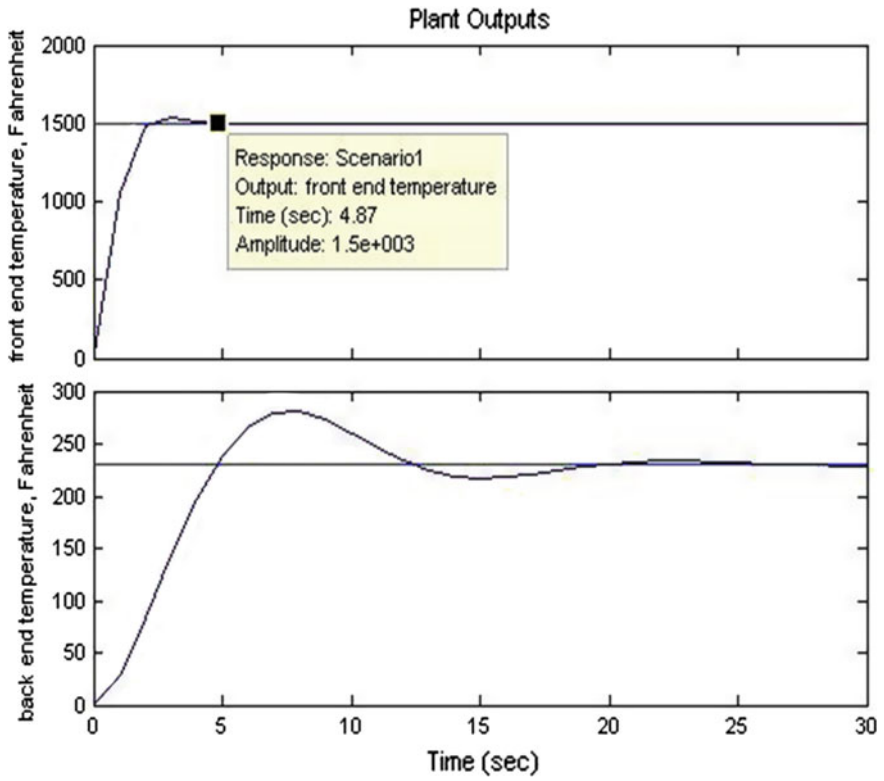

Fig. 7 Set point responses with control horizon value of 2 and prediction horizon of value 4 (M/P=0.5)

4 Conclusion

It has been observed that the response of MPC controller is very fast with very small settling time and very good set point tracking performance. Further, it has been found that the same control horizon to prediction horizon ratio results in same controller performance and the increase in the value of input rate weight results in decrease in control moves in manipulated variables.

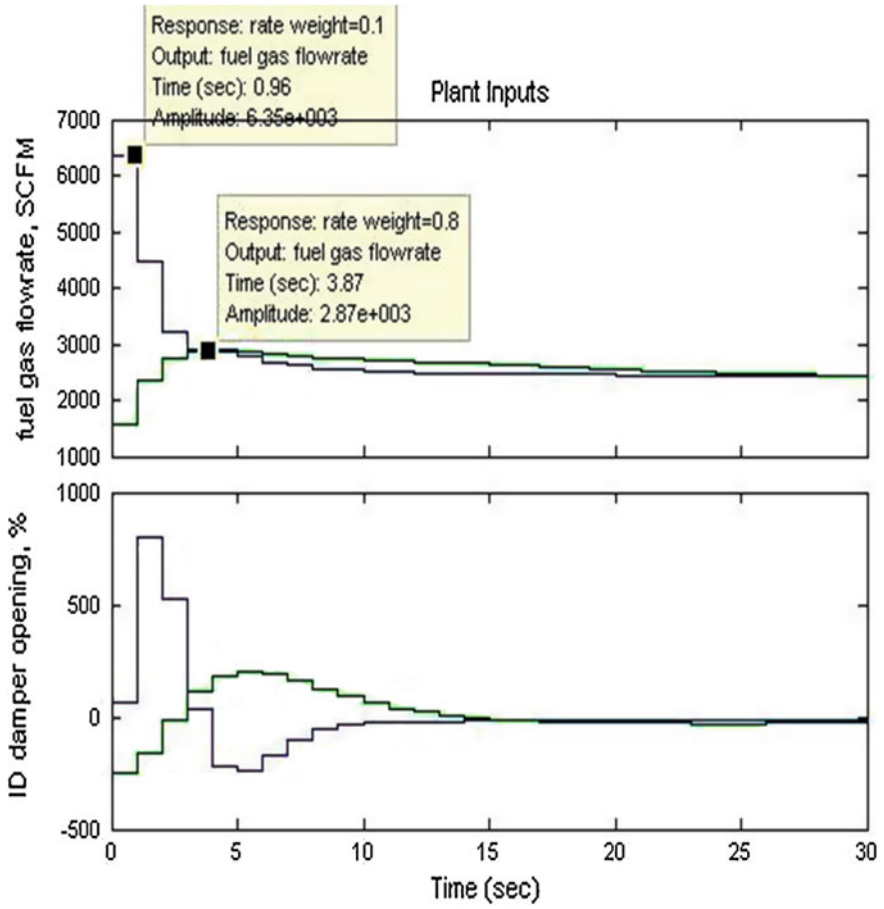

Fig. 8 Manipulated variable moves with input rate weight of value 0.1 and 0.8

References

1. Serge Naud, PE & Martin Emond, "Lime Kiln Control using Simple Advanced Regulatory Control Strategy", Presented at ISA EXPO 2007,2–4, Reliant Center, Houston, Texas, 2007.
2. Junxia Mu and David Rees, "Approximate Model Predictive Control for Gas Turbine Engines", Proceeding of the 2004 American Control Conference Boston, Massachusetts", 2004.
3. Rekha Rajan, Muhammed Salih. P and N. Anil Kumar, "Speed Controller Design for Steam Turbine", International Journal of Advanced Research in Electrical Electronics and Instrumentation Engineering", Vol. 2, Issue 9, 2013.
4. Goran Stojanovski and Mile Stankovski, "Advanced Industrial Control Using Fuzzy Model Predictive Control on a Tunnel Kiln Brick Production", Preprints of the 18th IFAC World Congress Milano(Italy) August 28–September 2, 2011.

5. M. Jarrensivu, K. Saari and S.L. Jamsa Jounela, “Control System of an Industrial Lime Kiln Process”, Control Engineering Practice 9 No. 6, pp. 589–606, 2001.
6. Lingli Zhu and Tao Zhang, “Implement and Research on the Expression Methods of Knowledge for the Expert System of Rotary Kiln”, Sensors and Transducers, Vol. 162, Issue 1, pp. 280–285, 2014.
7. Y. Bharadwaja, “Intelligent Control System of Lime Kiln Process by Programmable Logic Controllers”, Journal of International Academic Research for Multidisciplinary, ISSN: 2320-5083, Vol. 2, Issue 5, June 2014.
8. Xiaohong Wang, Qingjin Meng, Hongliang Yu, Zhugang Yuan and Xinhe Xu, “Distributed Control for Cement Production of Vertical Shaft Kiln”, International Journal of Information and Systems Sciences, Vol. 1, No. 3–4, pp. 264–274, 2005.
9. Pradeep Kumar Juneja, A.K. Ray, “Prediction Based Control of Lime Kiln Process in a Paper Mill”, Journal of Forest Products and Industries, 2(3), pp. 58–62, 2013.
10. Pradeep Kumar Juneja, A.K. Ray and R. Mitra, “MPC Based Controller Design for a Constrained Industrial Lime Kiln Process”, Journal of Forest Products & Industries, 2(6), pp. 7–9, 2013.

Design of Time-Delay Compensator for a FOPDT Process Model

Mayank Chaturvedi, Prateeksha Chauhaan and Pradeep K. Juneja

Abstract Majority of the chemical processes in process industry can be modeled as first-order plus dead time processes. In the present analysis, selected process model transfer function is taken into consideration and PID controllers are designed for the process using various tuning techniques and the effect of dead time is compensated using Smith predictor.

Keywords Delay · FOPDT · PID controller · Smith predictor

1 Introduction

Dead time can be referred as the time interval during which no response is observed for any given input, to the process. It occurs in the transportation of energy along a specified path. Delay appears naturally in a system and that is why a useful control system design technique must be capable of dealing with dead time [1, 2].

First-order plus Dead Time (FOPDT) processes are abundantly available in process industry like blending process, spray drying process, etc. For this kind of process, a lot of tuning rules are available in the literature. The first-order plus dead time processes can be modeled as

$$G(s) = \frac{Ke^{-\theta s}}{(1+\tau s)} \tag{1}$$

M. Chaturvedi (✉) · P. Chauhaan
Department of Electrical Engineering, Graphic Era University, Dehradun, India
e-mail: mayankchaturvedi.geit@gmail.com

P. Chauhaan
e-mail: chauhaan1411@gmail.com

P.K. Juneja
Department of Electronics & Communication Engineering, Graphic Era University, Dehradun, India
e-mail: mailjuneja@gmail.com

D.K. Lobiyal et al. (eds.), *Proceedings of the International Conference on Signal, Networks, Computing, and Systems*, Lecture Notes in Electrical Engineering 396, DOI 10.1007/978-81-322-3589-7_22

where θ is the dead time present and τ is the time constant [3].

The PID controller is the most common form of feedback. The reason for the popularity of PID controllers is its ease of implementation and flexibility of parameter variation. Tuning of a PID controller is very easy, i.e., its parameters can be easily adjusted to get the best control performance. All the advantages of PID make it a universal tool to achieve the best performance of feedback control loop [4–7].

Many tuning techniques are available in literature for PID controllers which can be used to derive the parameters of the controller. Some important tuning methods are Ziegler Nichols (ZN) [8], Cohen Coon [9], Wang Juang Chan (WJC) [10], Tyreus Luyben (TL) [11], Chien Hrones Reswick (CHR) [12], based upon process reaction curve. Internal Model Control and Skogestad [13] tuning techniques are some other important tuning techniques. As time delay is very common in practicing a process control loop, it is required to compensate the effect of dead time. To achieve this objective a dead time compensator can be used which improves the closed loop performance of a classical controller for processes with delay. To improve the performance of the controllers, Smith proposed the first dead time compensation structure as Smith Predictor in 1957. It became the most recognized algorithm to compensate dead time in the industry [13, 14].

2 Methodology

A process which can be modeled as FOPDT process model is selected for the present analysis. Controller parameters are calculated to design PID controllers using four tuning techniques, viz. IMC, WJC, CHR and ZN tuning methods. The closed-loop responses of the controllers designed using the above mentioned tuning techniques are compared and analyzed for determining the set-point tracking capability. Smith Predictor is then designed for various controllers to compensate the effect of dead time. The selected FOPDT system transfer function from literature is

$$G(s) = \frac{1.25e^{-13s}}{33s + 1} \tag{2}$$

where dead time = 13 s, process gain = 1.25, and time constant = 33 [15].

3 Results and Discussion

The simulation has been performed to compare set-point tracking capability of the controllers designed using IMC (various values of closed-loop time constant τ_c), WJC, CHR and ZN tuning techniques. Tuning parameters for the FOPDT model

using various tuning techniques are shown in Table 1. Using these controller settings, various controllers have been designed and compared through simulation.

Figure 1 shows the comparison of closed-loop responses of all the controllers designed and Table 2 shows the performance parameters obtained through these responses. It can be seen from Fig. 2 that least rise time is given by C_4 and lowest value of settling time and maximum percentage overshoot is given by C_5.

Table 1 PID controller settings

Tuning technique	Controller nomenclature	K_C	τ_I	τ_D
IMC (τ_c = 17)	C_1	1.345	39.5	5.43
IMC (τ_c = 20)	C_2	1.2	39.5	5.43
IMC (τ_c = 25)	C_3	1.003	39.5	5.43
CHR	C_4	1.939	46.2	6.11
WJC	C_5	1.427	39.5	5.43
ZN	C_6	1.218	24.55	6.14

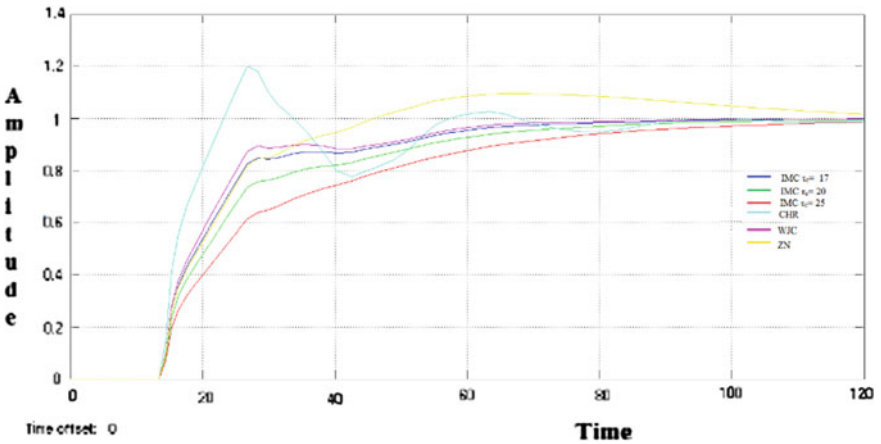

Fig. 1 Comparison of step response of PID controller designed using IMC τ_c = 17, 20, 25, CHR, WJC and ZN tuning techniques

Table 2 Performance parameters for various controller tuning techniques

Tuning method	Rise time	Settling time	% Overshoot
IMC (τ_c = 17)	34.5	74.1	0
IMC (τ_c = 20)	39.5	88.3	0
IMC (τ_c = 25)	51	109	0
CHR	7.21	87.5	22.5
WJC	21	66	0
ZN	19.8	116	9.49

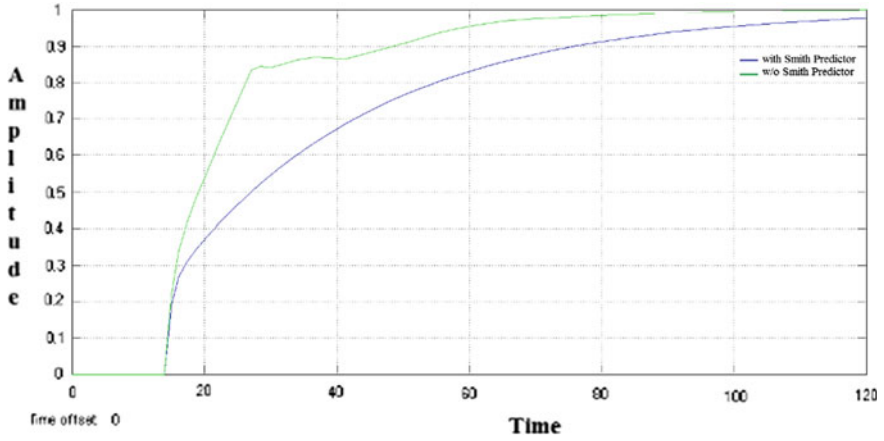

Fig. 2 Comparison of step response of PID controller designed using IMC (τ_c = 17) tuning technique with Smith Predictor and without Smith Predictor

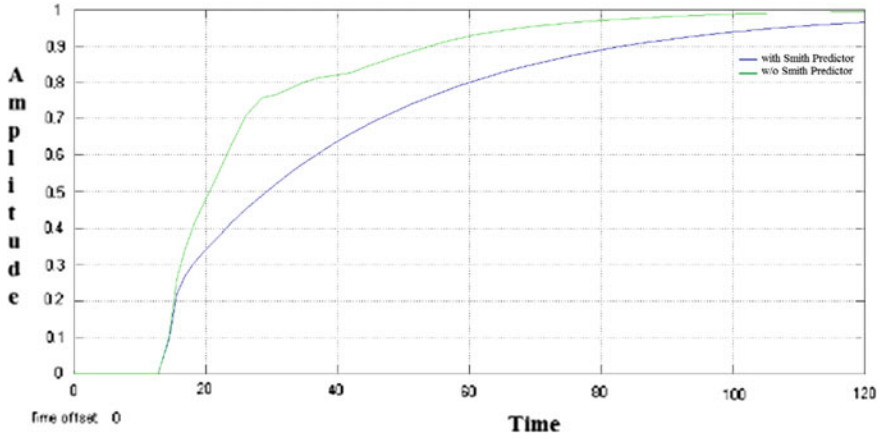

Fig. 3 Comparison of step response of PID controller designed using IMC (τ_c = 20) tuning technique with Smith Predictor and without Smith Predictor

The responses thus obtained after applying controller to the process are somewhat oscillatory and distorted. It can be easily seen that the set-point following is not gradual; it is due to the effect of delay. In order to compensate the effect of delay, a dead time compensator is used namely Smith Predictor.

Figures 2, 3, 4, 5, 6 and 7 show the comparative responses of all the controllers with and without using Smith Predictor. These figures clearly indicate the change in shape after applying Smith Predictor. The effect of delay is removed and the responses are smooth.

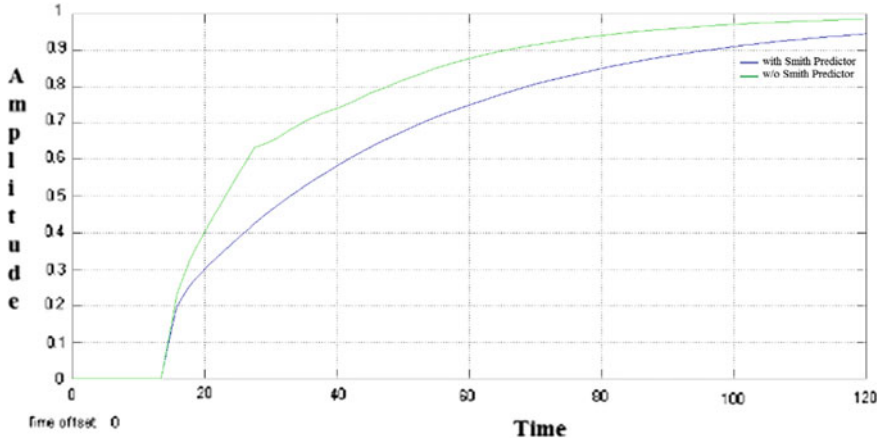

Fig. 4 Comparison of step response of PID controller designed using IMC (τ_c = 25) tuning technique with Smith Predictor and without Smith Predictor

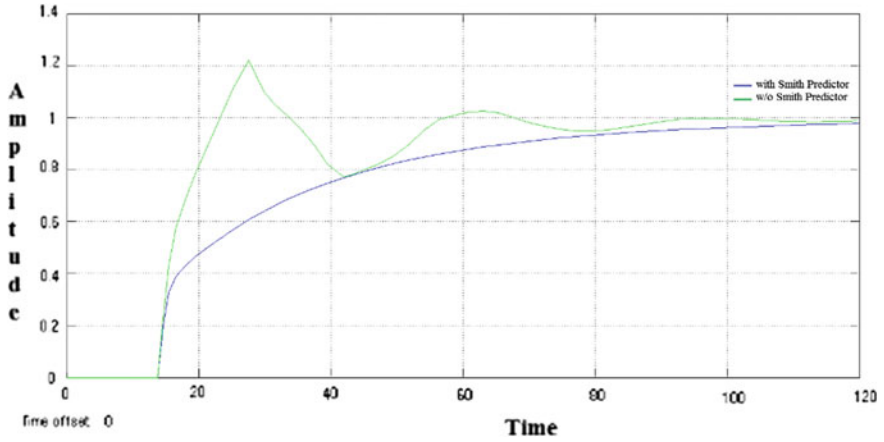

Fig. 5 Comparison of step response of PID controller designed using CHR tuning technique with Smith Predictor and without Smith Predictor

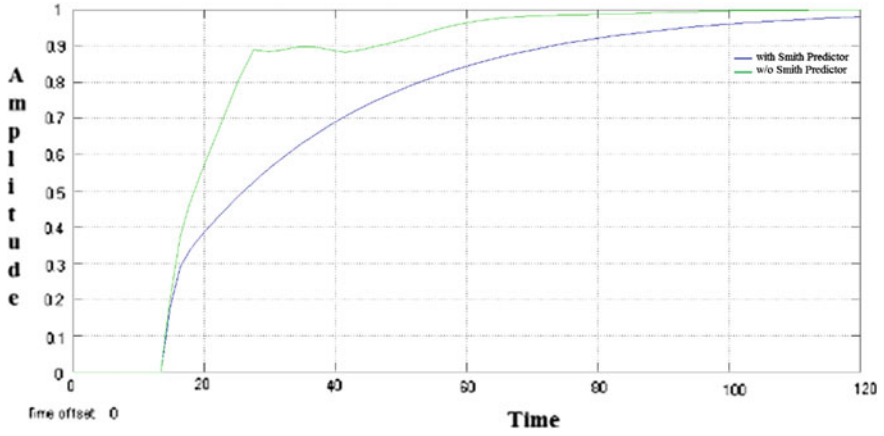

Fig. 6 Comparison of step response PID controller designed using WJC tuning technique with Smith Predictor and without Smith Predictor

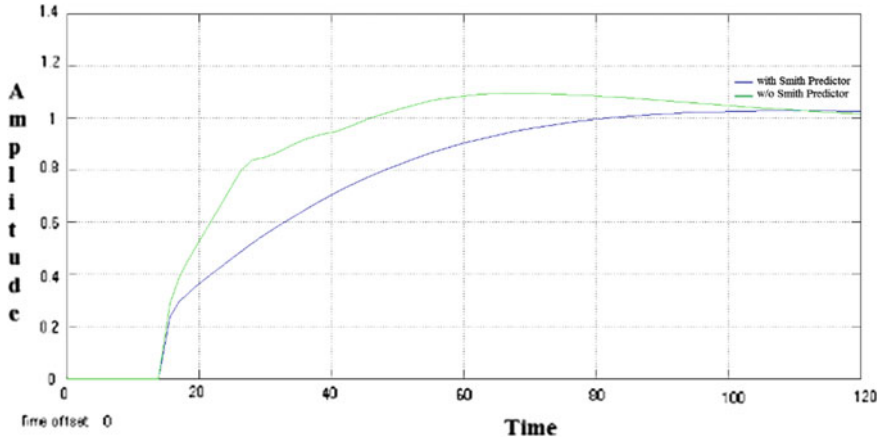

Fig. 7 Comparison of step response of PID controller designed using ZN tuning technique with Smith Predictor and without Smith Predictor

4 Conclusion

In present analysis, various PID controllers have been designed for selected FOPDT process model in order to get the satisfactory performance. The techniques used to design PID controllers are Internal Model Control, Chien Hrones Reswick, Wang Juang Chan, and Ziegler Nichols methods.

Among all the controllers designed for selected model Wang Juang Chan controller tuning technique gave best results in terms of settling time and percentage overshoot. The value of settling time and maximum percentage overshoot is least in

case of WJC controller. When Smith predictor strategy is applied to the designed controllers the effect of time delay is compensated and it also minimizes overshoot in most of the cases.

References

1. Shinskey, F. G.: Process Control Systems: Application, Design Adjustment, third ed., McGraw Hill, New York, (1988).
2. Chaturvedi, M., Juneja, P.K., Chauhaan, P.: Effect of Implementing Different PID Algorithms on Controllers Designed For SOPDT Process Proceedings of the International Conference on Advances in Computing, Communications and Informatics, ICACCI 2014, GCET Greater Noida, (2014) 853–858.
3. Chaturvedi, M., Juneja, P.: Effect of dead time approximation on controller performance designed for a second order delayed model. Proceedings of the International Conference on Advanced Electronic Systems, ICAES 2013, CEERI, Pilani, (2013) 313–315.
4. Cjevn, J.: Simple PI/PID Controller Tuning Rules for FOPDT Plants with Guaranteed Closed-Loop Stability Margin. Ročník 16, číslo 1, (2011) 17–25.
5. Visioli, A., Piazzi, A.: Improving Set-Point-Following Performance of Industrial Controllers with a Fast Dynamic Inversion Algorithm. Ind. Eng. Chem. Res., 42, (2003) 1357–1362.
6. Chen D., Seborg, D. E.: PI/PID controller design based on direct synthesis and disturbance rejection. Ind. Eng. Chem. Res., Vol. 41, (2002) 4807–4822.
7. Chauhaan, P., Juneja, P. K., Chaturvedi, M.: Controller Design and Its Performance Analysis for a Delayed Process Model. Proceedings of the International Conference on Advances in Computing, Communications and Informatics, ICACCI 2014, GCET Greater Noida, (2014) 859–862.
8. Ziegler, J. G., Nichols, N. B.: Optimum settings for automatic controllers. Trans. ASME 64, (1942) 759–768.
9. Cohen, G. H., Coon, G. A.: Theoretical considerations of retarded control. Trans. ASME 75, (1953) 827–834.
10. Xue, D., Chen, Y. Q., Atherton, D. P.: Linear feedback control analysis and Design with MATLAB. SIAM, (2007).
11. Tyreus, B. D., Luyben, W. L.: Tuning PI controllers for integrator/dead-time process. Ind. Eng. Chem. Res. 31, (1992) 2625–2628.
12. Astrom K. J., Hagglund, T.: PID Controllers: Theory, Design and Tuning. Instrument Society of America, (1995).
13. Seborg, D. E., Edgar, T. F., Mellichamp, D. A.: Process Dynamics and Control. Second ed., Wiley, New York, (2004).
14. Palmor, Z. J.: Time-delay compensation Smith predictor and its modifications. In W. Levine, editor, The Control Handbook. CRC Press, Boca Raton, FL, (1996).
15. Nancy, J., Sell, P.E.: Process Control Fundamentals for the Pulp and Paper Industry. TAPPI Process Control Textbook, Tappi Press, Atlanta, GA, (1995).

A Concept for Test Case Prioritization Based upon the Priority Information of Early Phase

Sushant Kumar, Prabhat Ranjan and R. Rajesh

Abstract The early information from requirement and design phase is very effective in software testing phase and it is also admitted by software requirement engineers (SRE) and software designer's community. However still most of the regression testing techniques work is performed by taking conventional information from software code. It will be more beneficial for software engineer if they use requirement priority information and design priority information in software testing to validate the process and find the fault easily. This will also provide the right direction of working of software and actual information is tested as per condition imposed. In this paper we scout that whether early phase (requirement and design) priority information associate with the tradition code analysis phase can improve the effectiveness of prioritization of test case techniques.

Keywords Test case prioritization · Test case selection · Requirement based prioritization · Model based prioritization · Early fault detection · SDLC

1 Introduction

Software testing is one of the crucial and important phases of software development life cycle (SDLC). The job is to intend to find the fault in software. Test case prioritization is an effective technique to find the test cases that determines faulty module. However in current software development it is mainly used in software testing phase to prioritize the test case. We cannot ignore the other phases of software development when we are preparing the test suite. We also need to give

S. Kumar (✉) · P. Ranjan · R. Rajesh
Central University of South Bihar, Patna 800014, Bihar, India
e-mail: sushantkumar@cub.ac.in

P. Ranjan
e-mail: prabhatranjan@cub.ac.in

R. Rajesh
e-mail: rajeshr@cub.ac.in

D.K. Lobiyal et al. (eds.), *Proceedings of the International Conference on Signal, Networks, Computing, and Systems*, Lecture Notes in Electrical Engineering 396, DOI 10.1007/978-81-322-3589-7_23

attention for requirement phase, design phase, code phase to gather the information to find the fault early in the software. So many researchers are looking to fill the gap of making test data using early phase information. Now many effective advanced soft computing techniques is being applied in different phase of the software to increase the quality of the product. In this paper we have focused on early phase of software development, why it is ignore in testing to make the prioritization of test suite. This research will be reducing the cost and time in software testing and maintenance. This new method is also increase the reliability of the software.

The phase wise fault identification is best supportive method to find the fault in early phase. The cost of find the fault in requirement phase is very low compare than other phases [1]. The requirement and analysis phase has almost 70 % work and more chance to fault here. Other phase has 30 % chance to fault. Design and code phase are reflection about requirement phase and if fault in requirement it will also persists in other phases of the software development. However we cannot ignore the importance of other phase like design phase and code phase for making to design of test case. All the phases have different type of information, that information is used to find the fault in software, Somerville [2] have explored the importance of every phases of SDLC. Indeed early phases provide much reliable information but always have a time bound in all phase so prioritization is provide good scope to find the critical area in all the phases. In software engineering prioritization is first introduce by Rothermal et al. [3] to find the fault in less time.

In this paper we utilize the information of requirement, design and code to make the test suite and prioritize the test data in test suite. The information from all the phases of software development life cycle (requirement, design, and code) has some own unique method like SRS (software requirement specification), UML (Unified modeling language), use-case, design patterns. These will help in software testing using their own ways for making test case prioritization. Software requirement specification document are prepared through requirement engineers using interaction with end users. SRS is give the input for prepare the design document, system designers preparer design document and design diagrams using SRS. And in the continuous process code is developed using design document by software developers. These three phases represents complete developed software before testing it will help in testing with different point of view with various priorities.

The complete goal of this paper is make the test case prioritization using gather the information from early phase (Requirement, Design and code). Large number of words in requirement phase to take decision for selecting the priority. Model based approach provide the design diagrams like different UML diagram it is extracted in XML format to take information from design like connectivity and flow of the model. And in last code based approach provide the static source code information using dependency call graphs.

2 Related Work

Prioritization of test case is very important in software testing and also it is effective technique for regression testing. Zhai et al. [4] has used test case prioritization for regression testing. He has prioritized the test case for location based service because it is always the requirement is changed in location based services so regression testing is used to assured the previously behaviors not having affected. Proper test case prioritization is effective to find the fault early and fix it.

Md. Siddik et al. [5] and Md. Arafeen [6] has proposed the requirement based test case optimization. Requirement clustering is used for cluster same type of software requirement specification. This method support the code based approach for test case prioritization. The requirement specification clustering is used text extraction, document matrix and term clustering to make priority based requirement. For the term clustering *K*-means algorithm has been used. Source code priority is decided by the combined priority by using lines of code, nested block depth and cyclomatic complexity of the code.

The slice based testing is the method of testing where code is divided in to slices, every slice are validate independently. Jeffrey et al. [7] has used slice based approach for test case prioritization. The requirement is divided into slice for find the fault early in the test execution.

Ant colony optimization has been used for test case optimization. Solanki et al. [8] has modified ant colony optimization (m-ACO) for test case prioritization in regression testing optimization. This approach is validated with various bench mark program, validation is performed by average percentage of fault detector (APFD) metric. Here food source represents the number of fault. Singh et al. [9] have proposed selection and prioritization approach using ACO to find the optimal solutions.

Regression testing has also very effective in embedded software, that always demands maintenance for added new features. Due to time constraint test case selection and prioritization have to up to mark in embedded software. Swarnendu et al. [10] has shown test case selection techniques for embedded software. He has proposed a model based regression test selection. He has also described different regression test selection techniques [11]. Most of the techniques are code based.

Rothermel et. al [3] has given the concept of test case prioritization to find the fault in specified time; faults are detected in testing process. In this paper he describes several techniques for test case execution to prioritize the test case for regression testing. The techniques are mainly focused on code coverage. For the validation he has taken 8 c programs has taken from Siemens corporate research.

Regression testing is an expensive process, number of methods of regression testing are used to improve its performance and these are retest all, test case selection, test case reduction, and test case prioritization. For increasing efficiency test case prioritization is being used for rearranging the test cases. A number of algorithms have been used for regression testing like greedy algorithm, 2-optimal greedy algorithm and now meta heuristic algorithm are using for solve the

prioritization problem [12]. The problem is always in regression testing is to select the techniques that is effective in terms of cover maximum software characteristics in minimum time [13].

A hybrid approach that combines the multiple criteria for regression testing is also very effective because it validate the process with different angle. Sampath et al. [14] have proposed a hybrid approach for regression testing based on rank, merge and choice based.

The formal testing techniques have reached high level of maturity in the last few years. But some common roots allowing to relate testing methods with each other are still missing in testing process. Classification of testing is one of the problems in software testing [15]. This paper tries to solve this type of problem.

Object oriented software is always having huge test case for validating the different behavior of object oriented functionality. Test case prioritization is one of the effective solutions for this is used by Abu Bakar et al. [16]. The goal of the work is to changes in a function body due to different relationship in object oriented program can be validate with optimized test case.

The test case with dependencies has taken extra time for checking same test case again and again. Asifa et al. [17] have proposed a dependency structures for prioritization. Functional test suites have been prioritized using dependency structures.

Srephen et al. [18] have proposed static test case prioritization using topic model. This method does not require the execution of each test case. The author has used black box static TCP in which source code is not available under test. This method used identifier, names, comments and string literals. This technique has applied on text analysis algorithm that uses the linguistic data information. This approach is compared with existing static black box TCP techniques.

Mei et al. [19] have proposed an approach to prioritized test cases in test suite in the absence of coverage information that will operate on java code and tested under JUnit framework. The JUnit test case prioritization framework have operated on the absence of coverage information (JUPTA). This technique analyzes the static call graphs to estimate the ability of each test case to achieve the code coverage, and the order of these test cases. For evolution of the effectiveness of JUPTA the author has conducted a study of 19 versions of java programs.

Multi-objective test case optimization is also very useful work in regression testing to complete more work on less time. The different algorithm are used in test case optimization like muti-objective genetic algorithm (MOGA), Diversity based genetic algorithm (DIV-GA) and many more. Annibale Panichella et al. [20] have used DIV-GA for solving the three objective in testing optimization problem and they are statement coverage, execution cost and past fault coverage.

In the testing process, possible to detect faults earlier and find more faults with test cases. A large number of test case prioritization papers are code based coverage. The code based approach has used number of statements covered, branch covered and basic block covered. Generally a test suite of 20 test cases having 20! Different ordering [21]. No algorithm has solve this problem more accurately. Some hope from meta- heuristic algorithm to solve this NP hard problem.

Table 1 The Phase wise cost of fixing the fault

Sr. No.	Phase name	Cost in units
1	Requirement	1
2	Design	10
3	Code	100
4	Test	1000
5	Maintenance	10,000

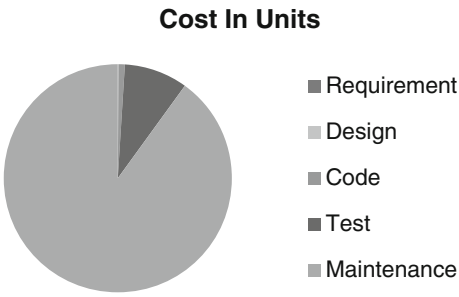

Fig. 1 The cost of fault in early phase of software development is very less

Chhabi et al. [22, 23] have propose a novel test case prioritization techniques based on dependence model for object-oriented programs. The author has first constructed intermediate model using source code. The purpose of this model is when the source code is modified model is also updated. This model represents different dependencies and information for object like association, inheritance and aggregation.

The observation from all the related work in test case prioritization shows that most of the work in prioritization is related to software testing like branch coverage, path coverage, probability based approach. The early phase is not much considered when making the prioritization of test suite. The gap is still open to effective utilization of the requirement, design and code phase to prioritize test case. If we take the help from early phase of software development it should great support for software testing to reduce the cost and time. Singh et al. [1] have also found the fault that is handle in maintenance phase is very costly compare than early phase of development. This can also define in give bar chart. The result from Table 1 and Fig. 1 shows that the cost of maintenance is very high.

3 Test Case Prioritization

3.1 Definition

Test case prioritization (TCP) is the problem of test case ordering in test suite of system under test (SUT). The goal of this is maximizing some goal criteria such as

fault detection rate of test cases. The ordering of test cases is for execution of test cases so that more important test cases is execute first. The definition of test case is defined with given rule.

Let T be test suite, PT is the set of permutation of T, and f is function from PT. Then $T' \in PT$ such that $\forall T''$ $(T'' \in PT)$ $(T'' \neq T')$ $[f(T') \geq f(T'')]$.

Here PT is the set of all possible prioritization of T. And f is a function applied to any ordering.

3.2 Metrics

Test case metrics is the measurement of test suite that finds the fault in fault is software. One popular measure is APFD (Average Percentage Fault Detection) the value of APFD is from 0 to 100, if number is higher means higher fault detection in software.

Let T be a test suite containing n test cases and suppose F be a set of m faults found by test suite T. Let TF_i is the first test case in ordering T′ of T which find fault i. The APFD for test suite T′ has performed the following given equation.

$$\text{APFD} = 1 - \frac{\text{TF1} + \text{TF2} + \text{TF3} + \ldots + \text{TF}m}{nm} + \frac{1}{2n}$$

This metric can be describe with taking one example consider a program with a test suite with 10 test cases A TO E in Table 2.

We consider the orders of test case one with no order and other with order. The first case is without order T1: ABCDEFGHIJ and other with order T2: IJEBCDFGHA. If calculate the value with equation of APFD it gives 43.75 % result in without ordering and 90 % with ordering. Figure 2 describes the result of APFD for both cases. The result shows the ordering of test cases has high value of APFD.

Table 2 Example for test case with fault covered

Test	Faults							
	1	2	3	4	5	6	7	8
A								
B	Y	Y						
C	Y	Y	Y					
D		Y	Y					
E	Y							Y
F								Y
G		Y						
H					Y			
I	Y	Y	Y	Y	Y	Y		
J					Y	Y		

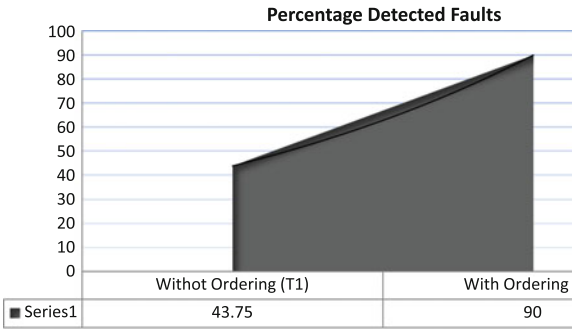

Fig. 2 Test case ordering in test suite for APFD calculation

4 A Conceptual Model for Test Case Prioritization

This concept combines the information from every phase of software development life cycle to take decision of priority of test cases. The first phase is SRS phase is take decision using requirement document that is carried out by requirement engineers with direct interaction with end users. Software design document (SDD) prepared with system designer with taking the document of requirement phase. And in code phase developed by software developers based on the software design document. These three phases represents software with different angle and with different priority, the combined information from SDLC phase is attached it identify the ordering of test case.

4.1 Priority Information from Software Requirement Specification (PISRS)

SRS has large number of requirements; the well documentation is primary need and mandatory for this phase for gaining information from requirement phase. The test that is similarities is combined in to a class or cluster. Grouping is form with syntactic and semantic; this concept is also used in text mining to find meaningful information [24]. All the requirements covered by some cluster based on the similarity information. Text extraction, term document matrix and term clustering are three major tasks in this process.

(i) Text extraction: The requirement is considered as a large number of words including meaningful and meaningless. The requirements are split into used words. The words that have no specific meaning like stop words or that are not related to goal like articles, propositions, conjunctions, etc have been eliminated. After eliminating all the non principle words the distinct terms regarding requirement are identified for next phase.

(ii) Term document matrix: After getting the different term from previous steps we create term document matrix. The matrix represents rows with requirements and columns with distinct terms across the all requirements. The matrix can be representing in many ways, like Boolean values in matrix cells indicate whether the terms are present in the requirement or not.

(iii) Term clustering: There are many clustering algorithms exist in clustering like agglomerative hierarchical clustering and *K*-means clustering. Charu et al. [24] Show that *K*-means clustering is suitable for document clustering. The *K*-means clustering approach specifies the number of clusters. The mapping of *K*-means algorithm in document matrix represents with n number of requirements and p number of terms. This algorithm allocates each requirement in to cluster, which have same or near to requirements.

4.2 Priority Information from Software Design Document (PISDD)

This is also the important document for software priority. For process in design document information comes from different design diagrams are used like UML, activity diagram, sequence diagram are used. This document is extracted in readable format. The UML reader takes UML diagram as a input and convert into the XML format that is provided by software designers. This is useful technique because we cannot take input directly in diagrams. XML is readable format and it used for many activities these activities can be prioritized according to their nature.

4.3 Priority Information from Software Code and Implementation (PISCI)

The code is widely used for testing purpose. This phase is the result of real development of software. The proper rule must be followed in software coding phase like naming convention. If we not follow the naming proper convention the checking of source code is very difficult as per requirements. Two methods are used for validation static and dynamic. Static method is used to check the software before execution. The different metric are used for to gain information from code to find the fault.

(i) *Lines of Code* (*LOC*) This is the measurement of lines of code in the software. In this method we have ignore the lines of comments and the blank line inside the code.

(ii) *Nested block statements* (*NBS*) It measures the number of nested statements in software nested statements have more chance for fault occurrence in the module and it is also cover more lines of code.

(iii) *Code Cyclomatic complexity* (*CCC*) This shows the number of linearly independent paths in the code. Number of independent path is important result to check the code for finding fault. The cc can be calculated by formula given McCabe $E - V + 2P$, where E is edges and V is nodes and P is the connected component.

According the above variables for each class or method code metric value (cmv) is calculated using the given equation.

$$\text{CMV} = \frac{\frac{\text{LOC}}{\max(\text{LOC})} + \frac{\text{NBS}}{\max(\text{NBS})} + \frac{\text{CCC}}{\max(\text{CCC})}}{3}$$

4.4 Integration and Mapping for Test Suite Cluster (IMTSC)

The priority calculated by requirement, design and code phase, the comparative priority is calculated by using all the three phases. This calculation is done by adding the priority value of all the SDLC phases. The integration add the priority information gather from requirement (PISRS), design (PISDD) and code PISCI this provide the result for combined priority of SDLC phase (IMTSC). Every phase has own purpose and all the phases is important, according to importance of phases we put the different weight on requirement, design and code.

$$\text{IMTSC} = \frac{\text{PISRS} + \text{PISDD} + \text{PISC}}{3}$$

The combined priority is used for making the requirement cluster in this approach and it has many similar requirements in one cluster (Table 3).

In Table 3 test cases 1 and 4 is used by requirement 1, and cluster 1 has 4 test cases (1, 4, 5 and 4) and the requirement covered is 1, 4 and 5.

4.5 Test Case Selection and Prioritization

After integration of all the phases and mapping of test cases the weight priority has used for test case prioritization and selection. The weight priority the sum of all requirement, design and code id is calculated. The weight may be varying according to the phase and importance. Let if the weight priority of requirements 1, 4 and 5 are 18.6, 13.4 and 15.0 respectively. The total sum of cluster 1 is 47 and using similar way let sum of cluster 2 is 26.6. The test case order is for first phase: 1, 4, 5 and 2 and for second phase are 3 and 2.

Table 3 Mapping of Requirement cluster into test mapping

Cluster 1	**Cluster 2**
M-1 ,M-4 , M-5	M-2,M-3

↓

REQUIRMENT ID	**TEST CASE ID**				
	TC 1	TC2	TC3	TC4	TC5
1	√			√	
2		√			
3			√		
4					√
5		√			√

↓

TEST MAPPING

↓

Cluster 1	**Cluster 2**
TC1,TC4,TC5 ,TC 6	TC2,TC3

5 Conclusion

This paper has used test case prioritization using early phase information. Most of the work in test case prioritization is performed by taking source code information. In this paper we have try to focus on the requirement and design phase of software. The concept find the fault in early phase if it is apply with code phase then more accurate result has come. Our testing result gives the more fruitful result for early fault identification.

References

1. Yogesh Singh, Arvinder Kuar, Bharti Suri, and Shweta Singhal: Systematic Literature Review on Regression Test Prioritization Techniques, Informatica 36(2012) 379–408.
2. Ian Sommerville: Software Engineering, Ninth Edition, Pearson, India, (2009).
3. Gregg Rothermel, Ronald H. Untch, and Mary Jean Harrold: Prioritizing Test cases for regression testing, IEEE Transactions on software engineering 27(2001) 929–948.
4. Ke Zhai, BoJiang and W.K. Chan: Prioritizing Test Cases for regression Testing of Location-Based Services: Metrices Techniques, and Case Study, IEEE Transactions on service computing, 7 (2014) 54–67.
5. Md. Saeed Siddik and Kazi Sakib: RDCC: An Effective Test case prioritization framework using software requirements, design and source code collaboration, 17 th International conference on computer and information technology, (2014)75–80.

6. Md. Junaid Arafeen and Hyunsook Do: Test case prioritization using requirement based clustering, IEEE 6th international conference on software testing, verification and validation, (2013) 312–321.
7. Dennis Jeffrey and Neelam Gupta: Test Case Prioritization Using Relevant Slices,30 th International conference on software and applications (2006) 411–420.
8. Kamna Solanki, Yudhvir Singh And Praveen Ranjan Srivastava: Test case prioritization: An approach on modified Ant Colony Optimization, Mathematical Problems in Engineering (2015).
9. Yogesh singh, Arvinder Kaur and Bharti Suri: Test case prioritization using ant colony optimization, ACM SIFSOFT Software engineering Notes (2010).
10. Swarnendu Biswas and Rajiv Mall: A Regression Test Selection Techniques for embedded software, ACM Transactions on Embedded computing systems, 13(2013) 47.1–47.39.
11. Swarnendu Biswas and Rajiv Mall: Regression Test Selection Techniques: A Survey, Informatica 35(2011) 289–321.
12. Sujata and G.N. Purchit: A schema support for selection of test case prioritization techniques, Fifth International conference on advanced computing and communication (2015) 547–551.
13. N. Sharma, Sujata and G.N. Purohit: Test case prioritization techniques "An empirical study" International conference on high performance computing and applications (2014)1–6.
14. Sreedevi Sampatt, Renee Bryce and Atif M. Memon: A Uniform Representation of hybrid criteria for regression testing, 39(2013) 1326–1344.
15. Ismael Rodriguez, Luis Llana and Pablo Rabanol: A General Testability Theory: classes Properties, complexity, and testing reductions, IEEE Transaction on software engineering, 40 (2014) 862–894.
16. Abu Bakar Md Sultan, Abdul Azim Abd Ghani, Salmi Baharom and Samaila Musa: An Evolutionary Regression Test Case Prioritization based on dependence graph and genetic algorithm for object-oriented programs, 2nd International conference on emerging trends in engineering and technology, (2014) 22–26.
17. Shifa-e-Zehra Haidry and Tim Miller: Using Dependency structures for prioritization of functional test suites, IEEE Transactions on software engineering 39(2013) 258–275.
18. Stephen W. Thomas, Handi Hemmati, Ahmed E. Hassan, Dorothea Blosrein: Static test case prioritization using topic model, Epmir software eng 19 (2014) 182–212.
19. Hong Mei, Dan Hao, Lingming Zhang, Lu Zhang, Ji Zhou and Gregg Rothermel: A Static Approach to Prioritizing JUnit test Cases, IEEE Transactions on software engineering 38 (2012)1258–1275.
20. Annibale Panichella, Rocco Oliveto, Massimiliano Di Pento and Ander De Lucia: Improving Multi–Objective Test Case Selection by injecting Diversity in Genetic Algorithms, IEEE Transactions on Software Engineering, 41(2015) 358–383.
21. Catgatay Catal: The Ten Best Practices for Test Case Prioritization, Communication as in Computer and Information Science 319(2012) 452–459.
22. Chhabi Rani Panigrahi and Rajiv mall: A heuristic-based regression test case prioritization approach for object-oriented programs, Innovations Syst Softw Eng 10(2014) 155–163.
23. Chhabi Rani Panigrahi and Rajiv mall: Model-Based Regression Test Case Prioritization, Communications in computer and information science 54(2010) 380–385.
24. Charu C. Aggarwal and Cheng Xiang Zhai: a survey of text clustering algorithms, Mining text data (2012)77–128.

MEMS-Based Phase Shifters for Phased Array Applications Fully Integrated on PCB Substrates

Amrita Chakraborty and Arpan Kumar Kar

Abstract The present study discusses the design of microelectromechanical systems (MEMS)-based phase shifters and their application in phased array antenna (PAA) realization. Commercially available MEMS Single-Pole-Double-Throw (SPDT) switches have been employed for the phase shifter design at a frequency of 5.7 GHz (ISM band). These phase shifters are in turn integrated with the feed lines of a 4×1 planar patch antenna array such that electronic mode of antenna beamsteering is resulted. It has been observed that a progressive phase shift of 45° between successive patch antenna elements would generate 11° beam tilt with good directivity and a high gain of 9.5 dB. The entire PAA structure along with the antenna elements, phase shifter modules, and the corporate feed network are integrated on the same PCB laminate, Rogers Ultralam 2000™ having permittivity $\varepsilon_r = 2.5$, thickness $h = 30$ mil (0.762 mm), and a dissipation factor $\tan \delta = 0.0019$ in order to facilitate simplicity in fabrication process.

Keywords Beamsteering · MEMS SPDT switches · Patch antenna array · Phase shifter · Phased array antenna (PAA)

1 Introduction

MEMS technology, initially restricted to academic research field only during 1990s, has gradually gained potential in recent years. Several companies like Omron, Radant MEMS, Wispry, DelfMEMS, Raytheon, Skyworks, have launched packaged

A. Chakraborty (✉)
Department of Electronics and Telecommunication Engineering,
Jadavpur University, Kolkata 700032, West Bengal, India
e-mail: amrita.chakraborty2@gmail.com

A.K. Kar
Information Systems DMS, Indian Institute of Technology Delhi,
New Delhi 110016, India
e-mail: arpan_kar@yahoo.co.in

D.K. Lobiyal et al. (eds.), *Proceedings of the International Conference on Signal, Networks, Computing, and Systems*, Lecture Notes in Electrical Engineering 396, DOI 10.1007/978-81-322-3589-7_24

MEMS devices, commonly MEMS switches which are commercially available in market for employment in broader application areas. The present work deals with radio frequency microelectromechanical systems (RF MEMS), a specialized research area dedicated to the development of RF components like varactor, phase shifter, and filter circuits, all utilizing MEMS technology. All RF MEMS devices consist of an actuating part which actuates on the application of an external voltage (electrostatic actuation) to provide the required RF functionality. This work discusses the design of RF MEMS phase shifters and its application in the development of PAA [1, 2] system, all modules integrated on the same substrate. RF MEMS-based phase shifters have gained importance since it has numerous applications in the areas of telecommunication, satellite, and military warfare. RF MEMS phase shifter modules also form an integral part of the PAA system used in military applications and weather forecasting systems. RF MEMS phase shifters can be realized by the following approaches: (a) switched line approach [3], (b) reflective type phase shifter using the 3 dB coupler approach [3, 4] and (c) loaded line or the distributed MEMS transmission line (DMTL) approach [5–7]. A number of publications are available which report the development of PAA system using MEMS phase shifter [3–8]. Switched line method of phase shifter implementation is by far the simplest approach, both in terms of design, layout, and fabrication. Hence, switched line method has been chosen to be implemented along with the 4 × 1 patch antenna array for electronic beamsteering purpose. All simulations have been carried out in Ansoft HFSS v. 13 ®. The SKY13335-381LF: 0.1–6 GHz GaAs SPDT switches were procured for the realization of the switched line phase shifters.

2 Device Design Strategy

This section is divided into three broad categories, (i) the switched line phase shifter design, (ii) the 4 × 1 patch antenna array design, and (iii) the PAA design.

2.1 Switched Line Phase Shifter Design

Figure 1 shows the basic schematic behind the design strategy of the switched line phase shifter device. The basic principle revolves round the concept of introducing time delay difference between two direct paths to result in desired phase shift. The

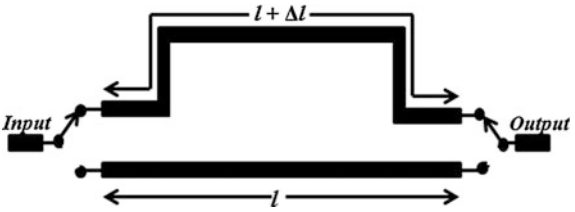

Fig. 1 Schematic layout of the switched line phase shifter

two transmission lines (i) reference line of length 'l' and (ii) the delay line of length '$l + \Delta l$' are of different path lengths which result in a phase delay (φ) of the RF signal at the output port governed by the expression [1]:

$$\varphi = (2\pi/\lambda)\Delta l \tag{1}$$

where, Δl = path difference and λ = wavelength of the input RF signal.

Switching between the reference line and the delay line segments are controlled by different switching modules, among which PIN diodes, FET switches and MEMS are most common. Switched line phase shifters have certain advantages over other phase shifters as φ is a linear function of frequency and independent of time and temperature changes since it is solely dependent on the length of the transmission lines.

2.2 4 × 1 Patch Antenna Array Design

The patch antenna array realization initially commences with the design of a single patch antenna followed by the four element array design such that the resonant frequency of the array is maintained at f_r = 5.7 GHz. Patch antenna design formulae are widely available in standard literatures [2] which have been adopted presently. Rogers Ultralam 2000™ having permittivity $\varepsilon_r = 2.5$, thickness $h = 30$ mil (0.762 mm) and a dissipation factor tan $\delta = 0.0019$ is considered as the substrate for the antenna design. The expressions to determine the width (W) and length (L) of the rectangular microstrip patch antenna element are as follows [2]:

$$W = (c/2f_r)\sqrt{(2/(\varepsilon_r + 1))} = 1.955 \text{ cm} \tag{2}$$

$$\varepsilon_{reff} = (\varepsilon_r + 1)/2 + 0.5(\varepsilon_r - 1)[1 + 12(h/W)]^{-1/2} = 2.369 \tag{3}$$

$$\Delta L/h = 0.412\frac{(\varepsilon_{reff} + 0.3)((W/h) + 0.264)}{(\varepsilon_{reff} - 0.258)((W/h) + 0.8)}, \therefore \Delta L = 0.039 \text{ cm} \tag{4}$$

$$L = (\lambda/2) - 2\Delta L = (c/2f_r\sqrt{\varepsilon_{reff}}) - 2\Delta L = 1.602 \text{ cm} \tag{5}$$

where, W, L = width and length of the rectangular microstrip patch antenna, c = velocity of light in vacuum (3×10^8 m/s), λ = wavelength of the input RF signal, ε_{reff} = effective dielectric constant of substrate and ΔL = effective length of patch antenna.

Simulations have been conducted in Ansoft HFSS v. 13 to obtain the Return Loss (S_{11} in dB) performance. For a single patch antenna element, $S_{11} = -29.12$ dB with a gain of 7.4 dB. The same element was cascaded to obtain a 4 × 1 linear array with an interspacing 'd' = 0.65λ between successive antenna elements. The factor 'd' was optimized by repeated simulations to a value of 0.65λ in order to

obtain perfect matching at the desired frequency of 5.7 GHz. For the 4 × 1 patch antenna array, S_{11} of −26.78 dB and a gain as high as 9.5 dB is obtained.

2.3 Phased Array Antenna (PAA) Design

The basic PAA consists of a series of radiating elements, each connected with a phase shifter module. The relative phases of the RF signals feeding the antenna elements are varied in manner so that antenna beam is reinforced in a certain direction and nullified in the undesired direction. The phenomenon of electronic beamsteering enables the antenna beam to undergo a certain angular displacement, or steers the antenna beam through some prescribed angle in space, denoted by θ_0 in Fig. 2.

Schematic layout of the PAA system required to achieve electronic beamsteering has been shown in Fig. 2. It consists of three major components, viz., (i) a linear antenna array, consisting of 4 × 1 rectangular microstrip patch antenna elements; (ii) phase shifter modules connected at the antenna feed elements and (iii) a power distribution network or the corporate feed network. It is to be noted that, in a PAA system [1–8], progressive phase shifts should be maintained among successive antenna elements as evident from Fig. 2. Starting from left to right, successive antenna elements maintain a constant phase shift of φ as $(3\varphi - 2\varphi)$, $(2\varphi - \varphi)$, $(\varphi - 0°)$. For the present study, progressive phase shift, $\varphi = 45°$ has been

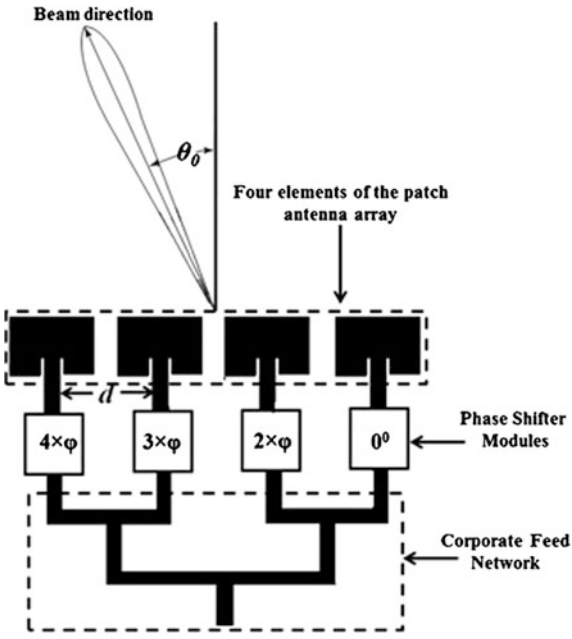

Fig. 2 Schematic layout of the Phased Array Antenna system showing beamsteering effect

considered to result in electronic beam steering effect. For four antenna elements, 0°, 45°, 90° and 135° switched line phase shifter modules are designed and verified for appropriate results.

3 Phased Array Antenna Implementation

Figure 3a shows the complete PAA implementation on the Rogers Ultralam 2000™ substrate. It consists of the 4-element patch antenna array, the switched line phase shifter modules and the corporate feed network, all integrated on a PCB surface of 12 cm × 7 cm only. This suggests minimum space requirement for the entire RF system integration and helps promote miniaturization. The lengths of the reference line and the delay line are calculated in relation to the mathematical expressions (5)–(8) shown as under. Here, L_0 denotes the length of the reference line, whereas, L_{45}, L_{90}, and L_{135} denotes the length of respective delay lines. Differences between the lengths of the reference and delay line would generate required phase shift in RF input signal. Figure 3b shows the S_{11} performance of the PAA system, both when the SPDT switches are connected to the reference states and the delay states. For both cases, it is observed that a perfect impedance matching is maintained since S_{11} is below −23 dB.

$$L_0 = (\lambda/\sqrt{\varepsilon_r})(1 - (\varphi/2\pi)) = (\lambda/\sqrt{\varepsilon_r})(1 - (0^\circ/360^\circ)) = 3.271\,\text{cm} \quad (6)$$

$$L_{45} = (\lambda/\sqrt{\varepsilon_r})(1 - (\varphi/2\pi)) = (\lambda/\sqrt{\varepsilon_r})(1 - (45^\circ/360^\circ)) = 2.862\,\text{cm} \quad (7)$$

$$L_{90} = (\lambda/\sqrt{\varepsilon_r})(1 - (\varphi/2\pi)) = (\lambda/\sqrt{\varepsilon_r})(1 - (90^\circ/360^\circ)) = 2.453\,\text{cm} \quad (8)$$

$$L_{135} = (\lambda/\sqrt{\varepsilon_r})(1 - (\varphi/2\pi)) = (\lambda/\sqrt{\varepsilon_r})(1 - (135^\circ/360^\circ)) = 2.044\,\text{cm} \quad (9)$$

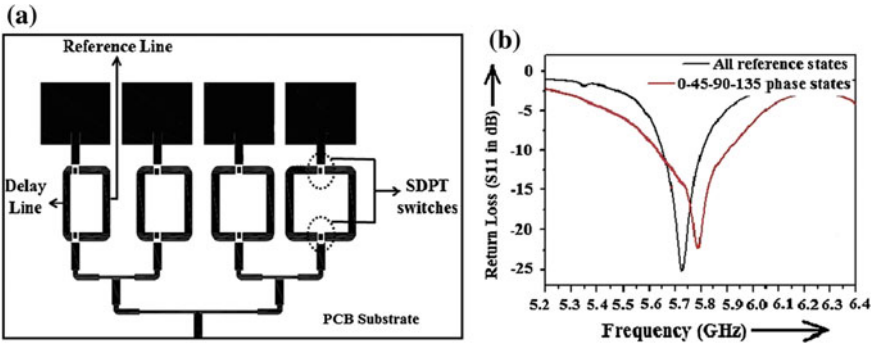

Fig. 3 **a** Schematic layout of the PAA system integrated with switched line phase shifter structure, **b** S_{11} performance with all the phase shifters both in reference and delay states

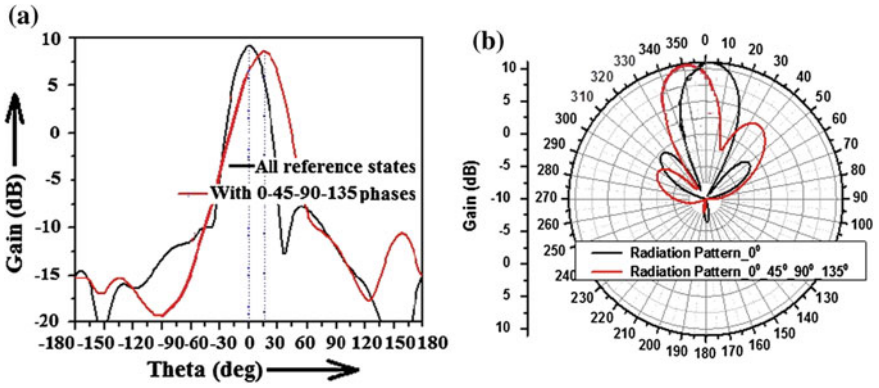

Fig. 4 **a** Rectangular plot of the antenna radiation pattern showing beam shift, **b** Polar plot of the antenna radiation pattern showing angular beam tilt

Corresponding to the theory of PAA, the beam steering angle (θ_0) maintains a relationship with the progressive phase shift (φ), which can be expressed as follows, where 'd' indicates the separation between successive antenna elements of the array:

$$\varphi = (2\pi/\lambda)d\sin\theta_0; \therefore \theta_0 = \sin^{-1}(\varphi\lambda/2\pi d) = 11.08^\circ \tag{10}$$

Hence, the major lobe of the antenna radiation patterns steers by approximately 11° with reference to original beam pattern where the major lobe is directed perfectly along the 0° line. The gain and the radiation pattern of the PAA have been shown as under in Fig. 4a, b. Figure 4a shows the rectangular plot whereas Fig. 4b shows the polar plot of the antenna radiation pattern along with a beamsteering of 11°.

4 Conclusion

MEMS switches have been employed in the design of switched line phase shifter device which is turn is an integral part of the PAA, a crucial RF system mandatory in military warfare. The three major RF subsystems, comprising of the antenna array, phase shifter modules and the corporate feed network have been integrated on a single PCB substrate of lateral dimensions 12 cm × 7 cm only, involving a planar RF system realization. The RF system development process is highly simplified, promoting miniaturization and is performance efficient in the frequency of interest in the Industrial, Scientific and Medical (ISM) radio band.

References

1. Mailloux R. J.: Phased Array Antenna Handbook. Second Edition. Artech House (2005).
2. Balanis C. A.: Antenna Theory: Analysis and Design. Third Edition. Wiley (2005).
3. Rebeiz G. M.: RF MEMS: Theory, Design and Technology. Second Edition. Wiley (2003).
4. Ko C. H., Ho K. M. J, Rebeiz G. M.: An Electronically-Scanned 1.8–2.1 GHz Base-Station Antenna Using Packaged High-Reliability RF MEMS Phase Shifters. IEEE TMTT 61, 2, 979–985 (2013).
5. Sundaram A., Maddela M., Ramadoss R., Feldner L. M.: MEMS-Based Electronically Steerable Antenna Array Fabricated using PCB Technology. J. MEMS 17, 356–363 (2008).
6. Goel P., Vinoy K. J.: A Low-cost Phased Array Antenna Integrated with Phase Shifters Cofabricated on the Laminate. Progress in Electromagnetics Research B. 30, 255–257 (2011).
7. Topalli K., Civi O. A., Demir S., Koc S., Akin T.: A Monolithic Phased Array Using 3-bit Distributed RF MEMS Phase Shifters. IEEE TMTT. 56, 270–277 (2008).
8. James C., Armenta A., Porter S., Marvin A.: Reconfigurable Phased Array Antennas with RF-MEMS on a PCB Substrate. Proc. IEEE AP Conf. 1–5 (2012).

A Novel Multipath Mitigation Technique for SPSGPS Receivers in Indian Urban Canyons

Bharati Bidikar, G. Sasibhushana Rao, L. Ganesh and M.N.V.S. Santosh Kumar

Abstract 3D Position, Velocity, and Time (PVT) provided by GPS receiver is biased by various errors and the incorrect measurement of the GPS observables. Among all the possible errors multipath phenomenon is of major concern, particularly in urban canyons, as it depends on the environment around GPS receiver antenna. Considering its importance, a number of studies were conducted to analyze the multipath effects on GPS signal, but most of the research concluded in the requirement of new architecture of GPS receiving antenna to reject the multipath signals or change in reflecting environment geometry around the GPS receiving antenna. But these conventional methods may not mitigate the multipath error of SPS (Standard Positioning Service) GPS applications in urban canyon, where the geometry or the reflection coefficient of nearby reflectors cannot be determined accurately. In this paper, the multipath error mitigation technique is proposed which is based on the linear combinations of pseudorange and carrier phase observations. The analysis of the error given in this paper will facilitate in processing the observables of satellites with high elevation angle and least signal multipath. The pseudorange correction and the analysis of the residual range error presented in this paper will be useful in selecting the low-multipath location for GPS receiving antenna placement, navigation, surveying, and ground-based geodetic studies.

Keywords GPS · SPS · Elevation · Pseudorange · Carrier phase range · Multipath error · Navigation solution

B. Bidikar (✉) · G. Sasibhushana Rao
Department of Electronics and Communications Engineering,
Andhra University, Visakhapatnam, India
e-mail: bharati.bidikar@gmail.com

L. Ganesh
Department of Electronics and Communications Engineering, ANITS,
Visakhapatnam, India

M.N.V.S.Santosh Kumar
Department of Electronics and Communications Engineering, AITAM,
Visakhapatnam, India

D.K. Lobiyal et al. (eds.), *Proceedings of the International Conference on Signal, Networks, Computing, and Systems*, Lecture Notes in Electrical Engineering 396, DOI 10.1007/978-81-322-3589-7_25

1 Introduction

SPSGPS position accuracy depends on the correctness of pseudorange. Pseudoranges are the measure of the transit time of the less precise Coarse/Acquisition (C/A) code. Though the Precision (P) code is also transmitted by the satellites, the SPSGPS receiver position is determined using the C/A code. The C/A code and the navigation message are modulated on the L1 (1575.42 MHz) and broadcast by the satellites to all the receivers on earth [1]. Precise measurement of the pseudorange determines the SPSGPS receiver accuracy.

These GPS measurements are biased by various error sources [2], but the common mode atmospheric, orbit, and satellite clock errors can be eliminated by differential operation [3]. But the multipath error caused by signal reflection and/or diffraction leads to multiple paths [4]. Although the line of sight (LOS) signal and the reflected signals have same emission time, the reflected signals are delayed due to longer propagation path leading to incorrect transit time determination by the GPS receiver correlator. These signals also interfere with the line of sight signal [5]. The resultant signal arriving at the receiver will have distorted amplitude, phase, and polarization [6]. These distortions and the time delays depend on the reflecting environment geometry near by the receiving antenna [7]. Multipath phenomenon also depends on the antenna gain pattern and the type of correlator used in the SPSGPS receiver. Hence, the multipath error is unique to each GPS receiver. These parameters limit the accuracy of the conventional multipath modeling. But in this paper the multipath error on pseudorange measurement of $L1$ is calculated using only the satellite transmitted ephemerides data and carrier frequencies for a SPSGPS receiver located in Indian Subcontinent (Lat:17.73°N/Long:83.319°E). Though the error is estimated for all visible satellites, the error analysis pertaining to only space vehicle pseudo random noise (SV PRN) 31 is presented in this paper. The multipath error analysis done in the paper will be a valuable for setting up the GPS receiver antenna for aircraft navigation, tracking, and for static SPSGPS receivers in urban canyon.

2 Multipath Error Modeling

The conventional method of multipath error mitigation is changing the receiver hardware and reflecting environment around the GPS receiver antenna. Few of the methods include directing the antenna in low-multipath direction or using multipath rejecting antennas like choke ring antenna [8]. But in this paper, the multipath error is estimated considering the satellite ephemerides data. Though the multipath error affects both the pseudorange and carrier phase measurements, the error on carrier phase measurements is negligible [9]. In this paper, the multipath error is modeled

on pseudorange of L1 frequency, considering the GPS observables and the carrier frequencies.

$$P_1 = \rho + c \times \Delta t^k + I_1 + MP_1 \tag{1}$$

where, 'P_1' is pseudorange on L1 frequency [m], 'ρ' is geometric range [m], 'I_1' is ionospheric delay on L1 frequency [m], 'MP_1' is multipath error on P_1 [m], 'Δt^k' is clock error of kth satellite [s] and 'c' is speed of light [m/s]

$$\phi_1 = \rho + c \times \Delta t^k - I_1 + \lambda_1 N_1 + M\phi_1 \tag{2}$$

$$\phi_2 = \rho + c \times \Delta t^k - I_2 + \lambda_2 N_2 + M\phi_2 \tag{3}$$

where, 'ϕ_1' is carrier phase measurement on L1 frequency [m], 'ϕ_2' is carrier phase measurement on L2 frequency [m], 'N_1' is integer ambiguity on L1 frequency, 'N_2' is integer ambiguity on L2 frequency, 'λ_1' is wavelength of L1 carrier frequency [m], 'λ_2' is wavelength of L2 carrier frequency [m], '$M\phi_1$' is multipath error on ϕ_1 [m] and '$M\phi_2$' is multipath error on ϕ_2 [m].

The expression for MP_1 can be obtained by forming the appropriate linear combinations (Subtract Eq. (2) from Eq. (1)).

$$\begin{aligned} P_1 - \phi_1 &= 2I_1 - \lambda_1 N_1 + MP_1 - M\phi_1 \\ MP_1 - M\phi_1 - \lambda_1 N_1 &= P_1 - \phi_1 - 2I_1 \end{aligned} \tag{4}$$

To represent the above equation in ionospheric (I_1) delay term free form, the Eq. (3) is subtracted from Eq. (2) and rearranged as below,

$$\phi_1 - \phi_2 = I_2 - I_1 + \lambda_1 N_1 - \lambda_2 N_2 + M\phi_1 - M\phi_2 \tag{5}$$

In the above equation I_2 is substituted in terms of I_1 where, the ionospheric delays (I_1 and I_2) are inter related to the respective carrier frequencies (f_1 and f_2) as,

$$\alpha = (f_1/f_2)^2 = I_2/I_1 \tag{6}$$

$$\begin{aligned} \phi_1 - \phi_2 &= \alpha \times I_1 - I_1 + \lambda_1 N_1 - \lambda_2 N_2 + M\phi_1 - M\phi_2 \\ \phi_1 - \phi_2 &= (\alpha - 1) \times I_1 + \lambda_1 N_1 - \lambda_2 N_2 + M\phi_1 - M\phi_2 \end{aligned} \tag{7}$$

Simplifying the Eq. (7) we get,

$$I_1 = \frac{(\phi_1 - \phi_2)}{(\alpha - 1)} - \frac{(\lambda_1 N_1 - \lambda_2 N_2)}{(\alpha - 1)} - \frac{(M\phi_1 - M\phi_2)}{(\alpha - 1)} \tag{8}$$

Substituting the above expression for I_1 in Eq. (4) we get,

$$MP_1 - \lambda_1 N_1 = P_1 - \phi_1 - \frac{2(\phi_1 - \phi_2)}{(\alpha - 1)} + \frac{2(\lambda_1 N_1 - \lambda_2 N_2)}{(\alpha - 1)} + \frac{2(M\phi_1 - M\phi_2)}{(\alpha - 1)} \tag{9}$$

Rearranging the terms in Eq. (9) we get,

$$MP_1 - \lambda_1 N_1 - \frac{2(\lambda_1 N_1 - \lambda_2 N_2)}{(\alpha - 1)} = P_1 - \phi_1 - \frac{2(\phi_1 - \phi_2)}{(\alpha - 1)} + \frac{2(M\phi_1 - M\phi_2)}{(\alpha - 1)} \tag{10}$$

In the above equation the term $\lambda_1 N_1 - \frac{2(\lambda_1 N_1 - \lambda_2 N_2)}{(\alpha - 1)}$ is constant provided the satellite signal tracking is continuous and no cycle slips in carrier phase measurements [10]. The multipath error on carrier phase measurements is negligible compared to the error on pseudorange. Hence the term $\frac{2(M\phi_1 - M\phi_2)}{(\alpha - 1)}$ is assumed to be zero.

Depending on these considerations the multipath error for each epoch is estimated and the change in multipath error from the instant the satellite is acquired is analyzed. The impact of the multipath error and its variation with respect to elevation angle of the satellites for the entire duration of observation are also analyzed. This analysis will be helpful in kinematic applications where multipath signal become more arbitrary, particularly in aircraft navigation and missile guidance where the reflecting geometry and the environment around the receiving antenna changes relatively in random way.

3 Results and Discussion

The statistical analysis of the results shows that multipath error is too large to neglect particularly at low elevation angle of the satellite. This error is estimated for geographical location (Lat:17.73°N/Long:83.319°E) in the Eastern coast of India for ephemerides collected on 11th March 2011 from the dual frequency GPS receiver located at ECE department, Andhra University College of Engineering, Visakhapatnam, India. The SV PRN 31 is tracked for 24 h and the analysis of the error, supported by the relevant graphs and the tables are presented in this paper. Though all the visible satellites are tracked and the errors are computed and analyzed but in this paper the multipath error estimated only for SV PRN 31 is presented. Navigation solution for each epoch is calculated using the pseudoranges (multipath error corrected) of all visible satellites.

Table 1 Pseudorange multiipath error for SV PRN 31 on L1 frequency and receiver position error

	Elevation angle (degrees)	Multipath error (m)	Residual range error (m)	Position error (x-) (m)	Position error (y-) (m)	Position error (z-) (m)
Min	5.17	2.57	6.44	−12.59	−27.97	−8.087
Max	80.8	4.53	160.1	7.715	25.71	12.07
Std	23.88	0.2076	45.92	4.082	10.86	3.814

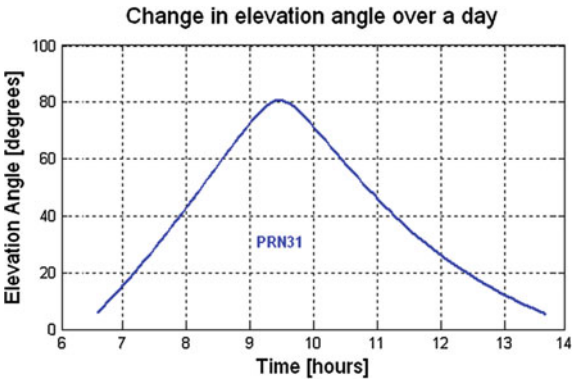

Fig. 1 Change in elevation angle of SV PRN 31 as tracked from GPS receiver located at Dept. of ECE, Andhra University (Lat:17.73°N, Long:83.31°E)

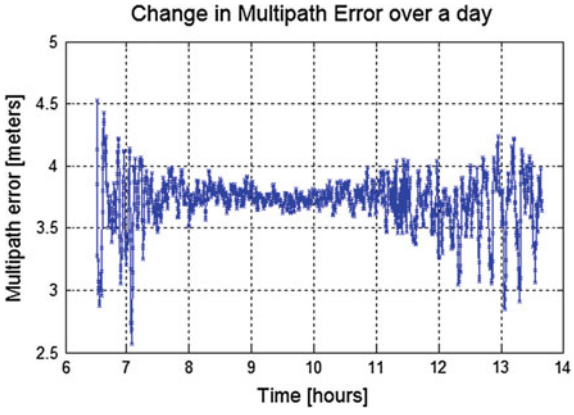

Fig. 2 SV PRN 31 pseudorange multipath error on L1 frequency for the observation period of 22 h

Table 1 details the multipath error and the error in receiver position coordinates. Figure 1 shows the change in elevation angle of Satellite 31 over the entire observation period. From Fig. 2 it is observed that the multipath error is as high as 4.53 m for the least elevation angle of 5.17° and as the satellite moves closer to the zenith the multipath error reduced to 2.51 m. Though the pseudorange was corrected for satellite clock error and multipath error, a residual error of as high as

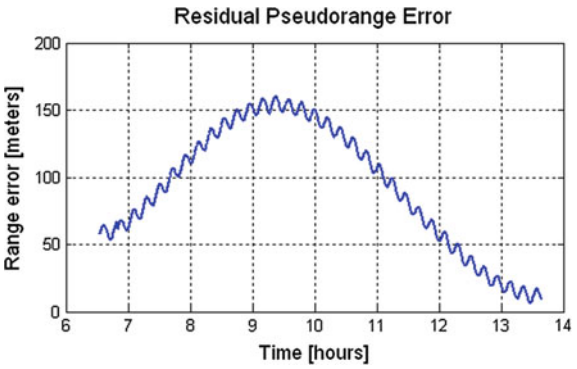

Fig. 3 Residual pseudorange Error of SV PRN 31

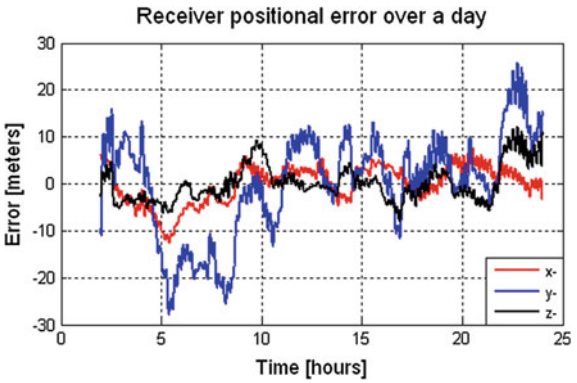

Fig. 4 Position Error of GPS receiver located at Dept. of ECE, Andhra University (Lat:17.73°N, Long:83.31°E)

160 m was observed (as shown in Fig. 3) compared to geometric range between SV PRN 31 and the SPSGPS receiver. Such residual errors in all the visible satellites resulted in inaccurate receiver position, as shown in Fig. 4.

4 Conclusions

The multipath mitigation technique is implemented on the dual frequency SPSGPS receiver ephemerides data collected from a geographical location (Lat:17.73° N/Long:83.319°E) over a Indian subcontinent. For this data the multipath error magnitude variations are investigated over the observation period of 22 h. The GPS signals are subjected to multiple reflections, and hence, the estimated multipath error was high. On implementing the technique it is found that the satellite acquired at low elevation angle resulted in high multipath error as signal traveled a longer path through the propagation medium. This multipath error mitigation technique does not require the geometry or the reflection coefficients of the nearby reflectors. It is also found that apart from the satellite clock error and the multipath error, a

number of other error sources affect the pseudorange, which intern degrade the receiver position. The impact analysis done in this paper will also be a valuable aid in selecting a location of least multipath error to set up the GPS receiver antenna for surveying in urban canyons, aircraft navigation, and tracking.

Acknowledgments The work undertaken in this paper is supported by ministry of Science and Technology, Department of Science and Technology (DST), New Delhi, India, under the woman scientist scheme (WOS-A). Vide sanction letter No: SR/WOS-A/ET-04/2013.

References

1. Bala Murugan, "The Land Based Positional Accuracy Of Gps And Gps Augmented By Gagan Over The Indian Geographical Region", International Journal of Scientific & Technology Research volume 3, Issue 4, 2014, pp 61–67.
2. G S RAO, "Global Navigation Satellite systems",1st ed, India: McGraw-Hill Edn., 2010.
3. He, X., et al. "Accuracy enhancement of GPS time series using principal component analysis and block spatial Filtering", Advances in Space Research, 03/2015, pp 1316–1327.
4. K.K. Fan, et al., "Estimation of GPS Carrier Phase Multipath Signals Based on Site Environment", Journal of Global Positioning Systems (2006) Vol. 5, No. 1–2:22–28.
5. Borre K. and Strang G., "Linear Algebra Geodesy and GPS", Wellesley-Cambridge Press, USA, 1997.
6. D. Manandhar, R. Shibasaki and H. Torimoto "GPS reflected signal analysis using software receiver", J. Global Positioning Syst., vol. 15, pp. 29–34 2006.
7. K. Boniface, et al.,' Comparison of Snow Data Assimilation System with GPS reflectometry snow depth in the Western United States', Hydrological Processes, Volume 29, Issue 10, pp. 2425–2437, 15 May 2015.
8. Pratap M. and Per E., "Global Positioning System: Signals, Measurements and Performance", Ganga-Jamuna Press, New York, Second Edition, 2006.
9. Kaplan E.D., "Understanding GPS: Principles and Applications", Second Edition, Artech House Publishers, Boston, USA, 2006.
10. Parkinson, B.W. and Spilker, J.R. Global positioning system: Theory and applications, American Institute of Aeronautics and Astronautics, Washington DC, 1996.

Controller Design for a TOPDT Process Model Using Integral Error-Based Tuning Techniques

Alka Patel, Pradeep Kumar Juneja, Mayank Chaturvedi and Jyoti Patel

Abstract It is very common to model an industrial sub-process transfer function by FOPDT. TOPDT models are also found in some situations as an appropriate model. A third-order transfer function composed of three first-order processes in series with delay function composes TOPDT. Scanty information is available for controller tuning techniques of TOPDT process. In present analysis, starting with the TOPDT model, converting it to SOPDT and then to FOPDT, controllers are designed using Integral error-based tuning techniques. Controllers are analyzed for their set-point tracking capacity.

Keywords PID controller · TOPDT · FOPDT · Integral error-based tuning techniques

1 Introduction

Proportional–integral–derivative (PID) controller has been used for a number of years in industries for process control applications. PID controller is implemented for most of the processes in control system in the world. The PID controller involves three constant parameters called the proportional (P), integral (I), and

A. Patel · M. Chaturvedi (✉)
Department of Electrical Engineering, Graphic Era University, Dehradun, India
e-mail: mayankchaturvedi.geit@gmail.com

A. Patel
e-mail: alkapatel27@gmail.com

P.K. Juneja · J. Patel
Department of Electronics & Communication Engineering, Graphic Era University, Dehradun, India
e-mail: mailjuneja@gmail.com

J. Patel
e-mail: jyotipatel74334268@gmail.com

D.K. Lobiyal et al. (eds.), *Proceedings of the International Conference on Signal, Networks, Computing, and Systems*, Lecture Notes in Electrical Engineering 396, DOI 10.1007/978-81-322-3589-7_26

derivative (D) values. P depends on the present error, I on the accumulation of past error, and D is a calculation of future error, based on current rate of change [1, 2]. The output of the controller can be given as:

$$Y(t) = e(t)K_{\mathrm{P}} + K_{\mathrm{I}} \int_0^t e(t) + K_{\mathrm{D}} \frac{\mathrm{d}e(t)}{\mathrm{d}t} \tag{1}$$

where e = Error signal; K_{P} = Proportional constant; K_{I} = Integral constant and K_{D} = Derivative constant

If the plant can be represented by first-order plus dead time (FOPDT) model, the typical PID controller can be empirically represented as:

$$G_{\mathrm{C}} = K_{\mathrm{C}} \left(1 + \frac{1}{sT_{\mathrm{I}}} + sT_{\mathrm{D}}\right) \tag{2}$$

$$K_{\mathrm{C}} = \frac{A}{K} \left(\frac{d}{\tau}\right)^B \tag{3}$$

$$\tau_{\mathrm{I}} = \frac{\tau}{A + B\left(\frac{d}{\tau}\right)} \tag{4}$$

$$\tau_{\mathrm{D}} = A\tau \left(\frac{d}{\tau}\right)^B \tag{5}$$

The main reasons of the popularity of the PID controller are the simplicity; robustness and effective cost-benefit ration [3–5]. Minimizing integral of time-weighted absolute error (ITAE) is commonly discussed to as a good performance index in designing PID controllers [6, 7].

Higher order processes are rich in dynamics and very less tuning rules are available in literature [8, 9]. A third-order transfer function composed of three first-order processes in series with delay function

$$G(s) = \frac{K\mathrm{e}^{-ds}}{(\tau_1 s + 1)(\tau_2 s + 1)(\tau_3 s + 1)} \tag{6}$$

where d is time delay τ_1, τ_2, τ_3 are times constant and K is process gain. Table 1 show the (A, B) pairs for FOPDT model.

Table 1 Set-point PID controller parameter [6]

Tuning Technique		P	I	D
IAE	A	1.086	0.74	0.348
	B	−0.869	−0.13	0.914
ITAE	A	0.965	0.796	0.308
	B	−0.855	−0.147	0.929
ISE	A	1.048	1.195	0.489
	B	−0.897	−0.368	0.888
ISTE	A	1.042	0.987	0.385
	B	−0.897	−0.238	0.906
IST^2E	A	0.968	0.977	0.316
	B	−0.904	−0.253	0.892

2 Methodology

In present analysis, process which can be modeled as TOPDT is taken below consideration. Then it is converted FOPDT models using Skogestad approximation, respectively.

The TOPDT transfer function selected from the literature can be given by [10]:

$$G(s) = \frac{2e^{-s}}{(2s+1)(s+1)^2} \tag{7}$$

The third-order plus dead time model can be converted into second-order plus dead time using Skogestad approximation.

$$G_1(s) = \frac{2e^{-1.5s}}{(2.5s+1)(s+1)} \tag{8}$$

The second-order plus dead time model can be converted into first-order plus dead time using Skogestad approximation.

$$GP_1(s) = \frac{2e^{-2s}}{(3s+1)} \tag{9}$$

Similarly, the selected TOPDT model can be converted into SOPDT and FOPDT process models using Taylor's series approximation technique as

$$G_2(s) = \frac{2e^{-2s}}{(2s+1)(s+1)} \tag{10}$$

And

$$GP_2(s) = \frac{2e^{-3s}}{(2s+1)} \tag{11}$$

Selected process model, is first reduced into lower order model. Different controllers have been designed based on various controller tuning techniques for FOPDT model.

3 Results and Discussion

The Result are obtained by comparing the important time response characteristics of closed loop step response using PID Controllers mentioned above and Performance Index criteria IAE, ITAE, ISE, ISTE, and IST^{2}E. The important time response characteristics are obtained, i.e., Settling time, Rise time, and % Overshoot.

Figure 1 shows the Comparison of closed loop step response of PID controller designed using IAE, ITAE, ISE, ISTE and IST^{2}E tuning technique for process GP_1. The Comparison of step response of a PID controller using IAE, ITAE, ISE, ISTE and IST^{2}E tuning technique for process GP_2 is given by Fig. 2.

Table 2 shows the comparison of all integral tuning technique for different controller for Skogestad approximated process model. Rise time is least in case of ISE, settling time is minimum in case of IST^{2}E while maximum percentage overshoot is least in case ITAE as compared to all other cases.

Table 3 shows the comparison of all integral tuning technique for different controller for Taylor series approximated process model. Rise time is least in case of ISE, settling time is minimum in case of ISTE and maximum percentage overshoot is least in case of IAE, ITAE and IST^{2}E.

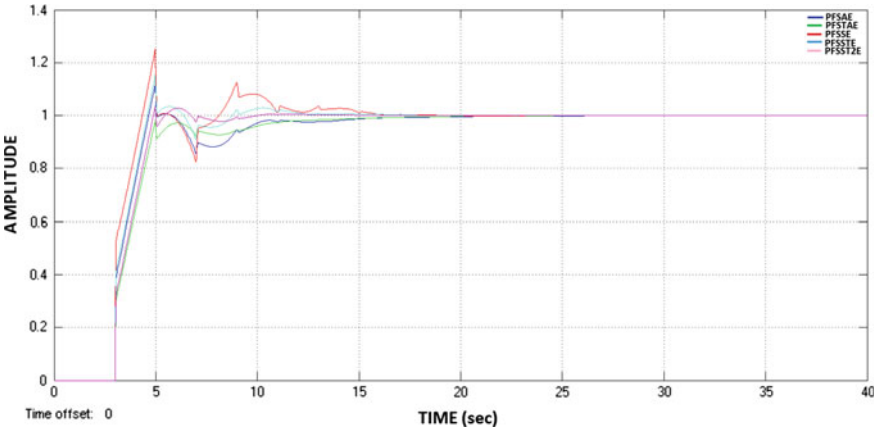

Fig. 1 Comparison of step response of a PID controller using IAE, ITAE, ISE, ISTE and IST^{2}E tuning technique for process GP_1

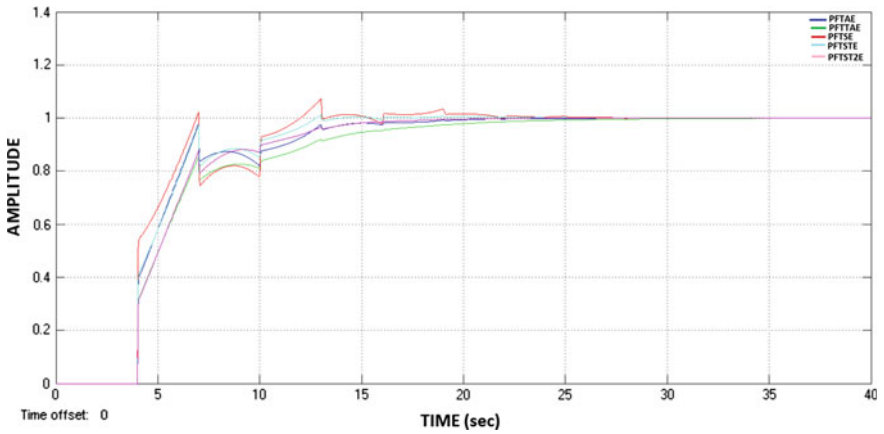

Fig. 2 Comparison of step response of a PID controller using IAE, ITAE, ISE, ISTE and IST^{2}E tuning technique for process GP_2

Table 2 Comparison of time response characteristics of PID controller designed using integral error-based tuning techniques for Skogestad approximated process model

Characteristics	IAE	ITAE	ISE	ISTE	IST^{2}E
Rise time	1.38	1.73	1.08	1.31	1.61
Settling time	12.9	10.8	13.7	10.2	7.54
% overshoot	12.2	0	24.7	15.9	2.75

Table 3 Comparison of time response characteristics of PID controller designed using integral error-based tuning techniques for Taylor Series approximated process model

Characteristics	IAE	ITAE	ISE	ISTE	IST^{2}E
Rise time	2.58	6.8	2.37	2.63	6.13
Settling time	15.1	15.1	18.1	11.4	13.8
% overshoot	0	0	6.96	1.21	0

The comparison of time response characteristics for PID controllers designed using integral error-based tuning techniques viz. IAE, ITAE, ISE, ISTE, IST^{2}E for Skogestad and Taylor approximated process models is shown in Table 4. Rise time and settling time is minimum in case of GP_1 while maximum % overshoot is less for GP_2 when PID controller is designed using IAE tuning method. For PID controller designed using ITAE tuning technique rise time is minimum for GP_2, settling time is minimum for GP_1, while maximum % overshoot is equal in both the cases. Rise time and settling time is minimum in case of GP_1 while maximum % overshoot is less for GP_2 when PID controller is designed using ISE tuning method. For PID controller designed using ISTE tuning technique rise time and settling time

Table 4 Comparison of time response characteristics for PID controllers designed using integral error-based tuning techniques for Skogestad and Taylor approximated process models

Tuning Method	Characteristics	GP_1	GP_2
IAE	Rise time	1.38	2.58
	Settling time	12.9	15.1
	% overshoot	12.2	0
ITAE	Rise time	1.73	6.8
	Settling time	10.8	15.1
	% overshoot	0	0
ISE	Rise time	1.08	2.37
	Settling time	13.7	18.1
	% overshoot	24.7	6.96
ISTE	Rise time	1.31	2.63
	Settling time	10.2	11.4
	% overshoot	15.9	1.21
IST^2E	Rise time	1.61	6.13
	Settling time	7.54	13.8
	% overshoot	2.75	0

are minimum for GP_1, maximum % overshoot is less in case of GP_2. Rise time and settling time is minimum in case of GP_1 while maximum % overshoot is less for GP_2 when PID controller is designed using IST^2E tuning method.

4 Conclusion

Different controllers are designed for the different integral tuning techniques. The controllers are evaluated for the set-point tracking capability. Transient and steady-state characteristics are evaluated. The complete study shows that all the integral tuning techniques exhibits the rise time and settling time are less for the skogestad approximation in the selected TOPDT model for PID controllers, so steady state is better. Maximum percentage overshoot and peak amplitude are better for Taylor approximation in the selected TOPDT model for PID controller.

References

1. Chaturvedi, M., Juneja, P. K., Chauhaan, P.: Effect of Implementing Different PID Algorithms on Controllers Designed For SOPDT Process. Proceedings of the International Conference on Advances in Computing, Communications and Informatics, ICACCI 2014, GCET Greater Noida, (2014) 853–858.
2. Kushwah, M., Patra A.: Tuning PID Controller for Speed Control of DC Motor Using Soft Computing Techniques-A Review, Advance in Electronic and Electric Engineering. ISSN 2231-1297, Volume 4, Number 2 (2014) 141–148.

3. Åström, K. J., Hägglund, T.: Revisiting the Ziegler-Nichols step response method for PID control. J. Process Control, 14, (2004) 635–650.
4. Martins, F. G., Coelho, M. A. N.: Application of feed forward artificial neural networks to improve process control of PID-based control algorithms. J. Computers and Chemical Engineering, 24, (2000) 853–858.
5. Chauhaan, P., Juneja, P. K., Chaturvedi, M.: Controller Design and Its Performance Analysis for a Delayed Process Model. Proceedings of the International Conference on Advances in Computing, Communications and Informatics, ICACCI 2014, GCET Greater Noida, (2014) 859–862.
6. Seborg, D. E., Edgar, T. F., Mellichamp, D. A.: Process Dynamics and Control. Wiley, New York (2004).
7. Fernando G. Martins," Tuning PID Controllers using the ITAE Criterion," Int. J. Engng Ed. Vol. 21, No. 5, (2005) 867–873.
8. Chaturvedi, M., Juneja, P.: Effect of dead time approximation on controller performance designed for a second order delayed model. Proceedings of the International Conference on Advanced Electronic Systems, ICAES 2013, CEERI, Pilani, (2013) 313–315.
9. Panda, R. C., Yu, C., Huang, H. P.: PID tuning rules for SOPDT systems: Review and some new results. ISA Transactions, Vol. 43, (2004) 283–295.
10. Kealy, T., and O'Dwyer, A.: Closed Loop Identification of a First Order plus Dead Time Process Model under PI Control. Proceedings of the Irish Signals and Systems Conference, University College, Cork, (2002) 9–14.

Effect of Variation in Filter Coefficients for Different PID Controller Structures on Performance of SOPDT Process

Mayank Chaturvedi and Pradeep K. Juneja

Abstract The proportional-integral-derivative controllers are being used by process industry to control various complex industrial processes, due to their simplicity and easy implementation. There are various structures of PID controllers available in the literature which makes it difficult to decide the selection of suitable controller structure for a particular industrial process model. This complexity further increases in case of structures with derivative filters. It is a matter of investigation to evaluate the effect of varying the filter coefficient on controller performance for such PID controller structures. The present analysis lay emphasis on the set-point tracking capability of the controller by weighting the filter coefficients of these structures.

Keywords Dead time · SOPDT · PID controller structures · Derivative filter · Filter coefficient

1 Introduction

While modeling any process, dead time naturally appears, where propagation of matter or energy is involved and characterizes a large class of industrial systems. Dead time can be responsible for poor performance, controller complexity, and even instability of the system [1]. The existence of delay is always a great apprehension to the process industry as it greatly affects the analysis and control design of a process [2].

M. Chaturvedi (✉)
Department of Electrical Engineering, Graphic Era University, Dehradun, India
e-mail: mayankchaturvedi.geit@gmail.com

P.K. Juneja
Department of Electronics & Communication Engineering, Graphic Era University, Dehradun, India
e-mail: mailjuneja@gmail.com

D.K. Lobiyal et al. (eds.), *Proceedings of the International Conference on Signal, Networks, Computing, and Systems*, Lecture Notes in Electrical Engineering 396, DOI 10.1007/978-81-322-3589-7_27

Second-order plus dead time process model represents a wide class of real-time industrial processes. PID controller is used to control such process as it is easy to implement and operate [3]. Very few tuning methods are available for SOPDT processes which are rich in dynamics [4]. Second-order plus dead time systems can be modeled as:

$$G(s) = \frac{Ke^{-\theta s}}{(1+\tau_1 s)(1+\tau_2 s)} \tag{1}$$

where K is process gain, θ is time delay, τ_1 is slow time constant, and τ_2 is fast time constant [5, 6].

PID control provides a generic and efficient solution to real-world process control problems [7]. PID controller is the first solution that should be tried to control an industrial process, due to simplicity and reasonable design effort. Processes with time delays can be controlled quite well with PID control [8]. Various structures of control have been proposed in the literature to overcome the limitations of PID controllers [9]. To obtain high performance while retaining simple implementation of the control system, different PID-based control structures have been formulated [10].

Broadly, there are five classifications of PID algorithms: parallel, parallel with derivative filter, series, series with derivative filter, and cascade [11, 12]. Controller transfer function for Parallel with derivative filter PID controller:

$$G(s) = K_c\left(1 + \frac{1}{\tau_I s} + \frac{\tau_D s}{\alpha\tau_D s + 1}\right) \tag{2}$$

Controller transfer function for Series with derivative filter PID controller:

$$G(s) = K_c\left(\frac{\tau_I s + 1}{\tau_I s}\right)\left(\frac{\tau_D s + 1}{\alpha\tau_D s + 1}\right) \tag{3}$$

In the feedback loop, a filter is an additional dynamic element that introduces additional phase lag. Subsequently, it reduces the stability margin for a feedback controller, compared to the situation where no filter is present. Thus any change in filter coefficient may require retuning of the controller [13]. Filter coefficient (α) should be between 0.05 and 0.2 and most often it is taken as 0.1 [14].

The tuning techniques play a vital role to design a controller for a process, consequently which tuning method is being selected effects the controller performance. Skogestad tuning relations for SOPDT system were derived by keeping the close loop time constant equal to the delay of the process model [15]. Ziegler Nichols et al. presented continuous cycling method to derive tuning relations in terms of ultimate gain and ultimate period [16]. A new approach using classical frequency response method has been proposed by Tyreus Luyben et al., avoiding the problem of poor control in case of IMC tuning method if a wrong value gets selected of closed loop time constant [17].

2 Methodology

In the present analysis, a process which can be modeled as SOPDT model is selected. Once a SOPDT model is selected, controller parameters are calculated to design PID controllers using Skogestad and Ziegler Nichols (ZN) tuning techniques. The controller parameters are then used to design parallel with derivative filter and series with derivative filter PID controllers, for α = 0.1, 0.05 and 0.2.

The closed-loop step responses of the feedback control system are compared and investigated to determine the effect of weighting filter coefficient on the set-point tracking capability of the controllers.

The selected SOPDT system transfer function is:

$$G(s) = \frac{5e^{-4s}}{(1+20s)(1+8s)} \tag{4}$$

where, process gain (K) = 5, dead time (θ) = 4 s, slow time constant (τ_1) = 20 s and fast time constant (τ_2) = 8 s [18].

3 Results and Discussion

Using Skogestad and ZN tuning methods the comparison of closed-loop step responses of the process with PID controllers in parallel with derivative filter form for the filter coefficients 0.1, 0.05, and 0.2 is shown in Figs. 1 and 2, respectively.

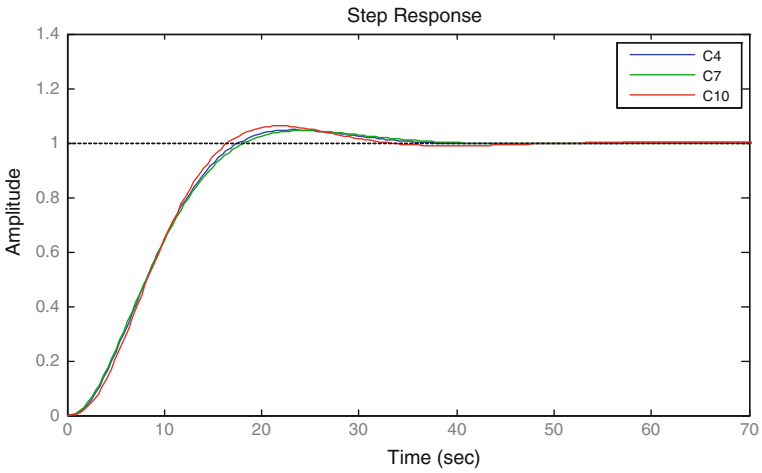

Fig. 1 Close loop response for parallel with derivative filter form PID controller, with α = 0.1, 0.05 and 0.2 respectively, using Skogestad tuning method

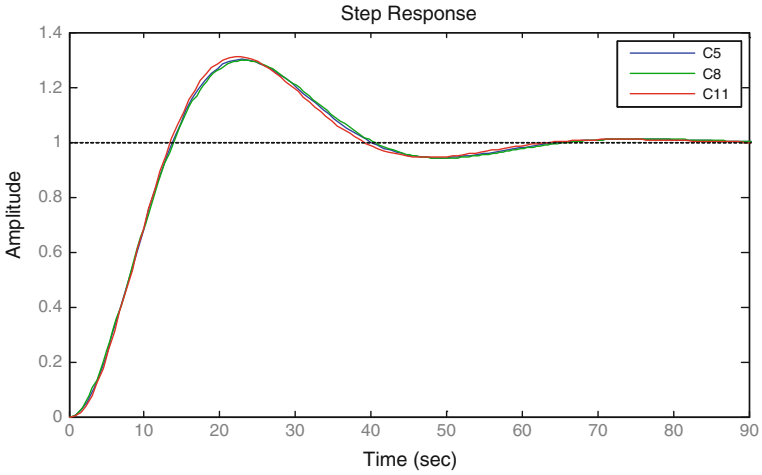

Fig. 2 Close loop response for parallel with derivative filter form PID controller, with $\alpha = 0.1$, 0.05 and 0.2 respectively, using ZN tuning method

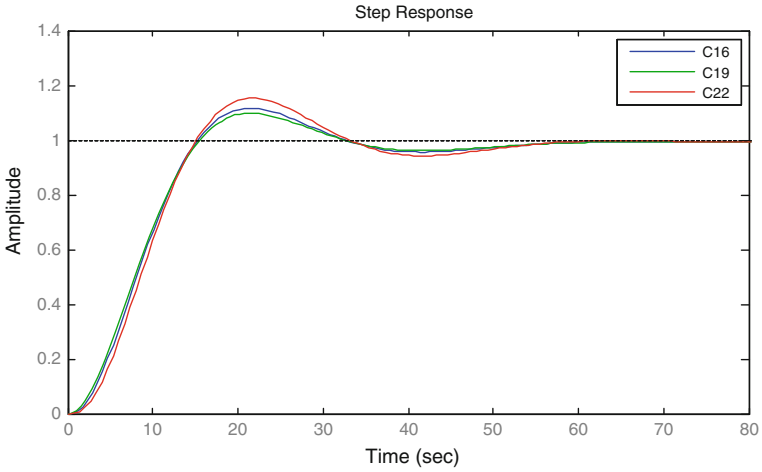

Fig. 3 Close loop response for series with derivative filter form PID controller, with $\alpha = 0.1$, 0.05 and 0.2 respectively, using Skogestad tuning method

Figures 3 and 4 shows the comparison of closed-loop step responses of the process with PID controllers in series with derivative filter form for filter coefficient 0.1, 0.05, and 0.2 using Skogestad and ZN tuning methods respectively.

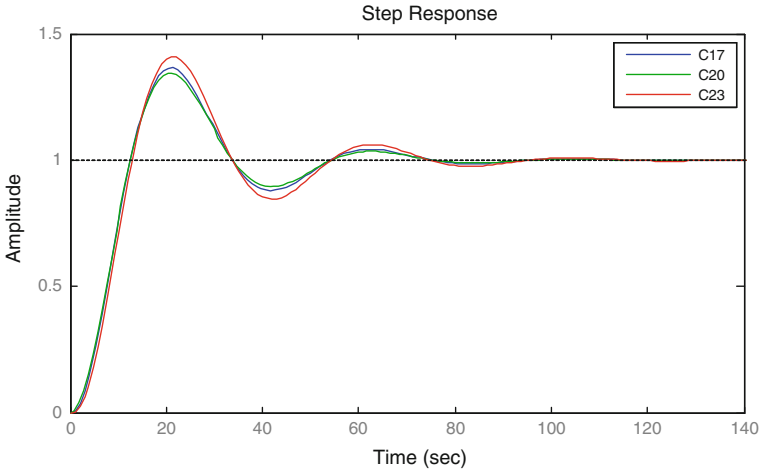

Fig. 4 Close loop response for series with derivative filter form PID controller, with α = 0.1, 0.05 and 0.2 respectively, using ZN tuning method

4 Conclusion

PID controllers based on different tuning techniques viz. Skogestad and Ziegler Nichols have been designed in present analysis, for selected SOPDT process, using parallel with derivative filter and series with derivative filter PID algorithm, for different values of filter coefficient. Filter coefficient 0.1 gives the best response with Skogestad tuning technique, in case of parallel with derivative filter form of PID controllers. While filter coefficient 0.05 gives the best response with Skogestad tuning technique, in case of series with derivative filter form of PID controllers. Parallel with derivative form of PID controller with filter coefficient 0.1 in comparison to any other filter coefficient selected for any other PID algorithm, exhibits optimum response while using Skogestad tuning technique for the selected SOPDT model.

References

1. Bhambhani, V., Chen, Y.Q., and Xue, D.: Optimal Fractional Order Proportional Integral Controller for Varying Time-Delay Systems. 17th IFAC World Congress, Seoul, Korea, (2008) 4910–4915.
2. Zhong, Q.C.: Robust control of time delay system. Springer, London, (2006).
3. Panda, R.C., Yu, C. C., Huang, H.P.: PID tuning Rules for SOPDT systems: Review and some new results. ISA Transactions, Vol. 43, (2004) 283–295.
4. Chaturvedi, M., Juneja, P.: Effect of dead time approximation on controller performance designed for a second order delayed model. Proceeding of ICAES 2013, CEERI, Pilani, (2013) 313–315.

5. Chen, D., Seborg, D.E.: PI/PID Controller design based on direct synthesis and disturbance rejection. Ind. Eng. Chem. Res., Vol. 41, (2002) 4807–4822.
6. Chauhaan, P., Juneja, P.K., Chaturvedi, M.: Controller Design and Its Performance Analysis for a Delayed Process Model. Proceedings of the International Conference on Advances in Computing, Communications and Informatics, ICACCI 2014, GCET Greater Noida, (2014) 859– 862.
7. Li, Y., Ang, K.H., Chong, G.C.Y.: PID control system analysis and design. IEEE Control Systems Magazine, 26(1) (2006) 32–41.
8. Åström, K.J., Häglund, T.: The Future of PID Control. Control Engineering Practice, Vol. 9, (2001) 1163–1175.
9. Åström, K.J., Albertos, P., Quevedo, J.: PID Control," Control Engineering Practice. Vol. 9, (2001) 1159–1161.
10. Visioli, A.: Research trends for PID controllers. Acta Polytechnica, Vol. 52, No. 5, (2012) 144–150.
11. Chaturvedi, M., Juneja, P. K., Chauhaan, P.: Effect of Implementing Different PID Algorithms on Controllers Designed For SOPDT Process. Proceedings of ICACCI 2014, GCET Greater Noida, (2014) 853– 858.
12. Juneja, P.K., Ray, A. K., Mitra, R.: Various PID controller algorithms for closed loop performance of consistency parameter of paper machine headbox in a paper mill. IPPTA Journal, Vol. 23, No. 2, (2011) 127–131.
13. Seborg, D.E., Edgar, T.F., Mellichamp, D. A.: Process Dynamics and Control. 2nd ed., Wiley, New York, (2004).
14. Shinskey, F. G.: Process Control Systems. Third ed., McGraw Hill, New York, 1988.
15. Skogestad, S.: Simple Analytic Rules for Model Reduction and PID Controller Tuning. J. Process Control, 13, (2003), 291–309.
16. Ziegler, J.G., Nichols, N. B.: Optimum settings for automatic controllers. Trans. ASME 64, (1942) 759–768.
17. Tyreus, B.D., Luyben, W.L.: Tuning PI controllers for integrator/dead-time process. Ind. Eng. Chem. Res. 31, (1992) 2625–2628,.
18. Sell, N. J.: Process Control Fundamentals for the pulp and paper industry. Tappi Press, Atlanta, GA, (1995).

Controller Capability Comparison for a Delayed First-Order Process Model

Pradeep Kumar Juneja, Mayank Chaturvedi and Manik Gupta

Abstract This paper analyses one of the most important control system design issues, the controller performance. A blending process which can be modeled as First-Order plus Dead Time is selected to design closed loop with a PID controller. The tuning of the controller parameters has been done using Ziegler Nichols and Tyreus Luyben tuning techniques. The performance of the PID controllers has been evaluated by comparing set-point tracking and disturbance rejection capabilities.

Keywords PID controller · Controller performance · Tuning technique · FOPDT · Dead time

1 Introduction

In recent decades, performance of the plant has become a greater attraction of the control engineers. The real challenge lies to improve performance even in inappropriate plant conditions. The performance of the controller plays a vital role in the overall plant performance. Set-point tracking and disturbance rejection capabilities are the two major design objectives to enhance the performance of the controller [1–3].

Most of the time the controllers have superior tracking performance but this can result to poor disturbance rejection. A trade-off between set-point tracking and disturbance rejection capabilities of the controller takes place, which makes it complex and thus need of appropriate tuning of the controller parameters arises [3, 4].

P.K. Juneja
Department of Electronics & Communication Engineering,
Graphic Era University, Dehradun, India
e-mail: mailjuneja@gmail.com

M. Chaturvedi (✉) · M. Gupta
Department of Electrical Engineering, Graphic Era University,
Dehradun, India
e-mail: mayankchaturvedi.geit@gmail.com

D.K. Lobiyal et al. (eds.), *Proceedings of the International Conference on Signal, Networks, Computing, and Systems*, Lecture Notes in Electrical Engineering 396, DOI 10.1007/978-81-322-3589-7_28

Blending process has been selected to depict the real challenges of the process industry. A stirred tank blending system is based on mass and component balance. The blending process can be modeled as First-Order plus Dead Time (FOPDT) process model [3]. The FOPDT process model transfer function can be given as

$$G(s) = \frac{Ke^{-\theta s}}{(1+\tau s)} \tag{1}$$

where, θ is dead time, K is process gain, and τ is time constant [5].

The dead time, delay or delay time are present naturally when a system is modeled. There are many causes of inherent presence of the dead time like energy propagation, sensor location, time taken by actuator, etc. [6–8]. Generally, the dead time makes system nonlinear, increases instability and difficult to control, which is undesirable for any industry.

The most extensively used controllers in process industry is Proportional–Integral–Derivative (PID) controllers, majorly because of its high cost/benefit ratio, simple structure, and easy implementation [9–11]. The PID controllers have three parameters: controller gain, integral time constant, and derivative time constant to control. For better controller performance, tuning of these parameters is necessary. The structure of a transfer function of the PID controller can be given as

$$G_c(s) = K_c\left(1 + \frac{1}{\tau_I s} + \tau_D s\right) \tag{2}$$

Controller tuning methods have been developed to optimize the performance of the controller. It is an important design decision to select a tuning technique because of the trade-off between set-point tracking and disturbance rejection capabilities of the controller. For a FOPDT process model, Ziegler Nichols (ZN) [12], Tyreus Luyben (TL) [13], Chien Hrones Reswick [14] are amongst the popular tuning techniques. In the present analysis, ZN and TL tuning techniques have been used to determine the controller parameter of PID controller.

2 Methodology

In the present analysis a process which can be modeled as FOPDT process model is selected. After selecting suitable process model, PID controllers have been designed and the controller parameters are calculated using Ziegler Nichols and Tyreus Luyben tuning techniques. The parameters can be calculated using Table 1.

Table 1 Controller parameters for PID controller

Tuning technique	Kc	τ_I	τ_D
ZN	$0.6K_{cu}$	$\frac{P_u}{2}$	$\frac{P_u}{8}$
TL	$0.45K_{cu}$	$2.2P_u$	$\frac{P_u}{6.3}$

Once the controller parameters have been calculated they are used to design PID controllers for constructing closed loop with unity feedback. The simulations have been performed and the results are compared to evaluate controller performance which is set-point tracking and disturbance rejection capabilities of the controllers. The selected FOPDT process model from the literature can be given as

$$G(s) = \frac{1.54e^{-1.075s}}{5.93s + 1} \tag{3}$$

where, Dead Time (θ) = 1.075 s, Process Gain (K) = 1.54, time constant (τ) = 5.93 s [3].

3 Results and Discussion

To evaluate controller performance of PID controllers designed using ZN and TL tuning techniques, the closed-loop system with unity feedback has been developed. The simulations have been performed for PID controllers implemented using controller parameters given in Table 2, calculated using both the tuning methods ZN & TL.

The comparison of closed-loop step responses with PID controllers designed using ZN and TL tuning techniques is given by Fig. 1. The step response settles

Table 2 PID controller settings

Tuning technique	K_c	τ_I	τ_D
ZN	2.154	2.195	0.548
TL	1.615	9.658	0.697

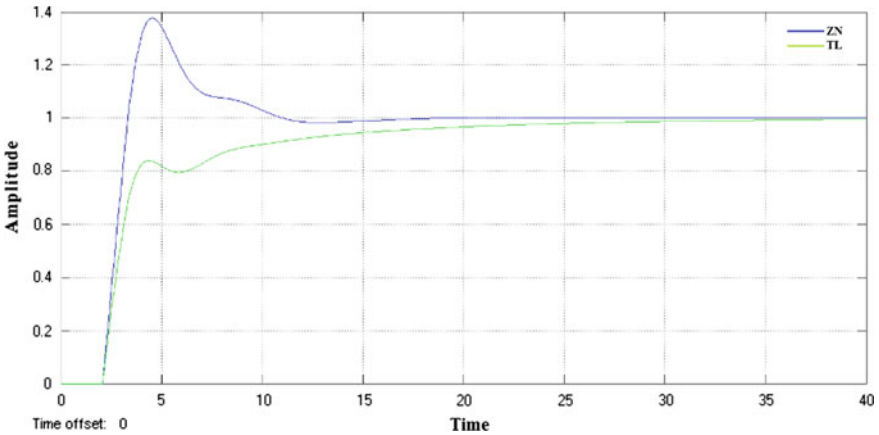

Fig. 1 Comparison of set-point tracking capability of PID controllers designed using ZN and TL tuning techniques

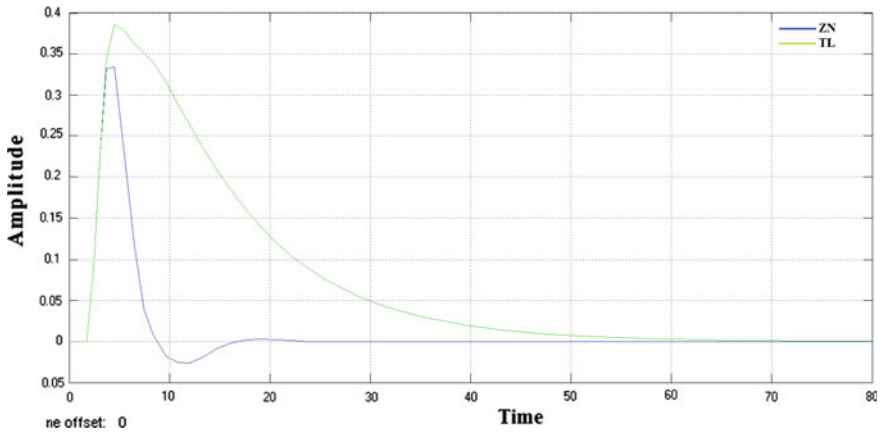

Fig. 2 Comparison of disturbance rejection capability of PID controllers designed using ZN and TL tuning techniques

Table 3 Comparison of important time response characteristics of PI controllers designed using ZN and TL

Tuning technique	ZN	TL
Rise time	0.997	7.73
Settling time	9.29	24.3
Overshoot (%)	37.7	0

more rapidly but has greater maximum percentage overshoot for PID controller designed using ZN tuning method in comparison with the step response obtained with PID controller designed using TL tuning technique.

Figure 2 exhibits the comparison of the disturbance rejection capability of the controllers designed using ZN and TL tuning techniques. In case of PID controller designed with ZN tuning method, the step disturbance settles more quickly, in comparison with PID controller designed by following TL tuning technique. The steady state and transient characteristics of closed-loop step responses for the selected FOPDT process with PID controllers designed using ZN and TL tuning methods are given in Table 3.

4 Conclusion

The controller performance has been assessed in terms of set-point tracking and disturbance rejection capabilities, while the PID controllers have been designed for a selected FOPDT process model, based on Ziegler Nichols and Tyreus Luyben tuning techniques. The PID controller designed using ZN tuning technique, exhibits optimum set-point tracking and disturbance rejection capabilities in comparison with controller designed using TL tuning technique.

References

1. Åström, K.J., Häglund, T.: PID Controllers: Theory, Design and Tuning. Second ed., Instrument Society of America, Research Triangle Park, NC, (1995).
2. Shinskey, F. G.: Process Control Systems. Third ed., McGraw Hill, New York, (1988).
3. Seborg, D.E., Edgar, T.F., Mellichamp, D.A.: Process Dynamics and Control, second ed., Wiley, New York, (2004).
4. W. Zhou, S. Shao, Z. Gao, " A Stability Study of the Active Disturbance Rejection Control problem by a Singular Perturbation Approach," Applied mathematical Sciences, Vol. 3, No. 10, (2009) 491–508.
5. Sánchez, J., Visioli, A., Dormido, S.: A two degree of freedom PI controller based on events. J. Process Control, Vol. 21 Issue 4, (2011) 639–651.
6. Chauhaan, P., Juneja, P.K., Chaturvedi, M.: Controller Design and Its Performance Analysis for a Delayed Process Model. Proceedings of the International Conference on Advances in Computing, Communications and Informatics, ICACCI 2014, GCET Greater Noida, IEEE Xplore, (2014) 859–862.
7. Chaturvedi, M., Juneja, P.: Effect of dead time approximation on controller performance designed for a second order delayed model. Proceeding of ICAES 2013, CEERI, Pilani, IEEE Xplore, (2013) 313–315.
8. Jangwan, R., Chaturvedi, M., Juneja, P. K., Sunori, S., Singh, P.: Comparative Analysis of Controllers Designed For Pure Integral Complex Delayed Process Model. Proceedings of the 2014 International Conference on Advances in Computing, Communications and Informatics, ICACCI 2014, GCET Greater Noida, IEEE Xplore, (2014) 712–717.
9. Visioli, A.: Research trends for PID controllers. Acta Polytechnica, Vol. 52, No. 5, (2012) 144–150.
10. Chaturvedi, M., Juneja, P. K., Chauhaan, P.: Effect of Implementing Different PID Algorithms on Controllers Designed For SOPDT Process. Proceedings of the International Conference on Advances in Computing, Communications and Informatics, ICACCI 2014, GCET Greater Noida, IEEE Xplore, (2014) 853–858.
11. Shi, J., Lee, W.S.: Set point response and disturbance rejection tradeoff for Second-Order plus Dead Time Processes. 5th Asian Conference, (2004) 881–887.
12. Ziegler, J.G., Nichols, N.B.: Optimum settings for automatic controllers, Trans. ASME 64, (1942) 759–768.
13. Tyreus, B.D., Luyben, W.L.: Tuning PI controllers for integrator/dead-time process," Ind. Eng. Chem. Res. 31, (1992) 2625–2628.
14. Chien, K.L., Hrones, J.A. and Reswick, J.B.: On the automatic control of generalized passive systems. Transactions of the ASME, (1952) 175–185.

Optimization Study on Quarter Car Suspension System by RSM and Taguchi

M.B.S. Sreekar Reddy, P. Vigneshwar, D. RajaSekhar, Katiki Akhil and P. Lakshmi Narayana Reddy

Abstract This paper presents on optimal vehicle seat suspension design for a quarter car model to reduce vibrations. With the aid of MATLAB/Simulink a simulation model is achieved. As the response surface methodology is a traditional technique for experimental process optimization. Recently a new approach to this problem has been tried with response surface methodology and Taguchi which is new in the statistical field. For the Response surface methodology, an experimental design was chosen in order and optimized for controlling parameters. Simultaneously, Taguchi optimization technique is implemented to know the effect of parameters over response.

Keywords Matlab simulink · Optimization · Response surface methodology · Comfortness · Taguchi method

1 Introduction

A good automotive suspension system should provide maximum rider comfortness having satisfactory road holding ability, when the vehicle is experiencing any road disturbance (i.e., cracks, uneven pavement, and pot holes), the vehicle body should

M.B.S. Sreekar Reddy (✉) · D. RajaSekhar · P. Vigneshwar · K. Akhil · P. Lakshmi Narayana Reddy
Mechanical Department, KL University, Vaddeswaram, Guntur, India
e-mail: mbssreddy@kluniversity.in

D. RajaSekhar
e-mail: drajasekhar283@gmail.com

P. Vigneshwar
e-mail: mallanjulap1@gmail.com

K. Akhil
e-mail: akhilaug31@gmail.com

P. Lakshmi Narayana Reddy
e-mail: reddypln16@gmail.com

D.K. Lobiyal et al. (eds.), *Proceedings of the International Conference on Signal, Networks, Computing, and Systems*, Lecture Notes in Electrical Engineering 396, DOI 10.1007/978-81-322-3589-7_29

have large damping coefficient or resistance to avoid large oscillations. The ride comfort can be defined according to axis and angular acceleration of front and rear car body, therefore, the angular acceleration and numerical axis must be minimize in order to attain higher ride comfort. Optimization of rider comfort is based on spring stiffness (K_s), damping coefficient (b), and sprung mass (m_s). Normally, these systems are developed by the empirical approach. The following is the literature review in this decade. Tak and Chung [1] a systematic approach was proposed to meet the optimum geometric design of suspension system with varied design variables for the best optimum rider comfortness. Koulocheris et al. [2] combined the deterministic and stochastic optimization algorithms for determining optimum vehicle suspension parameters and it has been noticed that this type of optimization was faster and flexible in rider comfortness. Weirs and Dhingra [3] designed the rear suspension system of racing motorcycle drive, and their designed increased the rear tire traction. Mitchell et al. [4] obtained the genetic algorithm optimization for best optimum parameters by considering the description of a suspension model and a scoring method. Raghavan [5] presented an algorithm to determine the attachment point locations of the tie rod of an automotive suspension.

Response surface methodology uses the various mathematical, graphical, and statistical techniques to develop, to improve and to optimize the experimental process. By attentive design of experiment and also several factors of independent variables (input variables) the objective of optimization of output variables will be approached [6]. Mithilesh Kumar [7] in his research work proved that quadratic model is best to fit for three variable designs through response surface. Priti Sonasale [8] proved that by using the method i.e,. DOE the welding parameters were optimized exactly. The explicitly designed experimental mode is necessary to analyses the performance uniqueness of system [9, 10]. Conventional methods cannot be used to evaluate the effect of input parameters on objective parameters because number of experiments increases when number of input parameters increase [11–14].

2 Formulation of Matlab/Simulink Model

Designing a passive suspension system for a car turns out to be an interesting design problem. When the suspension system is designed, a 1/4 car model (one of the four wheels) is used to simplify the problem to a one-dimensional spring-damper system ordinary differential equations (ODE) are derived from Fig. 1 as Eqs. (1) and (2) corresponding to sprung and unsprung mass respectively

$$m_u \ddot{x} = k_s(y - x) + b(\dot{y} - \dot{x}) - k_w(x - r) \tag{1}$$

$$m_s \ddot{x} = -k_s(y - x) - b(\dot{y} - \dot{x}) \tag{2}$$

Equations (1) and (2) are solved by the Simulink tool box which is provided in the Matlab ver, 2014. From this model RMS acceleration or the rider comfort RC is

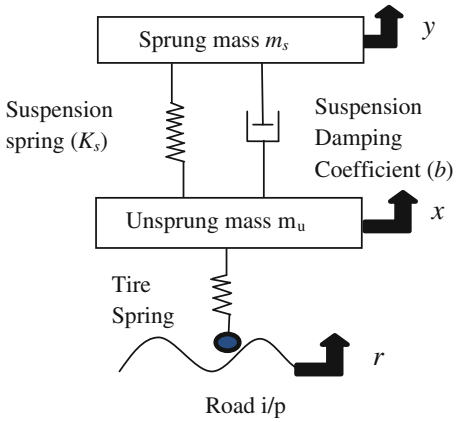

Fig. 1 Vehicle suspension system

Table 1 Three level factors for—Quater car suspension system

S. No.	Parameters	Level-1	Level-2	Level-3
1	Spring stiffness	8000	14,000	20,000
2	Suspension damping	500	1000	1500
3	Sprung mass	80	190	300

being solved for the various levels of data, i.e., spring stiffness (K_s), damping coefficient (b), and sprung $M_{u,}$ as shown below in Table 1. By keeping the unsprung mass and tire stiffness as constant values in the Simulink model as 40 kg and 120,000 N/m.

2.1 Road Profile

The effect of a sinusoidal road excitation of the ride comfort, road holding, and displacement of the head has been computed for the various bump width L with different vehicle velocity v. For an absolute time frame t represents the simulation time when wheel is just approaching a bump with a distance d. The mathematical expression of bump excitation on wheel is as follows [8]. With the same function following below a sine wave road profile was being developed for optimum conditions.

$$\begin{aligned} r &= 0; \quad \text{when} \quad t < \frac{d}{v} \\ &= h \sin\left[\frac{\pi v}{L}\left(t - \frac{d}{v}\right)\right] \quad \text{for} \quad \frac{d}{v} \le t \le \frac{d+L}{v} \\ &= 0 \quad \text{when} \quad t > \frac{d+L}{v} \end{aligned} \tag{3}$$

Table 2 Coded coefficients of three parameters

Terms	Effect	Coef	SE coef	*t*-value	*p*-value	VIF
Constant	–	1.2428	0.0247	50.42	0.000	–
Stiffness	0.3874	0.1937	0.0181	10.68	0.000	1.00
Damping	0.6024	0.3012	0.0181	16.60	0.000	1.00
Mass	−2.1367	−1.0683	0.0181	−58.89	0.000	1.00
Stiffness*stiffness	0.1453	0.0727	0.0266	2.73	0.034	1.01
Mass*mass	0.9471	0.4735	0.0266	17.78	0.000	1.01
Stiffness*damping	−0.1844	−0.0922	0.0257	−3.59	0.011	1.00
Stiffness*mass	−0.3340	−0.1670	0.0257	−6.61	0.001	1.00
Damping*mass	−0.6316	−0.3158	0.0257	−12.31	0.000	1.00

(*)-Multiplication Operator

Table 3 Model summary statistics

	Std.		Adjusted	Predicted		
Source	Dev.	*R*-Squared	*R*-Squared	*R*-Squared	Press	
Linear	0.34	0.8640	0.8327	0.7485	2.85	
2FI	0.34	0.8995	0.8392	0.6214	4.29	
Quadratic	0.050	0.9985	0.9965	0.9753	0.28	Suggested

2.2 Optimization of Response by RSM

By considering the goals and boundaries for each response, an optimum optimization of an individual was obtained by the following goals

- Response minimization
- Target the response
- Response maximize

In order to minimize the response, first a target value and the maximum response value are to be provided, if the response value is above the target value then desirability is considered as zero, and if the value is less than target value then it is unity. As the response approaches to the target value the desirability reaches one. From the model summary of the statistics it is clear seen that that regression model of quadratic is most fitted one when compared to linear (Tables 2 and 3).

2.3 Data Analysis of RC

In this present paper, Minitab-17 an excellent statistical package is used for analysis. From the statistical summary model, it is clearly understood that the response is good to have its nature in polynomial equation which is being formed by the three

independent variables, the final suggested regression equation in uncoded values is provided in the Eq. (4).

$$\mathrm{RC} = +1.85055 + 7.79328E-005K_s + 1.61257E-003b - 0.017164m_s - 3.07258E-008K_s b - 2.53004E-007K_s - 4.60132E-009bm_s + 1.18385E-009k_s k_s + 1.78235E-007bb + 4.17904E-005m_s m_s \quad (4)$$

The goodness of fit of the regression equation is verified with the following conditions:

- Quantitative checking for fitness between predicted model and observed model.
- Visual checking the validation of assumptions of random errors.
- Checking out for the *R*, Adjusted *R* Square, Predicted *R* square values in linear, quadratic.

The quantitative checking of the fitment of predicted model is shown in Table 4. It is clear from the table that the coefficient of determination R^2 is 99.85 % indicting that 99.85 % chances, the output matches with the observed values. It is observed that the adjusted R^2 value (99.65 %) is very close to the R^2 value (99.85 %) implying the model is not having any excess variable. The predicted R^2 value (97.53 %) indicates that 97.53 % times, the regression model is able to predict response for any value of input variable in the range. This implies that the model can be used for further process of optimization.

Table 4 Model analysis using ANOVA for RC

Source	DF	Adj SS	adj MS	*F*-value	*P*-value
Model	8	11.5397	1.44246	547.81	0.000
Linear	3	10.1568	3.38559	1285.75	0.000
K_s	1	0.3002	0.30017	114.00	0.000
B	1	0.7259	0.72589	275.67	0.000
m_s	1	9.1307	9.13070	3467.58	0.000
Square	2	0.8385	0.41926	159.22	0.000
K_s*K_s	1	0.0196	0.01962	7.45	0.034
m_s*m_s	1	0.8329	0.83288	316.30	0.000
Interaction	3	0.5444	0.18148	68.92	0.000
K_s*b	1	0.0340	0.03399	12.91	0.011
K_s*m_s	1	0.1115	0.11153	42.36	0.001
b*m_s	1	0.3939	0.39892	151.50	0.000
Error	6	0.0158	0.0158	–	–
Lack-of-fit	4	0.0158	0.0158	*	*
Pure error	2	0.0000	0.00000	–	–
Total	14	11.5555	–	–	–

(*)-Multiplication Operator

2.4 Analysis of Variance

The analysis of variance (ANOVA) was implemented to study the effect of the input parameters on the rider comfortness. Table 4 gives the statistics for the model summary. It reveals that the quadratic model is the best appropriate model. So, for further analysis this model was used which gives the estimated regression coefficients of rider comfortness for encoded units. The value "p" for the model is lower than 0.05 which indicates that the model significant, revealing that sprung mass is effective. The next contribution on the rider comfort is the damper and stiffness. Further, it is seen that the R^2 value is 0.9985 and the Adj.R^2 0.9965. The predicted value 0.9753 is in reasonable agreement with Adj.R^2 value. R^2 value in this case is high and close to 1, which is desirable.

2.5 Optimization Results of RSM

In Minitab17 the response optimizer helps to identify the combination of input variable settings that jointly optimized the single or the set of response with the help of the optimization plot which gives the optimal solution for the combination of input variables. The following is the plot which describes the above explanation (Fig. 2).

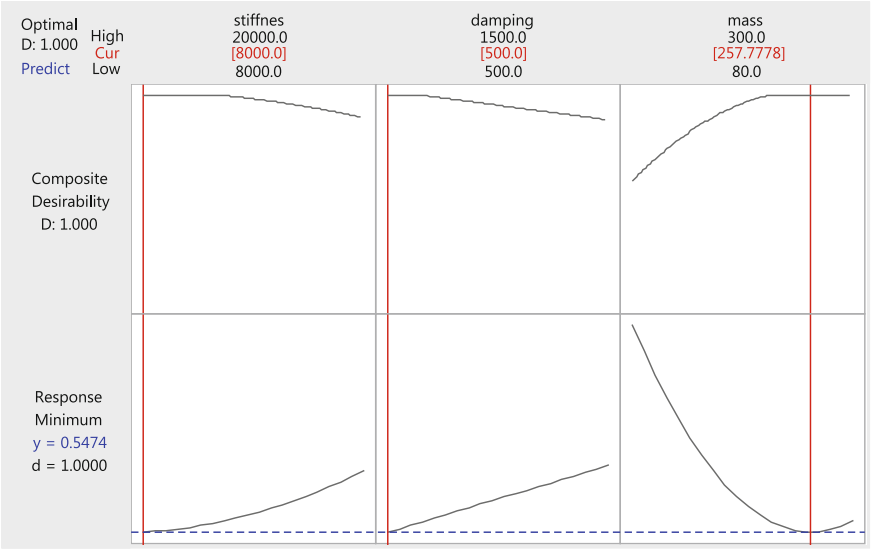

Fig. 2 Optimization plot of RC by RSM

3 Optimization Through Taguchi

Taguchi method requires minimum number of test runs and can be used to select best results by optimization of parameters. Prediction of optimum system parameters was done with Taguchi analysis and validation was done with Matlab/simulink. In Taguchi method process parameters are categorized into two main groups one is control factor and the other is noise factor, Control factors are nothing but design parameters and factors whose values are hard to control during normal process are called noise factors. Taguchi proposed orthogonal arrays as they play very important role in Taguchi design and can be used to estimate main effects using only a few experimental runs. Taguchi method uses a loss function to calculate the deflection between experimental values and aimed values. Using loss function signal to noise ratio is derived and signal to noise ratio or SN ratio is classified into three categories namely lower is better, nominal is best, higher is better. Signal to noise ratio need to be calculated for each experiment to determine the effect of each parameter on the output. In this paper three parameters are used as control factors and each factor is designed to have three levels. A L9 orthogonal array table with nine rows was chosen for the experiments. The steps to be followed Taguchi method are as follows:

1. Selection of suspension system constants.
2. Assignment of levels for each suspension constant.
3. Selection of Taguchi's orthogonal arrays.
4. Run the Taguchi L9 orthogonal array design for three factors.
5. Input the three trials responses for autogenerated nine levels.
6. S/N ratio is calculated for each obtained response RC.
7. Selection of optimum levels of process constants based on S/N ratio.
8. Evaluating simulation from obtained optimum process constants.

In this work, selection of suspension system parameters of three levels are same as in Table 1 With the proper selection of design of L9 orthogonal array with nine set of levels are being generated as follows in Table 5.

Table 5 Taguchi L9 Orthogonal array

Spring stiffness	Suspension damping	Mass
1	1	1
1	2	2
1	3	3
2	1	2
2	2	3
2	3	1
3	1	3
3	2	1
3	3	2

Table 6 S/N ratio of simulation results for quarter car model to obtain minimum response

Spring stiffness	Suspension damping	Mass	Trial 1	Trial 2	Trial 3	S/N Ratio	Mean
8000	500	80	2.8332	2.7821	2.9812	−9.14778	2.86550
8000	1000	190	2.1632	1.8621	2.1961	−6.35809	2.07380
8000	1500	300	1.0682	0.8912	1.0872	−0.16656	1.01553
14,000	500	190	1.2861	1.1921	1.2961	−2.00032	1.25810
14,000	1000	300	0.8614	0.7614	0.9612	1.25780	0.861333
14,000	1500	80	3.1632	2.8193	3.1821	−9.71277	3.05487
20,000	500	300	1.2861	1.0213	1.3029	−1.65804	1.20343
20,000	1000	80	1.8382	1.6912	2.1682	−5.61905	1.89920
20,000	1500	190	1.3261	1.2162	1.4612	−2.53079	1.33450

The mean S/N ratio from table is −3.992845

The corresponding responses for 3^{2-1} levels of basic three level designs are feed into run time analysis. The table which is filled up with proper sets of responses to the corresponding input parameters. With these factors as input autogenerated signal to noise ratio is analyzed with mean rates. Clearly results are related to the minimization of response, thus lower is the better equation used for mathematical calculation of signal to noise ratio. The calculated means S/N ratio for minimum response for quarter car model is shown in the Table 6 obtained by the nine simulation runs.

In quarter car suspension system for the selected suspension parameters with 3 dof, the mean S/N ratios are calculated in terms of mean response are shown in Tables 7 and 8. S/N ratio for mean response is presented in Figs. 3 and 4, helpful in selection of optimum combination of suspension parameters as mass (level-3), suspension damping (level-2), spring stiffness (level-3) having largest S/N ratio for individual suspension parameters.

Table 7 Smaller is better response table for signal to noise ratios

	Spring stiffness	Suspension damping	Mass
Level 1	−5.224146	−4.268713	−8.159866
Level 2	−3.485096	−3.573113	−3.629733
Level 3	−3.269293	−4.136706	−0.188933
Delta	1.954853	0.6956	7.970933
Rank	2	3	1

Table 8 Response table for mean

	Spring stiffness	Suspension damping	Mass
Level 1	1.985	1.776	2.607
Level 2	1.725	1.611	1.555
Level 3	1.479	1.802	1.027
Delta	0.506	0.190	1.580
Rank	2	3	1

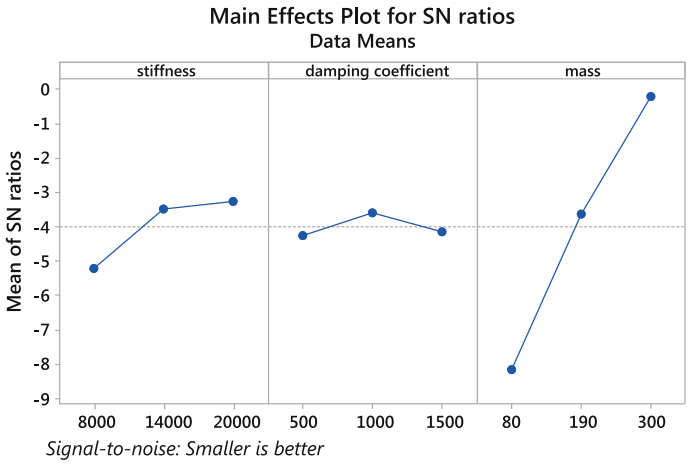

Fig. 3 Effect of suspension parameters on minimum response S/N ratio

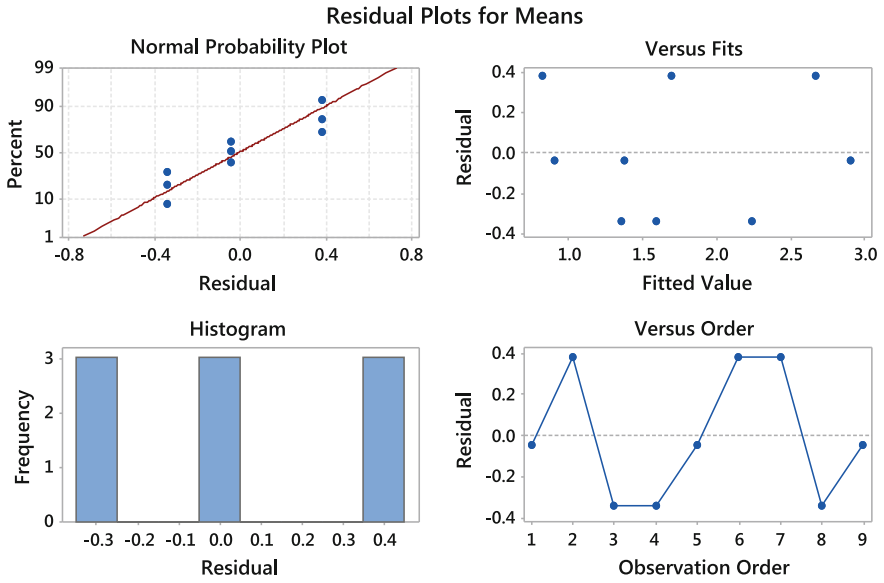

Fig. 4 Residual plots for means to obtain minimum response

4 Conclusion

From the above results of both RSM and Taguchi, in RSM composite desirability achieved i.e. $D = 1$ with the minimum response. Which is given as $y = 0.5474$. It is also shown that initial values of stiffness and damping are the control variables

effecting the response, where as in the case of sprung mass it is not the initial value instead the optimum value is 257.778 kg which is best control variable and effective variable in rider comfortness. While coming to Taguchi the best effective variable is chosen to be mass, i.e., is clearly seen from the ranks plot in Table 8 saying that the initial mass at level three is the best in minimizing the response. Therefore, this type of statistical approach and optimization techniques to quarter car suspension is efficient in technical analysis.

Acknowledgment This research was supported/partially supported by Prof. C.H. Ratnam, Mechanical Department, College of Engineering, Andhra University. We thank our Head of Department of Mechanical Engineering, Dr. Y.V. Hanumanth Rao. Dean of Research and Development, Dr. K.L. Narayana. And authors P. Vigneshwar and Rajasekhar would like to special thanks to Dr. Sumathi, Department of Humanities KL University, Pesaru Manjula Reddy Pesaru. Malla Reddy, and D. Kesava Reddy.

References

1. T. Tak and S. Chung, "An optimal design software for vehicle suspension systems," in SAE Automotive Dynamics & Stability Conference, Troy, Mich, USA, May 2000, SAE Paper no: 2000-01-1618.
2. D. Koulocheris, H. Vrazopoulos, and V. Dertimanis, "Optimization algorithms for tuning suspension systems used in ground vehicles," in Proceedings of International Body Engineering Conference & Exhibition and Automotive & Transportation Technology Conference, Paris, France, July 2002, SAE Paper no: 2002-01-2214.
3. P. C. Wiers and A. K. Dhingra, "On the beneficial effects of anti-squat in rear suspension design of a drag racing motorcycle," Journal of Mechanical Design, vol. 124, no. 1, pp. 98–105, 2002. View at Publisher · View at Google Scholar · View at Scopus.
4. S. A. Mitchell, S. Smith, A. Damiano, J. Durgavich, and R. MacCracken, "Use of genetic algorithms with multiple metrics aimed at the optimization of automotive suspension systems," in Proceedings of Motorsports Engineering Conference and Exhibition, Dearborn, Mich, USA, November 2004, SAE Paper no: 2004-01-3520.
5. M. Raghavan, "Suspension design for linear toe curves: a case study in mechanism synthesis," Journal of Mechanical Design, vol. 126, no. 2, pp. 278–282, 2004. View at Publisher · View at Google Scholar · View at Scopus.
6. R. Paneerselvam, Design and analysis of Experiments (PHI-Learning Pvt, Ltd, 2012).
7. Mithilesh kumar, Asit Baran puri, Atanu Maity "Experimental Study of cutting forces in Ball end milling of AL2014-T6 Using Response Surface Methodology" Procedia Material Science 6(2014) 612–622.
8. Priti Sonasale, "An approach to optimize Mig welding parameters by using Design of Experiments", IJAMM&C, Vol. 5, 2015.
9. M.S. Chua, M. Rahman, Y.S. Wong, H.T. Loh, Determination of optimal cutting conditions using design of experiments and optimization techniques, Int. J. Mach. Tools Manuf. 33(2) (1993) 297–305.
10. S.H. Lee, S.H. Lee, Optimization of cutting parameters for burr minimization in face-milling operations, Int. J. Prod. Res. 41(3) (2003) 497–511.
11. W.H. Yang, Y.S. Tarng, Design optimization of cutting parameters for turning operations based on the Taguchi method, J. Mater. Process. Technol. 84(1998) 122–129.
12. T.R. Lin, Optimization technique for face milling stainless steel with multiple performance characteristics, Int. J. Adv. Manuf. Technol. 19(2002) 330–335.

13. Boopathi, S., Sivakumar, K. and Kalidas, R. "Parametric Study of Dry WEDM Using Taguchi Method", International Journal of Engineering Research and Development (ISSN: 2278–800X), Vol. 2, No. 4, pp. 1–6, 2012.
14. M.B.S. Sreekar Reddy, Dr.S.S. Rao, P. Vigneshwar, K. Akhil, D. Raja Sekhar "An Intelligent Optimization Approach to Quarter Car Suspension System through RSM Modeled Equation", International conference on ICT for Intelligent Systems in press.

On Modeling and Analysis of Launch Vehicle System

Abhaya Pal Singh and Himanshu Agrawal

Abstract Modeling of dynamical systems is the primary attraction of many researchers from many decades. In this paper the modeling of Missile Launch Vehicle (MLV) System is reported. The detailed model analysis of the considered system is also reported. The model equations are found by using Euler–Lagrangian equation and comment on stability is given by using Lyapunove's theorem.

Keywords Dynamical system · Euler–Lagrangian equation (EL) · Lagrangian · Lyapunov stability · Launch vehicle (LV) · System modeling

1 Introduction

Modeling of dynamical systems is the primary attraction of many researchers from many decades. The main motivation is to have necessary information about automated control of the dynamical system. The dynamical systems may be classified as electrical systems or mechanical systems, etc., and can represent various other branches of science and technology.

In this paper a reusable Missile Launch Vehicle (MLV) system is considered. Missile launch vehicles are the need of today's defense organizations. Missile launch vehicles are those which carries missile to shoot in desire directions. This is related to security of ones nation hence there is a need of precise control of these launch vehicles.

There are various modeling strategies of dynamical systems are reported in the history. The backgrounds for modeling of dynamical systems are given in detailed in [1, 2]. The strategy of control of dynamical systems for both SISO and MIMO are reported in [3, 4]. The mathematical models of air turbulent are discussed in [5].

A.P. Singh (✉) · H. Agrawal
Symbiosis International University, Symbiosis Institute of Technology, Pune, India
e-mail: abhaya.aps@gmail.com

H. Agrawal
e-mail: himanshu.agrawal@sitpune.edu.in

D.K. Lobiyal et al. (eds.), *Proceedings of the International Conference on Signal, Networks, Computing, and Systems*, Lecture Notes in Electrical Engineering 396, DOI 10.1007/978-81-322-3589-7_30

In the paper [6] a qualitative modeling approach is proposed and uses the merits of the neural networks, fuzzy logic, and genetic algorithms. The paper [7] reports a sum of squares approach of modeling and control using polynomial fuzzy systems of nonlinear dynamical systems and paper [8] discusses about the observer design of nonlinear systems. In the paper [9] the changes in system's dynamics due to any fault are modeled as the nonlinear functions of input variables and states. Mathematical tool for building a fuzzy based model of a system to which fuzzy implications are used is presented in [10]. In [11] a survey on models is reported and this survey of models deals with the mathematical frameworks used for the modeling and think carefully about the challenging aim of modeling the complex systems. The paper [12–15] uses fractional calculus to model a system. Fractional order control of dynamical systems is reported in [16–20].

The paper [21] provides an overview of select Space Launch System (SLS) aerodynamic environments and describes the development choices and explains why are they made in a particular manner. The paper [22] provides the real-world examples, the lessons learned to illustrate common concerns by the use of simulations and models, this paper tells that modeling and analysis are important tools for the development of a system. This paper [23] introduces an approach which deal with reliability modeling method of Equipment System (ES), a case study on ES is carried in this paper. In [24] a modeling method is developed with objective of making potentially intractable problem of LV failure propagation. In the thesis [25] a research to formulate and implementation of a method is reported that is capable of evaluating vehicle architecture effects on safety and reliability. The modeling of missile salvos is reported in [26]. Paper [27] develops mathematical model of Launcher System and the control applications of the launcher through simulations. In [28] an Antiaircraft Missile cooperative guidance model is reported with different strategies. Paper [29] describes nonlinear control method of missile, in this paper the modeling of actuator is derived and this dynamics is used for control strategies. In [30] hybrid modeling is reported to design and improve performance of Hypersonic Vehicle. In [31] a patrol mission for unmanned surface vehicle are set up and modeled using C-BML.

For any control system design, it is essential to collect system's behavioral information. The important step for analysis of any system is to find the governing equation of the system. Modeling of any of the system will help to find the governing equation of the system. Hence, this paper gives the modeling and analysis of reusable MLV system. The considered system is having two degree of freedom one in the vertical direction and the other in the horizontal direction. Contribution of this paper.

- Modeling of MLV using EL equation.
- Linearizing the model of MLV.
- Analysis of the MLV system.
- Stability of the MLV system.

2 Modeling of Missile Launch Vehicle System

The schematic picture of MLV is shown in Fig. 1. It consists of two link, link 1 is having the Y-axis as axis of rotation and link 2 is having Z-axis as axis of rotation. Assuming all the masses are at the tip of the links, its equivalent dynamics is also shown in Fig. 1. Let m_1 and m_2 are the two masses and l_1 and l_2 are the link lengths of the link 1 and link 2 respectively. m_2 is the mass which is corresponding to the mass of the Missile. Let θ_1 is the angle of rotation along Y-axis and θ_2 is the angle of rotation along Z-axis and g as acceleration due to gravity.

Here, Euler–Lagrangian (EL) equation is used to find the governing equations of motion of the MLV system. The EL equation [32, 33] can be defined as

$$\frac{\mathrm{d}}{\mathrm{d}t}\left(\frac{\partial \pounds}{\partial \dot{x}}\right) - \frac{\partial \pounds}{\partial x} = F \tag{1}$$

where x is degree of freedom of the system in terms of positions and angles with F as a force applied to that system. £ is the Lagrangian which is difference between kinetic (KE) and potential energy (PE).

$$\pounds = KE - PE \tag{2}$$

To find KE of the considered system it is obvious to find the position of the first mass m_1 and the second mass m_2 and then first derivative will give the velocity of the two masses. So, the total KE will be the sum of the two kinetic energies and same for the potential energy. Therefore,

$$\mathrm{KE}_1 = \frac{1}{2} m_1 l_1^2 \dot{\theta}_1^2 \tag{3}$$

$$\mathrm{KE}_2 = \frac{1}{2} m_2 [l_1^2 \dot{\theta}_1^2 + l_2^2 \dot{\theta}_2^2 + l_2^2 \dot{\theta}_2^2 C_2^2 + 2 l_1 l_2 \dot{\theta}_1^2 \dot{\theta}_2^2 (S_1 - C_1) C_2] \tag{4}$$

$$\mathrm{PE}_1 = 0 \tag{5}$$

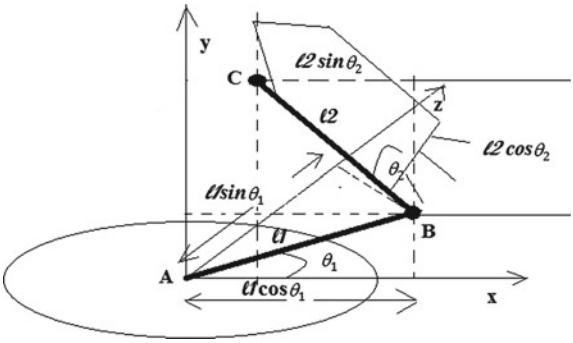

Fig. 1 Geometrical model closest to the actual model of reusable missile launch vehicle system (MLV)

$$\mathrm{PE}_2 = m_2 g l_2 C_2 \tag{6}$$

Now, using Eqs. (1), (2), (3), (4), (5), and (6) and with some mathematical manipulation we get

$$\ddot{\theta}_1 = \frac{E * A + m_2 l_1 l_2 (S_1 C_2 - C_1 C_2) * B}{C} \tag{7}$$

$$\ddot{\theta}_2 = \frac{m_2 l_1 l_2 (S_1 C_2 - C_1 C_2) * A - (m_1 + m_2) l_1^2 * B}{D} \tag{8}$$

Here,

$$\begin{aligned}
A &= \tau_1 - m_2 l_1 l_2 \dot{\theta}_2^2 (C_1 S_2 - S_1 S_2) \\
B &= \tau_2 + m_2 g l_2 S_2 + \frac{1}{2} l_2^2 m_2 \dot{\theta}_2^2 S2_2 - m_2 l_2 l_1 \dot{\theta}_1^2 (C_1 C_2 + S_1 C_2) \\
C &= E * (m_1 + m_2) l_1^2 - m_2^2 l_1^2 l_2^2 (S_1 C_2 - C_1 C_2)^2 \\
D &= m_2^2 l_1^2 l_2^2 (S_1 C_2 - C_1 C_2)^2 + (m_1 + m_2) l_1^2 (\frac{3}{2} l_2^2 m_2 + \frac{1}{2} m_2 l_2^2 C2_2) \\
E &= 0.5 l_2^2 m_2 (3 + C2_2)
\end{aligned}$$

where τ_1 and τ_2 are the input torque at the two joints and $C2_a = \cos 2\theta_a$ and $S2_a = \cos 2\theta_a$. Presenting Eqs. (7) and (8) into standard nonlinear state-space equations and after linearization of the nonlinear state-space matrix and considering $l_1 = 1\,\mathrm{m}$, $l_2 = 2\,\mathrm{m}$, $m_1 = 0.2\,\mathrm{kg}$, $m_2 = 20\,\mathrm{kg}$, $g = 9.8\,\mathrm{m/s^2}$, the linearized state-space form of MLV system will be

$$\begin{aligned}
\frac{\mathrm{d}(\delta \underline{z})}{\mathrm{d}t} &= \begin{bmatrix} 0 & 1 & 0 & 0 \\ 0 & 0 & -9.61 & 0 \\ 0 & 0 & 0 & 1 \\ 0 & 0 & -1.63 & 0 \end{bmatrix} \begin{bmatrix} z_1 \\ z_2 \\ z_3 \\ z_4 \end{bmatrix} \\
&+ \begin{bmatrix} 0 & 0 \\ 0.1 & -0.02 \\ 0 & 0 \\ -0.01 & -0.004 \end{bmatrix} \begin{bmatrix} \tau_1 \\ \tau_2 \end{bmatrix}
\end{aligned} \tag{9}$$

The output matrix will be

$$y = \begin{bmatrix} 1 & 0 & 0 & 0 \\ 0 & 0 & 1 & 0 \end{bmatrix} \begin{bmatrix} z_1 \\ z_2 \\ z_3 \\ z_4 \end{bmatrix} \tag{10}$$

3 Analysis of MLV System

Lyapunov's indirect method [34] uses the linearization of system to check the local stability of the considered system. In this the eigenvalues of the state matrix is found and if the real part of the eigenvalues are negative then only indirect method comment on the stability of the system else it fails. The indirect method does not give any information related how near to the origin it will give the guarantee stability. Here, the Lyapunov's direct method is used. In Lyapunov's Direct method a Lyapunov candidate function $V(x)$ is used which should be positive definite over the entire state space and it is needed to check that $\dot{V}(x)$ is negative definite then the system will be stable. Considering Eq. (9), the state matrix A is given by

$$\begin{bmatrix} 0 & 1 & 0 & 0 \\ 0 & 0 & -9.61 & 0 \\ 0 & 0 & 0 & 1 \\ 0 & 0 & -1.63 & 0 \end{bmatrix} \tag{11}$$

The eigenvalues can be found to be are $0, 0, +1.2801i, -1.2801i$. Hence, Lyapunov's indirect method fails to comment on the stability of MLV system. Let us consider sum of Eqs. (3, 4, 5 and 6) as a Lyapunov's candidate function, as this is the sum of total KE and total PE of the system which is positive definite. So,

$$\begin{aligned} V(z) = &\frac{1}{2}m_1 l_1^2 z_2^2 + \frac{1}{2}m_2[l_1^2 z_2^2 + l_2^2 z_4^2 + l_2^2 z_4^2 C_{z_3}^2 \\ &+ 2l_1 l_2 z_2^2 z_4^2 (S_{z_1} - C_{z_1}) C_{z_3}] + m_2 g l_2 C_{z_3} \end{aligned} \tag{12}$$

Taking first derivative of $V(z)$, assuming $\tau_1 = \tau_2 = 0$ (no external torque), and with some mathematical manipulation,

$$\begin{aligned} \dot{V}(z) = &- [z_3[194.12z_2 + 134.4z_4 + 40[9.61z_4(S_{z_1}S_{z_3} \\ &- C_{z_1}C_{z_3}) + 1.632z_2(S_{z_1}C_{z_3} - C_{z_1}C_{z_3}) - z_2^2 C_{z_1}C_{z_3}]] \\ &+ 40z_4[S_{z_3}(2z_4^2 + 9.8) + z_2(z_4 S_{z_1}S_{z_3} - z_2 S_{z_1}C_{z_3} \\ &- z_4 C_{z_1}S_{z_3})]] \end{aligned} \tag{13}$$

Hence, $V(z)$ will be negative definite only if the expression in the square bracket [.] right hand side of Eq. (13) is positive, if this satisfies the MLV system will be a stable system in Lyapunov sense.

4 Conclusion

In this paper the modeling of Missile Launch Vehicle (MLV) is reported and its governing equations of motion are found. Then the system is linearized for the analysis of the local behavior of the MLV system. Analysis of the system is carried

out to gather information about the MLV system. In analysis using Lyapunov's direct and indirect method it is obtained that Lyapunov's indirect method fails to comment upon the MLV systems stability. So, direct method of Lyapunov is used for further investigation of the stability. Using direct method a condition (Eq. 13) for stability of MLV system is obtained. Future work will be is to design a control law which can control the angles of MLV system to launch the missile in the desired direction.

References

1. Zhang, Chunwei, and Jinping Ou. "Modeling and dynamical performance of the electromagnetic mass driver system for structural vibration control." Engineering Structures 82 (2015): 93–103.
2. Branicky, Michael S. "General hybrid dynamical systems: Modeling, analysis, and control." Hybrid Systems III. Springer Berlin Heidelberg, 1996. 186–200.
3. Dorf, Richard C. "Modern control systems." Addison-Wesley Longman Publishing Co., Inc., (1995).
4. Stefani, Raymond T. "Design of feedback control systems." Oxford University Press, Inc., (1993).
5. SZABOLCSI, RÓBERT. "Stochastic Noises Affecting Dynamic Performances of the Automatic Flight Control Systems." Review of the Air Force Academy 1 (2009): 23–30.
6. Farag, Wael A., Victor H. Quintana, and Germano Lambert-Torres. "A genetic-based neuro-fuzzy approach for modeling and control of dynamical systems." Neural Networks, IEEE Transactions on 9.5 (1998): 756–767.
7. Tanaka, Kazuo, et al. "A sum-of-squares approach to modeling and control of nonlinear dynamical systems with polynomial fuzzy systems." Fuzzy Systems, IEEE Transactions on 17.4 (2009): 911–922.
8. Srivastava, Pallavi, et al. "Observer Design For Non-Linear Systems." International Journal of Applied Engineering Research 8.8 (2013).
9. Demetriou, Michael A., and Marios M. Polycarpou. "Incipient fault diagnosis of dynamical systems using online approximators." Automatic Control, IEEE Transactions on 43.11 (1998): 1612–1617.
10. Takagi, Tomohiro, and Michio Sugeno. "Fuzzy identification of systems and its applications to modeling and control." Systems, Man and Cybernetics, IEEE Transactions on 1 (1985): 116–132.
11. Bellomo, Nicola, and Christian Dogbe. "On the modeling of traffic and crowds: A survey of models, speculations, and perspectives." SIAM review 53.3 (2011): 409–463.
12. Machado, JA Tenreiro, and Maria Eugénia Mata. "Pseudo Phase Plane and Fractional Calculus modeling of western global economic downturn." Communications in Nonlinear Science and Numerical Simulation 22.1 (2015): 396–406.
13. Srivastava, Trisha, A. P. Singh, and Himanshu Agarwal. "Modeling the Under-Actuated Mechanical System with Fractional Order Derivative." Progr. Fract. Differ. Appl. 1, No. 1, (2015): 57–64.
14. Shah, Pritesh, S. D. Agashe, and A. P. Singh. "Fractional order modelling using state space theory." International Journal of Engineering and Technology 5.3 (2013): 2891–2894.
15. Singh, A. P., T. Srivastava, and P. Srivastava. "Fractional Equations of Motion Via Fractional Modeling of Underactuated Robotic Systems." IEEE ICARET (2013).

16. Dziwinski, Tomasz, et al. "Robust Non-integer Order Controller for Air Heating Process Trainer." Advances in Modelling and Control of Non-integer-Order Systems. Springer International Publishing, (2015). 249–256.
17. Singh, A. P., Faruk S. Kazi, Navdeep M. Singh, and Pallavi Srivastava. "$PI^{\alpha}D^{\beta}$ controller design for underactuated mechanical systems." In Control Automation Robotics & Vision (ICARCV), 12th International Conference on, (2012): 1654–1658.
18. Singh, A. P., et al. "Fractional Order controller design for underactuated mechanical systems." The 5th IFAC Symposium on Fractional Differentiation and its Applications-FDA. 2012.
19. Shah, Pritesh, Sudhir D. Agashe, and A. P. Singh. "Design of fractional order controller for undamped control system." Engineering (NUiCONE), 2013 Nirma University International Conference on. IEEE, 2013.
20. Singh, A. P., H. Agarwal, and P. Srivastava. "Fractional Order Controller Design For Inverted Pendulum On A Cart System (POAC)", vol-10, 2015, pp 172–178.
21. Blevins, John A., et al. "An Overview of the Characterization of the Space Launch Vehicle Aerodynamic Environments." (2014).
22. Hardy, Terry L. "MODELS AND SIMULATIONS: RISKS AND LESSONS LEARNED." JOURNAL of SPACE SAFETY ENGINEERING, Vol 1, No. 1, (2014).
23. Lin, Shaoyang, and Xiaoyue Wu. "Mission Reliability Modeling for Equipment System Based on the Operational Viewpoint of DoDAF 2.0." International Conference on Logistics Engineering, Management and Computer Science (LEMCS 2014). Atlantis Press, (2014).
24. Lawrence, Scott, Donovan Mathias, and Ken Gee. "A Failure Propagation Modeling Method for Launch Vehicle Safety Assessment." 12th International Conference on Probabilistic Safety and Management (PSAM12), Honolulu, HI. (2014).
25. Zwack, Mathew R. "CONTRAST: A Conceptual Reliability Growth Approach for Comparison of Launch Vehicle Architectures." (2014).
26. Milinovic, Momcilo, et al. "Discrete Deterministic Modelling of Autonomous Missiles Salvos." Defence Science Journal 64.5 (2014): 471–476.
27. Dokumaci, Korhan, M. Timur Aydemir, and Metin U. Salamci. "Modeling, PID control and simulation of a rocket launcher system." Power Electronics and Motion Control Conference and Exposition (PEMC), 2014 16th International. IEEE, (2014): 1283–1288.
28. Lei, Yu Yao, et al. "Modeling of Anti-Aircraft Weapon Systems Cooperative Guidance for Anti-Aircraft Missile." Applied Mechanics and Materials. Vol. 719. (2015): 504–513.
29. Chwa, D. O. N. G. K. Y. O. U. N. G. "Nonlinear longitudinal acceleration control of nonminimum phase missiles with actuator dynamics." Aerospace and Electronic Systems, IEEE Transactions on 50.3 (2014): 2369–2378.
30. Feng, Zhang, and Xue Hui-Feng. "A New Hybrid Modeling Method for Performance Digital Mock-Up of Hypersonic Vehicle." Appl. Math 9.1 (2015): 337–343.
31. Unal, Omer, and Okan Topcu. "Modelling unmanned surface vehicle patrol mission with Coalition Battle Management Language (C-BML)." The Journal of Defense Modeling and Simulation: Applications, Methodology, Technology 11.3 (2014): 277–308.
32. Otten, E. "Inverse and forward dynamics: models of multi–body systems." Philosophical Transactions of the Royal Society of London. Series B: Biological Sciences 358.1437 (2003): 1493–1500.
33. Spong, Mark W., Seth Hutchinson, and Mathukumalli Vidyasagar. "Robot modeling and control." Vol. 3. New York: Wiley, (2006).
34. Wang, Ruo Lin, H. Gu, and G. Song. "Adaptive Robust Sliding Mode Vibration Control of a Flexible Beam Using Piezoceramic Sensor and Actuator: An Experimental Study." Mathematical Problems in Engineering (2014):1–9.

Performance Evaluation of Tree-Based Classification Techniques on Intrusion Dataset

Moninder Kaur, Ramesh Kumar, Santosh Kumar Sahu and Sanjay Kumar Jena

Abstract Tree-based learning techniques are extensively used to solve classification problems on various domains. The underlying reason for that is due to its simplicity in implementation, easy to visualize, and more reliable compared to other learning techniques. To select an efficient classification algorithm for predictive analysis on intrusion detection is a challenging task. In this paper, we have tested 13 well-known tree-based classification techniques. The objective is to select the best algorithm among them for intrusion detection model. The tree-based classification techniques are used for prediction of attacks and normal instances on NSL-KDD dataset. The assessment of the methods are evaluated as per confusion matrix, mean absolute error, root mean square error, kappa statistics, ROC curve, accuracy, and execution time. The Weka API's are used with Java environment to implement the model. Experimentally, the LAD tree methods outperform in comparison with other tree-based algorithms.

Keywords Tree-based classifier · Intrusion detection · NSL-KDD

M. Kaur (✉) · R. Kumar · S.K. Sahu · S.K. Jena
National Institute of Technology, Rourkela, Odisha, India
e-mail: kaur.moninder5@gmail.com

R. Kumar
e-mail: connecting.ramesh@gmail.com

S.K. Sahu
e-mail: santoshsahu@hotmail.co.in

S.K. Jena
e-mail: skjena@nitrkl.ac.in

D.K. Lobiyal et al. (eds.), *Proceedings of the International Conference on Signal, Networks, Computing, and Systems*, Lecture Notes in Electrical Engineering 396, DOI 10.1007/978-81-322-3589-7_31

1 Introduction

Changes in life are not permanent, but change is. The world is evolving rapidly, hence the technology has significant impact on today's world. With the booming technology comes the boosted risks. Hence, it needs to adapt such technologies that we could cope with the risk.

Earlier, the hardware devices such as floppy disks, desktop computer, etc., were valuable, the thief targets them. But nowadays, the data or the information present in those floppy disks, hard disks, and computer system is valuable and became a viable target for the thief. In the early days, the attacks were minimum like mainframes required physical access to a dumb terminal to gain access. But with the change in technology came the client–server, peer-to-peer network, Internet wireless communication, and mobile computing, which significantly boosted the risk. Peer-to-Peer network has more vulnerabilities than client–server computing as each and every node is connected. For the protection, we used the firewall to filter traffic [1] and protect our private network from insecure networks. But the firewall was not enough as it checks only the header of the packet, and it failed to identify the malicious payload of the packet, therefore, is inadequate to counter an intrusion. An intrusion is an act of intruding or someone trying to get unauthorized access that is against system policies, and intrusion detection is a problem of great significance in this world of increasing cybercrime.

Therefore, we adapt Intrusion Detection System (IDS) which can analyze the network traffic to prevent system or network from malicious activity [2]. IDS monitors the network traffics, system level test data, and system status files as an input. It can detect attacks from a single PC to the entire enterprise network and countermeasures the intrusive efforts. An IDS is capable of identifying known as well as unknown attacks by examining the payload.

IDS are categorized into two types—anomaly-based IDS and misuse-based IDS. Anomaly-based IDS detects the outliers, it scans for the abnormal behavior of the system and conclude it as an attack. It generates many false alarms because it may be the case any authorized user can change its behavior. One advantage of this IDS system is that it can detect the variant of the attack. There are many approaches of the signature (anomaly) based detection like statistical approach, predictive pattern generation, neural networks, sequence matching, and learning, etc., while the misuse-based IDS is a knowledge base IDS, which has rules stored in its directory to be match with attacks. Whenever a network traffic is captured, it is matched with the rules, generate alarms accordingly. The main disadvantage of this system is that it can only detect the known attacks. It cannot detect changed attack pattern or variant of the attacks but generates less false alarms as it only matches with stored database.

The various approaches on misuse-based detection are Expert system, Keystroke monitoring, state transition analysis, and pattern matching. Some tools are available in the market to detect the intrusions like packet header anomaly detector(PHAD) and network traffic anomaly detector(NETAD) are the anomaly-based and snort is the misuse-based tool. IDS is very flexible as when new threats came, and we need

to update accordingly without modifying the entire core software package. It uses different data mining techniques to learn and develop rules for analyzing attacks. It may use several classification algorithms to discover and classify attacks patterns, etc. But not always an algorithm could accurately classify an attack or may add a lot of delay in the network. Therefore, to find an optimal tree-based learning algorithm for classification is a crucial task for the model formation process.

Many classification algorithms are available. To select a suitable technique, we need a comparative study to test various classification algorithms to analyze its efficiency and complexity. In this paper, the comparison of different tree-based algorithms are applied on NSL-KDD intrusion dataset. The algorithms are AD tree [3, 4], BF tree [5], decision stump, FT [6], J48 [7], NB tree [8], J48 graft [9], Random forest [10], LMT [11], Simple cart [12], and many more and presenting a comparative performance metrics for each algorithm.

2 Related Works

A classification algorithm takes the records in the dataset as input and places it into different classes. For the intrusion detection, a two-class classifier divides the network traffic into normal or malicious. A multi-classifier divides those abnormal instances again into the type of attacks. There has been much research on tree-based classifier in different fields like video segmentation, and Lyme disease risk prediction. Dietterich [13] reviewed five approximate statistical test to compare the performance of learning algorithms over other on a particular learning task. Verlinde [14] compared three different classifiers to find the optimal algorithm for the decision fusion problem. Schutze et al. [15] compared different learning techniques based on statistical classification using three different classification techniques.

3 Objective

Several tree-based classification algorithms are available. To practice an efficient algorithm, we require to compare them. In this paper, the focus is on tree-based classifiers. The principal objective is to obtain an efficient and optimal tree-based classification algorithm by analyzing different performance metrics like accuracy, kappa execution time, etc.

4 Methodology

For the comparison, we chose NSL-KDD dataset and tested the algorithm using Weka API in java. The comparison is based on different performance metrics like accuracy, kappa statistics, mean absolute error, and root-mean-squared error.

4.1 Tree-Based Classification Algorithm

Decision tree-based classifiers are extensively used in diverse areas. The main reason behind use of tree-based classifier is due to its simpler decisions by breaking the complex decision-making process using divide conquer approach. In addition with, the tree-based classifiers take less time during learning process, and predict the output. Hence, in this experiment, the most popular 13 types of tree-based classifiers are considered for intrusion detection. The objective is to select the most appropriate classifier amongst for building intrusion detection model.

4.2 Performance Metrics

To evaluate the performance of tree-based classifiers,the evaluation parameters such as confusion matrix, ROC curve, kappa statistics, mean absolute error, root-mean-squared error, root relative squared error, precision, recall, and F-measured are used. Table 1 visualized the comparison amongst the tree-based classifiers on intrusion dataset.

Table 1 Statistics of tree-based learning algorithms

Actual index	Algorithm name	Accuracy	Kappa	MAE	RMSE	RAE	RRSE	Execution time(MS)
1	AD tree	79.5067	0.597	0.2452	0.4121	48.5801	81.4658	6
2	Decision Stump	79.9858	0.6096	0.2472	0.419	48.9876	82.8047	1
3	BF tree	77.8699	0.5677	0.2161	0.4558	42.8177	90.1057	29
4	FT tree	79.2761	0.5942	0.2074	0.45	41.1031	88.9776	51
5	J48	81.0548	0.6309	0.1792	0.413	35.5072	81.6584	5
6	J48 graft	77.9099	0.5733	0.2207	0.4655	43.7244	92.0365	13
7	NB tree	81.8178	0.6401	0.1791	0.4189	35.4784	82.828	138
8	LAD tree	84.5059	0.6951	0.1934	0.3806	38.3261	75.2395	47
9	REP tree	81.5916	0.636	0.1898	0.4281	37.6129	84.6475	6
10	Random forest	78.7881	0.5894	0.1985	0.3823	39.3356	75.5882	10
11	Random tree	83.0376	0.6634	0.1724	0.4123	34.1536	81.5098	5
12	Simple Cart	77.8389	0.5669	0.223	0.4682	44.1932	92.5708	67
13	LMT	80.2741	0.6164	0.1963	0.4368	38.897	86.3548	1277

5 Implementation

Scientific developments depend on the reproducibility of results so they can be autonomously validated, approved, and compared. A lot of the assessment in intrusion detection has been based on registered data, and results are not reproducible. One of the fundamental issues of releasing information originates from privacy concerns, and also it is difficult to simulate the diverse attack patterns of various attacks. To reduce this problem, we have different benchmark datasets available like KDDCup99, NSL-KDD, IDEVAL, etc. We have used NSL-KDD datasets to evaluate the performance of different tree-based classification algorithms. NSL-KDD is an updated version of KDD99, which overcomes the problems of redundancy of records. It eliminates the duplicity of records, so the classifiers will not be biased toward more conventional records hence improves the performance of the learners.

The framework of our approach is shown in Fig. 1. It contains the output of the performance metrics of various classification algorithms to find out the effective and efficient algorithms.

For the implementation of different classifiers, we have used WEKA API. Nowadays, WEKA is very popular and widely accepted in the area of machine learning and data mining. Data scientists use this tool and its algorithms for data analysis. It is freely available on web and provides free API for different algorithms. The JAVA API components of WEKA are accessed using Java code to perform data preprocessing, learning classifiers, evaluation (performance matrices like precision–recall), and attribute selection.

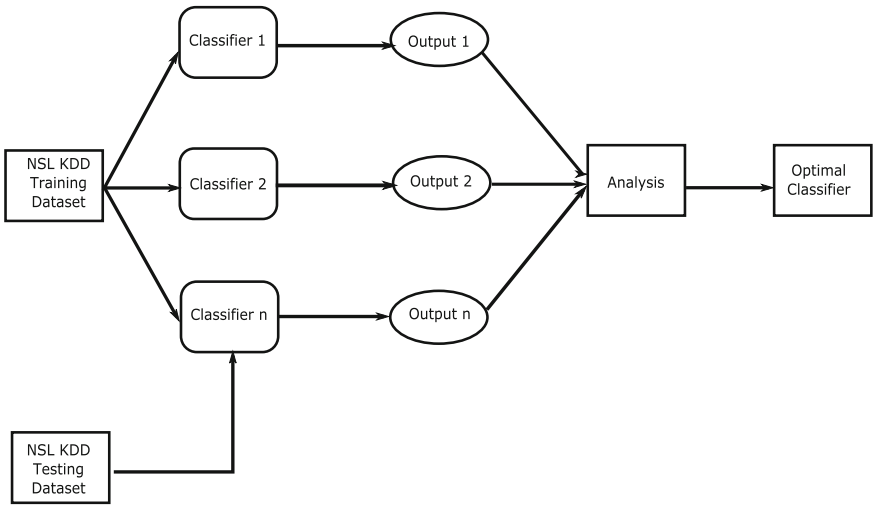

Fig. 1 Flow chart to find optimal classifier

6 Comparison

On analyzing the different tree-based classification algorithm by executing with the help of weka API, we obtained the following results. Table 1 contains the accuracy, kappa statistics, MAE, RMSE, RAE, and RRSE with execution time for different classifiers. The LAD tree provides the most accurate result (i.e., 84.5059 and kappa = 0.6951) followed by random tree (accuracy = 83.0376 and kappa = 0.6634) while the Simple Cart (accuracy = 77.8389 and kappa = 0.5669) has the least accuracy on NSL-KDD Dataset.

Figure 2 provides the trade-off between root-mean-squared error and mean absolute error. The decision stump has the highest mean absolute error (0.2472) followed by AD tree 0.2452 while random tree has the lowest mean absolute error (0.1724). The simple cart has the highest root-mean-squared error that is 0.4682 followed by the J48 Graft algorithm that has 0.4655 root-mean-squared error. LAD tree, on the other hand, has the least root-mean-squared error 0.3806.

Figure 3 provides the relative absolute error and root relative squared error. Decision stump has the highest relative absolute error 48.9876 followed by AD tree 48.5801 while random tree has the lowest relative absolute error 34.1536.

Simple cart has the highest root relative squared error that is 92.5708 followed by the J48 Graft algorithm that has 92.0365 root relative squared error. LAD tree, on the other hand, has the least root relative squared error 75.2395.

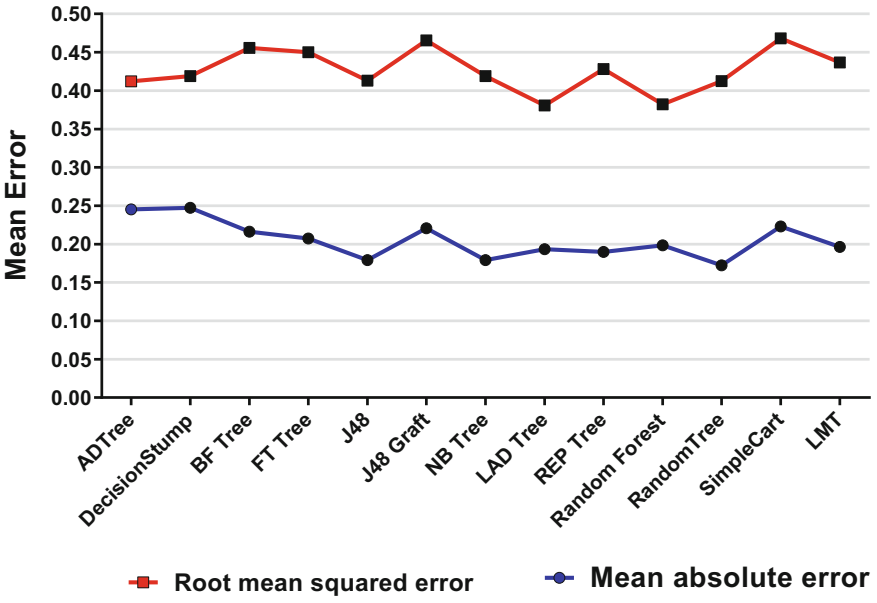

Fig. 2 Mean absolute error and root-mean-squared error

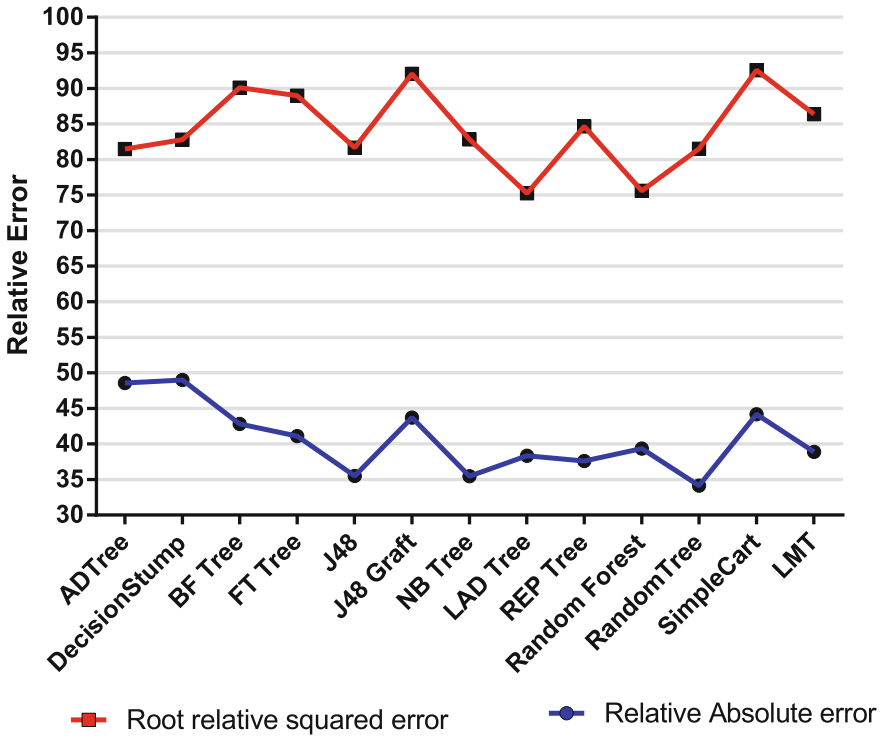

Fig. 3 Relative absolute error and root-mean-squared error

Table 1 provides the execution time as executed on a system with following configuration (Intel Core i5). LMT has the highest execution time of 1277 s followed by NB tree 138 s while decision stump has the least execution time of 1 s.

7 Result

We have analyzed the different classification algorithms on NSL-KDD dataset and we found that the LAD tree provides the most accurate result (84.5059) but its execution time is high, so there is a trade-off between execution time and accuracy. While, on the other hand, decision stump classification algorithm has the least execution time but its error rate is high, so again there is a trade-off between the execution time and failure rate. Following Tables 2 and 3 represent the confusion matrix of the LAD tree and decision stump tree by which we can analyze the performance.

Figures 4 and 5 represent the ROC curve for LAD tree and decision stump tree are as follows.

Table 2 Confusion matrix for LAD tree

Actual class	Predicted class	
	Class = Normal	Class = Intrusion
Class = Normal	9407	304
Class = Intrusion	3189	9644

Table 3 Confusion matrix for decision stump

Actual class	Predicted class	
	Class = Normal	Class = Intrusion
Class = Normal	9271	440
Class = Intrusion	8761	4072

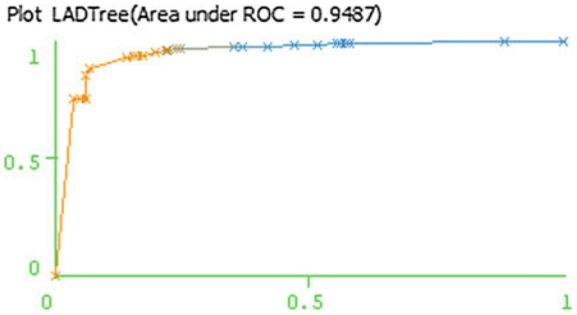

Fig. 4 ROC curve for LAD tree classifier

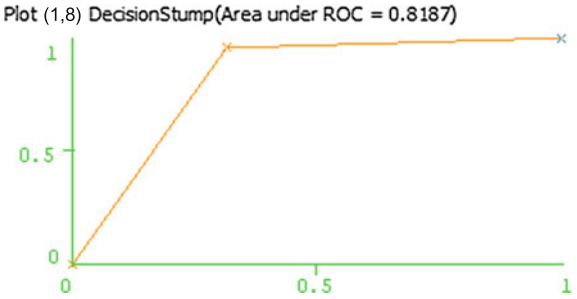

Fig. 5 ROC curve for decision stump classifier

8 Conclusion

In this paper, we have compared the different tree-based learning techniques using WEKA APIs in JAVA environment. There are 13 learning methods implemented and tested with NSL-KDD intrusion dataset. The well-known statistical evaluation parameters are considered for briefly reviewed amongst them. Empirically, the LAD tree outperforms in comparison to other techniques. The LAD tree learning

techniques provides the better result with stable output and least error rate. Hence, as per this experiment the LAD tree is the best tree-based classifier for intrusion detection.

References

1. Coley, Christopher D., and Ralph E. Wesinger Jr. "Firewall system for protecting network elements connected to a public network." U.S. Patent No. 6,061,798. 9 May 2000.
2. Sharma, Amit, and S. N. Panda. "Intrusion detection system." Enterprise Information Systems in 21st Century: Opportunities and Challenges (2009): 194.
3. Freund, Yoav, and Llew Mason. "The alternating decision tree learning algorithm." icml. Vol. 99. 1999.
4. Holmes, Geoffrey, et al. "Multiclass alternating decision trees." Machine learning: ECML 2002. Springer Berlin Heidelberg, 2002. 161–172.
5. Shi, Haijian. Best-first decision tree learning. Diss. The University of Waikato, 2007.
6. Gama, Joo. "Functional trees." Machine Learning 55.3 (2004): 219–250.
7. Quinlan, J. Ross. C4. 5: programs for machine learning. Elsevier, 2014.
8. Kohavi, Ron. "Scaling Up the Accuracy of Naive-Bayes Classifiers: A Decision-Tree Hybrid." KDD. 1996.
9. Webb, Geoffrey I. "Decision tree grafting from the all-tests-but-one partition." IJCAI. 1999.
10. Breiman, Leo. "Random forests." Machine learning 45.1 (2001): 5–32.
11. Landwehr, Niels, Mark Hall, and Eibe Frank. "Logistic model trees." Machine Learning 59.1–2 (2005): 161-205.
12. Breiman, Leo, et al. Classification and regression trees. CRC press, 1984.
13. Dietterich, Thomas G. "Approximate statistical tests for comparing supervised classification learning algorithms." Neural computation 10.7 (1998): 1895–1923.
14. Verlinde, Patrick, and G. Cholet. "Comparing decision fusion paradigms using k-NN based classifiers, decision trees and logistic regression in a multi-modal identity verification application." Proc. Int. Conf. Audio and Video-Based Biometric Person Authentication (AVBPA). 1999.
15. Schtze, Hinrich, David A. Hull, and Jan O. Pedersen. "A comparison of classifiers and document representations for the routing problem." Proceedings of the 18th annual international ACM SIGIR conference on Research and development in information retrieval. ACM, 1995.

Kinematic Modeling and Simulation of Manipulator for Executing Welding Operations with Arbitrary Weld Joint Profiles

B.B.V.L. Deepak, C.A. Rao, B.M.V.A. Raju and P.K. Singh

Abstract Current investigation deals with the development of an automated seam tracking methodology for the weld joints accessible in PC motor-assisted style setting. To perform welding operations, an industrial robot has been modeled in the CAD platform with three degrees of freedom. Later, kinematic models have been developed in order to navigate the end effector through the obtained weld seam path. Simulation results for different weld joints show the robustness of the developed methodology.

Keywords Seam tracking · CAD · Industrial robot · Forward and inverse kinematic · Weld seam path

1 Introduction

Nowadays, manufacturing industries require more and more automated machines to compete and fulfill the global requirements within given time limit. Proper motion planning algorithms are necessary for robotic systems, may be of manipulator or mobile platforms, in order to execute their specific tasks [1, 2]. Motion planning of industrial robots is a critical issue because of its end effectors path constraints [3, 4]. Whereas, the motion control of mobile robots or the mechanical behavior of the

B.B.V.L. Deepak (✉) · C.A. Rao · B.M.V.A. Raju · P.K. Singh
Automation Lab, Industrial Design Department, NIT-Rourkela, Rourkela, India
e-mail: deepak.bbvl@gmail.com

C.A. Rao
e-mail: bahubalendruni@gmail.com

B.M.V.A. Raju
e-mail: 213ID1358@nitrkl.ac.in

P.K. Singh
e-mail: 214ID1444@nitrkl.ac.in

D.K. Lobiyal et al. (eds.), *Proceedings of the International Conference on Signal, Networks, Computing, and Systems*, Lecture Notes in Electrical Engineering 396, DOI 10.1007/978-81-322-3589-7_32

robot depends upon the wheel geometric constraints while the robot is in motion [5, 6]. Bae et al. [7] used image processing algorithm to get the weld pool center and also investigated that how fuzzy logic approach can be used to monitor the manipulator and welding torch. Motion planning of mobile robot deals with generation of safest and shortest pats while reaching its target position [9–11]. There are several motion planning techniques have been developed based on artificial intelligence algorithms [12–15]. But these techniques are not suitable for performing welding operation.

This work describes about CAD-based robot modeling as well as simulation. The new method is based on sewing technique and simulation in CAD environment. The development of CAD-assisted robot welding covers mechanical design, extraction of coordinate data, importing the coordinate data to MATLAB, inverse kinematic solution, and simulation.

2 Kinematic Model of 3-Axis Robot

In robotics, manipulator kinematic analysis means forward and inverse kinematic analysis, it refers to calculate the relations between end effectors and joint angles. So for forward kinematics, the joint angles are the inputs and the outputs would be the coordinates of the end effectors. On the other hand for inverse kinematics, the given inputs are the coordinates of the end effector and the output to calculate would be joint angles (Fig. 1 and Table 1).

2.1 Arm Matrix Determination

Direct kinematics for the most part alludes to position examination of the tool. Therefore, forward kinematic examination is equal to finding of manipulator network with joining change frameworks as described in Eq. (1).

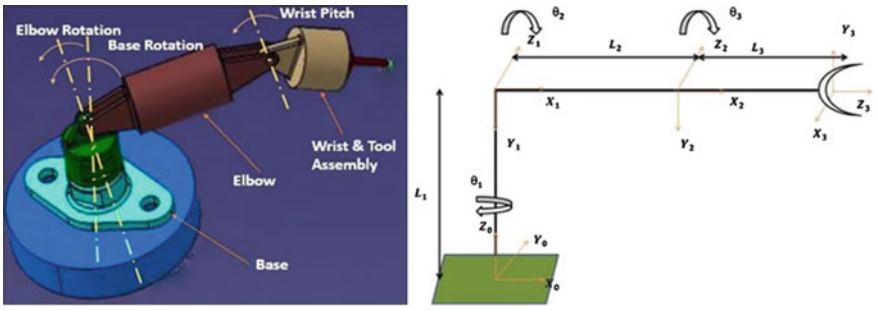

Fig. 1 3-axis manipulator in CAD environment and its coordinate reference frame

Table 1 Considered robotic arm stipulations

Element specification	Quantity	Measurement
DOF corresponds to each axis	Three	Rotational motion
Number of rigid elements/links	Three (base, elbow, and wrist)	
Link length of the above	70,100 and 70	mm
Work-volume	Link-1 turn: 360 Link-2 turn: 180, −180 Link-3 turn: up to 270°	Rotation in degrees

$$T_3^0 = T_0^1 * T_1^2 * T_2^3 \tag{1}$$

Therefore, the arm equation of the developed manipulator is

$$T_3^0 = \begin{bmatrix} \cos(\theta_1+\theta_2+\theta_3) & -\sin(\theta_1+\theta_2+\theta_3) & 0 & r_{14} \\ \sin(\theta_1+\theta_2+\theta_3) & \cos(\theta_1+\theta_2+\theta_3) & 0 & r_{24} \\ 0 & 0 & 0 & 0 \\ 0 & 0 & 0 & 1 \end{bmatrix} \tag{2}$$

where

$$r_{14} = l_1 \cos\,\theta_1 + l_2 \cos(\theta_1+\theta_2) + l_3 \cos(\theta_1+\theta_2+\theta_3);$$
$$r_{24} = l_1 \sin\,\theta_1 + l_2 \sin(\theta_1+\theta_2) + l_3 \sin(\theta_1+\theta_2+\theta_3)$$

represent the Cartesian coordinates of the end effector position.

2.2 End Effector Position Estimation

A basic mathematical methodology is actualized to take care of the backward kinematic issue. Figure 2 represents the line diagram of the modeled manipulator. From the time when the point (θ_3) relies on upon elbow edge (θ_2), so there will be ″2 wrist edges comparing to every connection development (left and right or upward and descending).

The base point can be controlled by Eq. (3)

$$\text{Base point}\,\theta_1 = \arctan(r_{14}/r_{24}) \tag{3}$$

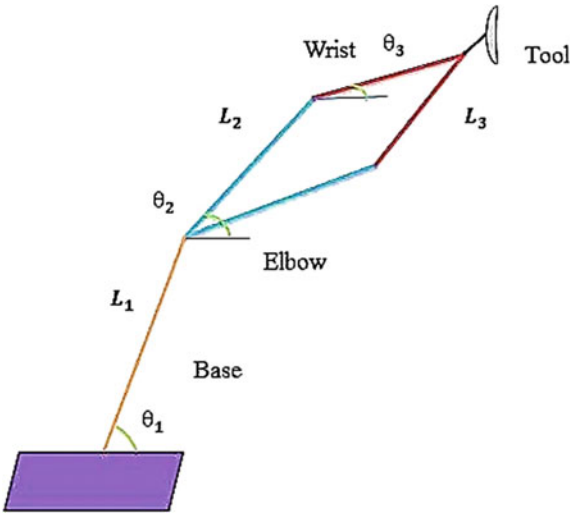

Fig. 2 Line diagram for performing kinematic analysis

Subsequent to finding θ_1, a three-revolute issue can be changed over to two-revolute planar issue. Therefore, two joint points ($\pm\theta_3$) will be obtained for the same instrument point as follows:

The controller end point worldwide location is given as per Eqs. (4) and (5)

$$Y = l_2 \cos\ \theta_2 + l_3 \cos(\theta_2 + \theta_3) \tag{4}$$

$$Z = l_2 \sin\ \theta_2 + l_3 \sin(\theta_2 + \theta_3) \tag{5}$$

Therefore,

$$\theta_3 = \cos^{-1}\left(\frac{Y^2 + Z^2 - l_2^2 - l_3^2}{2l_2 l_3}\right) \tag{6}$$

To calculate θ_2, arc tan function can be used as per Eq. (7)

$$\theta_2 = \pm a\tan 2\sqrt{\frac{(l_2 + l_3)^2 - (Y^2 + Z^2)}{(Y^2 + Z^2) - (l_2 - l_3)^2}} \tag{7}$$

These two arrangements are rung as elbow up and down positions and corresponding joint angle θ_2 are given by

$$\theta_2 = a\tan 2\frac{Z}{Y} + a\tan 2\left(\frac{l_3 \sin\ \theta_3}{l_2 + l_3 \cos\ \theta_3}\right) \quad \theta_2 = a\tan 2\frac{Z}{Y} - a\tan 2\left(\frac{l_3 \sin\ \theta_3}{l_2 + l_3 \cos\ \theta_3}\right)$$

3 Seam Tracking Approach

For the available 3D model, it is anything but difficult to know the geometry of the weld crease shape. Current methodology, control positions are reflected alongside the length/outskirts of the weld job. These points of inverse edges are associated through a bend further these bends are drawn along the whole length. By joining the center points of every bend, we would get a way and that way is only weld seam as appeared in Fig. 3. This systematic approach is called as sewing strategy and it can be displayed in CATIA which appeared in Fig. 4.

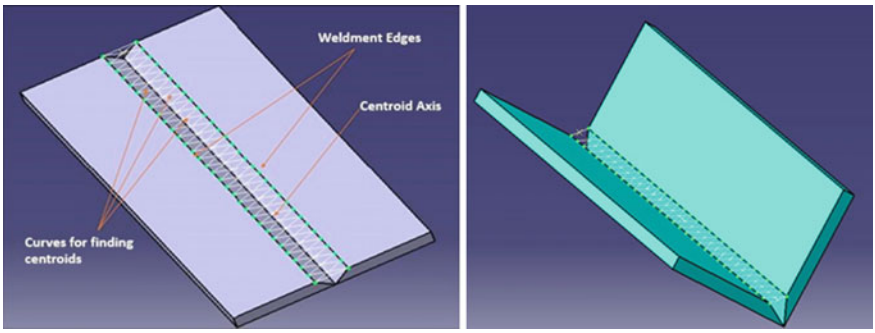

Fig. 3 Sewing technique for butt and L-shape joints

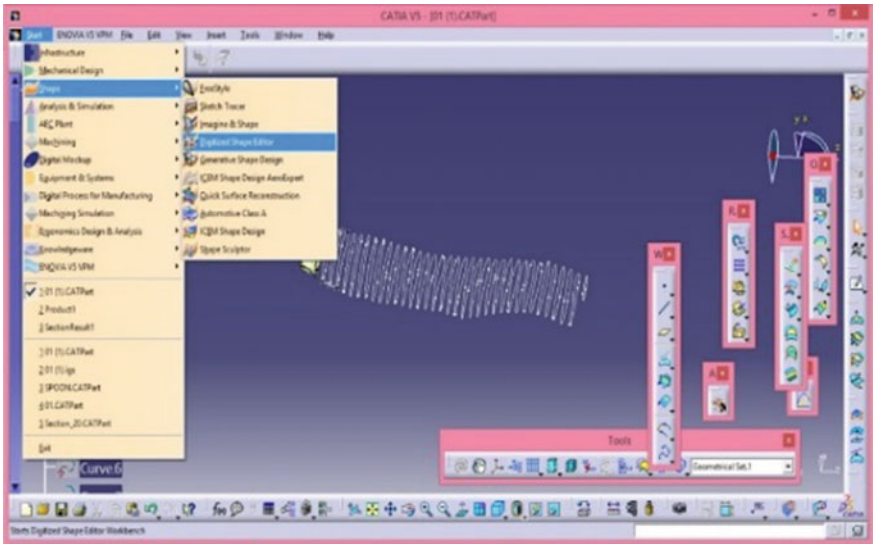

Fig. 4 Sewing diagram in CATIA

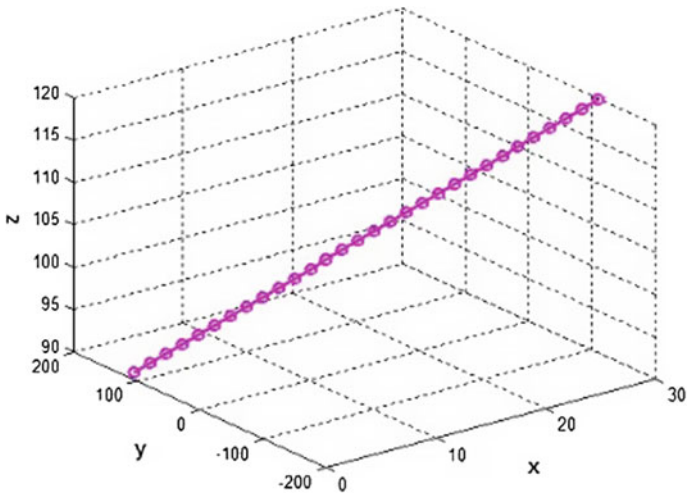

Fig. 5 Weld seam to be followed by robot

3.1 Extracting Coordinate Data from CAD Geometry of Weld Joints and Importing Same to MATLAB

The crease coordinate information from sewing procedure can extricate effortlessly. The project has been produced in CATIA to separate the point coordinate information into Excel. By opening CATIA window with seam path and by clicking on the program directly we can get the point coordinates in Excel sheet and then imported the same data to MATLAB. The 3D plot has been generated there for the weld seam coordinate data and it is shown in Fig. 5. With the known weld crease arranges it is anything but difficult to get the parameters of a robot controller. At long last, the robot would operate the welding task.

4 Welding Task in Virtual Environment

The got geometric way (crease way) and motion requirements will be input information to the modeled automated robot to execute welding operation. This manipulator is referred to the info parameters prior to execute welding. Present study deals with the examination the path planning is performed by third-order cubic spline introduction.

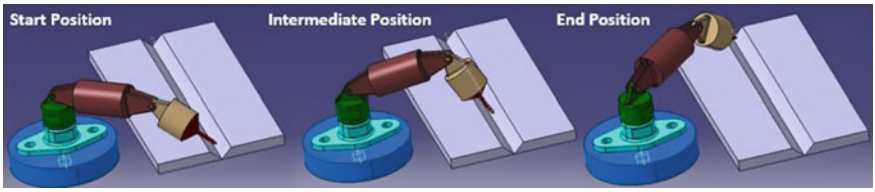

Fig. 6 Welding task for butt joint in virtual environment

Equation (8) represents the cubic spline trajectory representation with necessary boundary constraints:

$$\begin{aligned} &S(t) = \mathrm{b1} * t^3 + \mathrm{b2} * t^2 + \mathrm{b3} * t + \mathrm{b4} \\ &\text{At } t = 0, \mathrm{b4} = S_0(\text{given}) \text{ and } v_0 = \mathrm{b3};\ \text{At } t = 1, \mathrm{b1} + \mathrm{b2} + \mathrm{b3} + S_0 = S_f \\ &v_f = \left(3\mathrm{b1} * t^2 + 2\mathrm{b2} * t + \mathrm{b3}\right);\ a_f = (6\mathrm{b1} * t + 2\mathrm{b2}) \end{aligned} \tag{8}$$

The developed method is implemented to perform welding operation in the virtual environment. A typical operation for butt welded joint is represented in Fig. 6.

5 Assessment with Earlier Research

A percentage of the previous exploration showed speaks to the different philosophies for performing seam tracking and welding task. An itemized correlation is illustrated in Table 2.

Table 2 Evaluation with earlier techniques

Past work	Technique for seam tracking	Recognition of seam start and end points	Trajectory with respect to kinematics
[7]	Perception with optic sensor	Yes	No
[8]	Perception with laser sensor	No	Yes
[13]	Computer modeling	No	Yes
Current study	CAD assisted	Yes	Yes

6 Conclusion

The current research work meted to mimic the 3-pivoted automated manipulator in computer-aided atmosphere for executing welding task despite the fact taking after the weld crease way and its posture analysis requirements. Another crease following philosophy, named sewing procedure has presented for the welded joints accessible in virtual workspace. Acceptance of the created technique performed through reenactment outcomes while carrying out welding processes with various weld contours.

References

1. Ali T. Hasan, A.M.S. Hamouda, N. Ismail, H.M.A.A. Al-Assadi, (2006) An adaptive-learning algorithm to solve the inverse kinematics problem of a 6 D.O.F serial robot manipulator, Advances in Engineering Software, 37(7), pp. 432–438.
2. Deepak, B. B. V. L., Parhi, D. R., & Raju, B. M. V. A. (2014). Advance particle swarm optimization-based navigational controller for mobile robot. Arabian Journal for Science and Engineering, 39(8), 6477–6487.
3. Eliot, E., Deepak, B., Parhi, D., & Srinivas, J. (2013), Design & Kinematic Analysis of an Articulated Robotic Manipulator. International Journal of Mechanical and Industrial Engineering, 3(1), 105–108.
4. Deepak, B. B. V. L., Parhi, D. R., &Jha, A. K. (2011). Kinematic Model of Wheeled Mobile Robots. Int. J. on Recent Trends in Engineering & Technology, 5(04).
5. Parhi, D. R., & Deepak, B. B. V. L. (2011). Kinematic model of three wheeled mobile robot. Journal of Mechanical Engineering Research, 3(9), 307–318.
6. Dayal R P, Deepak B, Nayak D, Anand A. (2012), Forward and Inverse Kinematic Models for an Articulated Robotic Manipulator, International Journal of Artificial Intelligence and Computational Research, 4 (2): 103–109.
7. Bae, K. Y., Lee, T. H., &Ahn, K. C. (2002). An optical sensing system for seam tracking and weld pool control in gas metal arc welding of steel pipe. Journal of Materials Processing Technology, 120(1), 458–465.
8. Yoo, W. S., & Na, S. J. (2003). Determination of 3-D weld seams in ship blocks using a laser vision sensor and a neural network. Journal of manufacturing systems, 22(4), 340–347.
9. Deepak, B. B. V. L., Parhi, D. R., & Kundu, S. (2012). Innate immune based path planner of an autonomous mobile robot. Procedia Engineering, 38, 2663–2671.
10. Deepak, B. B. & Parhi, D. R. (2013, December). Target seeking behaviour of an intelligent mobile robot using advanced particle swarm optimization. In Control, Automation, Robotics and Embedded Systems, 2013 International Conference on (pp. 1–6). IEEE.
11. E.J Van Henten, J Hemming, B.A.J Van Tuijl, J.G Kornet and J Bontsema, (2003), Collision-free Motion Planning for a Cucumber Picking Robot, Biosystems Engineering, 86 (2), pp. 135–144.
12. Deepak, B. B. & Parhi, D. (2013). Intelligent adaptive immune-based motion planner of a mobile robot in cluttered environment. Intelligent Service Robotics, 6(3), 155–162.
13. B.B.V.L. Deepak & Dayal R. Parhi (2016), Control of an automated mobile manipulator using artificial immune system, Journal of Experimental & Theoretical Artificial Intelligence, 28:1–2, 417-439.

14. K.K. Kumar, Dr. A. Srinath, G. J. Anvesh, R. P. Sai and M. Suresh, Kinematic analysis and simulation of 6- DOF KUKAKr5 robot for welding application, International journal of Engineering Research and Applications, Vol. 3, no. 2, 2013, PP. 820–827.
15. M.V.A. Raju Bahubalendruni, Deepak B B V L Bibhuti Bhusan Biswal, (2016), "An advanced immune based strategy to obtain an optimal feasible assembly sequence", Assembly Automation, Vol. 36 Iss 2, doi:10.1108/AA-10-2015-086.

Modeling and Simulation for Conductivity of Germanium and YBCO

Rakesh Mohan Bhatt

Abstract With the advent of computer, modeling and simulation techniques have achieved a new height. To address the various issues related to the model of a system, simulation techniques have become the essential tool where the model represents the best understanding of the proposed system in an abstract way to explain and verify the actions affecting the real-world system. The present paper explores the simulation process in measuring the conductivity of Germanium (Ge) semiconductor and YBCO superconductor by deploying the mathematical model and simulation approach. Mathematical model has been considered as per Callaway et al. [1] in a modified form. Interesting results have been noticed in both the cases as far as the behavior of various scattering strengths involved in the thermal conduction is concerned. Thus, modeling and simulation not only estimates the results but also enables to understand the behavior of terms or components involved in the process.

Keywords Modeling · Simulation · Conductivity · YBCO · Germanium

1 Introduction

In addressing various issues related with the model of a system, simulation technology has become an essential tool in the age of digital computing. A system comprises of several components and their interfaces which is simplified and represented in the form of a model to mimic the real-world situation. However, simulation can only reduce the resources and time involved; it does not replace the actual/real experimental work. Besides that, it also enables to perceive the

R.M. Bhatt (✉)
Department of Computer Science & Engineering, HNB Garhwal University, Srinagar, Uttrakhand, India
e-mail: rmbhatt77@yahoo.com

D.K. Lobiyal et al. (eds.), *Proceedings of the International Conference on Signal, Networks, Computing, and Systems*, Lecture Notes in Electrical Engineering 396, DOI 10.1007/978-81-322-3589-7_33

interactions that would otherwise not be possible. Almost in every area, it maybe physics, chemistry, or economics, modeling and simulation have been carried out [2, 3].

Due to increased demand of Germanium, the research has been going on for its applications in fiber optics communication networks, infrared night vision systems, etc. Earlier approaches have also been studied [4, 5]. Further, superconducting systems promise wide applications for human welfare, particularly in the areas of communication, medical scanners, etc. [6, 7]. Thus, the estimation of the thermal conductivity of $Yba_2Cu_3O_7$ superconductors has been a great interest among the researchers [8, 9].

2 Modeling and Simulation

Some decades back, computer facility was used as a supplement but now Modeling and Simulation based on computer has become the most important methodology in many areas of applications [10]. System modeling, system studies are generally conducted with a model of the system. The present study considers maximum details of the system as a model is not a substitute for a real system, but simplifies the system taken into account. A model is manipulated through the simulation to enable to compress time and space [11]. The present approach is an extension of the previous work [5] which enables to accomplish a time and space compression between the interrelationships within a system.

Naylor [12] proposed 12 reasons so as to consider the simulation be useful for particular applications. In the present context, some of them are

(i) Simulation can be used to experiment with new situations about which little or no information is available, so as to prepare for what may happen.
(ii) Simulation can serve as a "pre-service test" to try out new policies and decision rules for operating a system, before running on the real system.

3 Germanium Semiconductor

In estimating phonon conductivity of the Germanium semiconductor, the Callaway's phenomenological model [1], workers have directly assumed that the relaxation rates due to isotopic impurities ($\tau_D^{-1} \sim A\omega^4$) and anharmonic interactions ($\tau_A^{-1} = B\omega^2 T^3$) are independent of each other. The present analysis discusses the inter-dependence of these relaxation rates in the form of a cross term (Γ^{AD}) [4] and its role in estimation of the phonon conductivity in the temperature range of 2–100 K.

4 YBCO Superconductor

Research investigation in the field of high-temperature superconductors have been carried by several workers due to its peculiar and inherent properties. This has provided a gate through to open the theoretical and experimental investigations for the industrial applications [10]. For high-temperature superconductors, transport properties have been reviewed by Tewordth and Wolkhausan theory [8], and Ravindran et al. [13]. This inclusion shows the good impact on the conductivity calculations. In the present analyses, conductivity has been measured in the temperature range of 10–240 K.

5 Analyses

The analyses of thermal conductivities of Germanium and YBCO have been done in adopting their respective conductivity model in the following subsections.

5.1 Germanium Conductivity Model

The thermal conductivity of Germanium (Ge) has been analyzed in the range 2–50 K by Srivastav and Kumar [14], where it has been shown that by using Callaway's model. The present analysis is based on the modified version [4] of Callaway's model [1] which includes the term $D\omega^3 T$ with the following expression for τ^{-1}

$$\tau^{-1} = v/FL + A\omega^4 + (B_1 + B_2)\omega^2 T^3 + D\omega^3 T \tag{1}$$

Here, v is the velocity, L is the Casimir length, F denotes the acoustic mismatch, A is the isotopic scattering, B_1 + B_2 are normal and Umklapp scattering processes, D is interaction parameter, ω is the angular frequency, and T is temperature. The term $D\omega^3 T$ depicts the interaction between mass defect and cubic anharmonic parameters.

5.2 YBCO Conductivity Model

The present model is different from the approach of Ravindran et al. [13]. Here, the interference scattering term $\delta x^3 t^4$ have also been considered [4]. Thus, the thermal conductivity model of Callaway's [1] is given by [4] has been taken for the estimation of thermal conductivity of the $YBa_2Cu_3O_7$ superconductor as follows:

$$\mathrm{K} = At^3 \int x^4 \mathrm{e}^x \Big/ \left[(\mathrm{e}^x - 1)^2 \cdot F(t,x)\right] \mathrm{d}x. \tag{2}$$

where $F(t, x)$ is

$$F(t,\, x) = \left[1 + \alpha x^4 t^4 + \beta x^2 t^2 + \gamma t x g(x,y) + \delta x^3 t^4 + \in x^2 t^4\right]. \tag{3}$$

In the above equation, the parameters A, α, β, γ, δ, and $\in$ refer the boundary scattering, point defect scattering, sheet-like fault, electron–phonon scattering, interference scattering (between point defect and 3-phonon processes) and 3-phonon scattering, respectively. Another term, t (= T/T_c) is the reduced energy, where T_c is the transition temperature of $YBa_2Cu_3O_7$ superconductors. Further, $g(x, y)$ is the BRT function, defined by Bardeen et al. [15].

6 Result

Following sections discusses the result of thermal conductivity measurements in both the materials using modeling and simulation technique on the above models.

6.1 Conductivity Estimation for Germanium

It is obvious from Fig. 1, through simulation process by taking different values such as F, B (= $B1$ + $B2$), and D, elevated conductivity is obtained nearly at the same temperature. Table 1 illustrates the value of the parameters and the corresponding conductivity value has been tabulated in Table 2 and the temperatures range from 2–100 °K.

6.2 Conductivity Estimation for YBCO

If interference scattering strength (δ) is increased from 225 to 235 as shown in Table 3, then the maximum conductivity shifted from 50 K to 40 K with slightly lower value, i.e., from 3.9596 (at δ = 225 K) to 3.8766 (at δ = 235). Further, by increasing the value of boundary scattering strength (A) from 4.10 to 4.25, increase in the value of conductivity from 3.9566 to 4.1044 has been observed as shown in Table 4. The results have also been graphically shown in Fig. 2.Values of other scattering strengts are taken as 20.0 for the point defect, 35.0 for sheet-like fault, 50.0 for electron-phonon scattering, and 3-phonon scattering strenghts in the present computations.

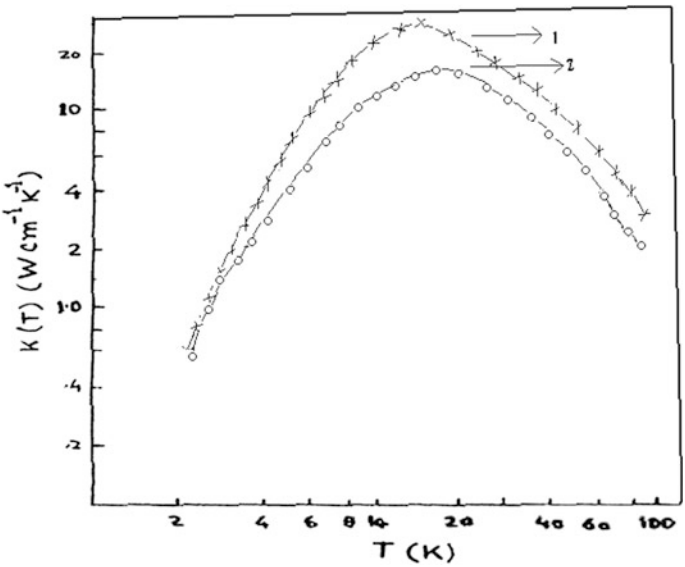

Fig. 1 Germanium conductivity

Table 1 Parameters for Germanium

Set/parameters	V ($\times 10^5$ cm/s)	L	F	ΘD	A ($\times 10^{-44}$ s^3)	$B1 + B2$ ($\times 10^{-23}$ s K^{-3})	D ($\times 10^{-33}$ s^3 K^{-1})
1	3.5	0.24	0.75	376.0	2.40	3.43	1.203
2	3.5	0.24	0.77	376.0	2.40	3.43	1.203

Table 2 Conductivity values for Germanium

Parameters	Value-1	Value-2	Parameters	Value-1	Value-2
2	00.4642	00.4566	50	07.9046	05.1480
10	15.3128	09.7649	74	04.0591	02.7145
22	19.9798	12.0494	86	03.1013	02.0952
30	15.7141	09.7505	94	02.6398	01.7943
42	10.2995	06.6168	100	02.3585	01.6098

Table 3 Conductivity values at $A = 4.10$ for YBCO

Temp. (K)	$\delta = 225$	$\delta = 230$	$\delta = 235$
10	1.5735	1.5694	1.5645
30	3.7439	3.7114	3.6796
50	3.9596	3.9148	3.8712
70	3.7024	3.6563	3.6114
110	2.8752	2.8365	2.7988
150	2.1511	2.1220	2.0938
190	1.6470	1.6253	1.6042
210	1.4587	1.4398	1.4214
240	1.2332	1.2176	1.2024

Table 4 Conductivity values at $A = 4.25$ for YBCO

Temp. (K)	$\delta = 225$	$\delta = 230$	$\delta = 235$
10	1.6311	1.6268	1.6225
30	3.8808	3.8472	3.8142
50	4.1044	4.0581	4.0129
70	3.8379	3.7900	3.7435
110	2.9804	2.9402	2.9012
150	2.2298	2.1997	2.1704
190	1.7073	1.6848	1.6629
210	1.5121	1.4925	1.4734
240	1.2783	1.2622	1.2464

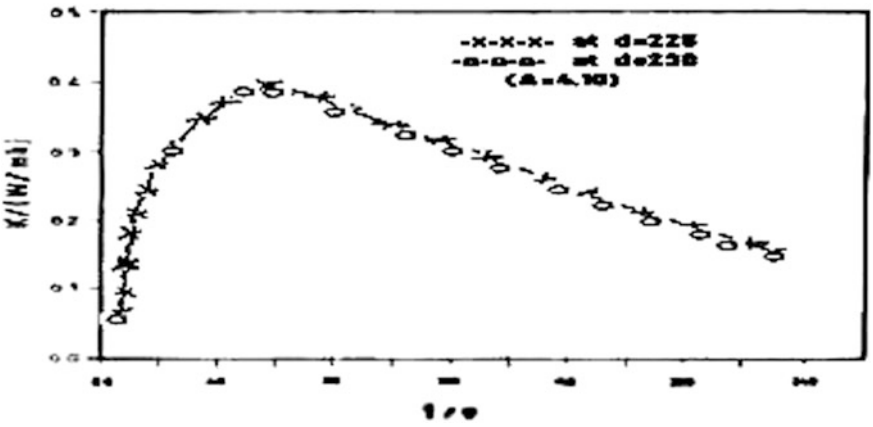

Fig. 2 YBCO conductivity

7 Conclusion

In both the material, simulation process has shown interesting results in reflecting the behavior of various parameters involved such as by increasing the value of boundary scattering strength (A), increase in the value of conductivity has been observed.

References

1. Callaway, Joseph, Phys. Rev. Vol. 113 (1959) 1046.
2. Naylor, T.H., Chang, Computer simulation experimentation with models of economic systems, John Wiley and sons, New York (1971).
3. Osetsky, Yu N. Computer-simulation study of high temperature phase stability in iron, Phys. Rev. B-57, No. 2 (1998) 755–763.

4. Gairola, R.P., Phys. St. Sol. (b) Vol. 125 (1985) 65.
5. Bhatt, R.M., Gairola, R.P., Simulation Analysis for Phonon Conductivity of Germanium. In: Chakravarthy, C.R., Patnaik, L.M., Ravi, M.L., Sabapathy, T., (eds.): Harnessing and Managing Knowledge, CSI Publication (2002) 220–223.
6. Vail, J.M., Emberly, E., Lu, T., Simulation of point defects in high-density lumeinscent crystals: oxygen in barium fluoride, Phys. Rev. B-57, No. 2, (1998).
7. Choi, Hyo-Sang, Bae, Ok, Kim, Hye-Rim, Park, Kwon-Bae, Switching Properties of a Hybrid Type Superconducting Fault Current Limiter Using YBCO strips, IEEE transaction on applied superconductivity, Vol. 14, No. 3, (2002) 1833–1837.
8. Teward, L., Wolkhausan, Th., St. Commun., Vol. 70, (1989) 839.
9. Srinivasan, R., Studies on High Temperature Superconductors, Anant Narlikar (ed): Superconductors, Nova Science Publisher, NY, Vol. 6, (1989) 263.
10. Shanon, R.F., Simulation: A survey with research suggestions, AIIE Transaction 7(3) (1975).
11. Law, Avril M. (ed.): Simulation Modeling and Analysis, Tata McGraw Hill, 4th Edition, (2008).
12. Naylor, T.H. (ed.): Computer simulation experiments with models of economic systems, John Wiley and sons, New York, (1971).
13. Ravindran, T. R, Sankaranarayana, V., Srinivasan, R. Pramana-J. Physics, Vol. 32, (1992) 109.
14. Srivastava, G.C., Kumar, Anil, Phys. Rev. B-25 (1982) 2560.
15. Bardeen, J., Rickayzen, G. Tewordt, L., Phys. Rev., Vol. 113 (1959) 982.

Cryptoviral Extortion: Evolution, Scenarios, and Analysis

Bharti Nagpal and Vinayak Wadhwa

Abstract "Cryptography" is a blessing to cyber security. People can store information securely and communicate privately over long distances. It is rapidly advancing and improving, but it is also making a ladder for cryptography-based viral attacks. This paper gives better understanding of the concept of "Cryptovirology" which presents how cryptography can also be misused in the world of cyber crime. Cryptovirology gives malware enhanced privacy and such malwares are not easily reverse engineered. Moreover, it gives the attacker enhanced obscurity while the Cryptovirus is communicating with attacker. Loss of access, confidentiality and leakage of critical data can be achieved with the help of same cryptographic concepts. Analysis and understanding of such attacks leads us to many fascinating methodologies and conclusions.

Keywords Cryptovirology · Ransomware · Cryptovirus · Information extortion attack

1 Introduction

Cryptography has been a boon to information security society. It is rapidly advancing and improving but is also making a ladder for cryptography-based viral attacks. Cryptovirology is the study of application of cryptography to build malicious software (Malwares) [1]. The scope of cryptovirology has expanded ever since its birth in academia [2]. Cryptography has been used to make malicious creation more rigid in detection and analysis.

Extortion-based Cryptovirus or better termed as "Ransomware" is relatively old. It may be generally defined as, "Ransomware, a kind of malware which demands a

B. Nagpal · V. Wadhwa (✉)
Ambedkar Institute of Advanced Communication Technologies and Research, Delhi, India
e-mail: vkw1954@gmail.com

B. Nagpal
e-mail: bharti_553@yahoo.com

D.K. Lobiyal et al. (eds.), *Proceedings of the International Conference on Signal, Networks, Computing, and Systems*, Lecture Notes in Electrical Engineering 396, DOI 10.1007/978-81-322-3589-7_34

payment in exchange for a stolen functionality" [3]. This field emerged with the concept that public key cryptography can create asymmetry between what a virus writer knows about virus and what a virus analyst can know by analysis of virus. This asymmetry can be exploited, as in case of Ransomwares. They are used for mass extortion, being widely spread in forms of cryptovirus, cryptotrojan, and cryptoworm.

Ransomwares have been in existence for over a decade. Earlier examples were either ineffective or easily mitigated, dating back to 1989, when a logic bomb named AIDS Trojan encrypted victim's files with monoalphabetic substitution cipher and asked ransom claim to decrypt hard disk. With the advent of such a phenomenon, researchers like Adam L. Young and Moti M. Yung, investigated and introduced the idea of Cryptovirology in a paper called "Cryptovirology: Extortion-based security threats and countermeasures" [2]. They suggested amalgamation of strong cryptography algorithms with computer virus like Trojan horse technology, which can allow virus writer or attacker to gain explicit access control of the victim's critical data that virus has access to. Experts at protection mechanisms need to be well aware and comprehend the potential ferocity and sophistication of such cryptographic viruses.

In late 2013, a potent wave of ransomwares appeared beginning with a version that was dubbed the name "Cryptolocker." This malware had the capability to encrypt whole windows drive in 30 min. It started a countdown timer for 72 h, notifying victim of the situation and demanding money in exchange for the data. When timer was over, the malware destructed the key to decrypt the data, and access to that data was lost forever. A new development over Ransomwares has been in action recently, called Ransomweb. Cybercriminals are making malwares that encrypt websites/server database and are demanding money against decryption. There are a number of vulnerable servers that are not updated frequently and are therefore susceptible to such attacks hence payloads to such viruses are crafted in a way that vulnerable server's critical data is encrypted. Information extortion attacks have also been around, wherein cybercriminal encrypts critical data forcing victim to give desired data in exchange. As an attacker, these attacks are relatively rare and require more skill. This paper highlights and explores the evolution of a Cryptovirus including extortion attack methodologies and scenarios. Further, an analysis of recent Cryptovirus trend is also given.

2 Attack Methodology and Scenarios

2.1 Cryptoviral Extortion Attack Methodologies

Cryptoviral Extortion

Cryptoviral extortion is a denial of resource (DOR) attack, which exploits the asymmetric nature of public key cryptography to make critical data unintelligible to

victim. It uses hybrid cryptosystem. Critical data is encrypted, while the original data is either overwritten or deleted in the process. It can be well understood in three phases of the attack. The attack is also inferable via diagrammatic representation in following section hybrid approach to cryptoviral extortion, in Fig. 2. The first phase begins with attacker generating an asymmetric key pair, keeping its secret key with himself and exporting public key with the Cryptovirus. In the second phase, Cryptovirus is activated across hundreds of victim computer systems. On each machine, the Cryptovirus will be generating a symmetric encryption key pair and an initialization vector. This is done with the help of a true random number generator. Critical data in the system will be encrypted using such symmetric encryption key pair and an initialization vector. The initialization vector and symmetric key is then concatenated and encrypted by the asymmetric public key and is sent to virus writer. The third phase is where the encrypted data is held for ransom and victim is asked to give ransom over some anonymous e-cash platform. With the ransom paid, virus writer decrypts the initialization vector and symmetric key via the private asymmetric key he possesses, and accordingly sends decrypted symmetric encryption key and an initialization vector to victim. Victim is finally able to recover data by decrypting his critical data with received symmetric encryption key and an initialization vector. Different methodologies for the attack have been explored below.

Native Methodology [2]

Asymmetric encryption is used in native approach, demonstrated in Fig. 1. Personal data is encrypted via an asymmetric encryption algorithm like RSA using asymmetric public key, corresponding private key of which is with the attacker. Attacker demands ransom in return for providing victim with the private key and procedure to decrypt the personal data.

Hybrid Methodology [2]

The Cryptovirus is implemented using a hybrid cryptosystem in hybrid methodology. It has a powerful random number generator and a strong seeding process. Figure 2, shown in the next page, demonstrates this methodology. The virus writer embeds true random number bit generator in the Cryptovirus, which generates initialization vector IV and random session key Ks. Assuming that

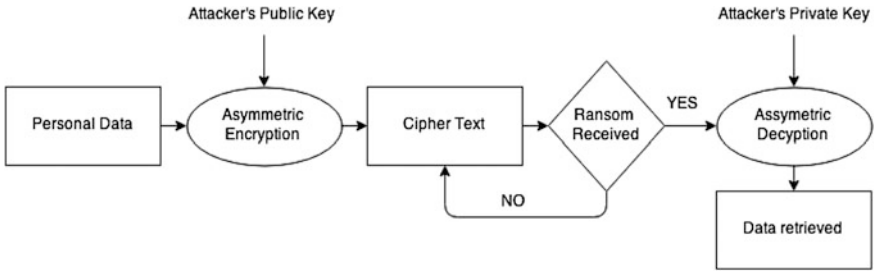

Fig. 1 Native methodology of cryptoviral extortion attack

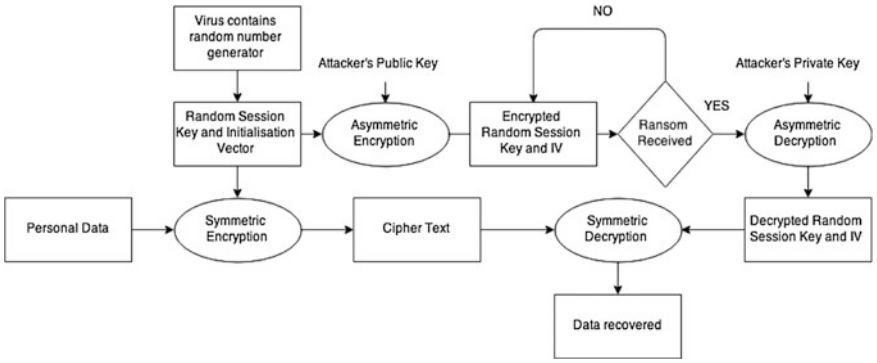

Fig. 2 Hybrid methodology of cryptoviral extortion attack

victim's system/network is already compromised by the attacker, which subsequently leads to attacker encrypting victim's critical data by a symmetric algorithm using generated IV and Ks. The session key and IV are itself encrypted with the help of asymmetric algorithm, using asymmetric public key already embedded in the virus by the attacker. The critical data is overwritten with the encrypted data. Now, victim is notified about the seizure of data and ransom details. If victim has paid the ransom, the attacker decrypts IV and Ks with the private asymmetric key and sends it to victim and accordingly victim can retrieve his/her critical data.

Table 1 given below compares the different methodologies discussed so far.

Table 1 Comparison between different methodologies for Cryptoviral extortion attack

Features	Native methodology	Hybrid methodology
Simplicity	Fairly simple	Complex
Encryption used to encrypt critical data	Asymmetric encryption to encrypt data like RSA	Symmetric encryption for encrypted data like AES, and asymmetric encryption to encrypt symmetric key and initialization vector
Risk of getting caught	Very high	Fairly low
Drawbacks	Asymmetric secret key is given to the victim, who may release it to everyone. To overcome above problem, it leads to increase in overhead of key management. Encryption of data directly with asymmetric public key is time consuming. This was overcome with development of hybrid methodology	Hybrid encryption requires a true random number generator to be embedded in virus; it must be able to generate truly random numbers. Hybrid encryption can be interrupted before it communicates with virus author, and can be reverse engineered to find IV and Symmetric shared key
Advantages	It is fairly simple and native in approach. It lays the basics of attack	It is complex and has a faster approach than native

2.2 Cryptoviral Extortion Attack Scenarios

Scenario 1—Cryptoviral Monetary Extortion based on Hybrid cryptosystem

The hybrid cryptosystem attack is based on hybrid encryption algorithm. The critical data is encrypted and is overwritten or deleted from victim's system.

The attack scenario procedure: A pair of public and private key (Asymmetric key pair) is generated by attacker and the public key is embedded in virus. The private key from pair is managed and is handled exclusively by the attacker. Attacker then launches the virus through the internet spreading it via spam mails, malicious files, and other general initial attack vectors. The victim is compromised if defense mechanism is not up to the mark. The Cryptovirus, essentially the payload, now comes in action and a random symmetric key (Session key) is generated. Initialization Vector (IV) is also generated for seeding. Critical data files are now encrypted and chained using chaining modes like Cipher Block Chaining (CBC). The critical data now maybe deleted or overwritten. Session key and IV are now concatenated and encrypted using public key (embedded in Cryptovirus). Now, Cryptovirus discloses its presence and holds the critical data for ransom. After the payment is successful (using anonymous payment methods) the attacker asks victim to send the encrypted IV and session keys. Attacker decrypts them with his private key and sends them to the victim.

Scenario 2—Cryptoviral Information Extortion based on Hybrid Cryptosystem

Just as monetary gain is achieved by hijacking data, similarly trade between desired information is done, to let go of the encrypted critical data. This may be used for information warfare or as a tool for espionage. Additional feature of authenticating the desired data is also displayed in the flow charts.

First, the Critical Data C is found from the whitelist that Cryptovirus has (based on extensions); then this data is encrypted using session key and an IV (Initialization Vector). Critical Data is deleted and only its encrypted copy remains. This is visible in Fig. 3 that is shown in the next page. Now, Desired Data H is

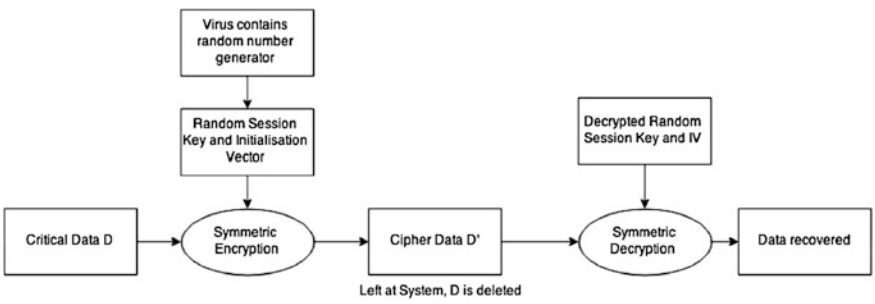

Fig. 3 Encryption and decryption of critical data in information extortion attack

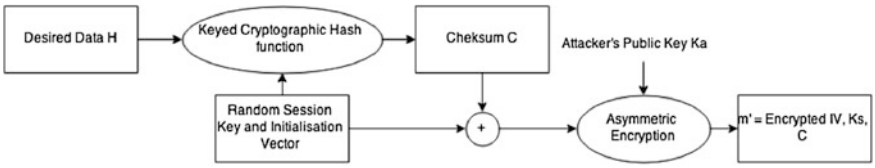

Fig. 4 Encryption and authentication of desired data in information extortion attack

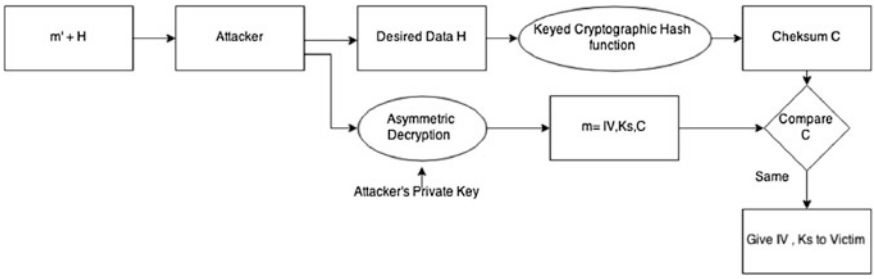

Fig. 5 Decryption and authentication of desired data by attacker in information extortion attack

found and keyed cryptographic hash function is taken of H using Initialization Vector IV and Session key, namely Ks. It results in a Checksum. This Checksum along with Session key and IV are encrypted with the public key of attacker. This is referred as m'. This is demonstrated in Fig. 4, shown in next page. Now, the victim is made to know about the attack and is demanded to send m' and the desired data H. Victim is unable to cheat attacker by sending altered H or m', as forgery to this must be done without the knowledge of Checksum, IV, and Session key. Once victim sends H and m', attacker decrypts m' to get session key, IV, and Checksum. Now, attacker authenticates that H is authentic by taking its checksum and comparing it with the decrypted one, as demonstrated below in Fig. 5 in next page.

3 Latest Trends Observed in Ransomwares/Cryptoviral Extortion Attacks

Following trends are observed in current wave of ransomwares:

- Critical Data is chosen according to whitelist of possible extensions for critical data.
- Shared Secret key, using access controls within network to implement an attack as mentioned previously.

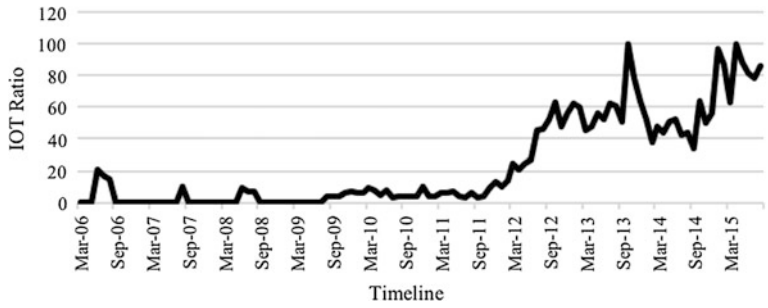

Fig. 6 "Ransomware"—Interest Over Time (IOT) [6]

- Takedown Resistant Command and Control Servers (C&C)—It is achieved by use of anonymizing networks nowadays. Earlier, peer to peer networks with resistance were achieved by the use of Domain Name Generation Algorithms (DNGA).
  - Peer to peer Networks: Infected systems interact with each other to relay commands from attacker.
  - Domain Generation Algorithms: Generation of possible C2C domains that vary over time. Example—Conficker Virus was able to generate 50,000 domains in a day at its peak [4].
  - Abusing Anonymizing Tor Network: Exploited by Cryptolocker version 2.0, use of such networks allow to hardcode C&C URLs instead of using DNGA.
  - Abusing I2p networks: Exploited by Cryptolocker v3.0, I2p users are offered anonymity for I2p services and anonymous web access.
- Usage of hard to trace anonymous Bitcoin crypto currency.
- Evolution of Encryption is actually a boon to development of such viruses which use practically unbreakable algorithms for encryption.
- Use of droppers, anti analysis and persistence increases the survivability of such viruses, with complex obfuscations [5].

Figure 6, given below, illustrates the Interest Over Time (IOT) trend of the term "Ransomware". IOT Ratio signifies how often a particular search is entered in comparison to global search volume across world [6]. It is justified as the potential wave of Cryptoviruses which has been spreading worldwide beginning 2012, with Reveton, followed by Dirty Decrypt, Cryptolocker, CryptoWall in 2013 and more devious Citroni/CBT Locker, TorrentLocker in 2014.

4 Countermeasures

Table 2 given below, explains briefly about the plausible countermeasures for defense against cryptoviral attacks.

Table 2 Defense measures: Cryptoviral extortion attacks

S. No.	User defense measures	OS defense measures	Cryptoviral specific defense measures
1	Regular backup of critical data	Use of smart card or Pluggable Authentication Module (PAM) for authentication to System's cryptographic API	Installing triggers on known attack file—locations for a Cryptovirus
2	Regularly update antivirus and use of firewalls and Intrusion detection and prevention systems	Public encryption key must be taken from trusted certificate	Use of tools like PowerShell to batch commands and filter out infected areas with the help of registry

References

1. Kumar, M., Kumar, R.: Cryptoviral Extortion: A virus based approach. In: International Journal of Computer Trends and Technology (IJCTT), Volume 4, Issue 5, pp. 1149–1153. International Journal of Computer Trends and Technology (2013).
2. Young, A., Yung, M.: Cryptovirology: extortion based security threats and countermeasures. In: IEEE Symposium on Security and Privacy, pp. 129–141. IEEE Computer Society Press, Oakland (1996).
3. Gazet, A., Comparative analysis of various ransomware virii. In: EICAR 2008 Extended Version, Journal in Computer Virology, Volume 6, Issue 1, pp 77–90. Springer-Verlag (2010).
4. Anandrao, S., Cryptovirology: Virus Approach In: International Journal of Network Security & Its Applications (IJNSA), Vol. 3, No. 4, pp 33–46. (July 2011).
5. Kotov, V., Rajpal M.: Report on Understanding Crypto-Ransomware, In-Depth analysis of most popular malware families, Bromium. http://www.bromium.com/sites/default/files/bromium-report-ransomware.pdf, (Sep 2014).
6. Google Trends for term "Ransomware", http://www.google.co.in/trends/explore#q=Ransomware&cat=0-5.

Utilization of Fractal Geometry for Phase Shifter Implementation

Amrita Chakraborty and Arpan Kumar Kar

Abstract This paper reports a study on the modified implementation of MEMS-based phase shifter devices. The field of Microelectromechanical Systems or MEMS had gained prominence in academic research during 1990s and has proved capability in the design and development of several RF devices, phase shifters being a crucial member in the group. Fractal curve, an iterative structure, mapping several points in two-dimensional space is employed to modify the structural layout of MEMS-based phase shifters. Higher order phase shifters like 90° and 180° require several MEMS bridges cascaded linearly on a Coplanar Waveguide (CPW) based transmission line (t-line), thus occupying large lateral length (∼few mm) and involving immense substrate wastage. MEMS phase shifters designs based on the iterative structure of Fractal Curve occupies lesser space and reports much lower loss performance when compared with linear cascaded structures in RF simulators.

Keywords Coplanar waveguide · Fractal curves · Moore curve · MEMS phase shifter · Miniaturization · Space-filling curves

1 Introduction

Microelectromechanical Systems or MEMS technology was initially restricted entirely for device fabrication in the field of microelectronics and device physics. However, MEMS technology was later utilized for development of devices operating at microwave and millimetre wave frequencies and hence, the term Radio

A. Chakraborty (✉)
Department of Electronics and Telecommunication Engineering,
Jadavpur University, Kolkata 700032, India
e-mail: amrita.chakraborty2@gmail.com

A.K. Kar
Information Systems, DMS, Indian Institute of Technology Delhi,
New Delhi 110016, India
e-mail: arpan_kar@yahoo.co.in

D.K. Lobiyal et al. (eds.), *Proceedings of the International Conference on Signal, Networks, Computing, and Systems*, Lecture Notes in Electrical Engineering 396, DOI 10.1007/978-81-322-3589-7_35

Frequency Microelectromechanical Systems (RF MEMS) came into limelight. RF switches, switched capacitors, tunable filters, resonators and phase shifters [1–10] constituted majority of the RF devices which were fabricated by the MEMS technology. It is a mandate for RF MEMS devices to (i) maintain all lateral dimensions of the device in micron and submicron order, (ii) contain an actuating portion capable of undergoing vibrations when subject to external voltage and (iii) adhere to the CMOS-based IC fabrication techniques only while implementing the devices. These conditions however, underline the fact that MEMS technology encourages the concept of miniaturization, without compromising on the overall device performance. Hence, authors have proposed the concept of introduction of Fractal geometry [11, 12] in the development of RF MEMS-based phase shifter structures. Fractal curves or the space-filling curves possess an inherent characteristic of accommodating a large line length within a fixed and compact area, thus reducing the overall device lateral dimensions manifold.

In [11, 12], authors have discussed the design of Fractal curve-based MEMS phase shifter structure employing Peano Curve and modified Hilbert Curve [13–16] based designs. The present work, however, reports the phase shifter design based on a Fractal curve known as the Moore Curve [13, 14], which is yet unexplored. Figure 1 shows the basic Moore Curve schematic and the iterations on which the phase shifter design has been based. It shows the first three iterations of the Moore curve, where, Fig. 1a shows the first iteration, Fig. 1b shows the second iteration and Fig. 1c shows the third iteration, respectively, based on which the MEMS-based phase shifter design has been structured.

The phase shifter design has been conducted using the Ansoft High Frequency Structure Simulator (HFSS) v.13 [17] software to obtain the S-parameters (in dB) to account for loss performance and differential phase shift at a frequency of 22 GHz, respectively. The frequency of 22 GHz falls under the K band (18–26 GHz by IEEE nomenclature) and is primarily suited for RADAR and satellite communications.

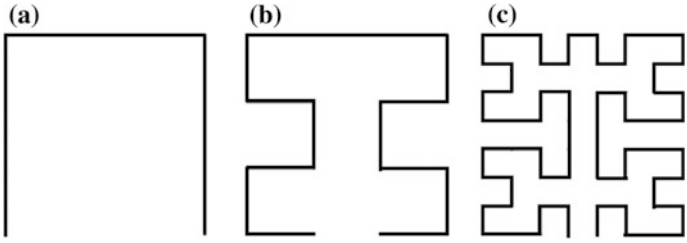

Fig. 1 Moore curve **a** first iteration, **b** second iteration and **c** third iteration

2 Device Design Strategy

The phase shifter is designed according to the Distributed MEMS Transmission Line (DMTL) principle, by which several similar bridge or beam-like structures are arranged on a Coplanar Waveguide (CPW) based transmission line (t-line) structure by means of mechanical supports/fixed anchors on either sides of the bridge. The CPW is housed in a 2-in, high resistivity (5–10 kΩ cm), p-type, <100> orientation, 250 µm thick silicon substrate [11, 18]. The silicon wafer has a 1 µm thick layer of silicon dioxide (SiO_2) layer grown on its surface by thermal oxidation technique in a quartz furnace at 1100 °C. The layer of SiO_2 acts as a passivation layer to isolate the silicon substrate material from active participation in current conduction, since SiO_2 is a popularly known dielectric material. The CPW line consisting of three parallel conducting lines, all fabricated of gold, are 1 µm in thickness. The central conductor is the signal line, carrying the RF signal from the input to the output port. On either sides of the signal line, two ground planes, each of 3–5*w* (where, *w* is the width of the CPW central conductor) in width run in parallel such that the bridges can be permanently anchored on the ground planes by means of mechanical supports or metal posts. A thin layer of silicon nitride (Si_3N_4) of 0.15 µm in thickness is deposited on the central conductor, where the bridges are about to make contact during actuation. This is done to ensure a perfect dielectric/capacitive contact between the bridges and the CPW signal line, where both are conducting layers. The structure hence resulted is known as the switched capacitor. The presence of the dielectric layer provides a high capacitive impedance path to the RF signal flow thus resulting in phase shift of the RF signal between the up and down states of the bridges. Figure 2a, b show the top view and the cross-sectional views of MEMS phase shifter implementation on CPW-based t-line. This diagram shows that four switched capacitors are required to generate a prescribed minimum phase shift of 30° at 22 GHz frequency. The idea is to cascade multiple numbers of such smaller phase shifter entities (known as unit cell phase shifter) to generate higher order phase shifters of 90°, 180° and so on. The designed unit cell phase shifter is 750 µm in

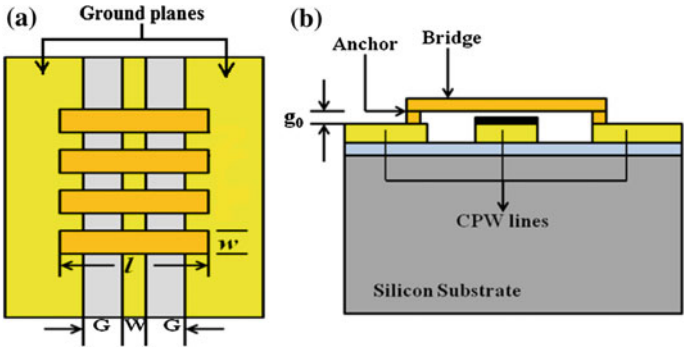

Fig. 2 **a** Top-view of the phase shifter, **b** cross-sectional view of the phase shifter

length. The CPW based t-line was designed in a way such that an unloaded characteristic impedance of 70 Ω is maintained throughout. On placement of the switched capacitors on the CPW t-line, the loaded characteristic impedance of the CPW t-line reduces to 50 Ω. The G/W/G configuration of the CPW t-line is set to 9.5 µm/5.5 µm/9.5 µm such that a characteristic impedance of 70 Ω is maintained [11, 12, 18]. Simulations also affirm that a total of four switched capacitors with each bridge dimension having length 'l' = 25 µm, width 'w' = 12 µm and thickness 't' = 0.3 µm, respectively, are appropriate in generating 30° phase shift at 22 GHz frequency.

2.1 Moore Curve-Based 180° Phase Shifter Design

The unit cell phase shifter structures when cascaded can yield higher order phase shifters having 90°, 180° or 270° phase shifts. The simplest design strategy to generate a higher order phase shifter is to arrange several similar unit cells in a linear fashion as shown under in Fig. 3. It is obtained from simulations that a total of seven similar unit cells are capable of generating 180° phase shift at a frequency of 22 GHz. The overall structure occupies a lateral length of 5.25 mm which is quite large as compared to the concept of MEMS technology which encourages the development of miniaturized structures. Hence, the concept of employment of fractal curves [13–16] was introduced. Third iteration of the Moore curve was the geometry employed to design the 180° phase shifter structure.

The Moore curve employs several meander-type structures and hence is capable of accommodating a large line length within a fixed area. Figure 4 shows the Moore Curve-based 180° phase shifter structure. It is evident that this structure accommodates a total of seven unit cells and is capable of generating 180° phase shift at 22 GHz frequency. It is also noteworthy that this phase shifter occupies a lateral area of 1.5 mm × 1.5 mm only which is a marked improvement over the earlier reported linear phase shifter design. The CPW-based t-line has only been shaped in the form of the Moore curve of third iteration in order to obtain space reduction, thus saving immense substrate area and ensuring a cost-effective outcome. In the following section, it will be observed that, the Moore Curve-based 180° phase shifter not only promotes miniaturization but also provides better RF performance as compared to the linear phase shifter equivalent.

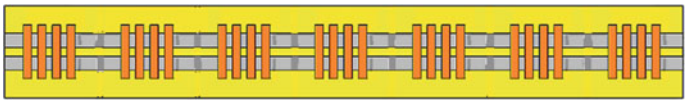

Fig. 3 Linear arrangement of the 180° phase shifter structure

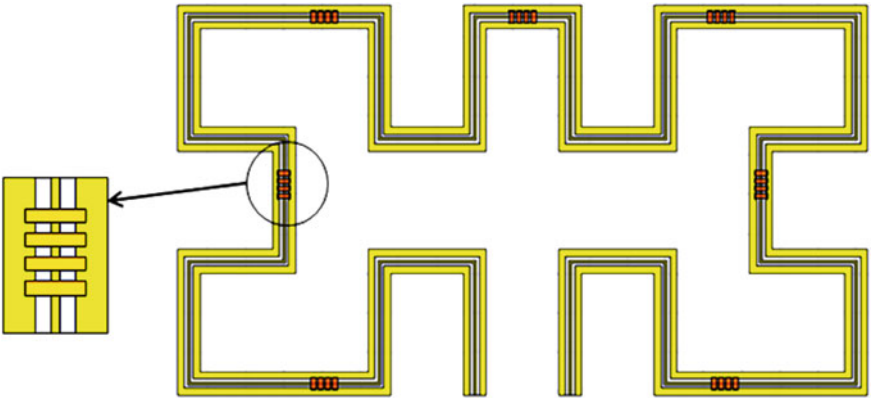

Fig. 4 Moore curve-based 180° phase shifter structure

3 Results and Observations

Simulations have been conducted for both the linear and the Moore Curve-based 180° phase shifter implementations and the results compared and contrasted to obtain the better outcome among the two designs. Figure 5a, b show the *S*-parameters performance (Return Loss (S_{11} in dB) and Insertion Loss (S_{21} in dB)) comparisons for both the up-state and down-state configurations. It is evident from both Fig. 5a, b that the Moore curve phase shifter implementation provides lower loss performance as compared to the linear phase shifter implementation. Figure 6 shows the differential phase shift, i.e. the differences between the phases of the up and down states of the bridges at 22 GHz. It is observed that 180° phase shift is resulted at the particular frequency of interest.

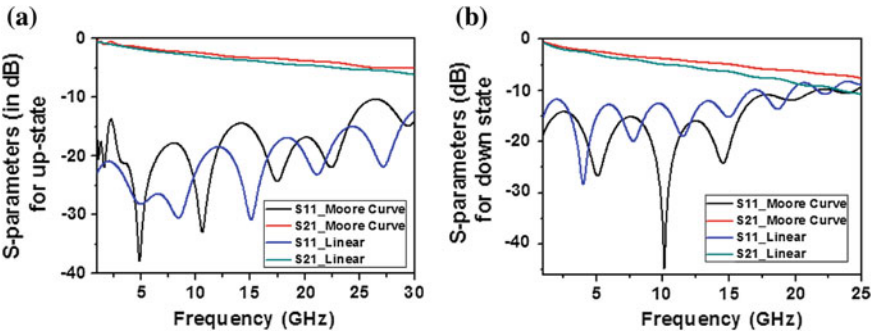

Fig. 5 *S*-parameters (dB) showing comparison between Moore curve based and linear 180° phase shifter structures **a** for up-state configuration, **b** for down-state configuration

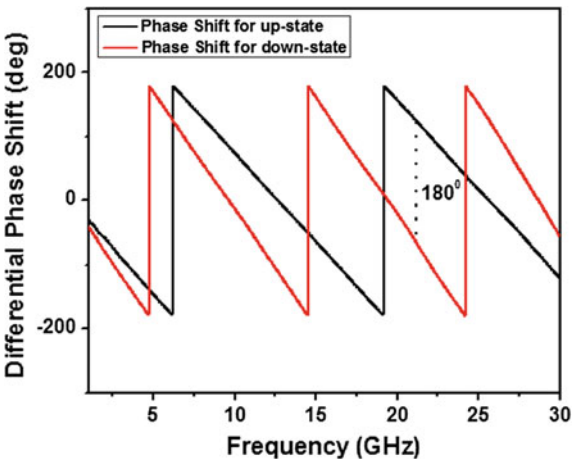

Fig. 6 Differential phase shift between the *up*- and *down-state* configurations showing 180° phase shift at 22 GHz frequency

4 Conclusion

A novel idea of Fractal Curve employment in the design of MEMS-based phase shifter structures is presented. Moore Curve of the third iteration is chosen as the geometry on which the CPW t-line shape is to be implemented. This strategy not only provides compact structures and promotes miniaturization, but also results in better RF performance as compared to the linear phase shifter equivalent. Considerable substrate area is saved in this technique thus ensuring cost-effective products.

References

1. Rebeiz G. M.: RF MEMS: Theory, Design and Technology. Second Edition. Wiley (2003).
2. S. Lucyszyn S.: Advanced RF Systems. Cambridge University Press. (2010).
3. Lacroix B., Pothier A., Crunteanu A., Blondy P.: Phase shifter design based on fast RF MEMS switched capacitors. Proc. IEEE 3rd European Microw. ICs Conf. 478–481 (2008).
4. Hayden J. S. and Rebeiz G. M.: One and Two-Bit Low-Loss Cascadable MEMS Distributed X-band Phase Shifters. Proc. IEEE MTT-S International Microwave Symposium Digest 161–164 (2001).
5. Lakshminarayanan B., Mercier D. and Rebeiz G. M.: High-reliability miniature RF-MEMS switched capacitors. IEEE Transactions on Microwave Theory and Techniques. 56. 971–981 (2008).
6. Mercier D., Caekenberghe K. V. and Rebeiz G. M.: Miniature RF MEMS switched capacitors. Proc. IEEE MTT-S Digest. 745–748 (2005).
7. Verger A., Pothier A., Guines C., Crunteanu A., Blondy P., Orlianges J. C., Dhennin J., Broue A., Courtade F. and Vendier O.: Sub-hundred nanosecond electrostatic actuated RF MEMS Switched Capacitors. J. Micromechanics Microengineering. 20. 2–8 (2010).
8. Rebeiz G. M., Tan G. L., Hayden J. S.: RF MEMS phase shifters: design and applications. IEEE Microwave Magazine. 72–81 (2002).

9. Unlu M., Demir S., Akin T.: A 15–40 GHz Frequency Reconfigurable RF MEMS Phase Shifters. IEEE Trans. on Microwave Theory and Techniques. 61.8 2865–2877 (2013).
10. Buck T. and Kasper E.: RF MEMS Phase Shifters for 24 and 77 GHz on High Resistivity Silicon. Proc. IEEE SiRF. 224–227 (2010).
11. Chakraborty A., Kundu A., Dhar S., Maity S., Chatterjee S., Gupta B.: Compact K-band distributed RF MEMS phase shifter based on high-speed switched capacitors. Proc. IEEE Mediterranean Microwave Symposium. 25–28 (2011).
12. Chakraborty A. and Gupta B.: A Novel Space Filling Curve Based 180° RF MEMS DMTL Phase Shifter. Proc. IEEE Mediterranean Microwave Symposium. 25–29 (2014).
13. http://en.wikipedia.org/wiki/Space-filling_curve.
14. https://en.wikipedia.org/wiki/Moore_curve.
15. Sun X., Ding G., Li B. and Shen M.: A Novel Meandered Coplanar Waveguide for RF MEMS Systems, J. Micromechanics and Microengineering. 27. 1628–1631 (2007).
16. Sagan H.: Space-Filling Curves. New York. Springer-Verlag. (1994).
17. www.ansys.com, Products, Electromagnetics.
18. Chakraborty A. and Gupta B.: Design, Fabrication and Characterization of Miniature RF MEMS Switched Capacitor based Phase Shifter. Microelectronics Journal. 45. 1093–1102 (2014).

Simulation Studies for Delay Effect on Stability of a Canonical Tank Process

Mayank Chaturvedi, Pradeep K. Juneja, Neha Jadaun and A. Sharma

Abstract Whenever the propagation of material or energy is modeled, dead time naturally comes into picture in the majority of the industrial process models. The existence of dead time is every time a great apprehension to the process industry. There are various limitations and constrains on the design of controllers, may be classical or intelligent, in the presence of delay time. Its presence also affects stability of the system. The present control system analysis focuses on the effect of dead time on stability of the selected process which can be modeled as first-order plus dead time model.

Keywords Dead time · FOPDT · Stability parameters · Stability

1 Introduction

Delay system represents a class which is widely used for analysis and modeling of transportation or propagation phenomena of matter, energy, or information. Naturally, appearance of these systems can be seen in modeling processes found in biology, physics, mechanics, physiology, chemistry, aeronautics, etc. When a process does not contain a delay, the electronic devices used in development of its

M. Chaturvedi (✉) · N. Jadaun
Department of Electrical Engineering, Graphic Era University, Dehradun, India
e-mail: mayankchaturvedi.geit@gmail.com

P.K. Juneja
Department of Electronics & Communication Engineering, Graphic Era University, Dehradun, India
e-mail: mailjuneja@gmail.com

A. Sharma
PDP, Graphic Era University, Dehradun, India

D.K. Lobiyal et al. (eds.), *Proceedings of the International Conference on Signal, Networks, Computing, and Systems*, Lecture Notes in Electrical Engineering 396, DOI 10.1007/978-81-322-3589-7_36

control law can generate required delays [1–3]. These delay systems can create a number of oscillations and may lead a process to instability. Delay is also known as dead time, transportation lag, or time lag [4].

For dynamic behavior representation of a complex process in industries as First-Order plus Dead Time (FOPDT) is to say that many storage elements can be represented by a single element. FOPDT is the system with delayed input, it is commonly used because of its less complexity. It is represented as [5]

$$G(s) = \frac{K\mathrm{e}^{-\theta s}}{\tau s + 1} \tag{1}$$

The dead time needs approximation in many processes as it is a nonlinear quantity, for its linearization purpose Taylor's series approximation technique is used in present analysis. Approximation of functions can be done using Taylor's series. Higher order models can be approximated with lower order models which have similar characteristics using first-order Taylor's series approximation [6].

$$\mathrm{e}^{-\theta s} = \frac{1}{(1 + \theta s)} \tag{2}$$

The first-order Taylor's series expansion of Eq. 1 is given as

$$G(s) = \frac{K}{(\tau s + 1)(1 + \theta s)} \tag{3}$$

Due to the presence of dead time, stability of a system or process leads toward instability, which is the biggest concern in the present industries. To analyze the stability of a process the Bode plot and Nyquist techniques are used in present analysis. Bode plot consists of two graphs, one is between magnitude and frequency and the other one is between phase angle and frequency. Nyquist plot, which is a polar plot is drawn in order to judge the stability of the time invariant linear systems in frequency domain.

Using these techniques many important stability parameters such as phase margin, gain margin, phase crossover frequency, gain crossover frequency, etc., can be calculated for stability analysis of different processes.

2 Methodology

In present analysis, process which can be modeled as FOPDT is taken under consideration.

The FOPDT transfer functions selected from literature are represented as [7]

$$D(s) = \frac{10\,e^{-156s}}{2344s+1} \tag{4}$$

$$E(s) = \frac{4.8\,e^{-530s}}{1652s+1} \tag{5}$$

$$F(s) = \frac{5.5\,e^{-469s}}{3749s+1} \tag{6}$$

The FOPDT models can be approximated with first-order Taylor's series approximation technique [4] as

$$\text{DWD} = \frac{10}{(2344s+1)(156s+1)} \tag{7}$$

$$\text{EWD} = \frac{4.8}{(1652s+1)(530s+1)} \tag{8}$$

$$\text{FWD} = \frac{5.5}{(3749s+1)(469s+1)} \tag{9}$$

The selected process models are of conical tank process and are taken to analyze the different behavior of dead time at different operating points in the process. To analyze the stability of the process models, Bode plots and Nyquist plots have been used. The stability margins of process with dead time and without dead time after approximation are compared for stability.

3 Results and Discussion

The simulations have been performed to analyze stability margins of selected FOPDT process models *D*, *E,* and *F* and their dead time approximated process models DWD, EWD, and FWD. Figures 1 and 2 show the Bode and Nyquist plots of process model D, respectively. The Bode and Nyquist plots of process model *E* is given by Figs. 3 and 4. Figures 5 and 6 exhibit the Bode and Nyquist plots of process model *F*, respectively.

Figures 7 and 8 give the Bode and Nyquist plots of process model DWD, respectively. The Bode and Nyquist plots of process model EWD are given by Figs. 9 and 10, respectively. Figures 11 and 12 show the Bode and Nyquist plots of process model FWD, respectively. Table 1 shows the stability margins of the selected FOPDT process models *D*, *E,* and *F*, with stability margins of dead time approximated process models DWD, EWD, and FWD.

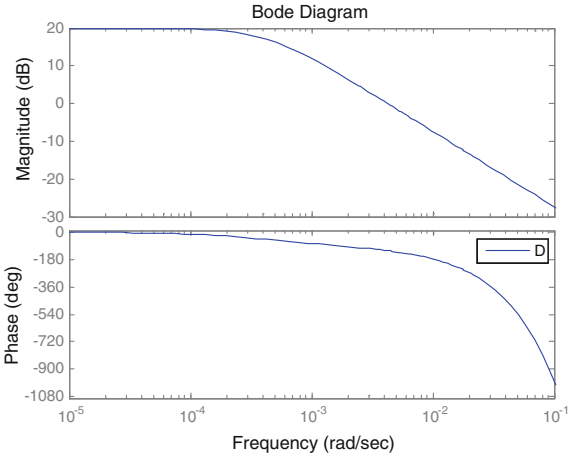

Fig. 1 Bode plot of D

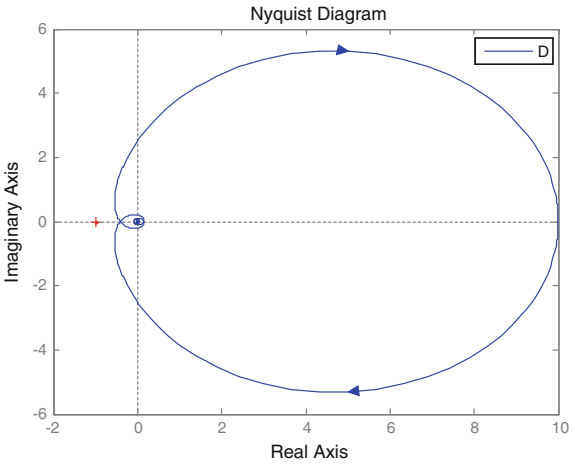

Fig. 2 Nyquist plot of D

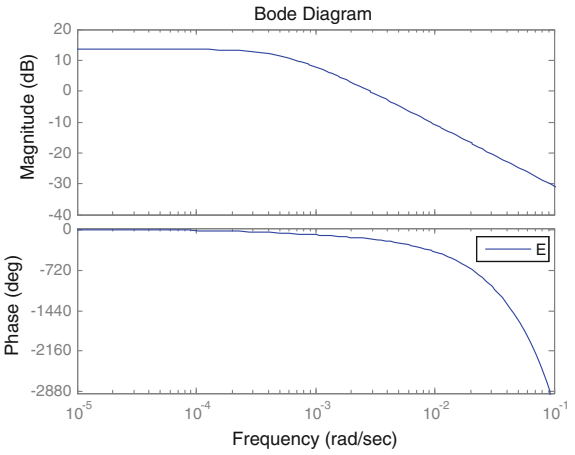

Fig. 3 Bode plot of E

Fig. 4 Nyquist plot of E

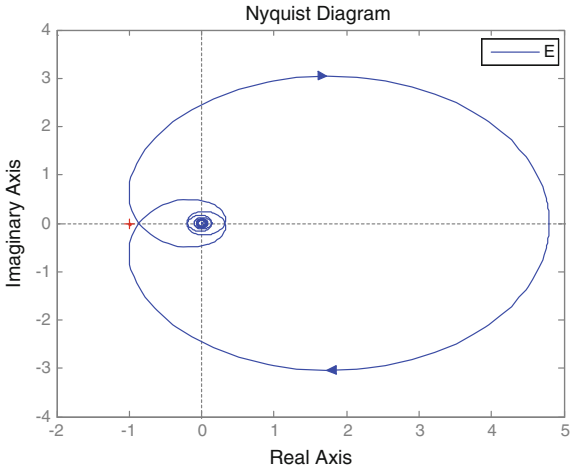

Fig. 5 Bode plot of F

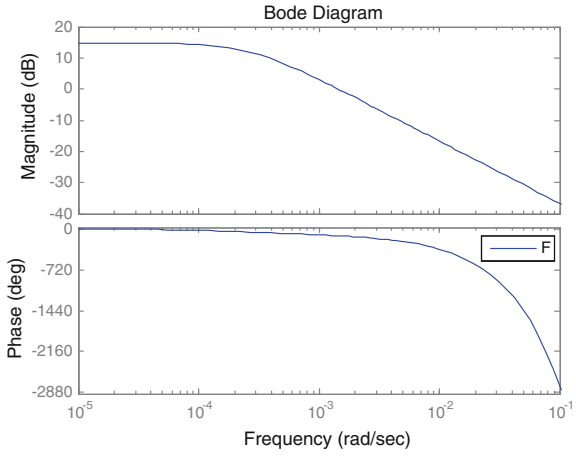

Fig. 6 Nyquist plot of F

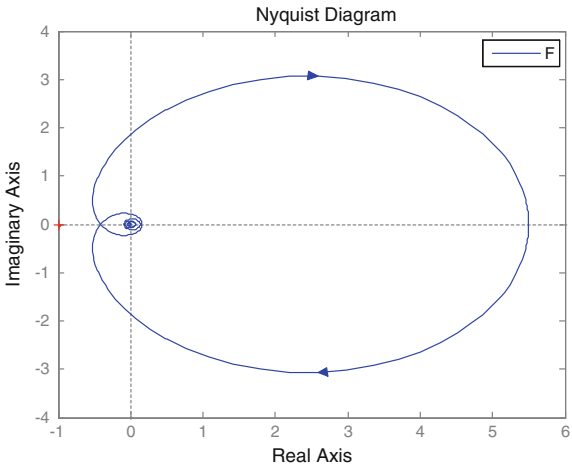

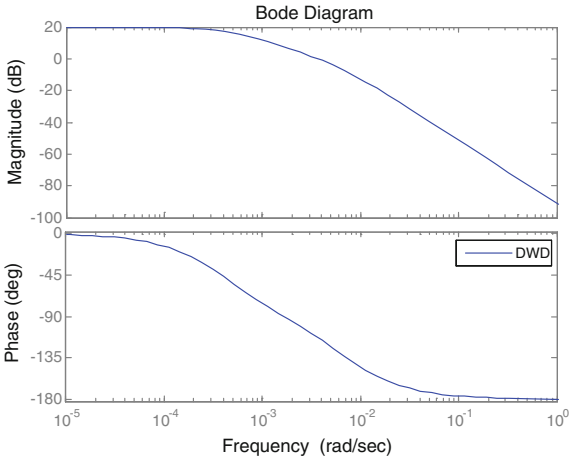

Fig. 7 Bode plot of DWD

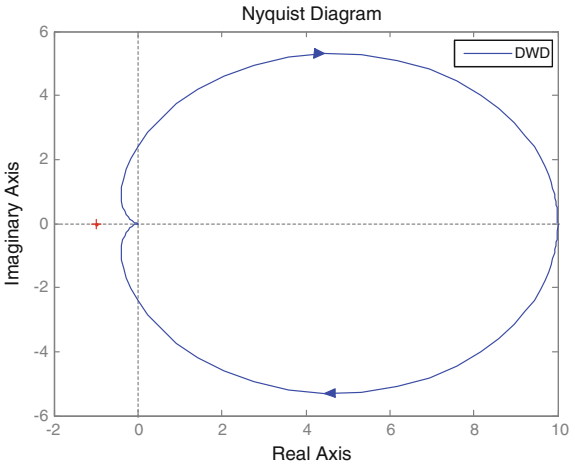

Fig. 8 Nyquist plot of DWD

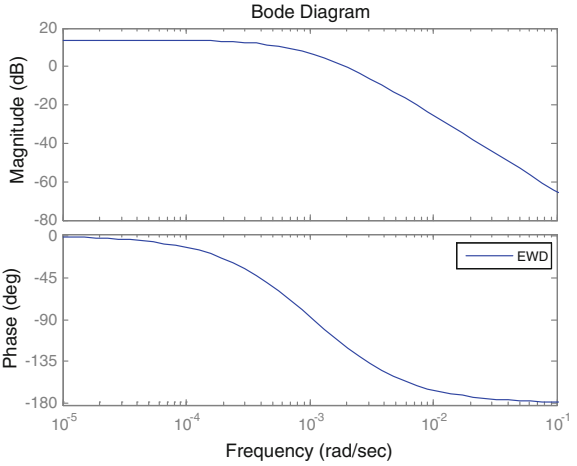

Fig. 9 Bode plot of EWD

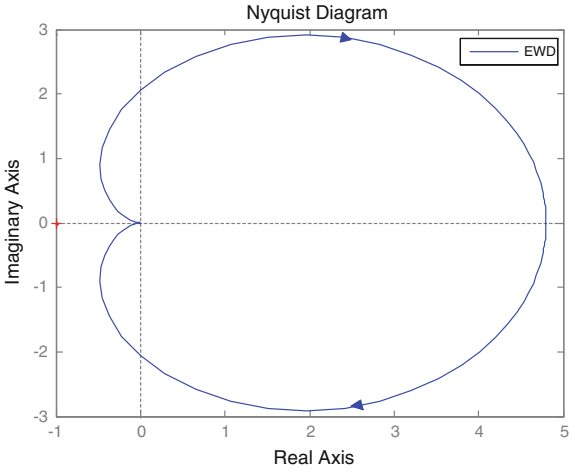

Fig. 10 Nyquist plot of EWD

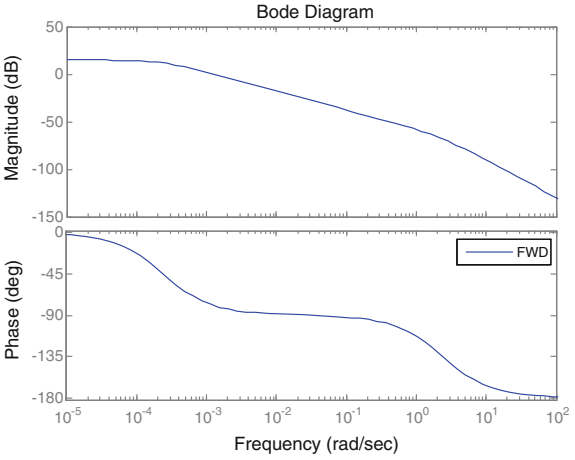

Fig. 11 Bode plot of FWD

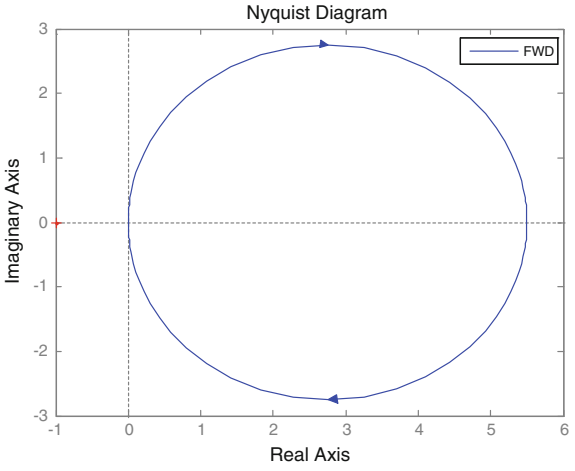

Fig. 12 Nyquist plot of FWD

Table 1 Comparison between stability parameters

System	G_m	P_m	ω_g	ω_p
D	7.69	57.8	0.0103	0.0042
DWD	Infinity	66.78	Infinity	0.0037
E	1.26	15.7	0.0033	0.0028
EWD	Infinity	61.6557	Infinity	0.0019
F	7.6	61.7	0.00351	0.0014
FWD	Infinity	100	Infinity	0.0012

4 Conclusion

In present analysis the selected FOPDT model is approximated using Taylor's series and using Bode and Nyquist techniques responses are drawn in results. By these responses certain stability parameters are achieved for different transfer functions. These parameters are compared.

The phase margin and gain margin in all the cases have been increased while comparing selected FOPDT process models with its dead time approximated process model. So it can be concluded that in the presence of dead time stability of a process decreases.

References

1. Farkh, R., Laabidi, K., Ksouri, M.: PI Control for Second Order Delay System with Tuning Parameter Optimization, International Journal of Electrical and Electronics Engineering, (2009) 1–7.
2. Chaturvedi, M., Juneja, P.K., Chauhaan, P.: Effect of Implementing Different PID Algorithms on Controllers Designed For SOPDT Process, Proceedings of the International Conference on Advances in Computing, Communications and Informatics, ICACCI 2014, GCET Greater Noida, IEEE Xplore, (2014) 853–858.
3. Chauhaan, P., Juneja, P.K., Chaturvedi, M.: Controller Design and Its Performance Analysis for a Delayed Process Model. Proceedings of the International Conference on Advances in Computing, Communications and Informatics, ICACCI 2014, GCET Greater Noida, IEEE Xplore, (2014) 859–862.
4. Seborg, D.E., Edgar, T.F., Mellichamp, D.A.: Process Dynamics and Control, second ed., Wiley, New York, (2004).
5. Cvejn, J.: Simple PI/PID controller tuning rules for FOPDT Plants with guaranteed closed-loop stability margin. Acta Montanistica Slovaca, (2011) 17–25.
6. Chaturvedi, M., Juneja, P.: Effect of dead time approximation on controller performance designed for a second order delayed model. Proceeding of ICAES 2013, CEERI, Pilani, IEEE Xplore, (2013) 313–315.
7. Dhanalakshmi, R., and Vinodha, R.: Design of Control Schemes to Adapt PI Controller for Conical Tank Process. Int. J. Advance. Soft Comput. Appl., Vol. 5, No. 3, (2013) 1–20.

Current Signature Analysis of Single-Phase ZSI-Fed Induction Motor Drive System

Vivek Sharma and Bhawana Negi

Abstract This paper presents THD responses of ZSI-fed induction motor drive system for the buck and boost operation. The proposed mechanism is simulated for various fault conditions, viz. MOSFET blown off fault, fault at MOSFET gate terminals for both the buck and boost operations. The simulation results are presented with corresponding THD values in this paper.

Keywords THD · MOSFET · Fault · Buck · Boost

1 Introduction

Traditional inverters provide efficient conversion from DC to AC but they lack reliability of operation. This in turn emphasizes on implementation of Zed source inverter. A three-phase single-stage Z-source inverter consists of inductance and capacitance connected in X shape [1–4]. By introducing LC impedance network the inverter can perform both buck as well as boot operations simultaneously depending upon the specifications of PWM strategies. Also, this inverter is immune to electromagnetic interference [5]. ZSI shows responses which are highly stable and it has unique property of showing boost as well as buck operations for the same specifications. But study of faults becomes an eminent part of research as the introduction of harmonics to the system leads to degrading of performance. Hence study of effect of faults is required for the implemented system [6]. It is studied that Z-source inverter finds its prominent application in variable speed control of drives, input for non-conventional sources of energy, sources with high power like fuel cells, rectification process or inversion process [7].

V. Sharma (✉) · B. Negi
Electrical Engineering Department, Graphic Era University, Dehradun, India
e-mail: vivek21@gmail.com

B. Negi
e-mail: bhawananegi105@gmail.com

D.K. Lobiyal et al. (eds.), *Proceedings of the International Conference on Signal, Networks, Computing, and Systems*, Lecture Notes in Electrical Engineering 396, DOI 10.1007/978-81-322-3589-7_37

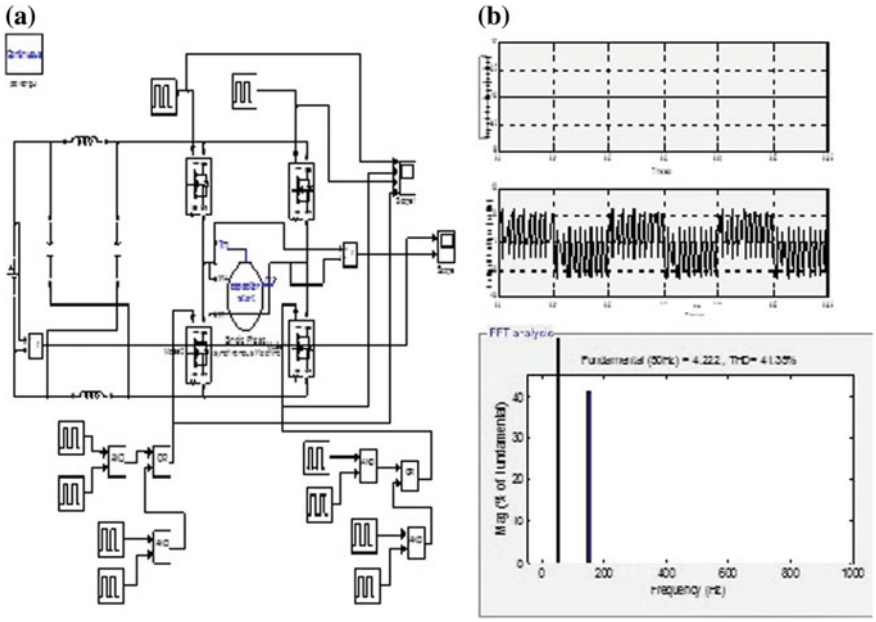

Fig. 1 **a** Simulink model of ZSI boost converter circuit **b** FFT spectrum

1.1 ZSI Boost Operation with Induction Motor Load

Figure 1 shows the MATLAB Simulink model of system implemented for boosted output.

This configuration shows a desirable boost operation of input voltage of 100 V to a high output of 200 V. The signature diagram of harmonics using fast Fourier transform is shown in Fig. 1b. The value of harmonic distortion at fundamental frequency is 41.35 %.

1.2 Fault at Gate Terminal of Phase A

The Simulink system of condition under consideration is presented in Fig. 2a. To depict this faulty condition, the gate terminal of MOSFET of one phase is grounded, i.e. not provided with gate pulse.

Introduction to such faults exhibits only one half of distorted output waveform. The percentage harmonics measured at 50 Hz is 37.42 %.

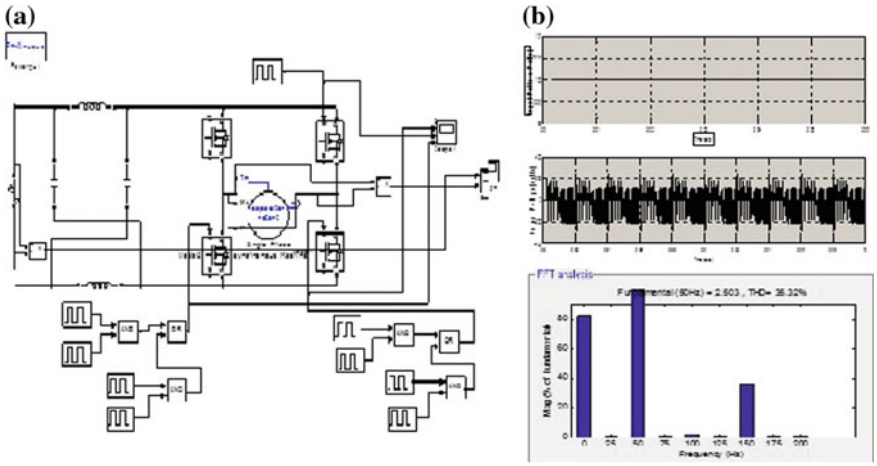

Fig. 2 **a** Simulink model of with gate grounded **b** FFT spectrum

1.3 High Resistance Condition Fault

This faulty condition resembles open circuiting of the phase A switch. In this case, the switch device is replaced by a high resistance of order of mega ohm. The current through this device is very small and it leads to high resistance low current fault.

Figure 3a shows the Simulink model for present faulty condition. The obtained output waveform is highly distorted and the % harmonics at operating frequency is 37.42 %.

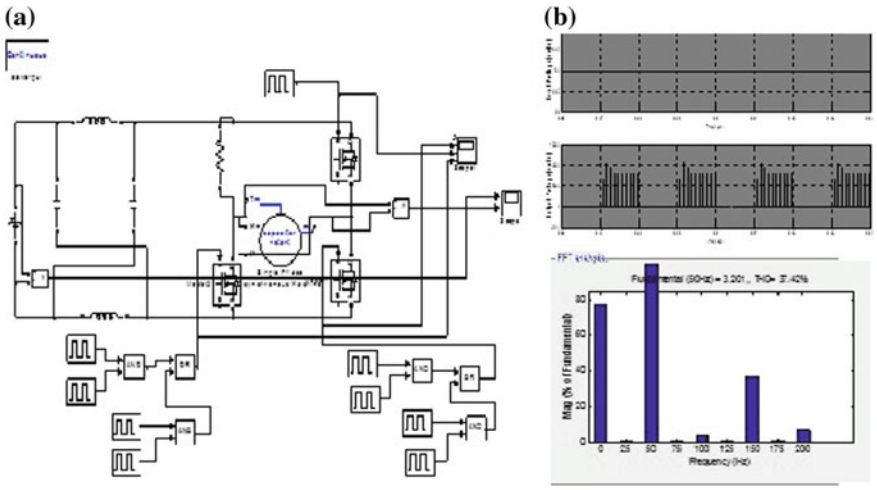

Fig. 3 **a** Simulink model for high resistance fault **b** FFT spectrum

2 Simulation Study for Buck Operation

2.1 With Induction Motor Load

To simulate practical conditions, the above system is simulated for induction motor load. The Simulink model for this condition is shown in Fig. 4a.

The output voltage waveform shows a reduced output of 50 V for an input supply of 100 V. The measured value of harmonics at fundamental frequency is 431.35 %.

2.2 Gate Terminal Grounded Fault

Figure 5a shows the Simulink circuit for gate terminal grounded fault under buck operation of CSI. In this topology, the gate of phase A MOSFET is deprived of the gate pulse.

In this faulty condition, only one half of distorted wave is obtained at the load with reverse polarity. The percentage value of harmonics at fundamental frequency is 310.18 %.

2.3 MOSFET Blown off Fault

The simulation equivalent for such circuit is obtained by replacing phase A MOSFET by high resistance as shown in Fig. 6.

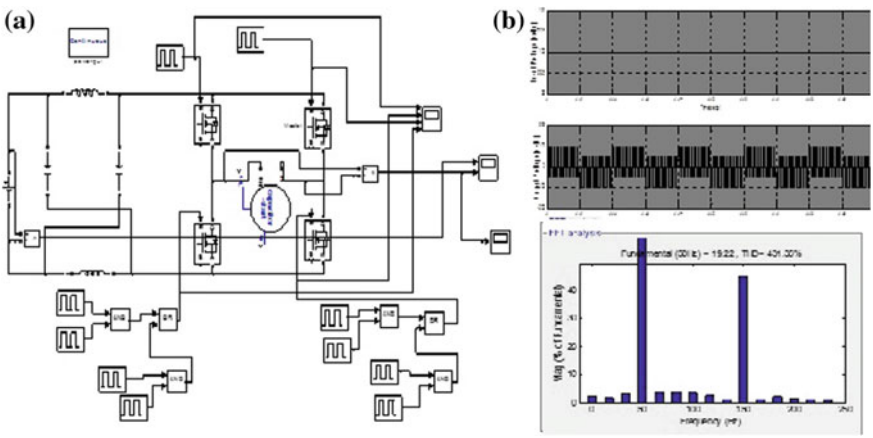

Fig. 4 **a** Simulink diagram of buck converter for IM load **b** FFT spectrum

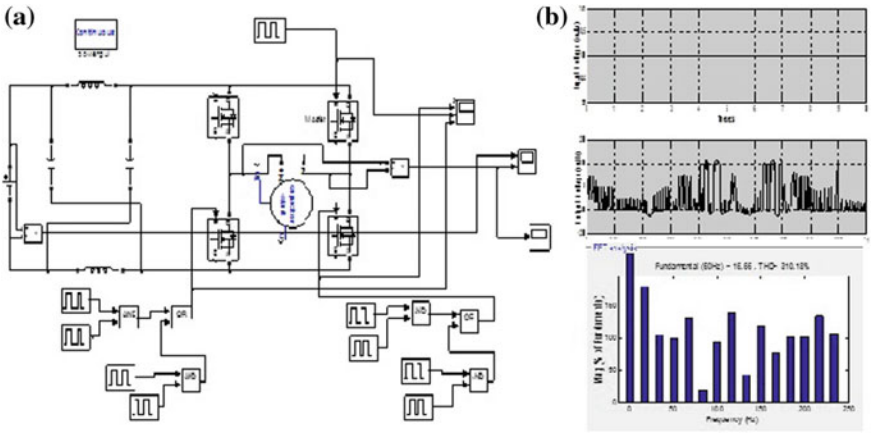

Fig. 5 **a** Simulink model of gate terminal grounded fault **b** FFT spectrum

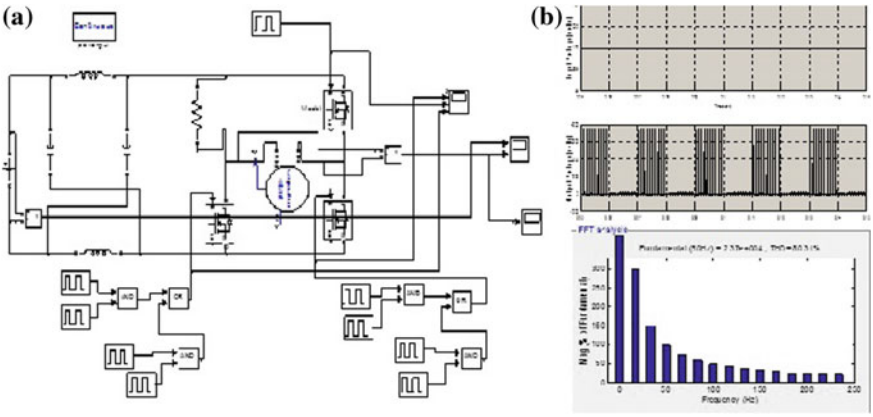

Fig. 6 **a** Simulink model with blown off fault **b** FFT spectrum

This condition depicts the replacement of power electronic switch of phase A with high resistance in the circuit. Due to high resistance in the converter side large value of distortion comes and the value of THD at operating frequency is 80.31 %.

The summary of fault is tabulated in Table 1. This study analyses both modes of operation, i.e. boost and buck modes of operation.

Table 1 Summary of FFT analysis

Type of fault	% THD	Load current (A)
Boost operation		
1. No fault	41.35	21
2. Gate grounded	36.32	27
3. High resistance at phase A	37.42	28
Buck operation		
4. Without fault	431.35	13
5. Gate grounded	310.18	18
6. High resistance at phase A	80.31	22

3 Conclusion

In this study, the variable frequency required for the harmonic control of single-phase AC motor is obtained from single-phase inverter. The magnetic saturation is avoided and constant flux operation is considered for the machine. The inverter uses PWM technique for voltage control and hence it has low ripples due to harmonics for no fault condition. For the faulty conditions, lower order harmonics are removed by switching of the device and the higher order harmonics are neglected by selective harmonic reduction method.

This study can be extended for three-phase systems with higher value of voltages.

References

1. Chandana Jayampathi Gajanayak, Fang Lin Luo, Hoay Beng Gooi, Ping LamSo, Lip Kian Siow, "Extended boost Z-source inverters." IEEE Transactions On Power Electronics, vol. 25, no. 10, pp. 2242–2252.
2. Vivek Sharma, Gaurav Mendiratta, "Harmonic Analysis of CSI-fed Induction Motor Drive", In Proceedings of the 8th INDIACom 2014 IEEE International Conference on "Computing for Sustainable Global Development", 2014.
3. Vivek Sharma, Chiranjeev panwar, "Comparative Analysis Of PV Fed Dc-Dc Converters," in proceedings of IEEE International Conference on Green Computing, Communication and Electrical Engineering (ICGCCEE 2014), 2014.
4. Vivek Sharma, Lokesh Yadav, "Harmonic Analysis of PWM Full Bridge Converter," in proceedings of IEEE International Conference on Power, Control and Embedded System (ICPCES-2014), 2014.
5. Vivek Sharma, Nikita Rawat, "Comparison of Interleaved Coupled-Inductor Boost Converter with Conventional DC Converters," in IEEE sponsored 4th International Conference on Computing of Power, Energy & Communication", ICCPEIC 2015, April 2015.
6. Vivek Sharma, Nikita Rawat, "Fault Diagnosis of Single phase Z-Source Inverter," International Conference on Advances in Computing & Communication Engineering ICACCE-2015, 2015.
7. B. Biswas, S. Das, P. Purkait, M.S. Mandal, D. Mitra, "Current Harmonics Analysis of Inverter-Fed Induction Motor Drive System under Fault Conditions", Proceedings of the International Multi Conference of Engineers and Computer Scientists 2009,Vol II IMECS 2009, March, Hong Kong, ISBN: 978-988-17012-7-5.

Kinematic Control of a Mobile Manipulator

B.B.V.L. Deepak, Dayal R. Parhi and Ravi Praksh

Abstract Proper motion planning algorithms are necessary for intelligent robotic systems in order to execute their specific tasks. To solve this problem, current research work introduces the inverse kinematic models for mobile manipulators. In general, a systematic closed-form solution is not available in the case of inverse kinematic models. To obtain elucidation for inverse kinematic problem is more complex as compared to direct kinematics problem. The current research work aims to combine the functionality of a robot arm with an autonomous platform. It means development of an autonomous wheeled mobile robot on which the robot arm is mounted. The purpose of this work is to integrate both the segments (i.e., mobile manipulator and mobile platform), such that the system can perform the constrained moves of the arm in the mean while as the platform is moving.

Keywords Robotic manipulator · Wheeled mobile platform · Inverse kinematic models · End effector constraints · Geometric wheel constraints

1 Introduction

Proper motion planning algorithms are necessary for robotic systems may be of manipulator or mobile platforms, in order to execute their specific tasks [1]. Motion planning of industrial robots is a critical issue because of its end effectors path

B.B.V.L.Deepak (✉) · D.R. Parhi
Department of Mechanical Engineering, National Institute of Technology-Rourkela, Rourkela, India
e-mail: bbv@nitrkl.ac.in

D.R. Parhi
e-mail: DRKPARHI@nitrkl.ac.in

B.B.V.L.Deepak · R. Praksh
Department of Industrial Design, National Institute of Technology-Rourkela, Rourkela, India
e-mail: 113ID1274@nitrkl.ac.in

D.K. Lobiyal et al. (eds.), *Proceedings of the International Conference on Signal, Networks, Computing, and Systems*, Lecture Notes in Electrical Engineering 396, DOI 10.1007/978-81-322-3589-7_38

constraints [2]. Whereas, the motion control of mobile robots or the mechanical behavior of the robot depends upon the wheel geometric constraints while the robot is in motion [3, 4]. To sustenance the progress and to enlarge the solicitation potential of robotic manipulators (industrial robotics), it is coherent to integrate locomotion features with manipulation capabilities, hereby developing wheeled mobile manipulators [5, 6].

Matched to conventional industrial robotic arms, mobile manipulators adapt to environmental changes for performing wide range of manufacturing tasks. Another benefit of this category of robotic systems is that the existing industrial environments do not have to be altered or modified as in the case of Automated Guided Vehicles (AGV's), where permanent cable layouts and/or markers are required for navigation [5]. In past [4, 7], authors dealt with kinematic models of wheeled mobile robots to generate trajectory within its environments. The developed kinematic models according to the wheel geometric constraints: Wheel sliding constraint and Wheel rolling constraints. But the kinematic analysis of manipulators is quite different from as compared to wheeled mobile robots. Kinematics deals with joint space coordinates, link reference frames, and end effector reference frames [1, 8]. To obtain solutions of inverse kinematics, several algorithms have been developed subjected to end effector constraints [9]. Motion planning of mobile robot deals with generation of safest and shortest pats while reaching its target position [10–12]. Several motion planning techniques have been developed based on artificial intelligence algorithms [13, 14]. But these techniques are not suitable for mobile manipulator control [15, 17, 18].

In this paper, we propose inverse kinematic solutions for both the mobility platform and robotic manipulator. The purpose of this work is to integrate both the segments (i.e., mobile manipulator and mobile platform), such that the system can perform the constrained moves of the arm in the mean while as the platform is moving.

2 Mechanical Design Architecture of Mobile Manipulator

The main characteristic of an automated mobile manipulator is its flexible operational workspace. Coordinated motion of the manipulator and mobile platform leads to a wide range of redundancy. Owing the velocity restrictions enforced on the mobile base, the WMM is a nonholonomic system. So it is required to develop a kinematic controller to make the robot system follow a desired end effector and platform trajectories in its workspace coordinates simultaneously.

In the current research work, a wheeled mobile manipulator is considered with a 4-axis manipulator equipped on a nonholonomic differential wheeled mobile platform. For the considered 4-axis manipulator coordinate frames for the manipulator are assigned as shown in Fig. 1 and corresponding kinematic parameters are represented in Table 1.

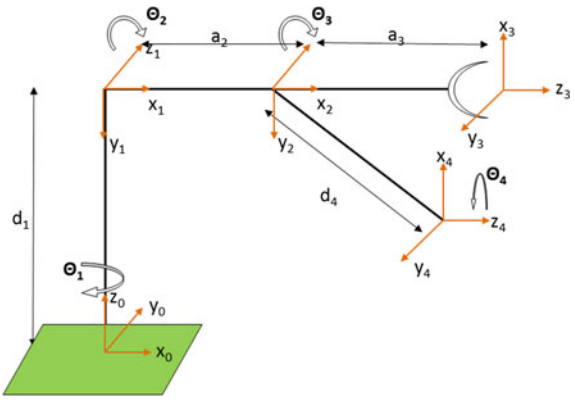

Fig. 1 Link coordinate frame of the manipulator

Table 1 Kinematic parameters of the manipulator

Axis	θ	d (mm)	a (mm)	α
1	θ_1	$d_1 = 70$	0	$-\pi/2$
2	θ_2	0	$a_2 = 100$	0
3	θ_3	0	$a_3 = 70$	$-\pi/2$
4	θ_4	$d_2 = 45$	$a_4 = 0$	0

The arm equation is obtained using D–H notation [16] as represented in Eq. (4), which is function of θ_1, θ_2, θ_3, and θ_4. The arm equation consists of six elements; three correspond to the end effector's position and the remaining three represent yaw, pitch, and roll orientations of the tool.

Using a homogeneous coordinate transformation matrix, the relation between adjacent links is given in Eq. (1).

$$T_i = \text{Rot}(z, \theta_i) * \text{Trans}(0, 0, d_i) * \text{Trans}(a_i, 0, 0) * \text{Rot}(x, \alpha_i) \tag{1}$$

$$= \begin{bmatrix} C\theta_i & -S\theta_i C\alpha_i & S\theta S\alpha_i & a_i C\theta_i \\ S\theta_i & C\theta_i C\alpha_i & -C\theta_i S\alpha_i & a_i S\theta_i \\ 0 & S\alpha_i & C\alpha_i & d_i \\ 0 & 0 & 0 & 1 \end{bmatrix} \tag{2}$$

Here, $C_i = \cos(\theta_i), S_i = \sin(\theta_i)$

On replacing the kinematic parameters illustrated in Table 1 in Eq. (2), individual transformation matrices T_0^1 to T_4^5 can be found and the global transformation matrix T_0^5 of the robot arm is found according to Eq. (3).

$$T_{\text{base}}^{\text{tool}} = T_{\text{base}}^{\text{wrist}} * T_{\text{wrist}}^{\text{tool}} = \begin{bmatrix} m_x & n_x & o_x & p_x \\ m_y & n_y & o_y & p_y \\ m_z & n_z & o_z & p_z \\ 0 & 0 & 0 & 1 \end{bmatrix} = \begin{bmatrix} R(\theta)_{3x3} & P_{3x1} \\ 0 & 1 \end{bmatrix} \tag{3}$$

where $T_{\text{base}}^{\text{wrist}} = T_0^1 * T_1^2$ and $T_{\text{wrist}}^{\text{tool}} = T_2^3 * T_3^4$

Where (p_x, p_y, p_z) represents the position and $R(\theta)_{3\times3}$ represents the rotation matrix of the end effector. Tool configuration is six-dimensional because arbitrary is specified by three position coordinates (x, y, z) and orientation coordinates (yaw, pitch, roll).

$$X = \begin{Bmatrix} p_x \\ p_y \\ p_z \\ y \\ p \\ r \end{Bmatrix} = \begin{Bmatrix} c_1(a_2c_2 + a_3c_{23} - d_4s_{23}) \\ s_1(a_2c_2 + a_3c_{23} - d_4s_{23}) \\ d_1 - a_2s_2 - a_3s_{23} - d_4c_{23} \\ -[\exp(\theta_4)/\pi]c_1s_{23} \\ -[\exp(\theta_4)/\pi]s_1s_{23} \\ -[\exp(\theta_4)/\pi]c_{23} \end{Bmatrix} \tag{4}$$

The time derivative of the end effector's position gives the linear velocity of the end effector. The position of the end effector $[p_x \quad p_y \quad p_z]^T$ is a function of (θ_1, θ_2, θ_3) because θ_4 indicates the orientation of the tool.

$$\begin{Bmatrix} v_x \\ v_y \\ v_z \end{Bmatrix} = \frac{\mathrm{d}}{\mathrm{d}t} \begin{Bmatrix} p_x \\ p_y \\ p_z \end{Bmatrix} = [J_M]_{3\times3} \begin{Bmatrix} \dot{\theta}_1 \\ \dot{\theta}_2 \\ \dot{\theta}_3 \end{Bmatrix} \tag{5}$$

where $[J_M]_{3\times3}$ is manipulator velocity Jacobean matrix and is equal to

$$\begin{bmatrix} -s_1(a_2c_2 + a_3c_{23} - d_4s_{23}) & -a_2^2s_2c_1 - a_3^2s_{23}c_1 - d_4c_{23}c_1 & -a_3s_{23}c_1 - d_4c_{23}c_1 \\ c_1(a_2c_2 + a_3c_{23} - d_4s_{23}) & -a_2s_1s_2 - a_3s_1s_{23} - d_4s_1s_{23} & s_1(-a_3s_{23} - d_4s_{23}) \\ 0 & -a_3c_{23} + d_4s_{23} & -a_3c_{23} + d_4s_{23} \end{bmatrix} \tag{6}$$

2.1 Inverse Kinematic Model

This section describes the development of inverse kinematic models of an arm based on its link coordinate systems. From Eq. (9), it is observed that there is a possibility of getting two wrist angles ($\pm\theta_3$) for the same tool position. Since the elbow angle (θ_2) depends on θ_3, two elbow angles will obtain corresponds to each θ_3.

The base angle can be found easily by Eq. (7).

$$\text{Base angle } \theta_1 = \arctan\left(p_y/p_x\right) \tag{7}$$

where p_x and p_y are determined from Eq. (8) and from the arm equation, the global pitch angle θ_{23} can be found as follows:

$$\theta_{23} = \arctan((c_1y + s_1p)/r) \tag{8}$$

The wrist angle can be found as follows:

$$\theta_3 = \pm \arccos\left(\left(\left\|b^2\right\| - a_2^2 - a_3^2\right)/p_x\right) \tag{9}$$

where $\left\|b^2\right\| = b_1^2 + b_2^2$; and $b_1 = c_1 p_x + c_2 p_y + d_4 s_{23}$ and $b_2 = d_1 - d_4 c_{23} - p_z$.

Once θ_3 is known then elbow angle θ_2 can be found from the global pitch angle θ_{23}.

$$\because \theta_{23} = \theta_3 + \theta_2 \Rightarrow \theta_2 = \theta_{23} - \theta_3 \tag{10}$$

The final joint parameter θ_4 can be found from the arm Eq. (14) as follows:

$$\text{Tool roll angle } \theta_4 = \pi * \ln \sqrt{(y^2 + p^2 + r^2)} \tag{11}$$

2.2 *Velocity Jacobean of Mobile Platform*

There are three constraints for a differential platform: first one corresponds to move the platform in the direction of axis of symmetry and the remaining two are rolling constraints, not allow the wheels to slip. The motion equation of a differential mobile platform is a function of left wheel and right wheel velocities (v_{Lt}, v_{Rt}) as represented in Eq. (12).

$$\dot{\xi}_I = \begin{Bmatrix} \dot{x} \\ \dot{y} \\ \dot{\psi} \end{Bmatrix} = \frac{1}{2s} \begin{bmatrix} s * \cos\psi & s * \cos\psi \\ s * \sin\psi & s * \sin\psi \\ -1 & 1 \end{bmatrix} * \begin{Bmatrix} v_{Rt} \\ v_{Lt} \end{Bmatrix} \tag{12}$$

While moving the mobile platform with a heading angle ψ, the following kinematic Eq. (13) is used which relates the linear velocity of the mobile platform reference frame to the wheel velocities.

$$\begin{Bmatrix} V_x \\ V_y \end{Bmatrix} = [J_{\text{MP}}]_{2\times 2} \begin{Bmatrix} \dot{\theta}_{rt} \\ \dot{\theta}_{lt} \end{Bmatrix} \tag{13}$$

where $[J_{\text{MP}}]_{3\times 3}$ is mobile platform velocity Jacobean matrix and $\dot{\theta}_{rt}$ and $\dot{\theta}_{lt}$ are angular velocities of right and left wheels, respectively.

Velocity Jacobean matrix $[J_{\text{MP}}] = \frac{1}{2r} \begin{bmatrix} \cos\psi & \cos\psi \\ \sin\psi & \sin\psi \end{bmatrix}$

2.3 Velocity Jacobean of Mobile Manipulator

The differential kinematics of the mobile manipulator is obtained by combining the kinematic Eqs. (5) and (13) of a 4-axis manipulator and the differential mobile platform as shown in Eq. (14). The first three parameters in the above equation relate to the manipulator and the remaining two correspond to the differential platform.

$$\{\dot{q}\} = \begin{Bmatrix} \dot{\theta}_1 \\ \dot{\theta}_2 \\ \dot{\theta}_3 \\ \dot{\theta}_{rt} \\ \dot{\theta}_{lt} \end{Bmatrix} = [J_{\mathrm{WMP}}]_{5\times 5} \begin{Bmatrix} \dot{\theta}_1 \\ \dot{\theta}_2 \\ \dot{\theta}_3 \\ \dot{\theta}_{rt} \\ \dot{\theta}_{lt} \end{Bmatrix} \tag{14}$$

where $[J_{\mathrm{WMP}}]$ is the Velocity Jacobean of Mobile Manipulator and is represented as follows:

$$[J_{\mathrm{WMP}}] = \begin{bmatrix} [J_{\mathrm{WMP}}]_{11} & [J_{\mathrm{WMP}}]_{12} & [J_{\mathrm{WMP}}]_{13} & [J_{\mathrm{WMP}}]_{14} & [J_{\mathrm{WMP}}]_{15} \\ [J_{\mathrm{WMP}}]_{21} & [J_{\mathrm{WMP}}]_{22} & [J_{\mathrm{WMP}}]_{23} & [J_{\mathrm{WMP}}]_{24} & [J_{\mathrm{WMP}}]_{25} \\ [J_{\mathrm{WMP}}]_{31} & [J_{\mathrm{WMP}}]_{32} & [J_{\mathrm{WMP}}]_{33} & [J_{\mathrm{WMP}}]_{34} & [J_{\mathrm{WMP}}]_{35} \\ [J_{\mathrm{WMP}}]_{13} & [J_{\mathrm{WMP}}]_{13} & [J_{\mathrm{WMP}}]_{43} & [J_{\mathrm{WMP}}]_{44} & [J_{\mathrm{WMP}}]_{45} \\ [J_{\mathrm{WMP}}]_{13} & [J_{\mathrm{WMP}}]_{13} & [J_{\mathrm{WMP}}]_{53} & [J_{\mathrm{WMP}}]_{54} & [J_{\mathrm{WMP}}]_{55} \end{bmatrix}$$

where

$$[J_{\mathrm{WMP}}]_{11} = -s_1(a_2c_2 + a_3c_{23} - d_4s_{23});\ [J_{\mathrm{WMP}}]_{12} = -a_2^2s_2c_1 - a_3^2s_{23}c_1 - d_4c_{23}c_1;$$
$$[J_{\mathrm{MP}}]_{13} = -a_3s_{23}c_1 - d_4c_{23}c_1;\ [J_{\mathrm{WMP}}]_{14} = [J_{\mathrm{MP}}]_{15} = 0;$$
$$[J_{\mathrm{WMP}}]_{21} = c_1(a_2c_2 + a_3c_{23} - d_4s_{23});\ [J_{\mathrm{WMP}}]_{22} = -a_2s_1s_2 - a_3s_1s_{23} - d_4s_1s_{23}$$
$$[J_{\mathrm{WMP}}]_{23} = s_1(-a_3s_{23} - d_4s_{23});\ [J_{\mathrm{WMP}}]_{24} = [J_{\mathrm{MP}}]_{25} = 0;\ [J_{\mathrm{WMP}}]_{31} = 0$$
$$[J_{\mathrm{WMP}}]_{32} = -a_3c_{23} + d_4s_{23};\ [J_{\mathrm{WMP}}]_{33} = -a_3c_{23} + d_4s_{23};\ [J_{\mathrm{WMP}}]_{34} = [J_{\mathrm{MP}}]_{35} = 0$$
$$[J_{\mathrm{WMP}}]_{41} = [J_{\mathrm{MP}}]_{42} = [J_{\mathrm{MP}}]_{43} = 0;\ [J_{\mathrm{WMP}}]_{44} = [J_{\mathrm{MP}}]_{45} = (\cos\psi)/2r$$
$$[J_{\mathrm{WMP}}]_{51} = [J_{\mathrm{MP}}]_{52} = [J_{\mathrm{MP}}]_{53} = 0;\ [J_{\mathrm{WMP}}]_{54} = [J_{\mathrm{MP}}]_{55} = (\sin\psi)/2r$$

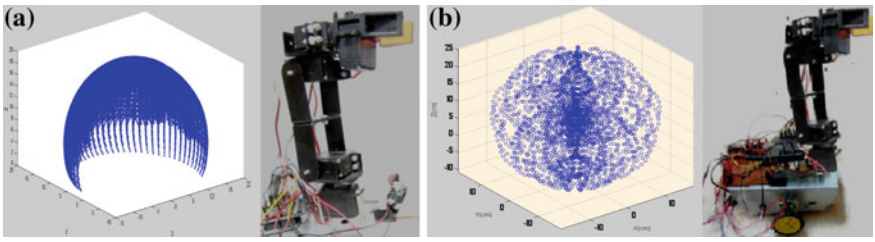

Fig. 2 Workspace generated by **a** Fixed manipulator and **b** WMM

Figure 2 represents the workspace generated by the mobile manipulator, when it is at a specific position. The developed hybridized system extends the workspace of a fixed manipulator by two times as shown in Fig. 2.

3 Conclusion

This study integrates the kinematic models of a 4-axis manipulator and a differential mobile platform. The motion of the developed WMM is controlled by five parameters in which three parameters give the velocity information of the manipulator and the remaining two correspond to the differential mobile platform. Finally, comparison has been performed in between the theoretical result obtained from the current analysis with the experimental results of a fabricated real mobile manipulator (4 DOF).

References

1. Ali T. Hasan, A. M. S. Hamouda, N. Ismail, H. M. A. A. Al-Assadi, (2006) An adaptive-learning algorithm to solve the inverse kinematics problem of a 6 D.O.F serial robot manipulator, Advances in Engineering Software, 37(7), pp. 432–438.
2. Deepak, B. B. V. L., Parhi, D. R., & Jha, A. K. (2011). Kinematic Model of Wheeled Mobile Robots. Int. J. on Recent Trends in Engineering & Technology, 5(04).
3. Parhi, D. R., & Deepak, B. B. V. L. (2011). Kinematic model of three wheeled mobile robot. Journal of Mechanical Engineering Research, 3(9), 307–318.
4. Hamner, B., Koterba, S., Shi, J., Simmons. R., Singh, S. (2009). An autonomous mobile manipulator for assembly tasks, Autonomous Robot, vol. 28, pp. 131– 149.
5. Deepak, B. B. V. L., Parhi, D. R., & Amrit, A. (2012). Inverse Kinematic Models for Mobile Manipulators. Caspian Journal of Applied Sciences Research, 1(13).
6. Deepak, B. B. V. L., & Parhi, D. R. (2011). Kinematic Analysis of Wheeled Mobile Robot. Automation & Systems Engineering, 5(2).
7. Manfred L. Husty,, Martin Pfurner, Hans-Peter Schröcker, (2007), Anew and efficient algorithm for the inverse kinematics of a general serial 6R manipulator, Mechanism and Machine Theory, 42(1), pp. 66–81.
8. Dayal R. P, Deepak B, Nayak D, Anand A. (2012), Forward and Inverse Kinematic Models for an Articulated Robotic Manipulator, International Journal of Artificial Intelligence and Computational Research, 4 (2): 103–109.
9. Deepak, B. B. V. L., Parhi, D. R., & Kundu, S. (2012). Innate immune based path planner of an autonomous mobile robot. Procedia Engineering, 38, 2663–2671.
10. Deepak, B. B. V. L., & Parhi, D. R. (2013, December). Target seeking behaviour of an intelligent mobile robot using advanced particle swarm optimization. In Control, Automation, Robotics and Embedded Systems (CARE), 2013 International Conference on (pp. 1–6). IEEE.
11. E. J Van Henten, J Hemming, B. A. J Van Tuijl, J. G Kornet and J Bontsema, (2003), Collision-free Motion Planning for a Cucumber Picking Robot, Biosystems Engineering, 86 (2), pp. 135–144.
12. Kundu, S., Parhi, R., & Deepak, B. B. (2012). Fuzzy-neuro based navigational strategy for mobile robot. International Journal of Scientific & Engineering Research, 3(6).

13. Deepak, B. B. V. L., Parhi, D. R., & Raju, B. M. V. A. (2014). Advance particle swarm optimization-based navigational controller for mobile robot. Arabian Journal for Science and Engineering, 39(8), 6477–6487.
14. Datta, S., Ray, R., Banerji, D. (2008). Development of autonomous mobile robot with manipulator for manufacturing environment, International Journal of Advanced Manufacturing Technology, Vol. 38, pp. 536-542.
15. Deepak, B B V L (2015), Design and Development of an Automated Mobile Manipulator for Industrial Applications, Ph.D. Thesis, National Institute of Technology—Rourkela, http://ethesis.nitrkl.ac.in/6652/.
16. Eliot, E., Deepak, B., Parhi, D., & Srinivas, J. (2013), Design & Kinematic Analysis of an Articulated Robotic Manipulator. International Journal of Mechanical and Industrial Engineering, 3(1), 105–108.
17. Deepak, B. B. & Parhi, D. (2013). Intelligent adaptive immune-based motion planner of a mobile robot in cluttered environment. Intelligent Service Robotics, 6(3), 155–162.
18. B.B.V.L. Deepak & Dayal R. Parhi (2016) Control of an automated mobile manipulator using artificial immune system, Journal of Experimental & Theoretical Artificial Intelligence, 28:1–2, 417–439.

Author Index

D.K. Lobiyal et al. (eds.), *Proceedings of the International Conference on Signal, Networks, Computing, and Systems*, Lecture Notes in Electrical Engineering 396, DOI 10.1007/978-81-322-3589-7